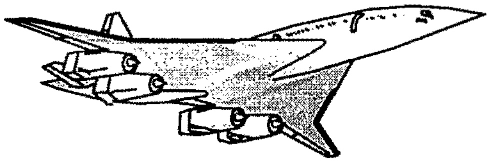

High Speed Research Program

HSR II - Airframe Task 20

Task 2.1 - Technology Integration

Sub-Task 2.1.3 Aeroelastic Concept Engineering

ACE Final Report

December 31, 1998

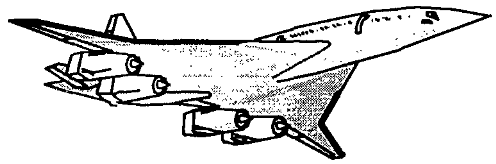

High Speed Research Program

HSR II - Airframe Task 20

Task 2.1 - Technology Integration

Sub-Task 2.1.3 Aeroelastic Concept Engineering

ACE Final Report

December 31, 1998

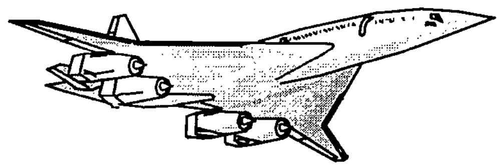

ACE Final Report

I - Introduction

Chris Borland
Joe Giesing

December 31, 1998

Table of Contents

Acknowledgements

Abdi, Frank	Alpha-Star Corp	Structures
Adamson, Eric	Boeing-Sea	Aero
Agrawal, Shreekant	Boeing-LB	Aero
Anderson, Mark	VPI	Controls
Arslan, Alan	Boeing-LB	Loads
Baker, Miles	Boeing-LB	Loads
Barclift, Bill	Boeing-Sea	Weights
Barkey, Derek	Boeing-LB	Structures
Barthelemy, Jean Francois	NASA LaRC	HPCCP
Becker, Brad	Boeing-Sea	Weights
Bharadvaj, Bala	**Boeing-LB**	**ACE Team**
Bhatia, Kumar	Boeing-Sea	Structures
Borland, Chris	**Boeing-Sea**	**ACE Team**
Boyd, Bill	Boeing-Sea	Flutter
Burggraf, Warren	Boeing-Sea	Aero
Buttrill, Carey	NASA LaRC	Controls
Carpenter, Jon	Boeing-LB	Weights
Carpenter, Paul	Boeing-Sea	Aero
Cayton, Mark	Boeing-Sea	Structures
Chaderjian, Neal	**NASA ARC**	**ACE Team**
Chang, Kwan	Boeing-Sea	Flutter

This report is the final documentation of the ACE Project, conducted as WBS 3.1.2 under the Technology Integration (Task 20) element of the High Speed Research - Airframe Technologies Contract NAS 1-20220.
The report was assembled by Chris Borland, Joe Giesing, and Dave Knoernschild of The Boeing Co. However, there are many individuals whose efforts contributed to the success of the ACE program, and there names are listed on this and the following pages. Apologies if names were omitteed.

Acknowledgements

Chen, Allen	Boeing-Sea	Aero
Churchill, Brett	Boeing-Sea	Controls
Clark, Tita	Boeing-Sea	Propulsion
Coen, Peter	NASA LaRC	TI
Conley, Walt	Boeing-Sea	Noise
Debrouwer, Giles	Boeing-LB	Structures
Dees, Paul	Boeing-Sea	Aero
Downs, Tony	Boeing-Sea	Structures
Ebner, Keith	Boeing-Sea	Aero
Flores, Servando	Boeing-Sea	Aero
Geertsema, Egbert	Boeing-Sea	Noise
Gelhausen, Paul	**NASA ARC**	**ACE Team**
Giesing, Joe	**Boeing-LB**	**ACE Team**
Gilbert, Bill	NASA-LaRC	TI
Giles, Gary L.	NASA LaRC	Structures
Goggin, Patrick	Boeing-LB	Loads
Green, Larry	**NASA LaRC**	**ACE Team**
Griffiths, Bob	Boeing-Sea	Aero
Guruswamy, Guru	NASA ARC	Loads
Henderson, Dennis	Boeing-LB	Controls
Johnson, Bryan	Boeing-Sea	Structures

Acknowledgements

Kimoto, Bruce	Boeing-LB	TI
Knoernschild, David	Boeing-Sea	DOSS
Kumar, Vasant	Boeing-Sea	Structures
Lam, Alfred	Boeing-LB	Weights
Lavelle, Tom	NASA LeRC	Graphics
Livne, Eli	U of Washington	Structures
McCullers, Arnie	Vigyan	DOSS
Meredith, Paul	Boeing-Sea	Aero
Merritt, Fergus	Adv. Scientific Computing	Graphics
Mitchell, Pat	Boeing-Sea	Weights
Moitra, Stuti	Boeing-Sea	Structures
Moore, Matt	Boeing-Sea	Noise
Murman, Scott	NASA-ARC	Loads
Narducci, Bob	Boeing-LB	Aero
Nazari, Mark	Boeing-Sea	Structures
Nelson, Chet	Boeing-Sea	Aero
Okazaki, Alan	Boeing-LB	DOSS
Parkan, Glenn	Boeing-Sea	Weights
Parker, Starr	Boeing-Sea	Loads
Pera, Ron	Boeing-Sea	TI
Peterson, Kevin	Boeing-Sea	Aero
Porter, Chris	Boeing-LB	Loads

Acknowledgements

Rams, Jim	Boeing-Sea	Weights
Rehder, Joe	NASA LaRC	HPCCP
Roth, Eric	Boeing-Sea	Aero
Sergev, Steve	Boeing-Sea	Structures
Shih, Michael	Boeing-LB	Structures
Sobieski, Jaroslaw	NASA LaRC	HPCCP
Stone, Steve	Boeing-Sea	Structures
Suju, Ludwig	Boeing-Sea	Structures
Tamigniaux, Terry	Boeing-Sea	Structures
Titzer, Chris	Boeing-Sea	Controls
Torres, Francisco	NASA ARC	Graphics
Tu, Eugene	**NASA ARC**	**ACE Team**
Vegter, Chris	Boeing-Sea	Aero
Viars, Phil	GE	Propulsion
Wakayama, Sean	Boeing-LB	DOSS
Waszak, Marty	NASA LaRC	Controls
Welge, Bob	Boeing-LB	TI
Wilhite, Alan	NASA-LaRC	TI
Yuan, Kuo-An	Boeing-LB	Loads

Section I
Introduction

Section I.1
Background, Goals, and Objectives

Aeroelastic Concept Engineering Team Charter

- Develop and validate processes/methods/tools to integrate advanced technologies from individual disciplines into the aircraft design procedure
  - ◊ include all key interdisciplinary interactions
  - ◊ include optimization whenever/wherever feasible
  - ◊ leverage, not duplicate, other elements of HSR
- Develop a new design - Optimized Aeroelastic Concept Airplane (9/98, Level II milestone)
- Guide the definition of the Technology Configuration (12/98, Level I milestone)

The Aeroelastic Concept Engineering project was initiated in 1994 as an effort to incorporate the potential benefits of Multidiciplinary Design Optimization into the configuration design and selection of the High Speed Civil Transport aircraft, as well as to improve the accuracy of the methods employed in conceptual and preliminary design. It was recognized early on that a fully-integrated or tightly-coupled MDO would not be feasible within the time and budgetary constraints of the HSR Program. It was deemed important to employ a methodology which would a) fit within the operational constraints of the existing discipline organizations, and b) make a positive contribution to the improvement of HSCT designs within the time and budget available. The Program Level II Milestone, Optimized Aeroelastic Concept, was chosen as the appropriate goal for the process, and the project name, Aeroelastic Concept Engineering, was chosen to reflect that goal. It was further decided that optimization methods would be used where feasible and appropriate, but not to the exclusion of more traditional trade study, analysis, and best practice approaches.

Goals for the ACE Team Optimization Process

- Minimize the MTOW with realistic airplane design constraints
- Practical and reliable
- Applicable at the conceptual and preliminary design phase
- Modified and augmented for the future
- Maintain the autonomy of individual contributing disciplines
- Improve the design, and understand the changes.

The ACE Teams goal was to develop, implement, and demonstrate a process that could be used to improve airplane design. Within the context of the HSR program, an "improved design" is by definition one with reduced gross weight while meeting all realistic airplane-level program constraints. The optimization process therefor used maximum take-off gross weight (MTOW) as the primary objective function. It was necessary that the process meet other requirements as well, listewd above. It was important the the individual disciplines providing data be able to oporate autonomously and maintain control of there data and processes. It was also critical that when and improved design was developed, that sufficient information be available so that the various design changes and sensitivities could be visible to and understood by the engineers concerned.

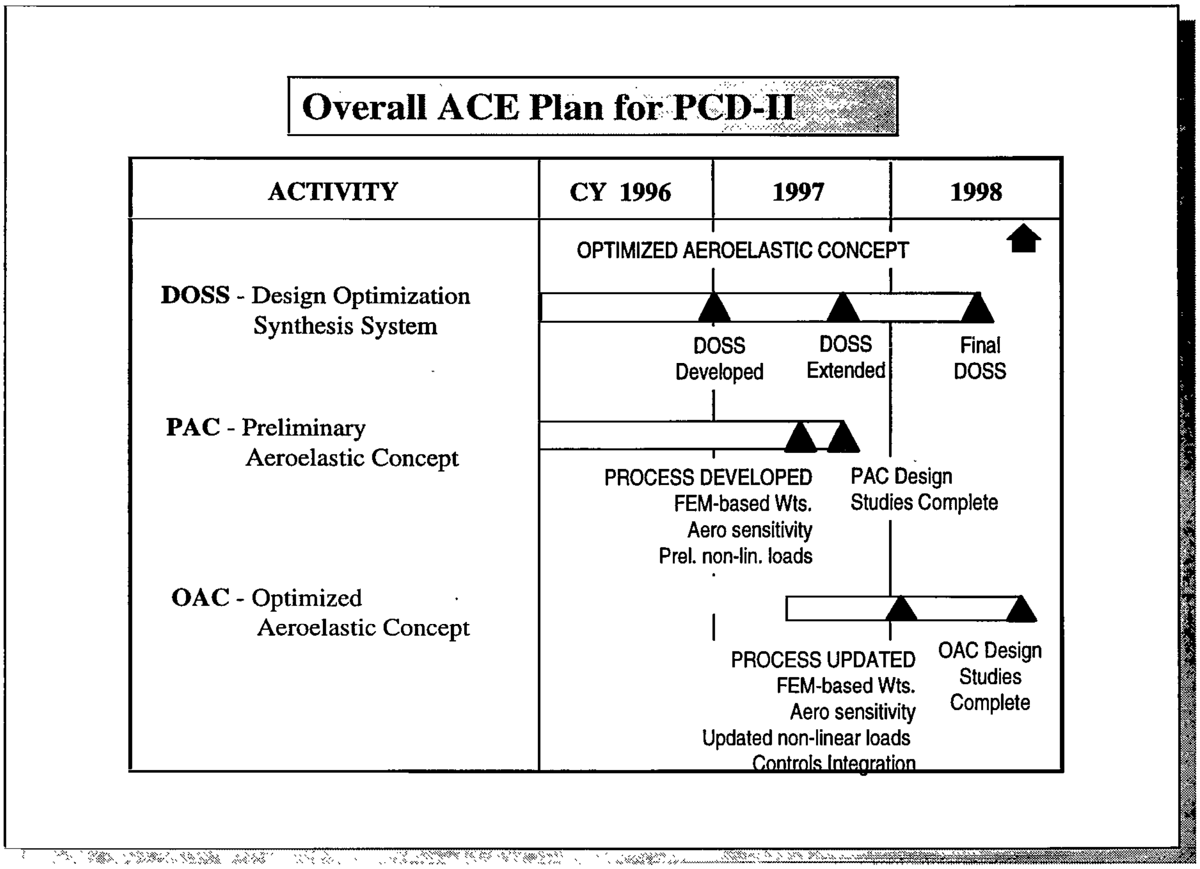

This page shows the schedule of the ACE program during the PCD2 timeframe, although the project had been initiated during PCD1 and was well underway by 1996. The ACE Team posed an imtermediate level milestone known as the PAC (Preliminary Aeroelastic Concept) to be used to check out and validate the methods and procedures being developed, in preparation for meeting the goals of the OAC. The system known as DOSS (discussed below) was developed during this period and an initial version using lower fidelity “advanced design” data was used for an initial configuration development. The system was extended for use with some higher-fidelity data for the PAC, and modified again for use on the OAC. The initial DOSS and PAC developments have been documented in earlier reports, listed in the References.

Strategy Adopted in the ACE Optimization Process

- Individual disciplines work concurrently and maintain autonomy.
- Local design variables determined through local optimization, analysis, or best practices.
- Disciplines provide data to global process.
- System deals with global design variables - with strong interdisciplinary coupling and/or significant impact on the airplane configuration.
- Global/local process can be iterative (formal or informal).
- Global optimization process includes airplane mission analysis.
- The design system includes realistic constraints.
- The system output helps the designer understand the design space.

DOSS - Design Optimization Synthesis System

The strategy adopted allowed the Team to reach the previously stated goals. Individual disciplines performed their own analysis and optimizations, using global level constraints and local design variables, and passed data and sensitivities to a global level process (DOSS) for optimization. The global design variables chosen were those that would have significant interdisciplinary interaction, such as planform parameters of aspect ratio, sweep angle, etc. The global process included a mission analysis module, since MTOW was chosen as the global objective function, but this is unique to the current HSR application, and not essential to the DOSS process as a whole. Iterations between global and local levels were conducted on an informal basis, updating the local configurations for optimization, rather than by a formal iteration process looking for convergence.

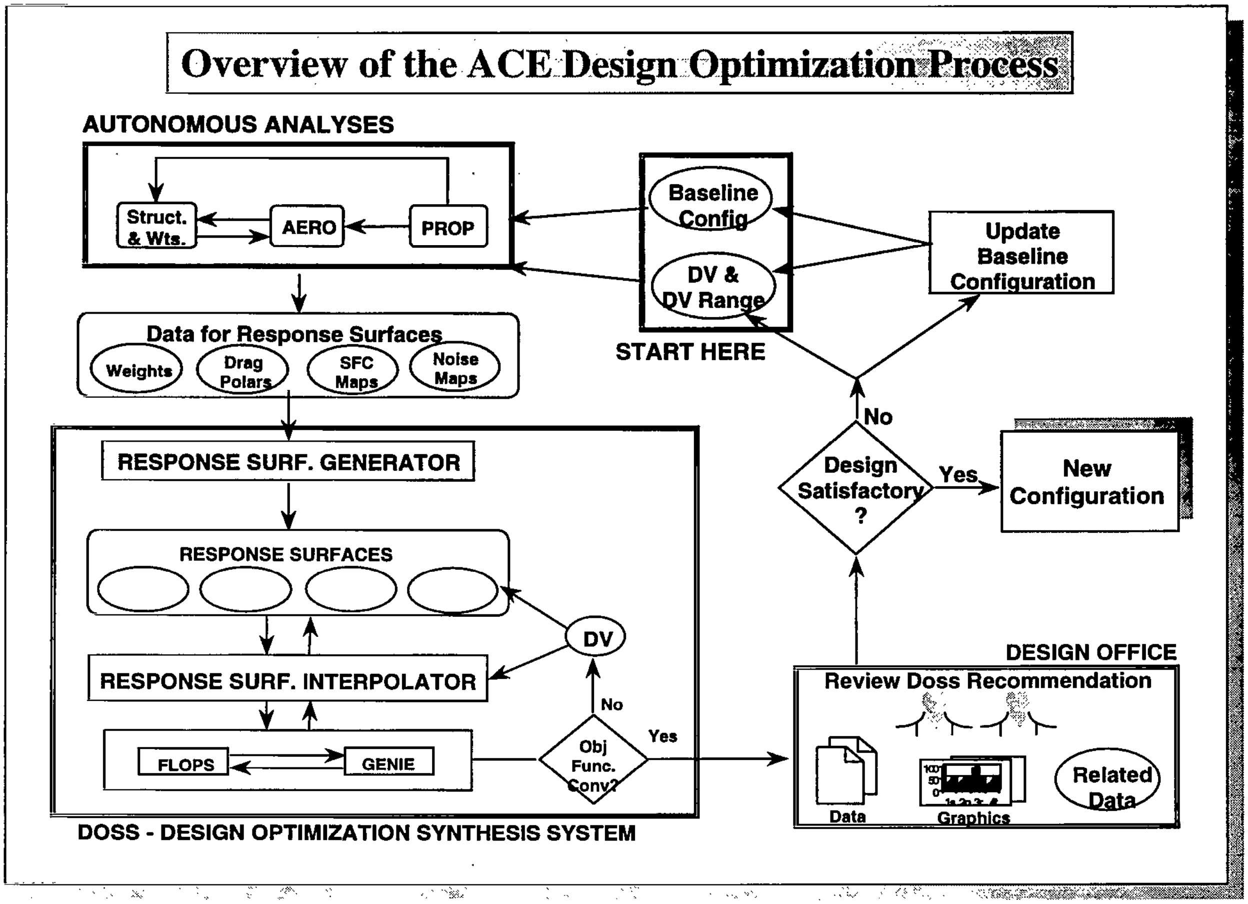

The ACE Process starts by chosing a baseline configuration and objective function, as well as global design variables and their ranges. These are then passed to the various disciplines for analysis and optimization, some of which may be interdisciplinary. For example, engine size effects both propulsion and aerodynamics, and planform affects both aerodynamics and structures. The disciplines produce results for a given set or range of design variables which are treated as constraints. Results are provided in the form of tables, equations, or individual analysis results. These results are then fitted using a response surface generator, to create a database which can be used by the global optimizer. The global optimizer and mission analysis operate within a framework known as GENIE. GENIE, the optimizer, mission analysis, and response surface generation and interpolation tools, together with an interactive data interface and graphics display package, form the Design Optimization Synthesis System, DOSS. Results from DOSS are reviewed by the engineering teams, incorporated with results from other studies and analyses, and form the basis for further design recommendations and baseline updates.

Section I.2
ACE Global-Local Process Overview

•Divide Design Variables
  1) Strongly Interacting Global Design Variables
  2) Weakly Interacting Local Design Variables

• Design/Optimize Local Design Variables at the Local Level
  •Perform a Local Design for Each Parameteric Variation of the Global Design Variables
  • Use Baseline Design for Needed Interactions with Other Disciplines
  • Output Local Data for Weight, Drag, SFC, etc. from Local Designs Versus Parametric Values of Global Design Variables

• Place Parametric Data for Weight, Drag & SFC Versus the Global Design Variables into the Global Level Optimization
  • Use Response Surfaces and Other Approximations

• Optimize the Global Design Variables
  • Using the Local Design Data
  • Using a Mission Module

• Update the Baseline and Response Surfaces and Repeat the Process If Necessary

The ACE process separates the design process into two levels; 1) the global level where a small number of global variables are optimized to minimize the objective function(in this case Max. Take-Off Gross Weight) and, 2) the local level where potentially a large number of local variables (e.g. skin gages and stringer areas) are optimized to minimize a local objective function (e.g. structural weight).
The effect of local variables across the disciplines is assumed weak and is taken care of by iteration. For instance the effect of elasticity on drag (a very small effect) can be taken care of by using the elasticity of the baseline design (and its subsequently updated values) during the optimization process.
The global variables interact with the local discipline designs by acting as parameters. The local designs are performed on parametric variations of the global design variables and performance data (weight, drag, etc.) are developed and fed to the global optimization process.

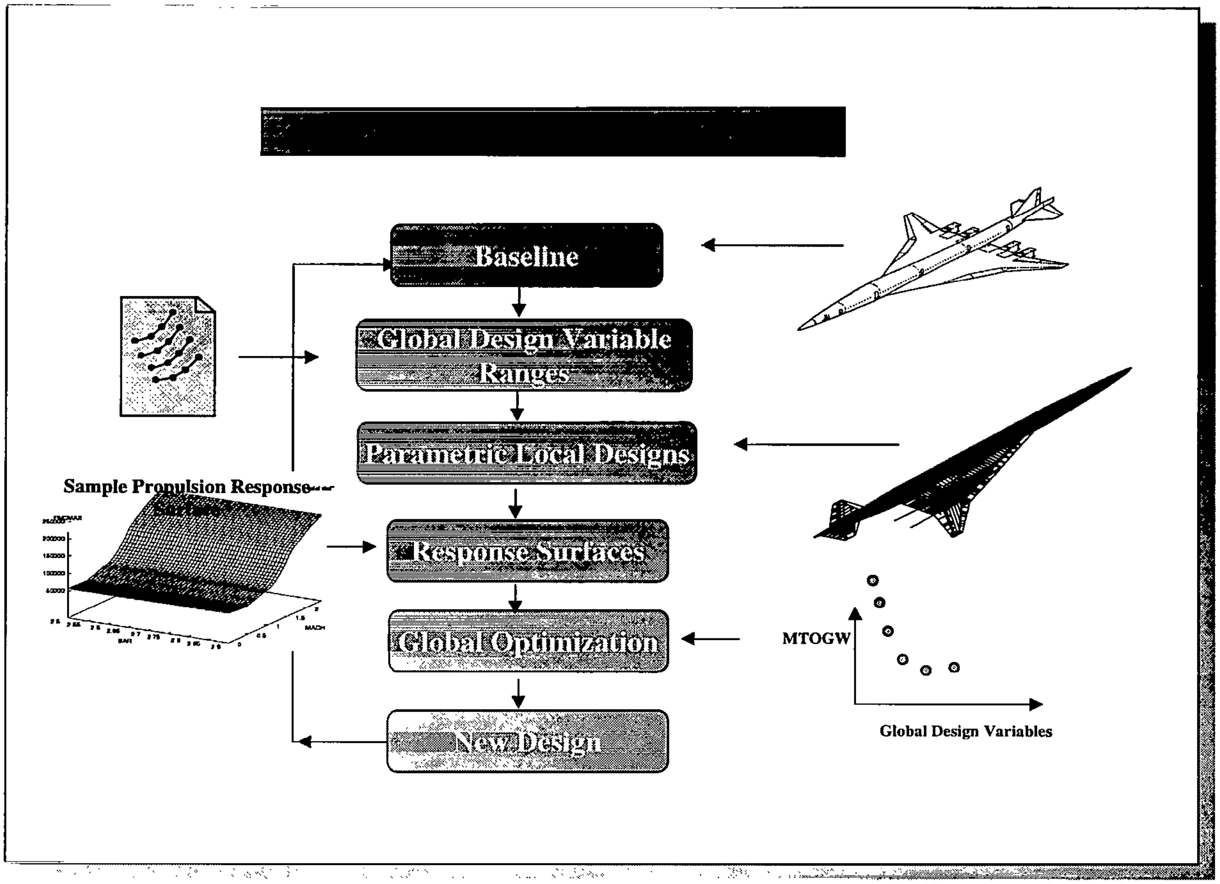

A flow chart of the global-local design process is given in this chart.

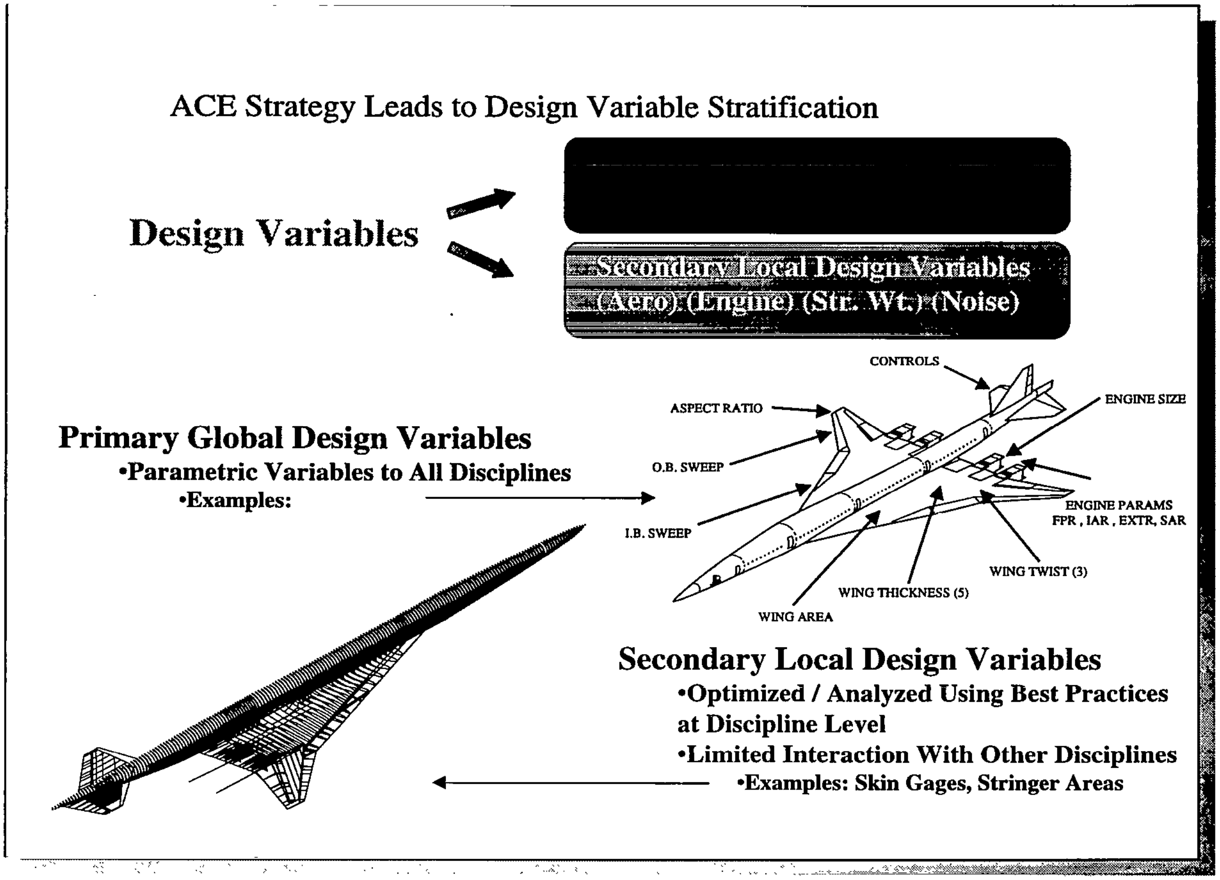

The ACE approach is to separate the design variables into global and local design variables. Global d.v. strongly affect two or more disciplines where local variables strongly affect one discipline and only weakly affect others. Global design variable examples are; wing area, sweep, aspect ratio, thickness, twist, engine thrust, fan pressure ratio and tail size. Local design variable examples are; skin gages, stringer area and shape, leading edge nose radius, and the details of the outer mould lines.

The control of the global and local design variables is up to the user who must consider the importance of the interaction, strength of the interaction, expense, and fidelity level desired. If a local design variable turns out to have a strong interaction it can be elevated to the global level. The importance and strength of interaction should be used to order the design variables (e.g. wing area, thrust, aspect ratio, sweep, engine by-pass ratio etc.). After they have been ordered the expense and fidelity level required to accommodate them can then be used to draw a line to separate global from local design variables. This will allow a proper interaction of the global variables and an approximate interaction for the weakly interacting variables. This process also allows high fidelity local optimization data (e.g. structural sizing FEM optimization for weight and drag and L/D optimization using CFD) to pass on to the global optimizer.

- Structures and Weights (Use Structural Sizing Optimization)
  - *F = OEW (Structural Weight)*
  - *g = Stress, Buckling, Loads, Flutter, Manufacuturability, etc.*
  - Output Weight and Internal Running Loads

- Aerodynamic Performance (Use a Combination of Optimization, & Corrections)
  - *F = High Speed Wave Drag, Low Speed L/D*
  - *g = Layout Constraints, Fuel Vol., Leading Edge Radius, TE Angle*
  - Drag Build-Up Best Practices
  - Correct Drag with CFD and Data
  - Output High/Low Speed Drag Polars and Aero. Coef.s

- Propulsion and Noise (Use Engine Company Best Practices)
  - Out Put Engine Data Deck
  - Add Engine Installation Increments

Local design variables and constraints are dealt with at the local level. For instance skin gages and stringer areas are sized for minimum OEW weight (Objective Function F) while satisfying aeroelastic load, and flutter constraints (g), buckling and material allowables, and allowing for fixed and as-built weights. The engine is designed to the engine company best practices. The aerodynamic drag is predicted using a combination of linear wave drag optimization, CFD & test corrections, and best practices, and analysis. The appropriate constraints are also satisfied at the local aerodynamic level.

ACE Strategy Leads to Independent Concurrent Parametric Data Approach

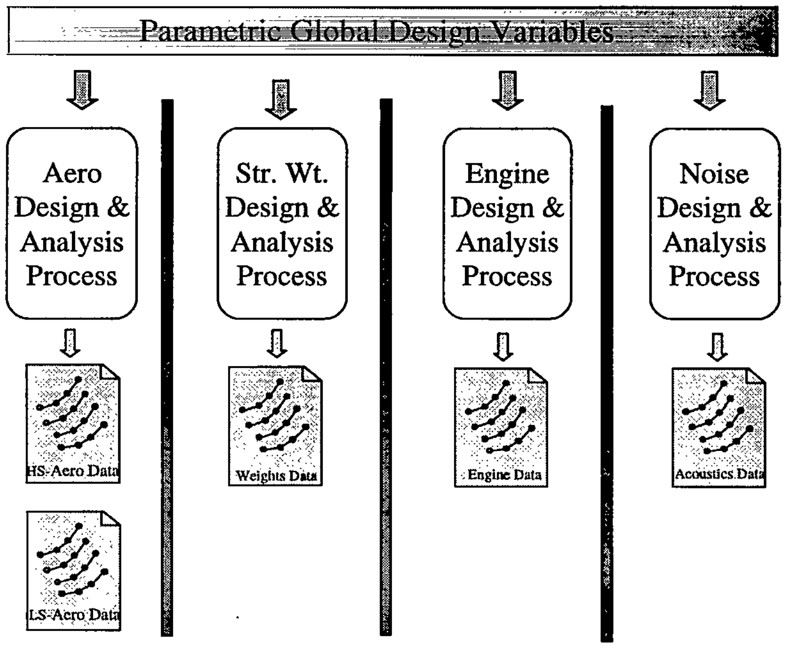

All data generation is done in parallel with minimal or no interaction. Aerodynamic drag is computed for the rigid aircraft since elastic effects are small. Corrections can be applied if necessary based on the baseline aircraft. In this case a small interaction or no interaction is needed. Structural sizing contains a linear loads and flutter aerodynamic segment which is developed by the Structures Group. If CFD corrections are needed, a selected set of CFD cases can be done ahead of time to furnish this data. The CFD data is generated using the baseline configuration and applied to correct the structural sizing aerodynamic data. In this case only a small interaction or no interaction is needed.

The engine propulsion and acoustics data is obtained independently by the engine company with very little or no data required from other disciplines.

- **Global Optimizer Minimize Objective Function (F) and Satisfy Constraints (g)**
  F = Maximum Take-Off Gross Weight
  g = Take-Off, Climb, Cruise, Landing, Noise Constraints
- **Use Mission Analysis Module (FLOPS) to Provide Objective Function (F) and Constraints (g)**

The global optimization process provides the Mission module (FLOPS) with configuration updates. The Mission module flies the updated configuration through the mission, determines the fuel and objective function (MTOGW) and the state of the mission constraints for take-off, noise, landing etc. It then feeds this data back to the optimizer. The optimizer compares the current state of the objective function and constraints with the desired results and comes up with a new configuration that it thinks will satisfy them. This new configuration update is used to repeat the process, and this repeats until convergence.

Advantages and Benefits of ACE Approach

- **Simple and Practical Process for Integrating/Optimizing Full Configuration**
  - Natural Extension of Aircraft Sizing Process
  - Easy Way to Integrate Dissimilar Disciplines
- **Process & Data Controlled by Disciplinary Experts & Organization**
  - Design Best Practices, Optimization or Analysis
- **Concurrent Data Generation (All Disciplines Working in Parallel)**
- **ACE Process Independent of Disciplinary Fidelity Levels**
  - Allows Variable Fidelity (By Discipline or By Update Levels)
  - Controlled by Discipline
  - DOSS Applicable from Conceptual Design, Through Preliminary Design

There are several very important advantages to the ACE approach. First, the ACE approach conforms to current industry organizational structure. In industry each discipline is responsible for the process and data quality it produces. The ACE process allows this responsibility to be carried on.
Second, each discipline can perform its data generation in parallel with the other disciplines allowing concurrent operation.
Third, the ACE process operates independent of the fidelity level of each of the disciplines. This allows each discipline to supply data rapidly and update the data as it matures.
Fourth, the ACE-DOSS process is very close to the Current Advanced Design Process. This provides for a smooth transition from current practices in configuration sizing to the advanced MDO practices of the future.

Section I.3
ACE Working Group Processes Overview

This section describes the ACE Working Groups commissioned to meet and carry out the challenges in the various disciplines. There are 5 working groups as follows.

- DOSS Working Group (Over-all global optimization process)
- Aerodynamics Working Group (Local Drag and Aero. Optimization Process, plus Propulsion data)
- Nonlinear Loads Working Group (Nonlinear Loads for Str. Sizing Opt. Process)
- Structures and Weights Working Group (Structural Sizing Optimization and Wt. Prediction)
- Controls Working Group (Tail Sizing and Active Controls)

A brief overview of each working group is given including its objectives and approach.

DOSS Working Group

Objectives

- Develop a **Practical MDO System** for Simultaneous Optimization of Multiple Global Design Variables
- Develop User Friendly GUI and Design Space Visualization Techniques
- Include All Required Disciplinary, Mission and Manufacturing Constraints
- Apply the DOSS Process to Find the ACE Optimized Aeroelastic Concept and Other TI Configurations

The objectives of the DOSS WG are to; 1) produce a practical user friendly configuration optimization MDO tool that lines up with the ACE strategy, 2) develop an architecture that is very general and a code that is easily modified, and 3) apply the process to the development of the ACE OAC configuration and assist in the development of the TC configuration.

DOSS Working Group

Approach

- Develop Response Surface Techniques for Utilizing Parametric Data From the Various Disciplines
  - RS Generator RSMAKE, SOCS
  - RS Reader RSREAD

Sample Response Surface for Aerodynamic Drag

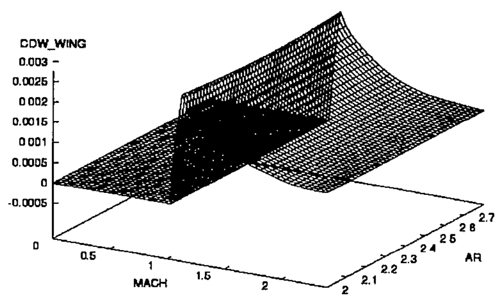

Sample Propulsion Response Surface

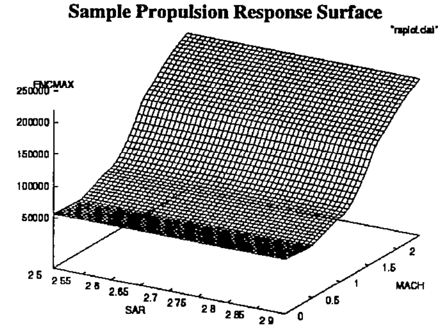

The details of the DOSS approach and process is given in Appendix A. One of the major components of DOSS is the Response Surface. Processes for making and using response surfaces as well as integrating them into the optimization process was the responsibility of the DOSS WG.

DOSS Working Group

Approach (Cont.)

- Employ and Extend the Genie Architecture and Optimization Capability

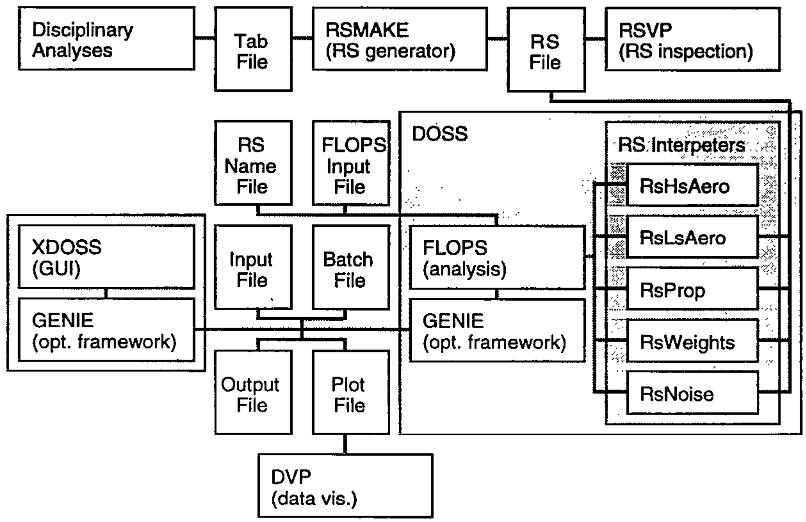

The Genie architecture is the backbone of the DOSS process that coordinates and drives the optimization process. Genie is a very general architecture and can easily accept new or modified modules/data.

DOSS Working Group

Approach (Cont.)

- Include the NASA FLOPS Mission Code

Mission Analysis

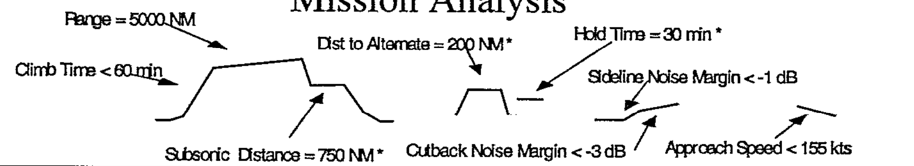

•Add a GUI and Design Space Visualization Code

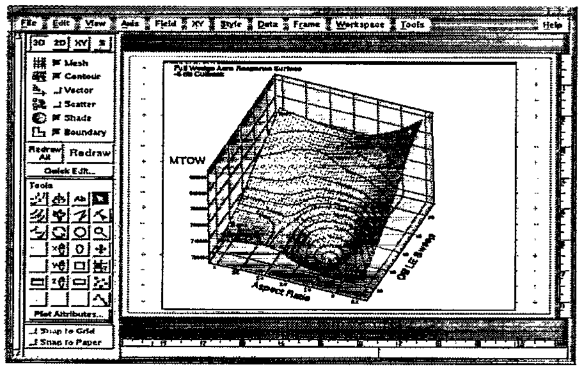

The NASA FLOPS code is the mission analysis that calls data from the response surfaces, flies the mission and, evaluates the state of the global level constraints and objective function (MTOGW).

A clear view of the design space is mandatory in addition to the optimized configuration. Thus the DOSS WG is required to provide creative graphics to help determine the shape of the multi-dimensional design space.

It is also the responsibility of the DOSS WG to develop a GUI to make sure that the code is user friendly.

DOSS Working Group

Advantages and Benefits of DOSS

- General Architecture Good for MDO of Many Classes of Vehicles
- Response Surface Approach Leads to;
    - Multiple Fidelity or Variable Fidelity
    - Concurrent Parametric Data Development
    - Data Interface, Rather than Code Interface
    - Disciplinary Experts Responsible for Parametric Data
    - Disciplines Can Use Best Practices or Optimize Parametric Data
    - Rapid Optimization
    - Smoothed Data for Increased Optimization Robustness
- Easy Design Space Visualization
- DOSS is a Natural Extension of Aircraft Sizing Process
- Easy Way to Integrate Dissimilar Disciplines at Different Stages / Levels of Automation and Robustness

HIGH SPEED RESEARCH
Aeroelastic Concept Engineering

Aerodynamic Performance Working Group

Objectives

- Develop an Improved Fidelity Aerodynamic Performance Process
  - For Predicting Drag and Other Aerodynamic Parameters
  - Include CFD
- Develop Low and High Speed Aerodynamic Data
  - for Parametric Variations of ACE Configurations
- Ensure Quality of Resulting Response Surfaces

The primary goals of the Aerodynamics discipline are to; 1) furnish a process for determining high fidelity parametric drag data ,2) determine this data for ACE configurations, and 3) make sure the resulting response surfaces are accurate.

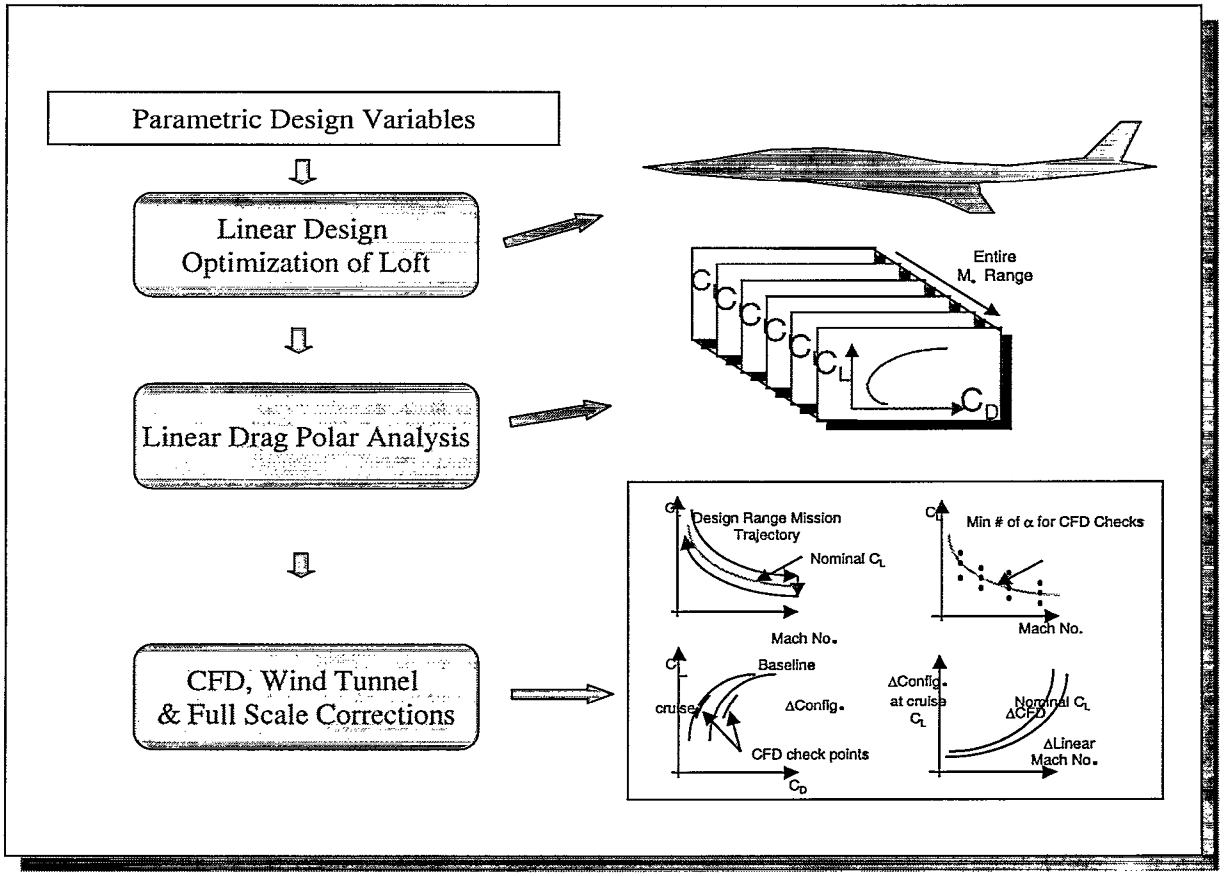

The aerodynamic process decided upon is given in this slide. Details of the process are found in Appendix B. The first step is to obtain viable linear optimized parametric configurations including fuselage area ruling and layouts. The second step is to determine the drag polars of the parametric configurations and the other lift and moment data. The third step is to perform CFD spot checks of the parametric set of configurations and to correct the linear data accordingly. Other corrections are also introduced using past configuration tests.

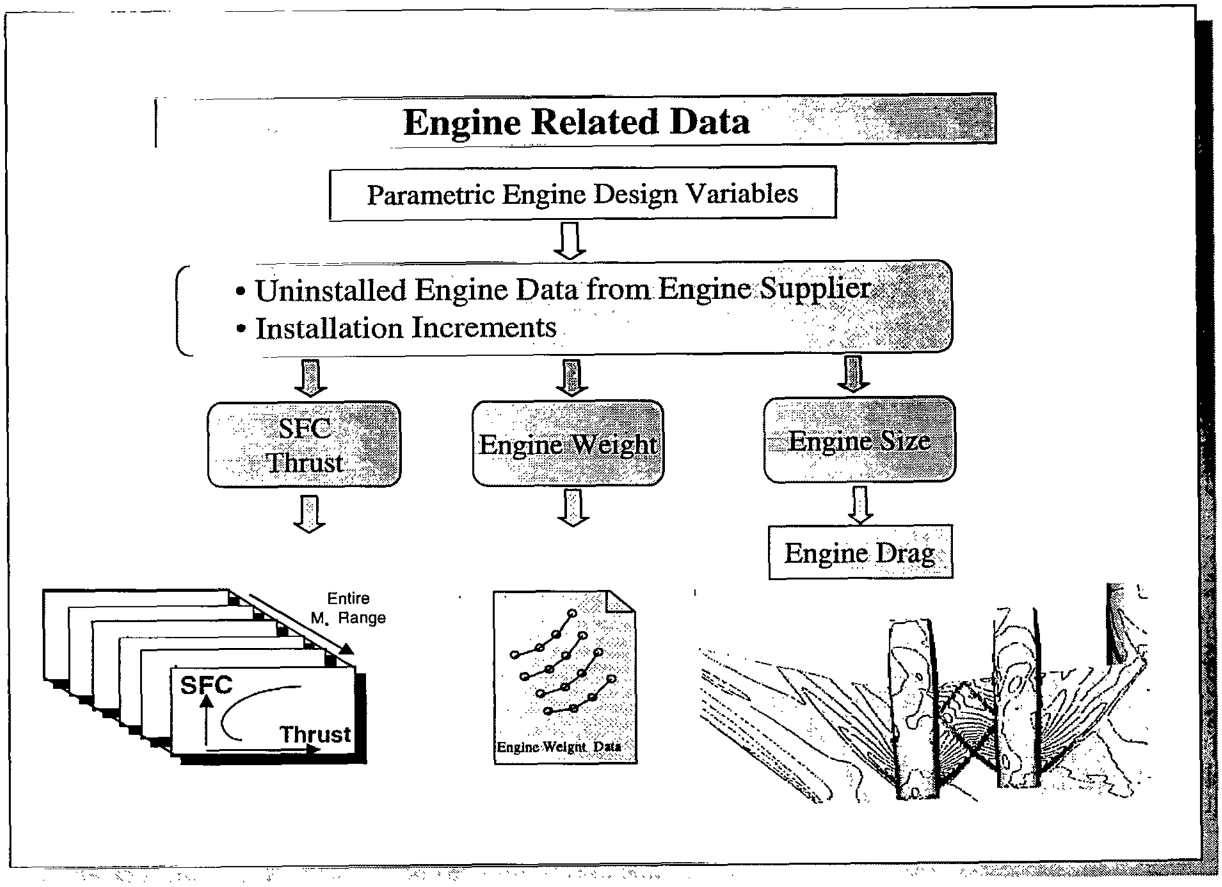

The Aerodynamics WB is also involved with the engine drag data. Nacelle and pylon effects are included in a drag build-up fashion. The engine also supplies engine weight data that is of interest to the Structures and Weights WG. The engine performance data is supplied in two parts; 1) the basic uninstalled data plus, 2) an installation increment.

Nonlinear Loads Working Group

Objectives

- Develop a **Practical High Fidelity** Nonlinear Structural Loads Identification and Analysis Process
  - CFD Based Process
  - Corrections to Linear Loads
- Develop CFD Methods for Extreme Load Conditions
  - Boeing Long Beach and NASA AMES
- Use CFD and Nonlinear Loads Process to Develop Loads for ACE and TI Configurations and Structural Sizing

Loads analysis involves sorting through hundreds or thousands of cases to determine the critical ones. High fidelity CDF can not be applied to each of these cases because of the expense and time involved. However, many of the load cases are nonlinear and can only be handled accurately using CFD. The challenge is to develop a process that captures the nonlinear aspects but is practical to use.
CFD itself may have problems performing the required calculations at the extreme conditions at which many of the critical loads are found. Also the criteria for convergence in loads is different from that encountered in drag performance.

Nonlinear Loads Working Group

CORRECT

- New Local Equivalence Correction Procedure
- Requires a Limited Data Base of CFD Solutions
- CFD/Linear Theo. Grid Conversion Employed (CFDDLM)
- Unique SVD Singular Value Decomposition Technique Used to Minimize CFD Cases

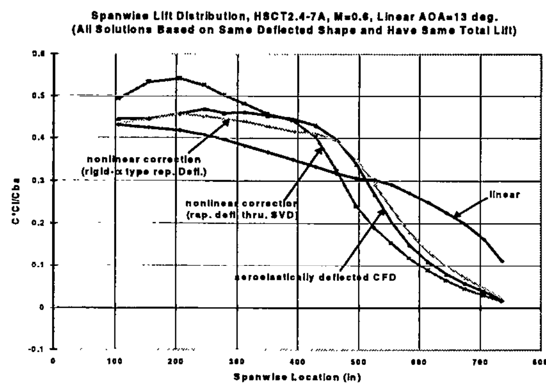

Appendix C presents the details of the nonlinear loads process and applications. The nonlinear loads process is based on a correction procedure and gives accurate results even when a small data base of CFD solutions is used. The process was verified by comparison with CFD analyses done on the aeroelastically deflected configurations.

Nonlinear Loads Working Group

CFD Technology for Loads

- New Convergence Criteria Needed (Sectional Lift/Moment)
- Some Static Load Cases Cause Unsteady Flow Conditions (Time Accurate Simulation)
- Increased Robustness Required for Some Load Cases

Flow Analysis for the PTC W/B/F/C Configuration

High Speed Aerodynamics, Long Beach
CFL3D N-S, Badwin-Lomax (Degani-Schiff), $Re_c = 40 \times 10^6$, $M_\infty = 0.80$, $\alpha = 9.57°$, $\delta_c = 12.42°$
W/B C-O (181x289x65) - LE 0/9° TE 0/0/3°

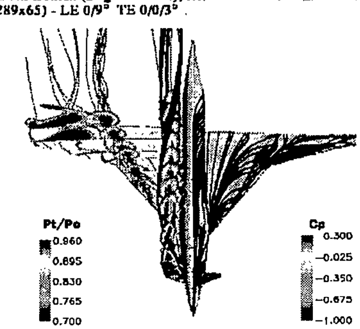

BOEING

New criteria for convergence was developed for CFD loads. CFD work was done at Boeing Long Beach using CFD3DAE.BA. It was verified by NASA AMES using the Overflow code and various turbulence models. AMES also provided some verification calculations using ENSAERO. Boeing Seattle (ISDS) assisted in solving grid overset difficulties for the canard.

Nonlinear Loads Working Group

CRLOAD

- New Critical Load Identification Procedure
- Based on Fully Stressed Design Weight

Fully Stressed Weight using Linear Sort Sequence (TCA)

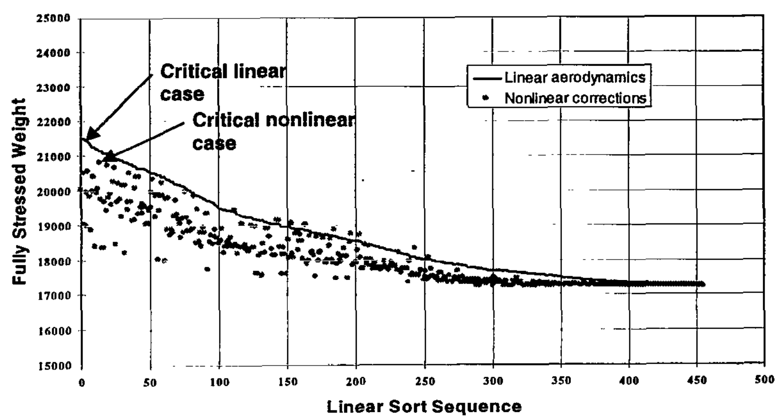

The new nonlinear loads process was applied to the TCA aircraft. 120 candidate critical load cases were screened. Many of the load cases that were critical for the linear loads screening (high angle of attack) were not critical for the nonlinear loads screening. Generally speaking nonlinearities tended to lower the loads. However, when one case is eliminated from the critical list there is always one just below it ready to take its place. As such applying nonlinear loads to the TCA reduced the weight by 4%.

Nonlinear Loads Working Group

- A New Nonlinear Loads Process Has Been Developed
  - Integrated With the DITS Structural Sizing Optimization Process
  - CORRECT, CRLOAD & CFDDLM Used

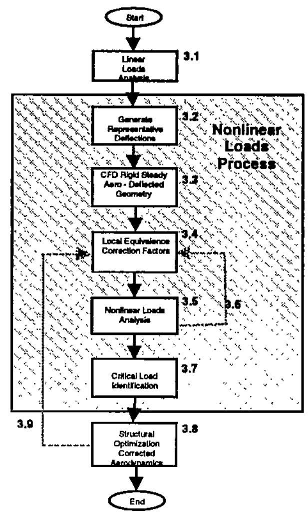

The new nonlinear loads correction process was imbedded into the structural sizing and optimization process.

Structures and Weights Working Group

Objectives

- Develop a **Rapid Improved Fidelity** Structural Sizing and **Weights** Process
  - Higher Fidelity than Parametric Weights
  - FEM Based (or Equivalent)
  - Within 5% of Current DITS Sizing Process Weight
  - Maintain Aeroelastic Loads and Flutter Mechanisms
- Use Process to Develop Weight Sensitivities of ACE Configurations
- Include FEM Weight Data into Weight Equations

High fidelity structures and weights data is very difficult to obtain. Usually parametric weight equations must have a large weight data base of similar aircraft to accurately predict weight and mass distribution. On the other hand weights based on finite element models require many months to determine each parametric data point. Thus the objectives of the Structures and Weights WB is to develop a more rapid high fidelity weights prediction process and apply it to parametric ACE configurations.

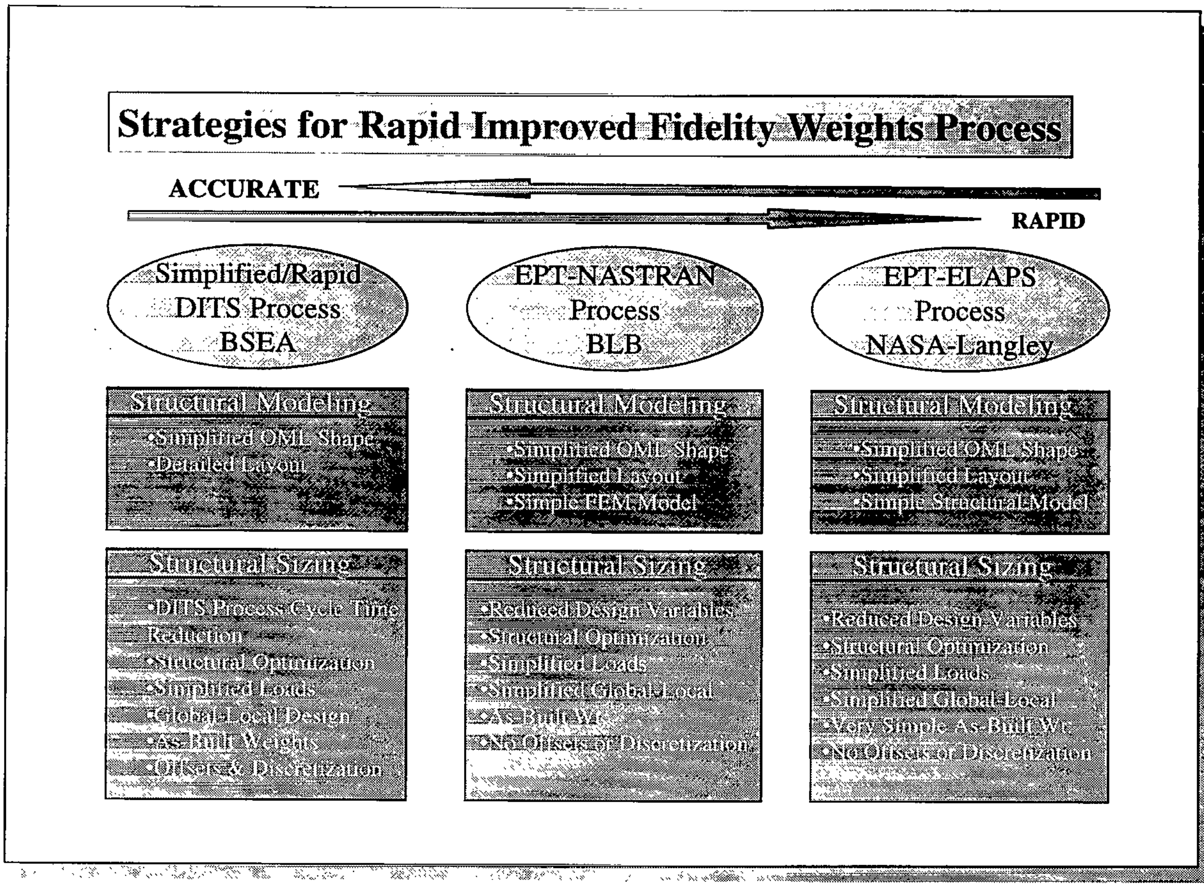

Since the process and data generation goals are so very ambitious, three approaches were developed at three separate sites. Each site was responsible for developing and verifying its own process. Each site was also responsible to generating a portion of the parametric weights data needed. A detailed description of each of these processes and some of the resulting data is given in Appendix D. Appendix D.1 describes the Elfini simplified DITS process, Appendix D.2, the EPT-NASTRAN process and Appendix D.3, the ELAPS process.

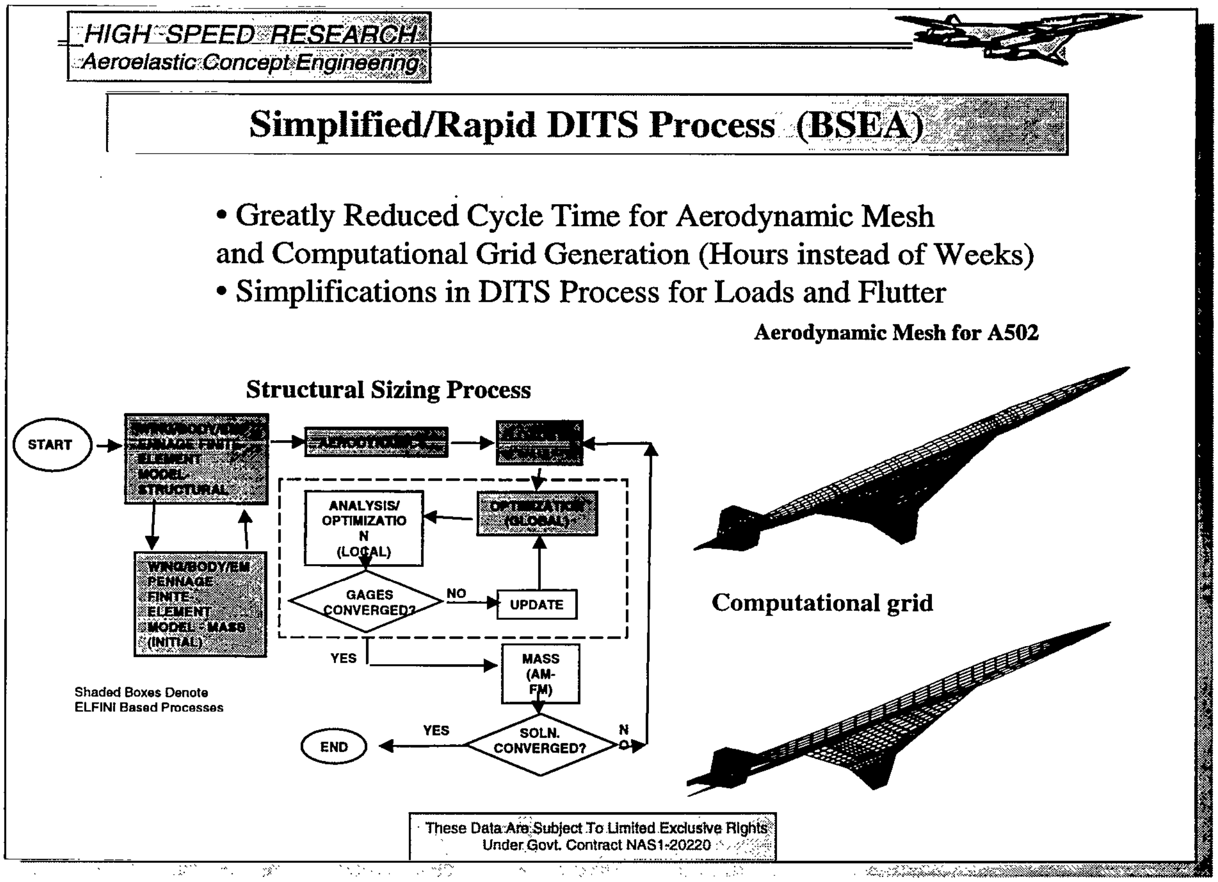

Appendix D.1 gives the details of the Elfini Simplified DITS process. The cycle time for the aero and computational grid generation has been greatly simplified. This process was applied to the baseline PTC aircraft and to one variant in break location. Strength only solutions were obtained.

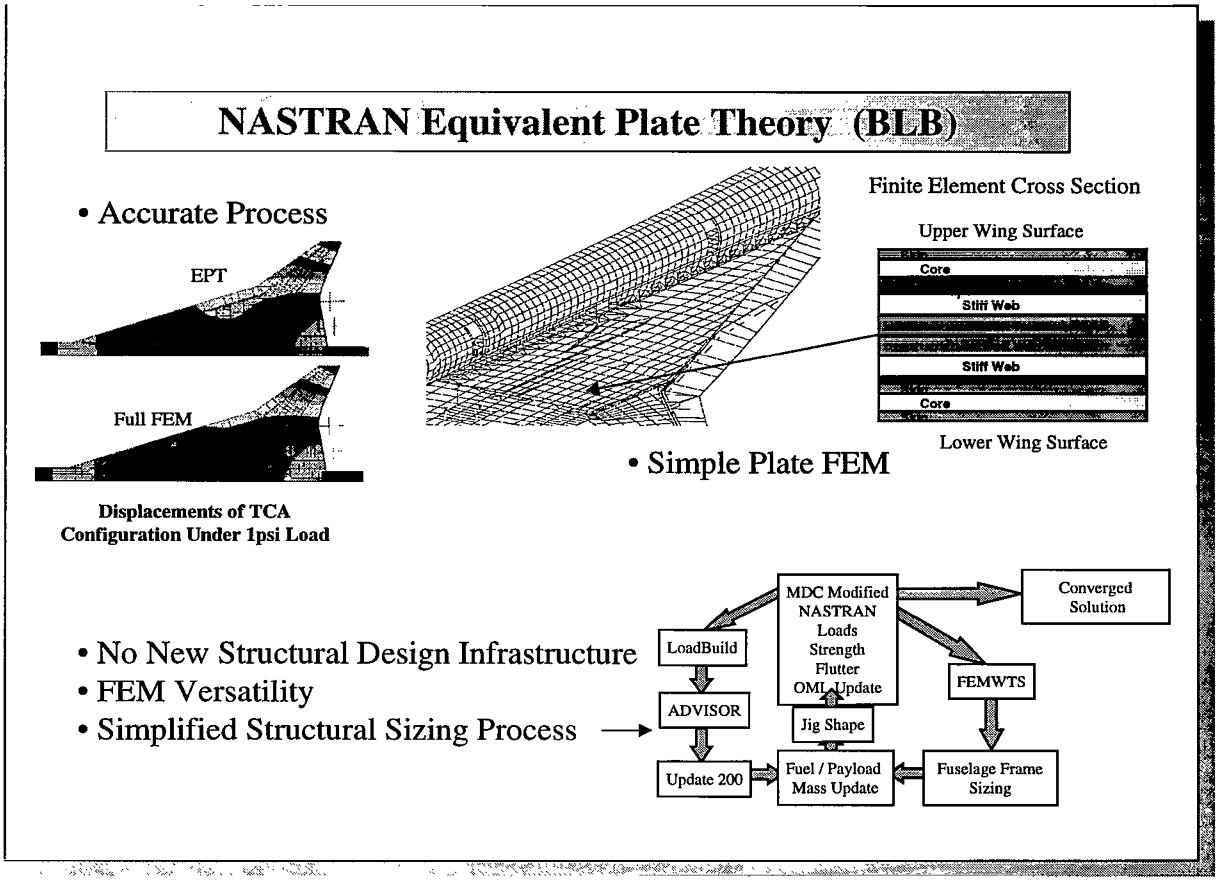

Appendix D.2 gives the details of the Equivalent Plate Theory FEM process in NASTRAN. A simple plate FEM or a mixture of plate and full FEM can be used . Each element contains the upper surface sandwich, sub structure spar and rib caps and webs and the lower surface sandwich. No new infrastructure is needed to perform the structural sizing optimization. A simplified version of the DITS-NASTRAN infrastructure was used.

Much time was spent verifying the process since it was new. Specifically the process was verified against the TCA DITS-NASTRAN sized configuration. The agreement was very good.

Data was also developed for the PTC, one sweep and one aspect ratio variation. These data were not verified in time to be used in the final optimization of the ACE OAC (Optimized Aeroelastic Concept).

ELAPS Equivalent Plate Theory Process (NASA Langley)

- Continuous Representation Structural Design (Non FEM Based)
- Simplified Plate Wing and Shell Fuselage
- Used With NASA Langley Infrastructure
  - Loads, Flutter, Buckling, Sizing Optimization

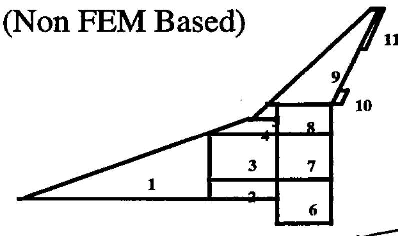

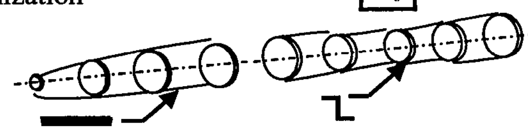

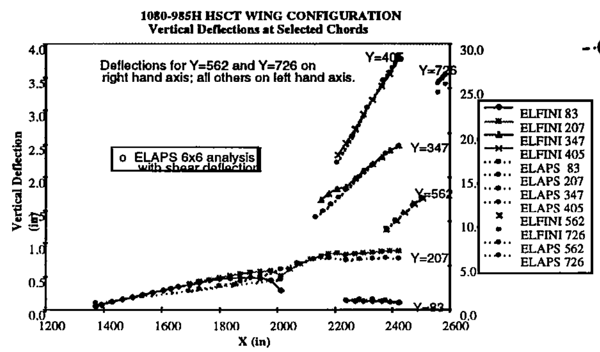

- Accurate Analysis

Appendix D.3 gives the details of the ELAPS Equivalent Plate Theory process. This process does not use finite element analysis but uses a continuous variation Rayleigh- Ritz approach based on the ELAPS process. NASA has also developed its own infrastructure to perform, loads, flutter, buckling, and sizing optimization in addition to the ELAPS code.

Much time was spent verifying the process since it was new. Initial verification shows the stress and deflection analysis to be quite accurate. Further verification of the design process has been done also but is not complete. Specifically the process is being verified against the TCA and PTC DITS-Elfini sized configuration. The parametric thickness data for the PTC has not been verified and thus was not used in the optimization of the ACE OAC configuration.

Controls Working Group

Objectives

- Investigate possible strategies for inclusion of control system parameters in DOSS optimization process
- Choose appropriate design variables and constraints which provide major interactions with configuration
- Provide data for incorporation into DOSS response surfaces

A Controls Working Group was established to review possible methods and strategies for including the control system design process into DOSS.
The Group was to choose appropriate design variables, from existing processes, that would be applicable, and could be included within the time and budget constraints of the ACE process. The Group was then to provide appropriate data.

Controls Working Group

Approach

Incorporate results from Stability and Control tail sizing process into DOSS "response surface"

- •Choose selected configurations from design space ("prism")
- •Perform standard tail sizing and balancing, observing constraints ("V-bar" or "scissors chart")
- •Determine effect of configuration variables on weight and drag due to tail surface variation
- •Incorporate data in DOSS response surface

After a considerable review, it was determined that, because of stability and control constraints that would not lend them selves to inclusion in the optimization process, that data for DOSS would be provided through the standard control sizing process. This process determines the minimum control size (and therefore minimum weight and drag) that would meet all the imposed S&C constraints (nose wheel lift off, pitch recovery, etc.)

A sets of configurations was chosen from the DOSS design space and the tail sizing procedure performed.. The effects of configuration variables on weight and drag of the minimum sized tail was then provided to DOSS as a response equation to supplement the weight and drag methods.

Results of the Control Working Group study are given in Appendix E

Section I.4
ACE Design Variables

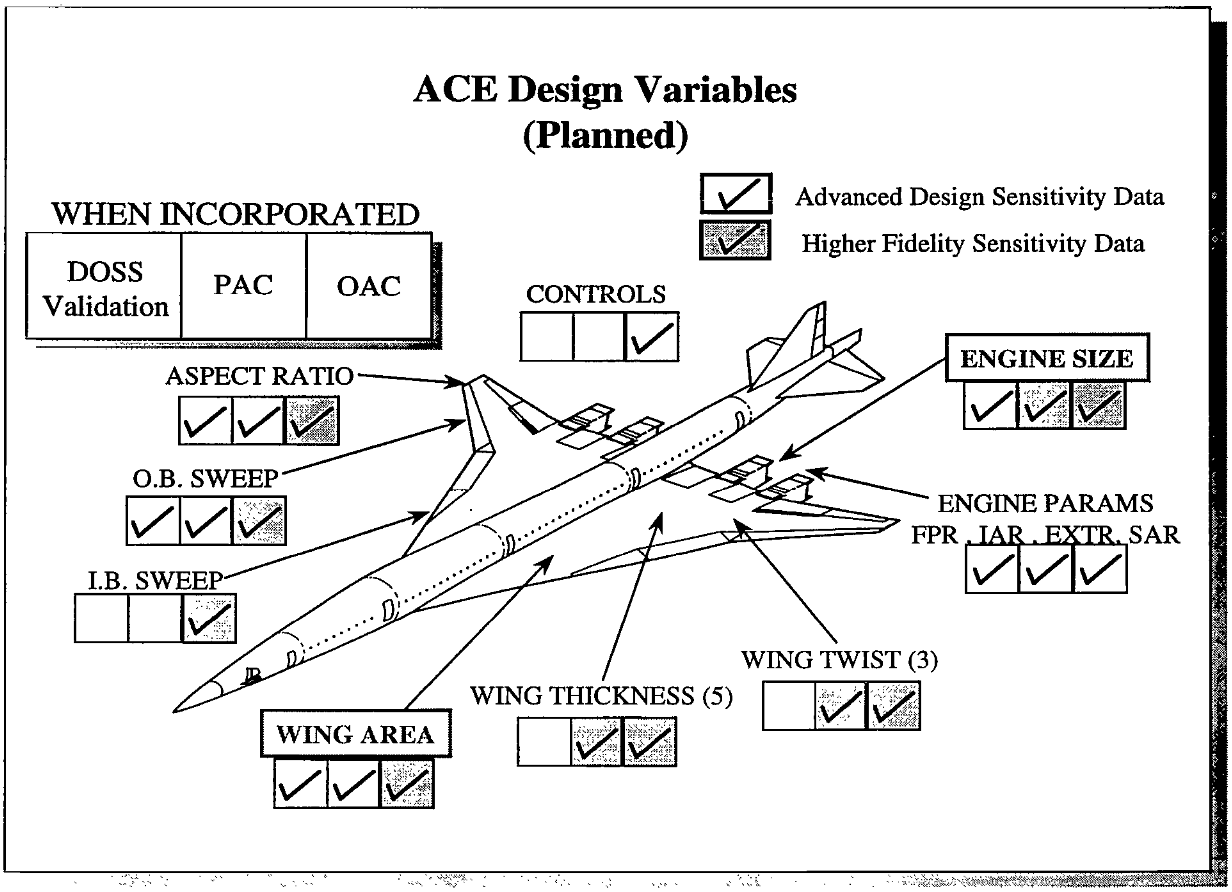

This figure shows the global design variables that were planned for various stages of the ACE project, and the level of analysis fidelity that was to be used. The basicairplane sizing variables of wing area and engine size were to be supplemented by the addition of engine cycle variables, planform variables, aerodynamic loft variables, and control surface variables. A check in an unshaded box indicates that the variable was to be included using advanced design or parametric data. This was the status for all data during the DOSS Validation phase, where results were compared with the results of the traditional trade study approach. For the PAC, higher fidelity information, obtained from Computational Fluid Dynamics (CFD) for performance aerodynamics and loads, and Finite Element Modeling (FEM) for structural analysis and sizing would be included for certain variables. For the OAC, this higher fidelity variable set would be extended.

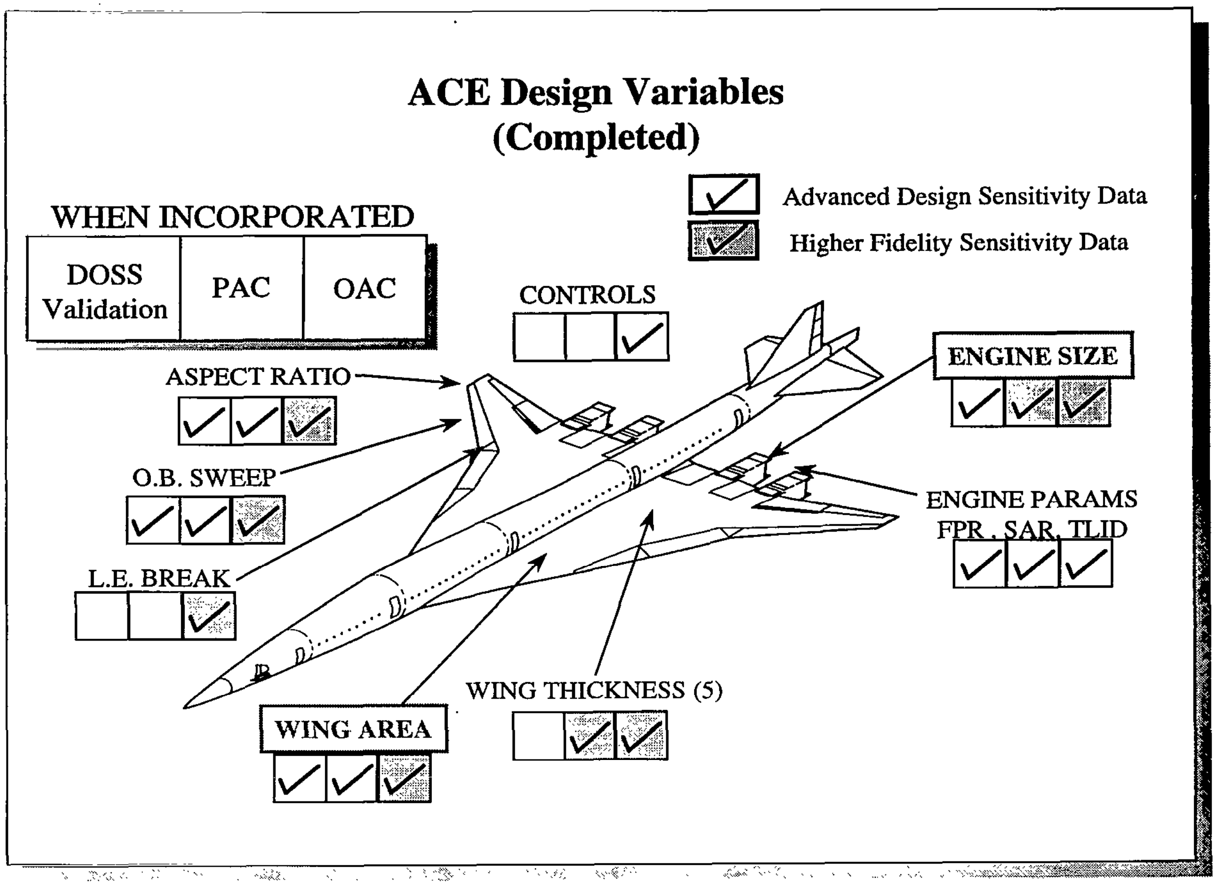

This figure shows the actual variables and fidelity levels that were used during the ACE Program. Changes from the planned set included the substitution of leading edge break location for inboard sweep angle, elimination of wing twist, and substitution of different engine variables to ease the problem formulation. For the final OAC results, the effect of wing thickness was included in the CFD-based aerodynamic calculations, but could not be included in the FEM-based structural weight calculations due to time constraints.

Results of the ACE studies leading to the OAC are described in the following section of this report.

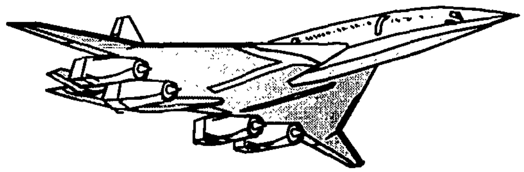

ACE Final Report

II - OAC Design Recommendations

David Knoernschild - Boeing Seattle

December 31, 1998

Optimized Aeroelastic Conept (OAC) Study

- II.1 OAC Data Space
- II.2 OAC Optimization Results
- II.3 Sensitivity Analysis
- II.4 Design Robustness

DOSS was used to perform a simultaneous wing planform, engine cycle, and wing thickness optimization study. The result of the study was the Optimized Aeroelastic Concept (OAC). The OAC was the primary input to the 1998 Technology Concept (TC).

OAC Design Variables

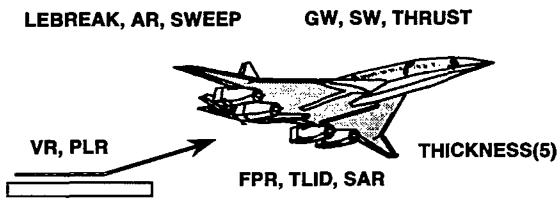

Total Design Variables: 16

The goal of the OAC effort was to provide an airplane configuration optimizing wing planform, wing thickness distribution, engine cycle, and takeoff flight profile parameters. The resulting optimization problem had 16 global design variables. Compare this to a typical sizing problem where only 5 design variables are used: GW, SW, THRUST, VR, and PLR.

OAC Thickness Permutation Variables

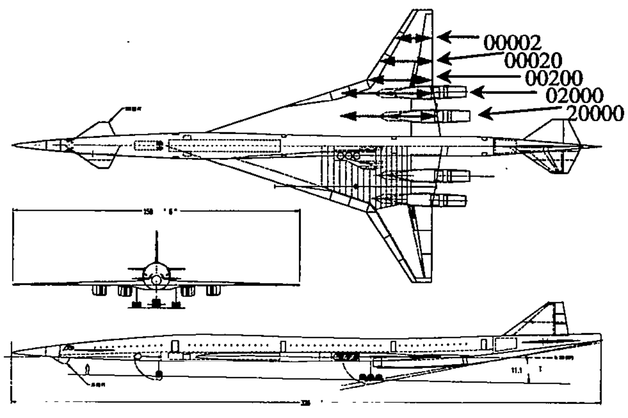

The ACE team defined five thickness perturbations to the baseline PTC loft. In the chord-wise direction, the mode shapes of the thickness perturbations are defined by Hicks-Henne mathematical functions. In the span-wise direction, the modes are defined by a linear "tent" shape.

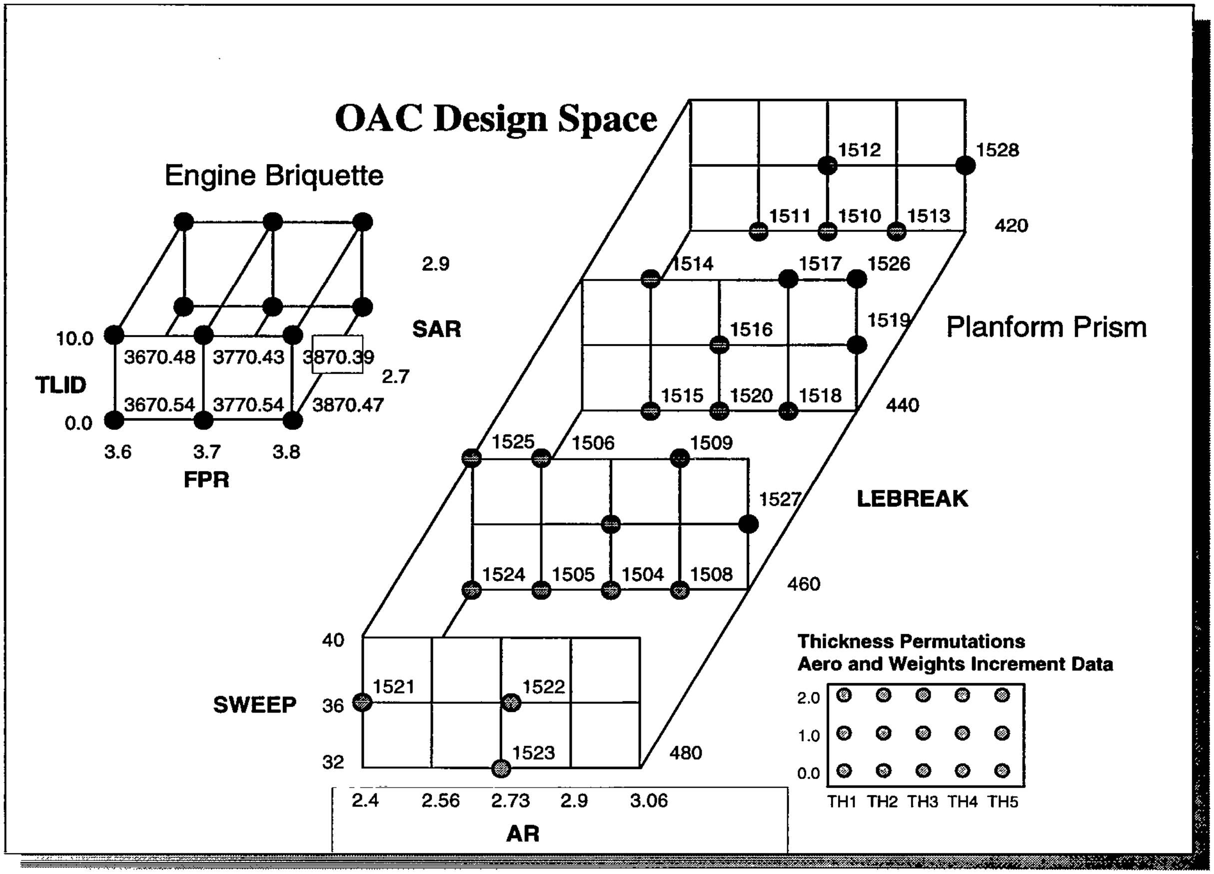

The design space covered by the OAC desing study is shown in the figure above. Data for the OAC study was developed in a series of configuration trades conducted during 1998.

The configuration trades consisted of two major efforts: a planform study, which analyzed various outboard planform options, and a propulsion study which explored various engine cycle concepts. Taken together, the configuration trades produced a total of 300 possible design concepts consisting of 25 aspect ratio/outboard sweep/leading edge break combinations, three engine fan pressure ratios, two thrust lapse rates, and two suppresser area ratios.

To include wing thickness sensitivity data, additional sets of incremental drag polars and weights increments were also used.

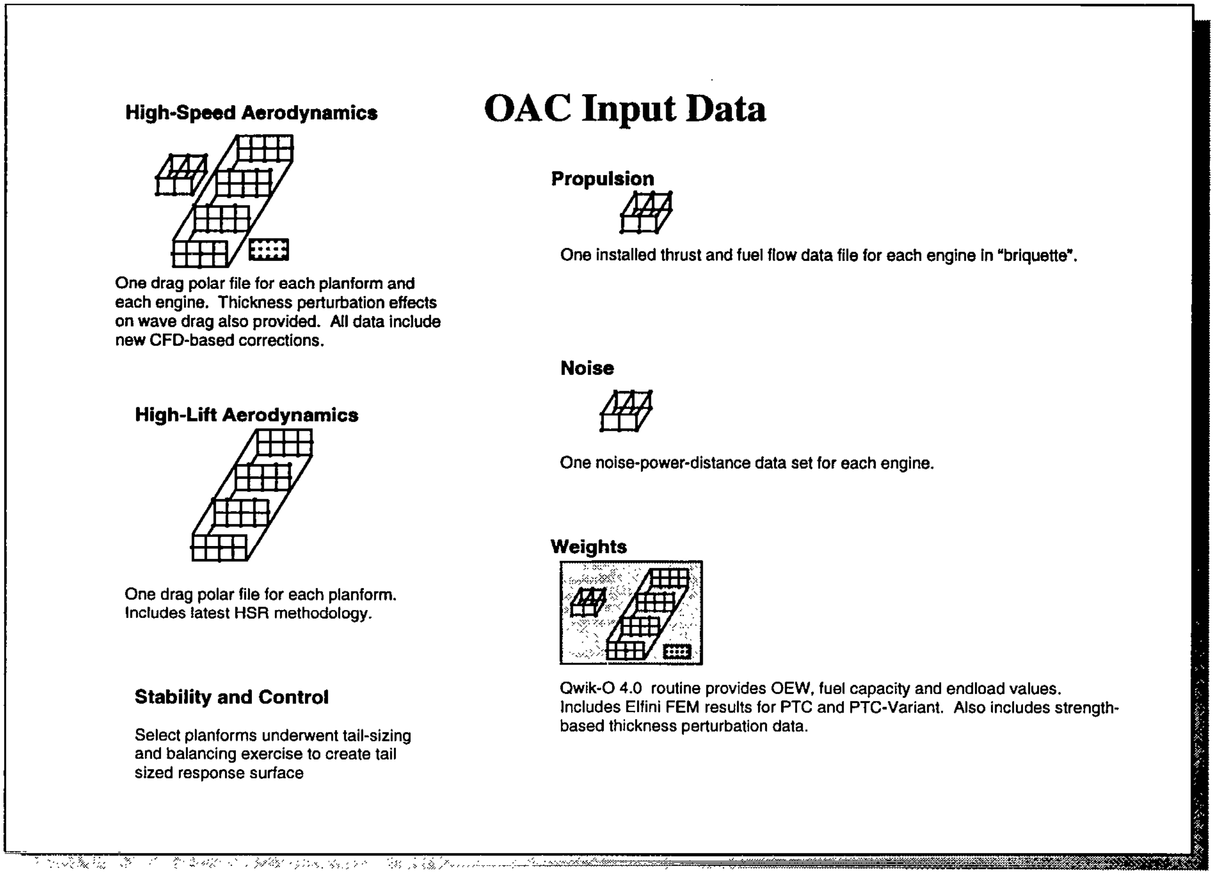

The high-speed aerodynamics, high-lift aerodynamics, stability and control, propulsion, noise, and weights engineering teams provided data for the studies leading up to the OAC. A large collection of data sets were generated and much effort was expended in upgrading and automating the data generation process.

The raw data sets were combined into single sets of response surfaces for each discipline.

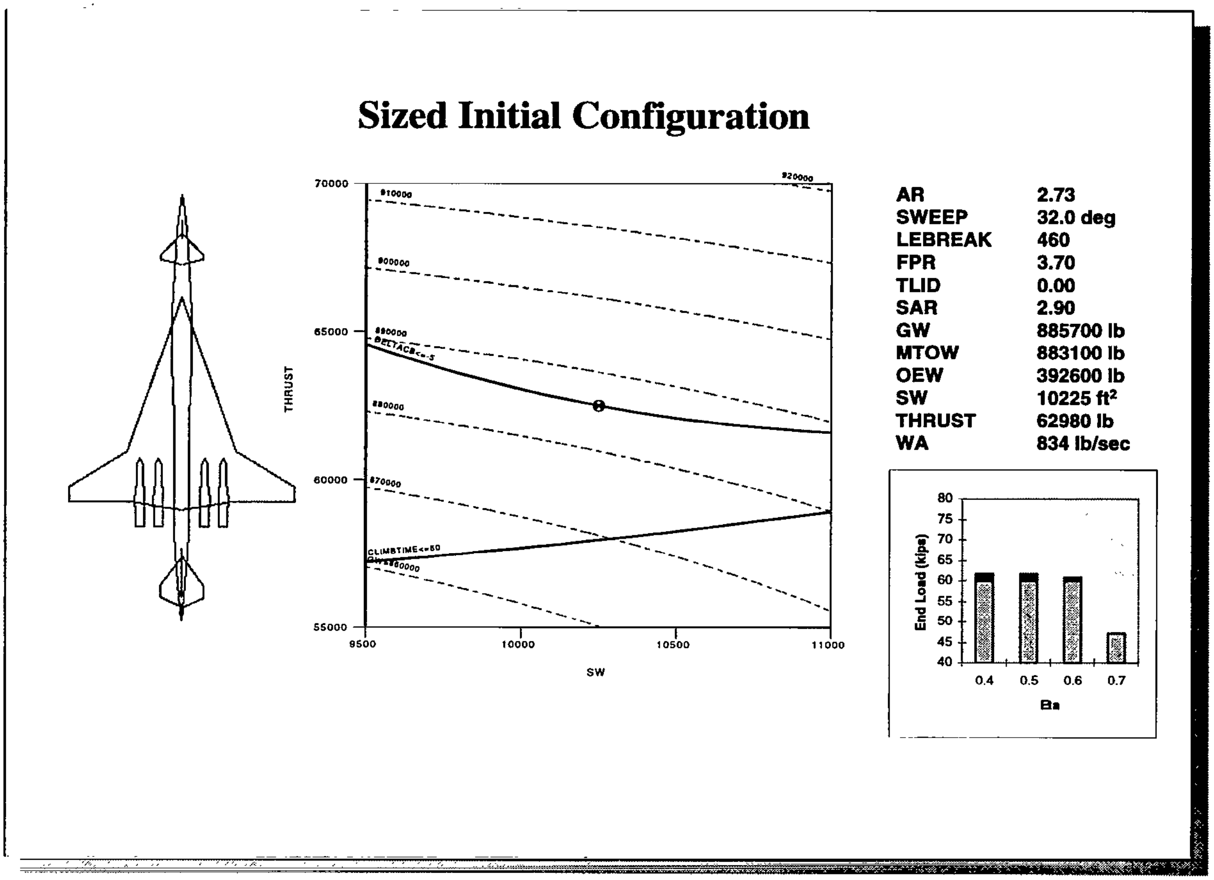

Once all the response surfaces were constructed a valid pre-optimized starting point was obtained by performing a re-sizing of the PTC wing area and engine thrust while fixing each of the other planform and engine design variables at their corresponding Preliminary Technology Concept (PTC) values. The sizing calculated by optimizing gross weight (GW), wing area (SW), and reference thrust (THRUST) to minimize GW while satisfying all of the performance constraints. Wing thickness permutation variables were set to their baseline (PTC) values. The resulting sized solution violated three of the four end load margin constraints. An attempt to satisfy all four end load constraints was made, however, for the given planform, no combination of wing size and engine size produced a satisfactory answer. The sized configuration had a gross weight of 885700 LB.

Optimized Configuration

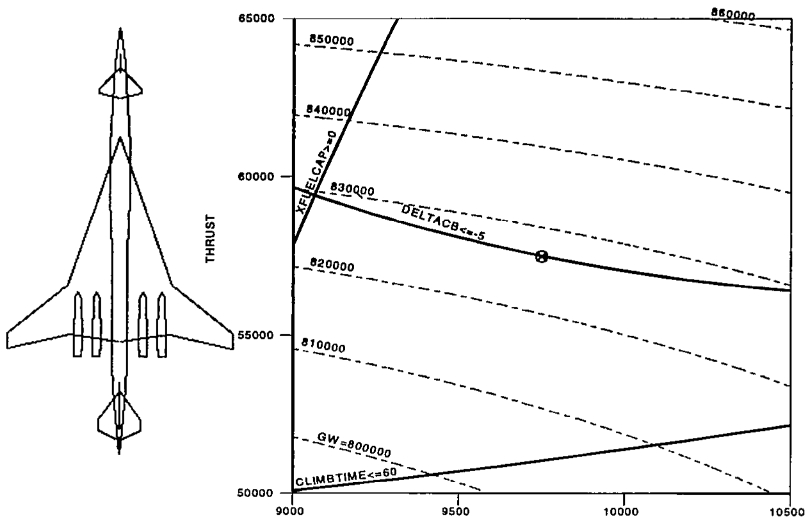

AR	2.86
SWEEP	40 deg
LEBREAK	460
FPR	3.80
TLID	0.00
SAR	2.70
GW	826500 lb
MTOW	824100 lb
OEW	355800 lb
SW	9520 ft^2
THRUST	57420 lb
WA	748 lb/sec

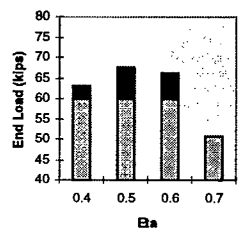

Next, a full configuration optimization was performed. All planform, engine, wing thickness, and sizing variables were allowed to vary. The result was a configuration with a 59000 LB (7%) lighter gross weight. The engine cycle increased in FPR and decreased in SAR. The wing planform increased slightly in outboard sweep. Wing thickness did not increase for any of the thickness modes. Note that the end load constraint violations become even larger for the optimized case. As in the previous case, wing area and engine size can not be adjusted to satisfy all four end load contraints.

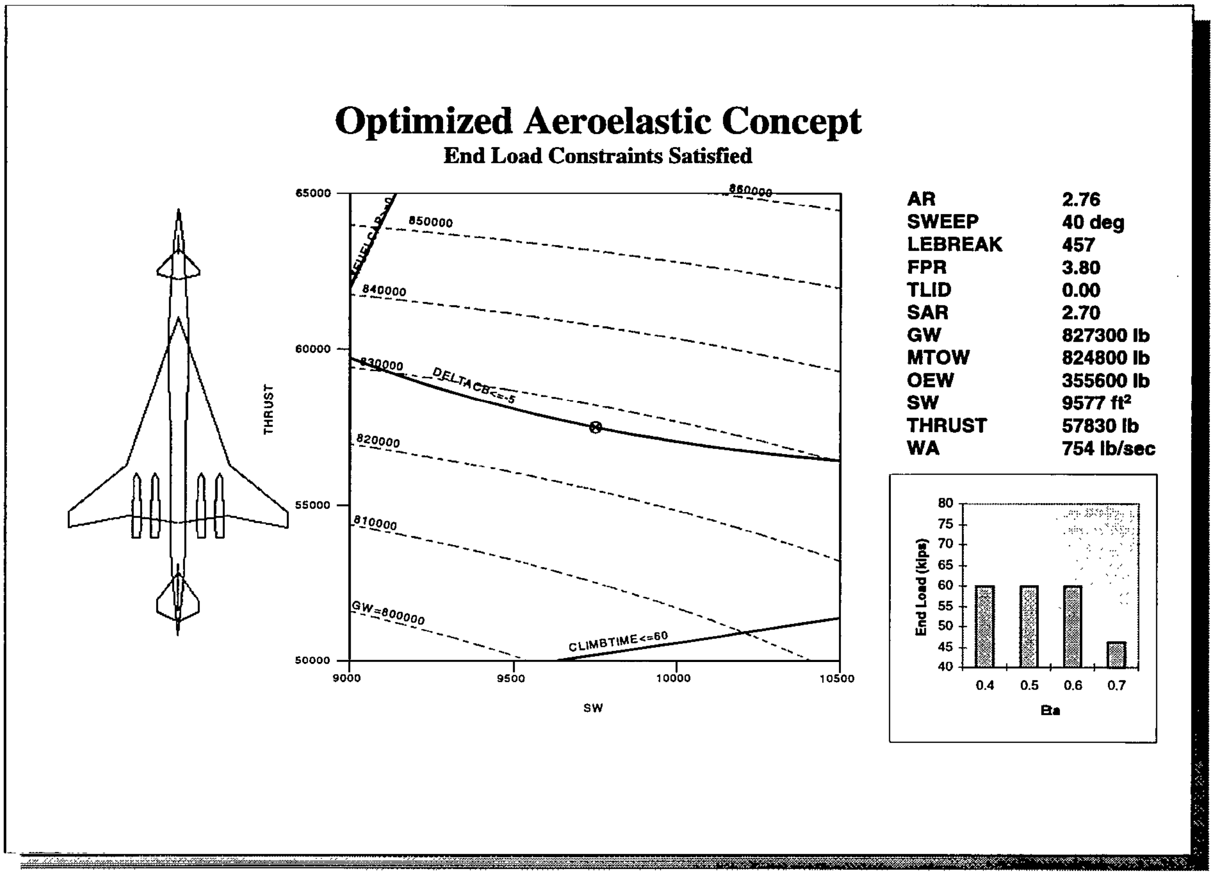

The optimization was re-computed, this time forcing satisfaction of the end load constraints. An optimized solution was found which satisfied all the end load constraints, with a gross weight only 800 lb greater than the preceding case. Slight reductions in aspect ratio and leading edge breaks are all that are needed to reduce the end loads to acceptable levels.

OAC Solution

Stage 3 -5 db Cutback, 60 kips Endload

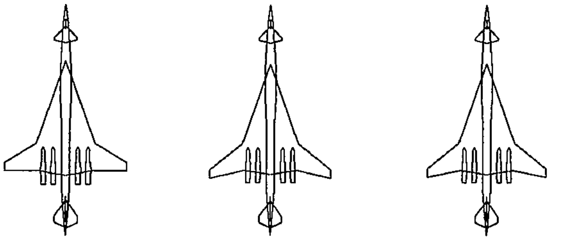

	PTC Endloads Ignored	Optimized Endloads Ignored	Optimized Endloads Honored
AR	2.73	2.86	2.76
SWEEP (deg)	32.0	40	40
LEBREAK	460	460	457
FPR	3.70	3.80	3.80
TLID	0.00	0.00	0.00
SAR	2.90	2.70	2.70
GW (lb)	885700	826500	827300
MTOW (lb)	883100	824100	824800
OEW (lb)	382600	355800	355600
SW (ft²)	10225	9520	9577
THRUST (lb)	62975	57420	57830
WA (lb)	884	748	754
Endload	Failed	Failed	OK

The sized baseline and optimized configurations are compared in the chart above. Simultaneous optimization of the wing and engine reduced maximum takeoff weight by 58,000 LB.

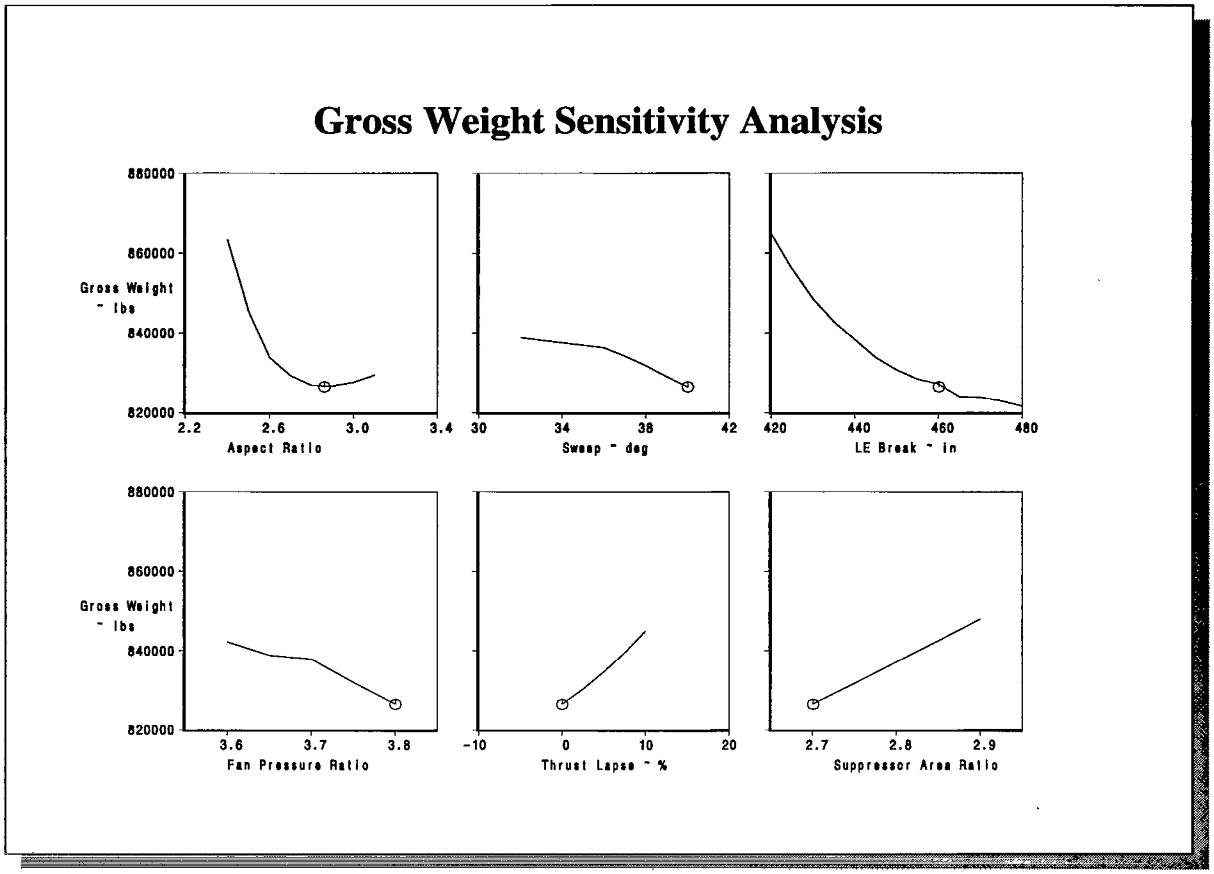

An optimized sensitivity analysis can be performed by varying a single design variable across the entire design space, while holding several other variables constant and optimizing the remaining variables. For this study, optimized sensitivities were obtained by varying the aspect ratio (AR) while holding outboard wing sweep (SWEEP), leading edge break (LEBREAK) and the engine variables (FPR, TLID, and SAR) constant, and optimizing all other input variables (wing area, engine size, gross weight, noise takeoff rotation speed, and programmed lapse rate). Sensitivities were also obtained with respect to SWEEP, LEBREAK, FPR, SAR, and TLID as the sensitivity variable.

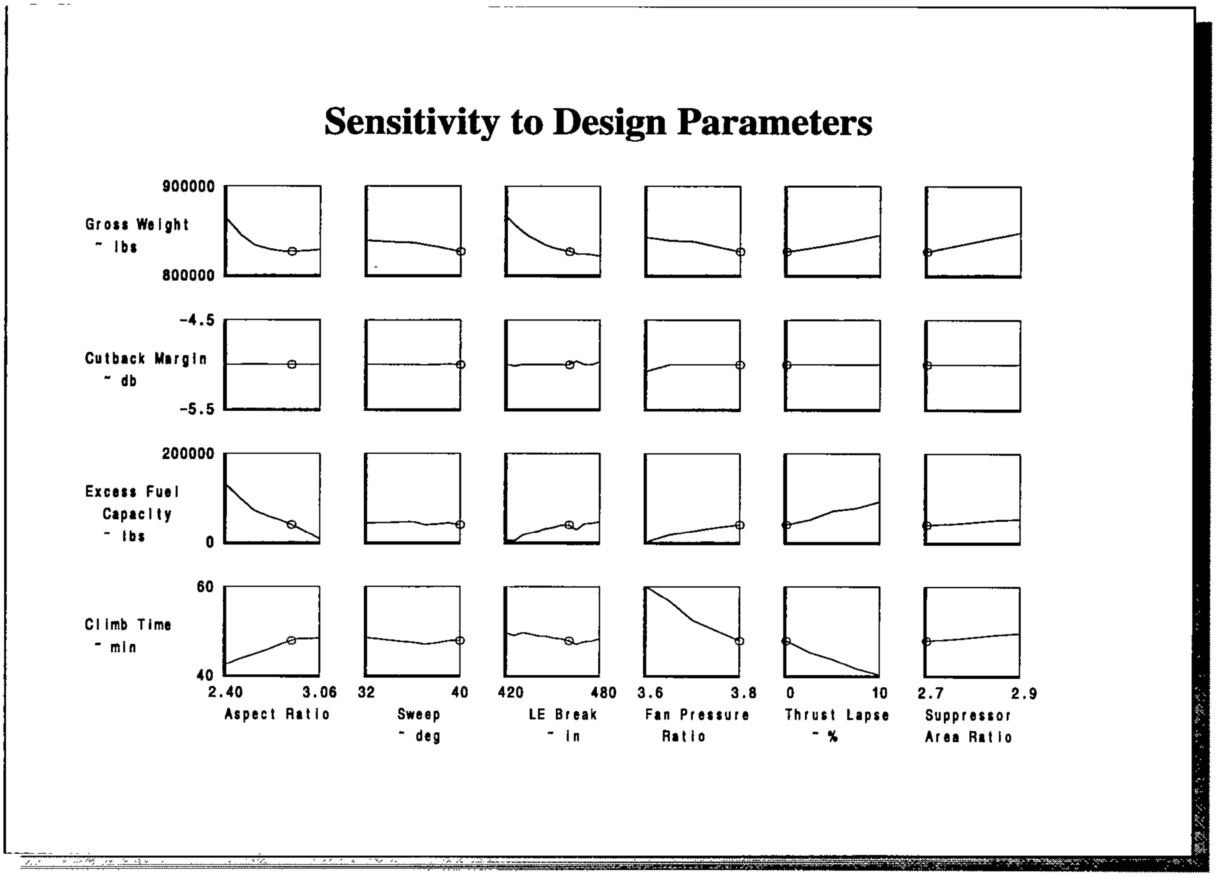

The figure above shows more details of the optimized sensitivity study presented on the previous page. Here the objective function and several of the constraints are shown varying as a function of the planform and engine cycle design variables.

End-load Sensitivities

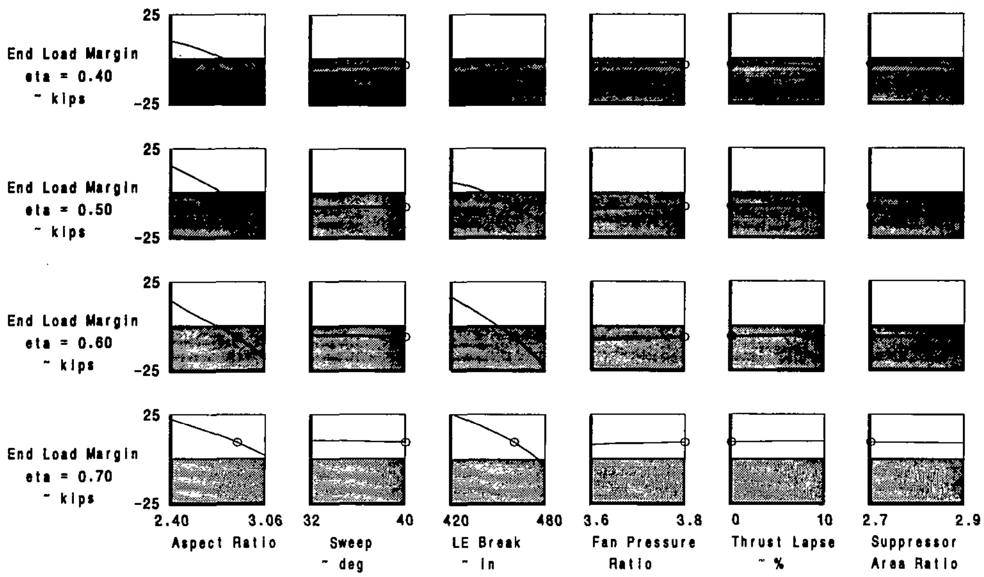

The end load margins are plotted above with respect to the design variables. End load margin is defined as maximum allowable end load minus the actual end load. Positive values of end load margin signify a satisfactory solution. The emphasized point shows the optimum solution obtained by ignoring the end loads. End load is most sensitive to aspect ratio and leading edge break.

Thickness Optimized Sensitivities

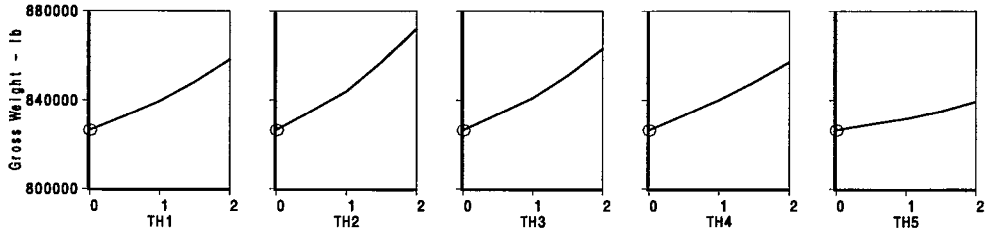

Optimized sensitivity analysis data are shown above for the wing thickness permutation variables. It should be noted that the wing thickness study presented in this document was performed using sample linear aero data and preliminary weights data. ELAPS simplified FEM data will be obtained for the thickness variables in the future and will be included in a future report. For this study, reductions in thickness were not allowed.

Given the linear data available, in no case does increasing thickness provide a benefit. The added drag due to increased thickness always over-powers the structural weight savings. This may change as higher-fidelity data become available or more advantageous thickness perturbation modes are selected.

OAC Noise Robustness
Cutback -7 dB, Endload 60 kips

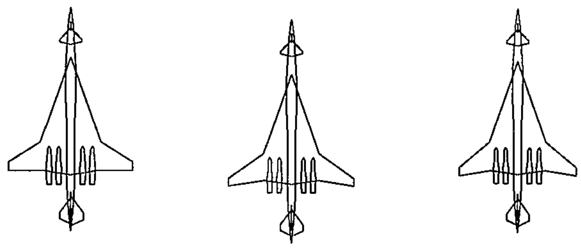

	PTC Configuration Endloads Ignored	Re-Optimized Endloads Ignored	Re-Optimized Endloads Honored
AR	2.730	3.060	2.664
SWEEP (deg)	32.0	36.0	40.0
LEBREAK	460.0	460.0	453.9
FPR	3.70	3.80	3.80000
TLID	0.00	0.00	0.00
SAR	2.90	2.70	2.70000
GW (lb)	955900	865100	877900
MTOW (lb)	953000	862500	875200
OEW (lb)	421900	377100	383500
SW (sq.ft)	11469	9981	10581
THRUST (lb)	72329	61725	64850
WA (lb/sec)	957.5	804.3	845.0
Endloads	FAILED	FAILED	OK

The effect of decreasing the noise constraint on the optimum configuration was studied. Cutback noise margin was reduced from -5 dB to -7 dB. Optimizing the configuration reduces the PTC (sized for Stage 3 -7 dB) from 955900 LB to 865100 LB, a 90800 LB savings. The planform is 3.06 aspect ratio, 36 degrees sweep, and 460 inch leading edge break. Compare this to the optimum Stage 3 -5 dB configuration weighing 826500 LB.

The configuration was then re-optimized for Stage 3 - 7dB, this time honoring the 60 kips end load constraints. The resulting airplane weights 877900 LB (12800 LB greater than the unconstrained case). The aspect atio, sweep, and LEBREAK change to 2.664, 40 degrees, and 453.9 inches, respectively.

The enforcement of end load constraints results in a Stage 3 - 7dB solution that has a lower aspect ratio than its Stage 3 - 5dB counterpart. This trend is reversed from the unconstrained case.

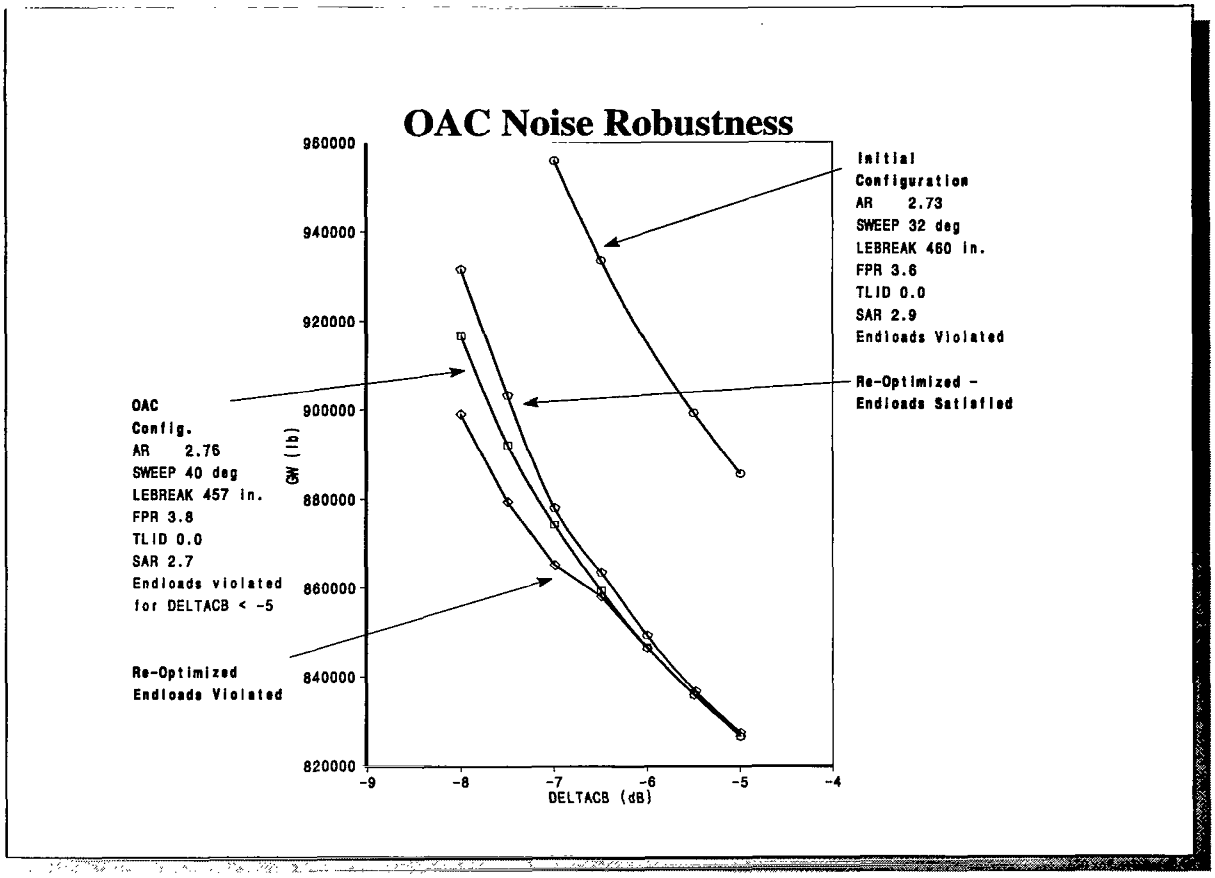
OAC Noise Robustness
960000
940000
920000
900000
880000
860000
840000
820000
GW (lb)
-9
-8
-7
-6
-5
-4
DELTACB (dB)
Initial
Configuration
AR 2.73
SWEEP 32 deg
LEBREAK 460 in.
FPR 3.6
TLID 0.0
SAR 2.9
Endloads Violated
Re-Optimized -
Endloads Satisfied
OAC
Config.
AR 2.76
SWEEP 40 deg
LEBREAK 457 in.
FPR 3.8
TLID 0.0
SAR 2.7
Endloads violated
for DELTACB < -5
Re-Optimized
Endloads Violated

Effect of Endload Constraint on Optimum Design (-5 dB Cutback)

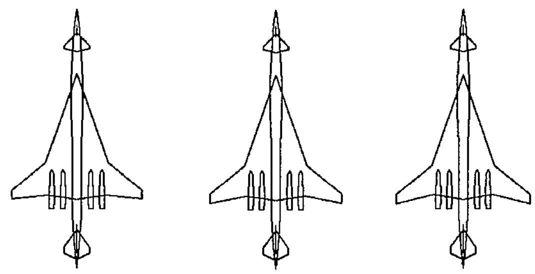

	55 kips	60 kips	80 kips
AR	2.592	2.764	2.859
SWEEP	40.0	40.0	40.0
LEBREAK	445.6	457.1	460.0
FPR	3.80	3.80	3.80
TLID	0.00	0.00	0.00
SAR	2.70	2.70	2.70
GW	830458	827279	826516
SW	9733	9577	9517
THRUST	58686	57830.3	57428
WA	764.8	753.6	748.4

The effect of changing the end load margin on optimum planform was analyzed. If the maximum allowable end load is decreased to 55 kips, a gross weight penalty of 3200 pounds is paid. Attempts to further reduce the end load constraint to 50 or 40 kips failed. The solution would not converge.

If maximum allowable end load is increased to 80 kips, gross weight is reduced by less than 800 pounds. At a constraint value of 80 kips, there is in effect, no active end load constraint.

The conclusion from this study are two-fold. First, the sensitivity of gross weight to end load constraint is fairly shallow. That is, changes in the end load constraint value have a weak effect on weight. However, if the desired end load is reduced below 55 kips, the solution will fail to close.

Effect of End-load Constraint on Noise Robustness

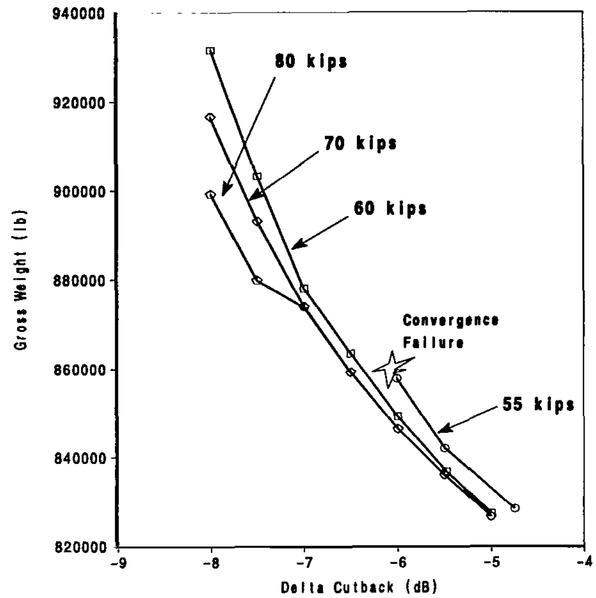

Conclusions

- The OAC configuration has been successfully optimized using 16 design variables.
- Simultaneous optimization of the wing planform and engine cycle saves 58000 LB in gross weight.
- All end load constraints can be satisfied with a slight planform change and a minimal gross weight penalty.
- Changing the cutback noise constraint from -5 dB to -7dB results in a solution with a lower aspect if the 60 kips end load constraints are enforced.
- Increasing the end load constraints from 60 to 80 kips will reduce gross weight by only 800 LB.
- If the end load constraints are reduced below 55 kips, no feasible solution is obtainable.

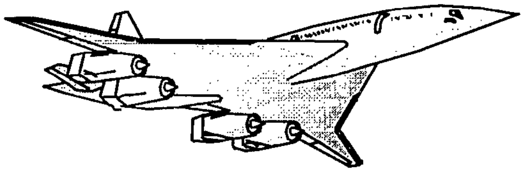

ACE Final Report

III - Future Developments and Transfer of ACE Technology

Chris Borland - Boeing Seattle
Joe Giesing - Boeing LB
David Knoernschild - Boeing Seattle

December 31, 1998

This section provides information on appropriate developments beyond or outside of the ACE project. This section is divided into several sections as follows:

- Current Activities
- List of Specific Items from the Final ACE Meeting
- Other Future Activities

Future Applications & Developments of ACE Technology--- Current Activities

DOSS--- Current Activities

- DOSS-FLOPS Integration into AFOSR MDO CRAD Project
- Implement Boeing Proprietary DOSS (DOSS-ASAP)
- Integrate DOSS-ASAP Technology into AVIDS (Aerospace Vehicle Integrated Define System)
- Make DOSS-ASAP Technology Available to BCAG Commercial A/C Projects

The DOSS process is being adopted for the AFOSR MDO CRAD project which will be placed into the MDISE architectural.
A Boeing version of DOSS using the ASAP proprietary sizing code in place of FLOPS is also in progress.
A new Boeing initiative for a general configuration design system (AVIDS) will integrate the design process for a variety of aerospace vehicles into one architecture. DOSS will have much to offer this new effort and collaboration between DOSS and AVIDS has begun.
Boeing Commercial Airplane Company has several special purpose sizing codes. DOSS-ASAP has much to offer BCAG as a general purpose sizing and configuration optimization process and code. Dialogue with BCAG on the benefits of DOSS has begun.

Future Applications & Developments of ACE Technology----Current Activities

ACE Rapid FEM Capability--- Current Activities

- EPT-NASTRAN IAD Project "Rapid Structural Sizing and Optimization"
  - ACE Concentrated on EPT-NASTRAN Verification
  - IAD Project Intended to Help EPT Reach Its Full Cycle Time Reduction Potential
  - Increased Automation of FEM and Sizing Process
  - Streamline Global-Local Design Process

- ELAPS Projects

  ELAPS Verification
  - Technology Transfer of ELAPS and NASA Loads/Flutter/Sizing Optimization Infrastructure to Boeing Seattle
  - Refinement of ELAPS and Design Process

  ELAPS In AFOSR MDO Program
  - ELAPS and Structural Sizing Infrastructure Will be the Technology Used for the Rapid Weight Estimation in MDOP

The EPT (Equivalent Plate Theory)- NASTRAN process has been developed and verified under the ACE project. Some of the potential for reduced cycle time has yet to be tapped because most of the ACE effort was spent in development, training, and verification. An increase in automation for the simple FEM model and its subsequent sizing optimization will speed up this already rapid process. A streamlining of the global-local process will reduce the number of global design cycles reducing the cycle time even further.

The ELAPS (Equivalent Plate Theory using a continuous representation) also has the potential to be very rapid. This process was developed at NASA Langley A CRAD contract is planed with Boeing Seattle in order to facilitate its development, verification and technology transfer to industrial applications.

ELAPS is also being considered for use in the Boeing AFOSR MDO CRAD program.

Future Applications & Developments of ACE Technology--- List of Specific Items from the Final ACE Meeting

- DOSS Maintenance and Support
- Modify DOSS for Innovative HSR Concepts
  - Boost Engine and Engine Placement
  - Integrated Wing-Body and/or Swing Wing
  - Other
- Continue Improving DOSS Graphics (DOSS Visualization Program)
- Upgrade Manufacturing Constraint Determination Process
  - Response Surface for Load Center of Pressure
  - Move Process to the Structural Sizing Optimization Process and Include Weight Penalty Determination
  - Include the Weight Increase Due to Changing Constraint Values
  - Include Other Constraints Over and Above Running Loads
  - (e.g. Laminate Thickness)

Continued on Next Page

DOSS is a very effective tool for configuration optimizaton and as such must be maintained and supported.
DOSS will require some modifications (DOSS is an easily modified code) to accommodate the new innovative HSR concepts (e.g. engines that are scheduled will require modifications to the Mission and other modules).
The DOSS graphics are advanced state of the art and continued improvements of them will have a high pay-off.
The running load manufacturing constraints in DOSS had a considerable influence on the selection of the Optimized Aeroelastic Concept configuration. It is important therefore that it produce high fidelity level results. The current running load manufacturing constraint module in DOSS is a stand-alone calculation based on simple processes. The addition of a load center of pressure will help increase the fidelity with a modest effort. The greatest fidelity will be achieved however if the process is moved to the structural sizing process from the stand-alone module that it currently is . This will also allow provision for computing the added weight due to changing of this constraint.

Future Applications & Developments of ACE Technology--- List of Specific Items from the Final ACE Meeting (Cont.)

(Continued)

- Upgrade Weights Calibration Using Recent Data
  - Wing ITD Data
  - EPT-NASTRAN Aspect Ratio and Sweep Data
  - NASA ELAPS Thickness Data (in the future when it becomes available)
- Prescribe Techniques for applying Plate Theory to Integrated Wing-Body and/or Swing Wing Concepts
- Re-Evaluate Critical Linear Load Cases in Light of Nonlinear Critical Loads
  - Eliminate Va Cases and Compare with Nonlinear Results
- Automate Linear Aero. Drag Calculations
- Complete ENSAERO Validation of Nonlinear Loads Process
- Complete PTC Nonlinear Loads Evaluation
- Re-evaluate Inner Wing Box Chord Variations with Wing Area

The current weight equation calibration does not include some recent(and future) data. This data should be included as it becomes available.
The plate theory methods have the potential to provide rapid evaluation of the new innovative HSR concepts. The most effective procedure for doing this should be developed.
The EPT NASTRAN process has been proven accurate and should now be applied to the most recent concepts. When the ELAPS process has been verified it can also be applied.
The evaluation of the TCA nonlinear loads showed that the effect of nonlinearity was to eliminate the low speed load cases (Va) from the critical list. It would be instructive to find out if the same weight can be obtained simply by eliminating these cases from the linear loads process.
The linear wave drag process is a good candidate for automation since it is a robust process and does not require much computer time.
The nonlinear loads evaluation of the PTC was not completed under the ACE project. It would be beneficial and informative to complete this study and take advantage of the CFD data that has been generated for this case.
The ground-rules for changing the inner wing box with changes in wing area may need to be revisited. Currently the ground-rules fix the inner wing box chord length and do not allow it to change with wing area.

Future Applications & Developments of ACE Technology--- Other Future Activities

- Propose DOSS Technology and Extensions for Launch Vehicles for the Up-coming(1999) NASA Langley ISE (Intelligent Synthesis Environment)
- Add CORBA Process to DOSS-Genie
- Include Controls Design Variables and Processes into DOSS
- Boeing-NASA Collaboration on MDO Architecture using DOSS-Genie
- Include Design of Experiments in DOSS
- Include Batch processing of input data in DOSS
- Incorporate In-line engineering codes in DOSS

NASA Langley will be instituting a new initiative in 1999 called the Integrated Simulation Environment (ISE). Integration of current launch vehicle optimization processes with DOSS could provide an effective tool for ISE for both space and aircraft applications.
The HSR project is currently investigating configurations with innovative blended wing/body planforms. DOSS and the rapid structural sizing optimization are ideal for these studies and therefore should be used.
CORBA is a commercial code "wrapping" process that is gaining acceptance world wide. It would be beneficial for the Genie architecture in DOSS to adopt this standard.
Active controls are increasingly playing a part in producing efficient and high performing aerospace vehicles (HSCT is a prime example). As such the benefits of this discipline must be captured by DOSS to take maximum advantage this newly emerging technology.
The use of design of experiments (DOE) to pick points from design space for analysis will produce more efficient and more accurate response surfaces.
Automated data generation processes(for Aero, Prop, Noise, etc.) for driving codes in batch mode to create full design space data sets overnight will allow more efficiency, reduced errors, reduced turn-around time, and greater consistency of data.
Putting engineering codes in-line with the DOSS system is appropriate if they are automated, robust, and require small computer CPU time.

Future Applications & Developments of ACE Technology--- Other Future Activities

- Add Trajectory optimization in DOSS
- Include **ACTIVE CONTROLS** In the Structural Sizing Optimization Process
    - Structural Design with Prescribed Controls
    - Design of Structures and Controls Together
- Integrate ACE **NONLINEAR LOADS** Process into the Structural Sizing Optimization Process and Apply to the **INNOVATIVE HSR CONFIGURATIONS**

The incorporation of trajectory optimization (like OTIS or SOCS) will allow a better optimization for noise in the DOSS process.
Active controls need to be dealt with at the DOSS global level(as suggested previously) and at the local structural sizing optimization level also. The aeroelastic mode, load and flutter control can be optimized at the FEM sizing optimization level.
The new blended wing body HSR innovative configurations will be even more susceptible to nonlinear load effects that then current configurations. As such the inclusion of the newly developed nonlinear loads process will be very beneficial.

References

8.2.1 - DOSS Report - End of February 1997

8.2.2 - DOSS Extended Milestone - End of September 1997

Postscript File
MS Word Rich Text Format (RTF)
MS Word V6 for Windows

8.2.3 - Preliminary Aeroelastic Concept Report - Nov. 97

8.2.4 - Deliverable Report on Extended DOSS - Nov. 97

8.2.5 - Deliverable Report on Final DOSS - Aug. 98

The above Reference are available in the Technology Integration (TI) section of the HSR ADAPT Pages, under the ACE Page/Deliverables and Reports, section 8.2.

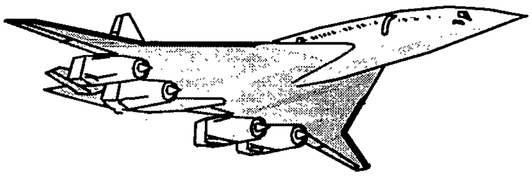

ACE Final Report

A.1 - Final DOSS System

David Knoernschild
Tom Lavelle
Fergus Merritt
Alan Okazaki
Sean Wakayama

December 31, 1998

Topics covered in DOSS Detailed Description

- DOSS Architecture
- GENIE Optimization Framework
- DOSS Interface File - Inputs and Outputs
- Response Surfaces
- Mission Analysis
- Optimization

Typical Sizing Code

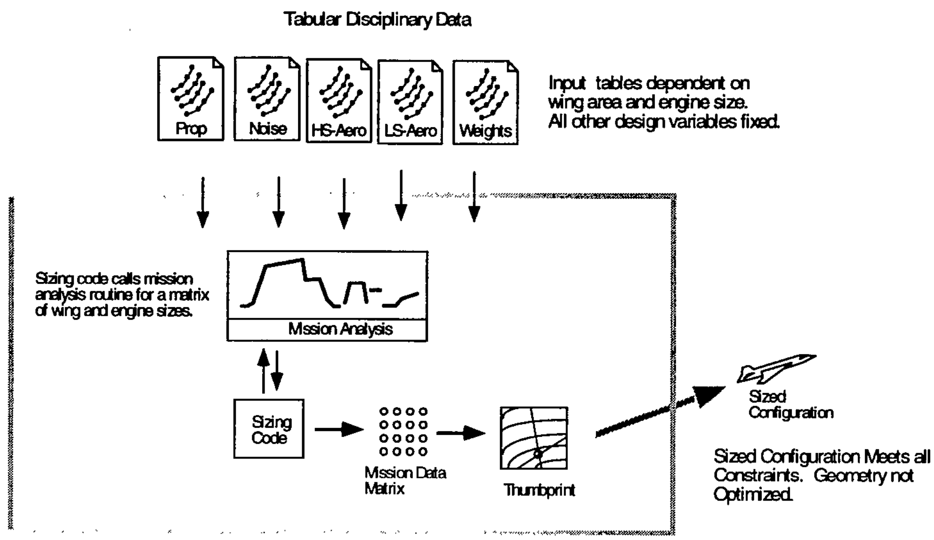

Traditional sizing codes consist of data modeling modules for each discipline and a central mission analysis routine. Data modeling is accomplished by a combination of table interpolators, and where appropriate, simple analysis routines. The mission analysis routine performs calculations along a detailed prescribed flight path by integrating the equations of motion. A matrix of gross weight solutions is produced over a grid of engine and wing size values. A sizing contour plot or "thumbprint" is then produced and a constrained minimum gross takeoff weight can be obtained, usually by visual inspection of the plot.

Design Optimization Synthesis System

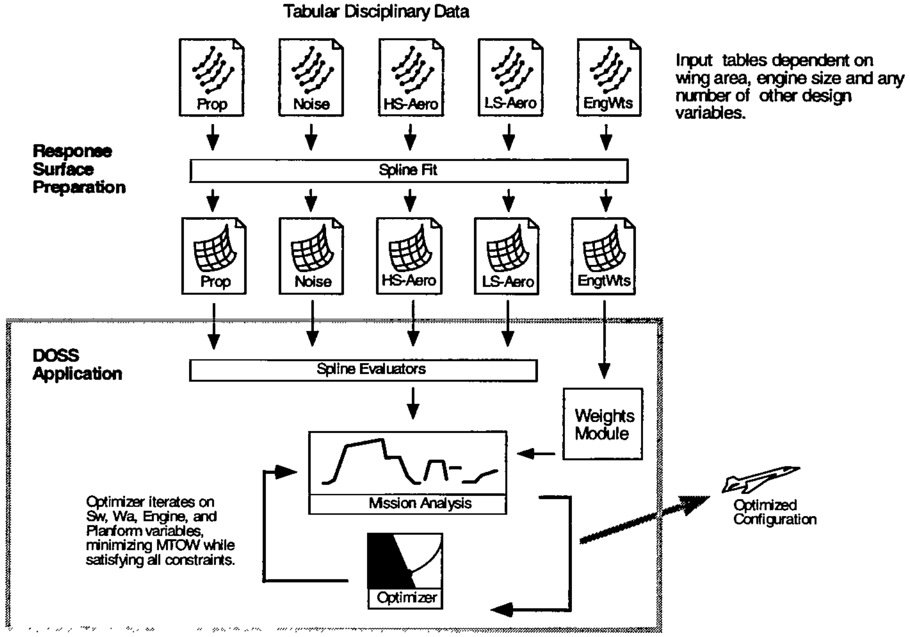

The DOSS process extends the methods of traditional airplane sizing systems and allows true multidisciplinary optimization. Disciplinary data is fed into the system as a series of response surfaces which cover the entire design space being studied. A nonlinear optimizer is used to optimize not just wing and engine size, but planform, engine, and other design variables as well. Rather than producing a sized aircraft for fixed values of various configuration parameters, the end result of a DOSS optimization is a configuration which optimized every design parameter that was permitted to change.

Outline of DOSS Architecture

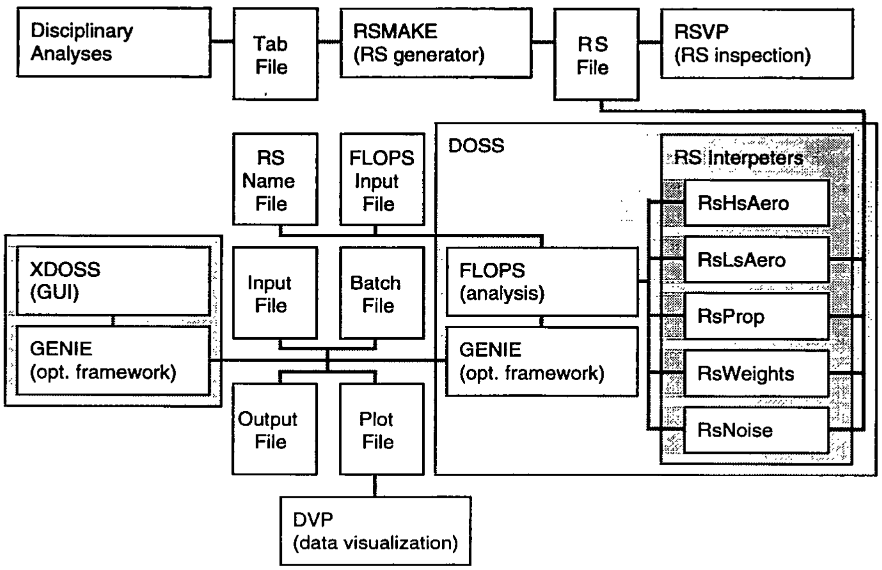

The major components of the DOSS Architecture are shown in this chart. Briefly, they can be described as follows:

RSMAKE:	Response surface fitting program.
RSVP:	Response surface viewing and checkout program.
RS Interpreters:	Response surface interpreters, linked to FLOPS.
FLOPS:	Mission analysis code.
GENIE:	Optimization framework.
XDOSS:	Graphical User Interface (GUI) to DOSS.
DVP:	(DOSS Visualization Program) Advanced thumbprint and graphics program.

DOSS Architecture - Files

- Tab (*.tab): Table file; contains data from disciplines for constructing response surfaces.
- RS (*.rs): Response surface file; contains the fitted data.
- Input (*.inp): GENIE input file; contains input and result values for optimization starting point.
- Batch (*.bat): GENIE batch file; contains set up data for optimization.
- Output (*.out): GENIE output file; same format as input file, but contains inputs and results for optimized design.
- Plot (*.plot): Plot file; contains data for plotting.

How to Work with DOSS

- The disciplines generate sensitivity input data and place them in tab files.
- Response surface generators are applied to the tab files generating RS files.
- The response surfaces can be inspected using the RSVP program.
- The user edits the rs.inp file to tell the system what RS files to use.
- While most of the variations between designs are captured by the response surfaces, some changes to the configuration or mission may require changes to the FLOPS input file.
- The user sets up the initial starting values by editing the input file. This can either be done through the XDOSS interface or a text editor.
- The user selects from standard batch files to set up sizing, thumbprint, or full optimization operations. These batch files may be edited to handle variations on the basic optimizations.
- Through either XDOSS or UNIX command line, the user runs DOSS with the selected batch file. DOSS performs the optimization or thumbprint generation task and saves the results in an output file or a plot file.
- Plots can be viewed through one of several plotting packages.

Working with DOSS is quite easy and logical.

Appendix B contains example problems that can be used as a starting point to further understand how to work with DOSS.

Genie Optimization Framework
(GENeric Interface for Engineering)

- Concept
  - Single interface powerful enough for most engineering problems.
  - Easy linkage to any analysis.

Genie, a GENeric Interface for Engineering, was originally developed at Stanford University as a shell for performing generic engineering optimization problems. The idea behind its development was to build a single interface that was powerful enough to be used for most engineering problems yet simple enough to be linked with any analysis code.

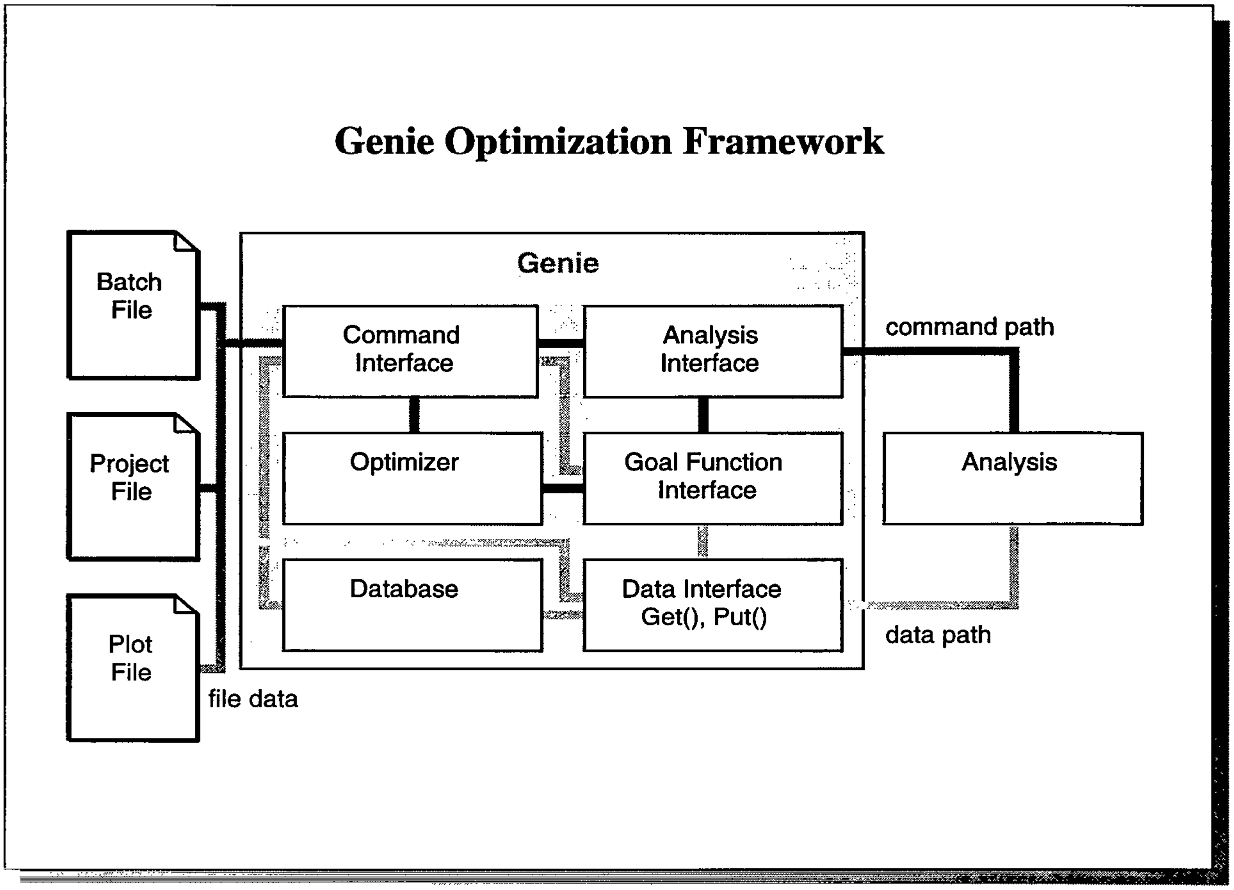

Architecturally, a Genie application has a few major components. The analysis performs the engineering calculations. A database handles communication and storage of data. The analysis gets input data from the database and puts results into the database for storage. An optimizer manipulates selected inputs to improve the design. The optimizer puts its design changes into the database, launches the analysis, and gets the resulting changes to the objective and constraints from the database. Finally, a command interface handles communication to the user. The command interface enables manipulation and retrieval of data. It enables optimization problem set-up and execution. It also provides hooks for communication with graphical user interfaces.

Linking an analysis to Genie is relatively easy. It involves writing a trivial analysis interface and communicating design data through simple data interface commands. The analysis interface takes commands from the command interface or the optimizer and simply calls the analysis with no arguments. The data interface provides simple functions that the analysis uses to get and put information from and to the database.

Genie Optimization Framework (GENeric Interface for Engineering)

- Capabilities
  - Command language:
    - Very flexible optimization set up.
    - Automated operation as Unix background job.
    - Data manipulation.
  - Output of plot data and data summaries.
  - Output of information to aid selection of optimization scaling.
  - Choice of optimizers (robust NLOpt, fast NPSOL).
  - Macintosh and X-Window graphical user interfaces.
- Benefits
  - Details of linking to optimizer are handled by the framework.
  - Investment in framework benefits multiple applications.

Genie enables easy linkage between the analysis and optimizer, allows automated data calculation, provides data output in useful formats, provides information to facilitate scaling design variables and constraints, provides a selection of optimizers, allows flexible definition of optimization problems, and works through graphical user interfaces on both Macintosh and UNIX platforms.

Recent Genie Improvements

Version	Improvement	Description
1.6.0	Fortran interface	Easier replacement of FLOPS input file.
1.5.6	Optimizer line search	Improve optimizer robustness.
1.5.5	Array output	Output arrays in DVP format to enable elimination of plot routines from XFLOPS.
1.5.4	Virtual scaling	Assist users with optimization scaling problems.
1.5.2	Optimization output	Cleaner output with better explanations as requested by users.
1.5.2	Critical constraint identification	Indicates least-satisfied constraint when optimizer cannot find feasible solution to help determine what is wrong with optimization.
1.5.0	Non-smoothness trap	Identifies points where the objective or constraints are not smooth to help in development of optimization-friendly analyses.

This lists the improvements made to Genie under ACE.

The improvements are listed along with a brief description of what they do.

The most-recent version of Genie on which significant work was done on the improvements is listed.

Renent Genie Improvements

Version	Improvement	Description
1.4.0	New optimization setup commands	Provide more-flexible optimization problem set up.
1.3.1	Hierarchic database	Support data structures to provide better organization of large amounts of data.
1.3.0	Variable types	Support types beyond double, including int, FILE, and String.
1.3.0	DVP output	Output data in DVP format.
1.3.0	Batch command	Allow commands to be executed from files to improve flexibility.
1.0.0	GUI interface	Commands provided to support X-Window GUI.

This lists the improvements made to Genie under ACE.

The improvements are listed along with a brief description of what they do.

The most-recent version of Genie on which significant work was done on the improvements is listed.

Response Surfaces - An Overview

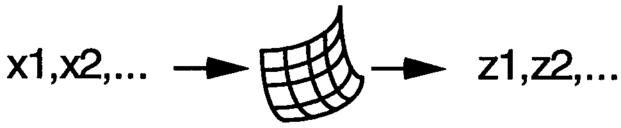

$$[z1, z2,...] = f(x1, x2,...)$$

Features

- Piecewise cubic polynomial representation of functions
- C2 continuity
- Any number of inputs and outputs
- Surfaces and variables designated by name
- Generic format for all data sets

In traditional mission performance and sizing codes, table lookups are used to obtain data such as thrust, fuel flow, drag, and community noise. For a general gradient-based optimization system like DOSS, data modeling via table lookup is not a viable solution for two reasons.

1. DOSS is designed to be flexible enough to allow the user to add design variables without recompilation of the code. This means that the underlying data modeling system must be capable of recognizing and using additional variables. Typical table lookup routines handle only a fixed number of independent variables. Response surface routines, on the other hand, can handle any number of independent and dependent variables.

2. Gradient-based optimization methods such as those used in DOSS, are very sensitive to discontinuities in the objective and constraint functions. Value, slope, and even inflection discontinuity in the underlying data modeling functions can cause discontinuities in the overall analysis. For best results, it is necessary to require that the analysis functions exhibit continuous second derivatives. This is called C2 continuity. For DOSS, it was deemed necessary to use data modeling methods that provide C2 continuity. Since almost all raw data for DOSS arrives in the form of discrete data points, the only feasible way to accomplish this is to fit piecewise cubic spines to all datasets.

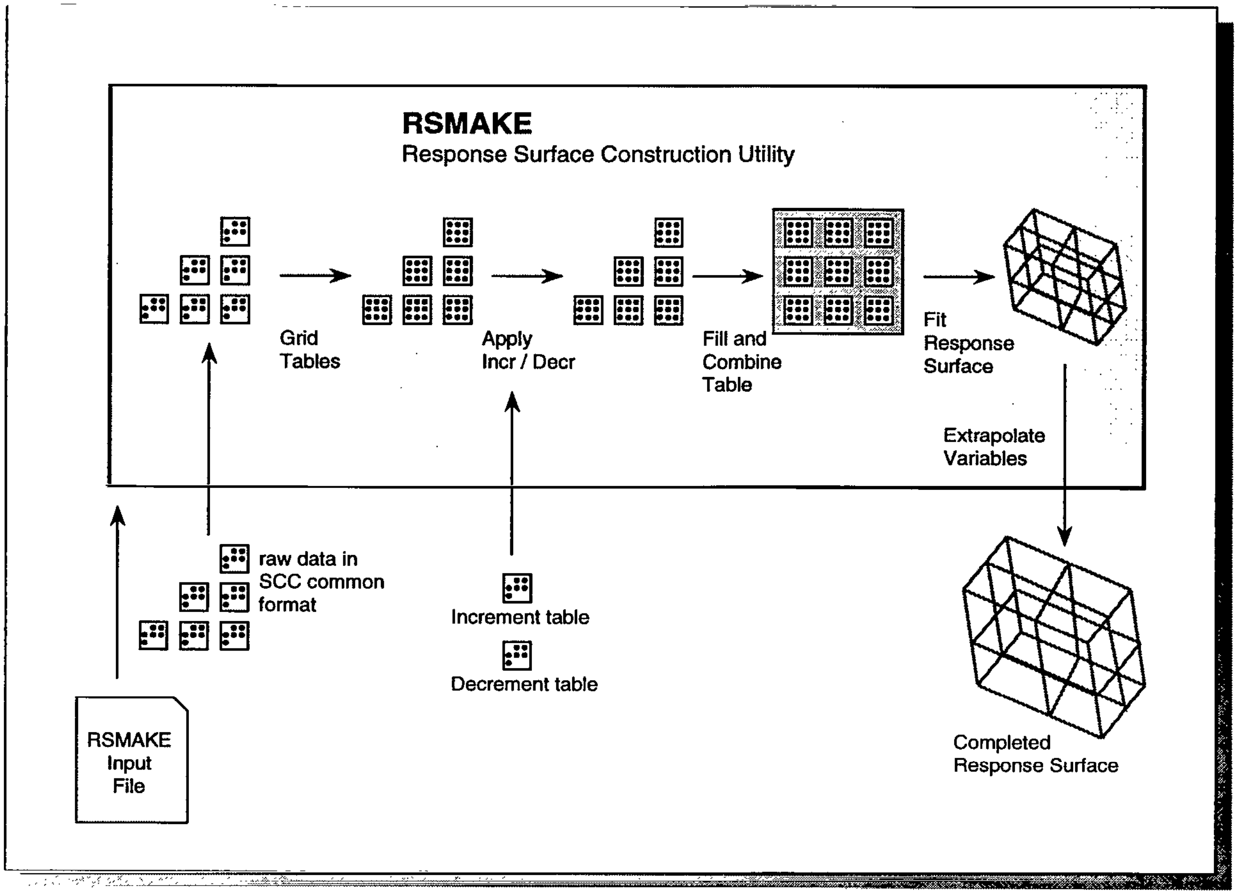

Once all the individual data subsets are in hand, the DOSS utility "RSMAKE" is used to merge the individual disciplinary datasets into single datasets for each discipline. "RSMAKE" is then used to construct response surfaces. Once complete, there exists a single response surface data file for each of the five major data categories -- high speed aerodynamics, low speed aerodynamics, propulsion, noise and weights. During the initial validation of DOSS, the weights response surface data contained only bare engine weight, length and CG data -- all other OEW calculations were done during execution by the parametric weights routines.

RSMAKE has the capability to create piecewise linear, quadratic and cubic spines. Although cubic splines were successfully generated using all the validation data, the linear splines were used for the validation process to increase the speed of execution of the main DOSS code. No apparent loss in accuracy or robustness resulted. This is probably due to the very robust nature of the NLOpt optimizer used.

RS Generation - RSMAKE

- Combines multiple data sets
- Works with all disciplines
- Automatically fills in missing data
- Can accommodate any number of independents
- Calls appropriate conversion utility from Sizing Code Calibration Team common format

RS Fitting Routines

SOCS-Based Spline Fitters in RSMAKE

- Sparse Nonlinear least squares optimization
- Exact Interpolation
- C2 Continuity
- No wiggles or oscillations
- Data sets with missing data can be easily handled

All DOSS response surfaces are created using spline generation software based on the Sparse Optimal Control Software (SOCS) developed by John Betts and Richard Mastro of Boeing Information and Support Services. The SOCS-based spline generation routines provide minimum curvature splines with C2 continuity and no wiggles. Datasets with missing data can be easily handled. SOCS is based on a sparse non-linear optimization scheme and can solve large problems very efficiently. A generic response surface generation application, TAB2RS, as well as a propulsion specific fitter, PROP2RS, are included in the current release of DOSS.

DOSS RS Data Modeling

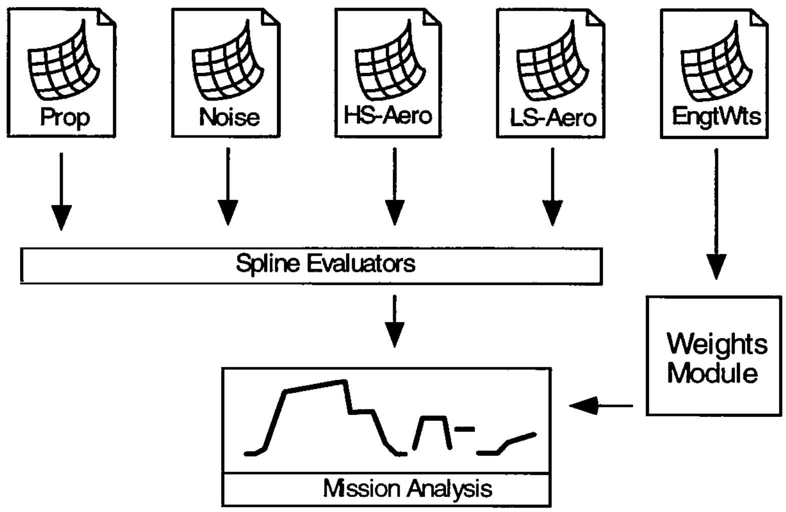

Data from five major disciplines are modeled in DOSS: propulsion, high speed aerodynamics, low speed aerodynamics, community noise, and weights. A set of one or more response surfaces is needed for each discipline. The weights data modeling method also includes two C-language modules for the parametric weight equations.

All response surfaces are created using a SOCS response surface data fitter to provide any combination of linear, piecewise quadratic, or piecewise cubic surfaces.

Propulsion Response Surfaces

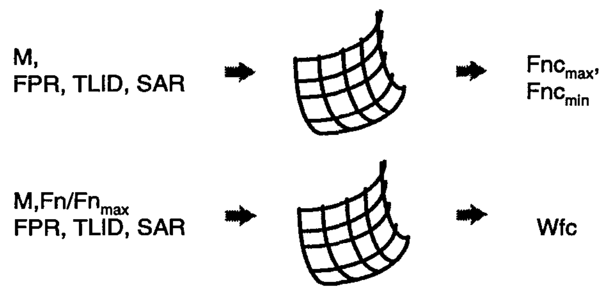

As obtained from the propulsion staff, raw installed thrust data for each combination of the global design variables are presented as tabular functions of Mach and altitude Fuel flow data are presented as functions of Mach, altitude, and throttle setting (Fn/Fnmax). Raw thrust and fuel flow data are then reduced and corrected for ambient conditions before response surface generation.

Sample Propulsion Response Surface

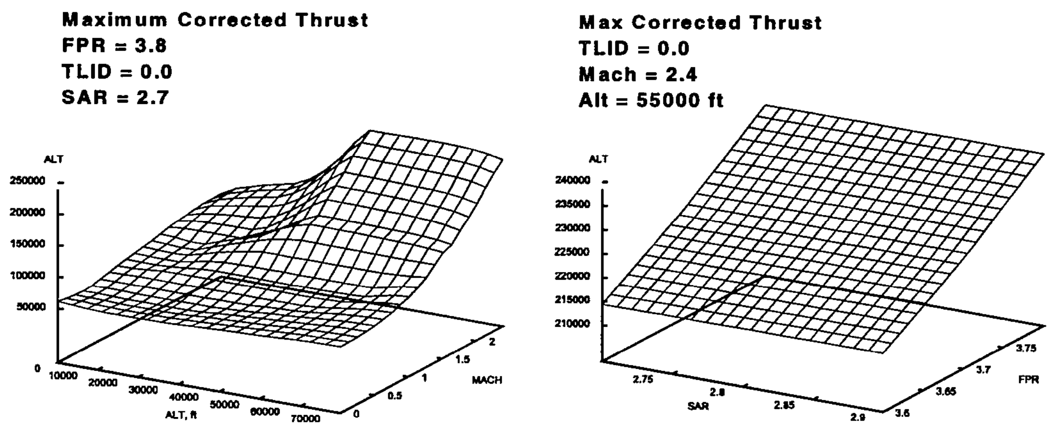

The figure above shows 3-D cuts through the response surface for maximum corrected thrust.

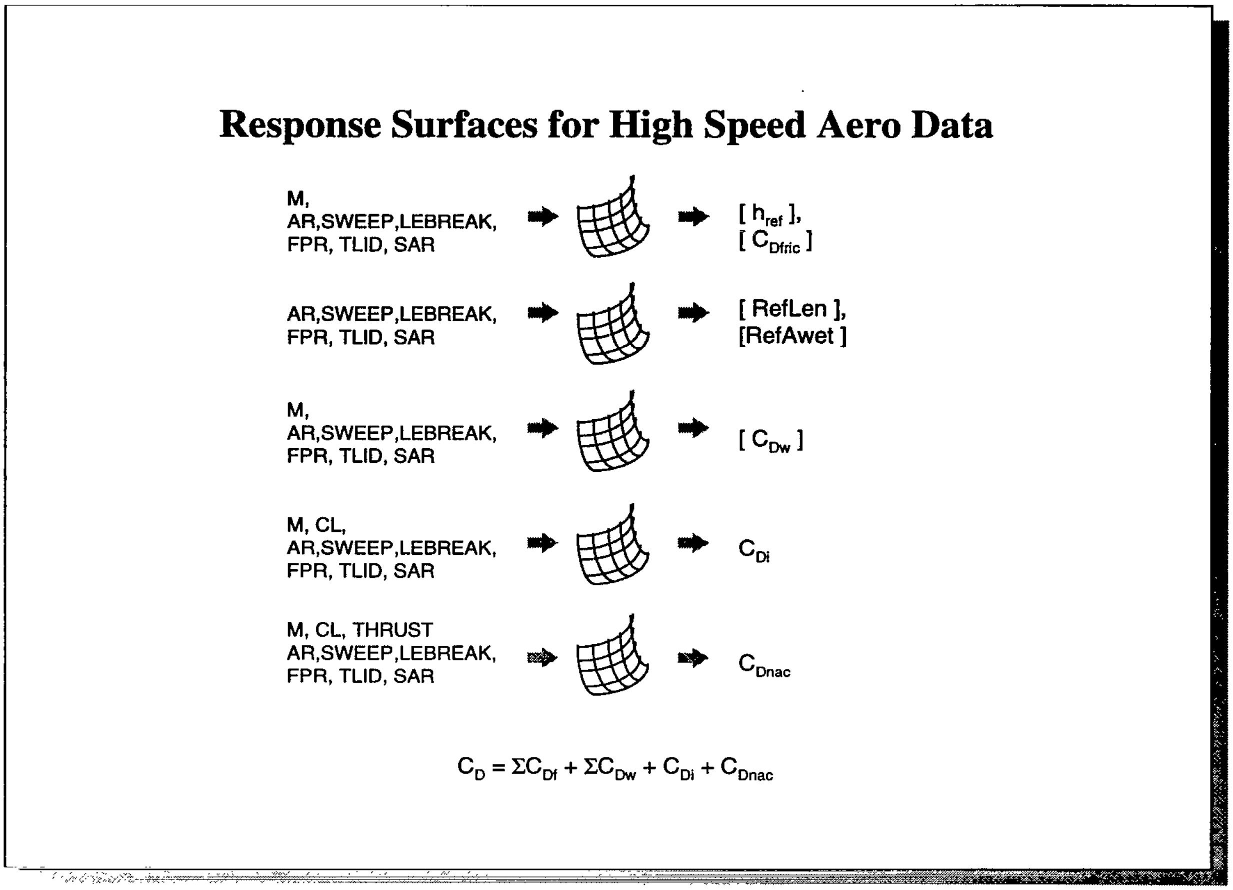

High speed drag is modeled using a component buildup approach. Response surfaces are constructed for the following:

1. Reference length and wetted area of each component (fuselage, wing, vertical tail, and horizontal tail) are given as functions of the global design variables. These quantities are used to predict component skin friction drag for any combination of Mach and altitude.

2. A reference set of skin friction drag coefficients are given for each component over a range of Mach numbers for a reference altitude. These values are obtained from higher-fidelity high speed aero codes and are used to correct the skin friction values calculated by the skin friction routine in DOSS.

3. Component wave drag is specified for a given Mach number and all global design variables.

4. Induced drag is provided as a function of Mach, lift coefficient, and all global design variables.

5. Nacelle drag, which is a combination of wave drag on the nacelles and lift and wave interference between the wing and nacelles, is given as a function of Mach, lift coefficient, engine scaling factor, and all global design variables.

As DOSS executes, total airplane drag is computed by summing up the individual components of drag for any given combination of altitude, Mach number, lift coefficient, and global design variables.

Sample Response Surface for Aerodynamic Drag

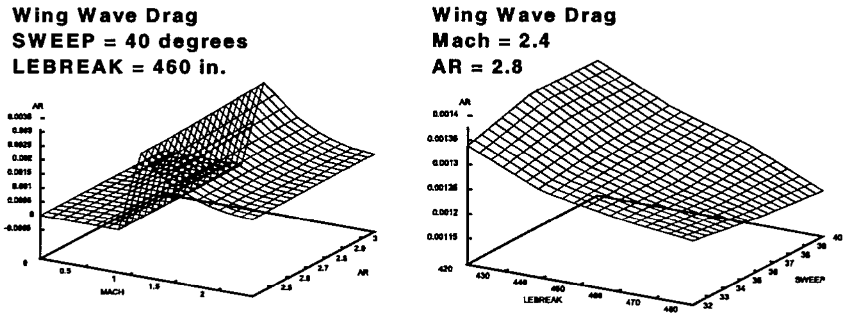

The figure above shows 3-D cuts through the wing wave drag response surface.

Response Surfaces for Low Speed Aerodynamics

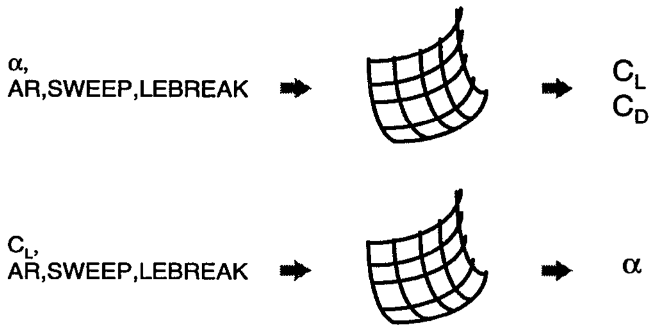

Low speed aero data is provided for takeoff flaps setting and optimized climbout flaps. Fundamentally, the data are used in DOSS exactly as they are in FLOPS, except that response surfaces are built from the raw data. Two response surfaces are generated for each flap setting. Lift coefficient and drag coefficient are given as functions of angle of attack and the global design variables. A separate response surface giving angle of attack versus lift coefficient and the global design variables is also provided to eliminate the need to perform reverse interpolation of the data.

Noise Response Surface

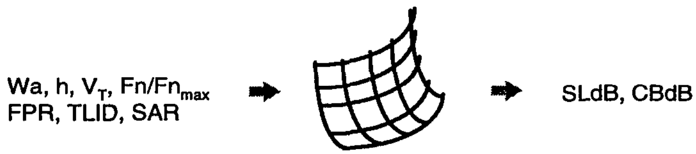

The noise dataset consists of a single response surface. Flare sideline noise, 700 ft sideline noise, and cutback noise (at a reference altitude) are given for two airspeeds as functions of throttle setting and any global design variables. Noise levels are corrected for the proper airspeed with linear interpolation while engine size scaling and cutback altitude variations are handled by simple log corrections.

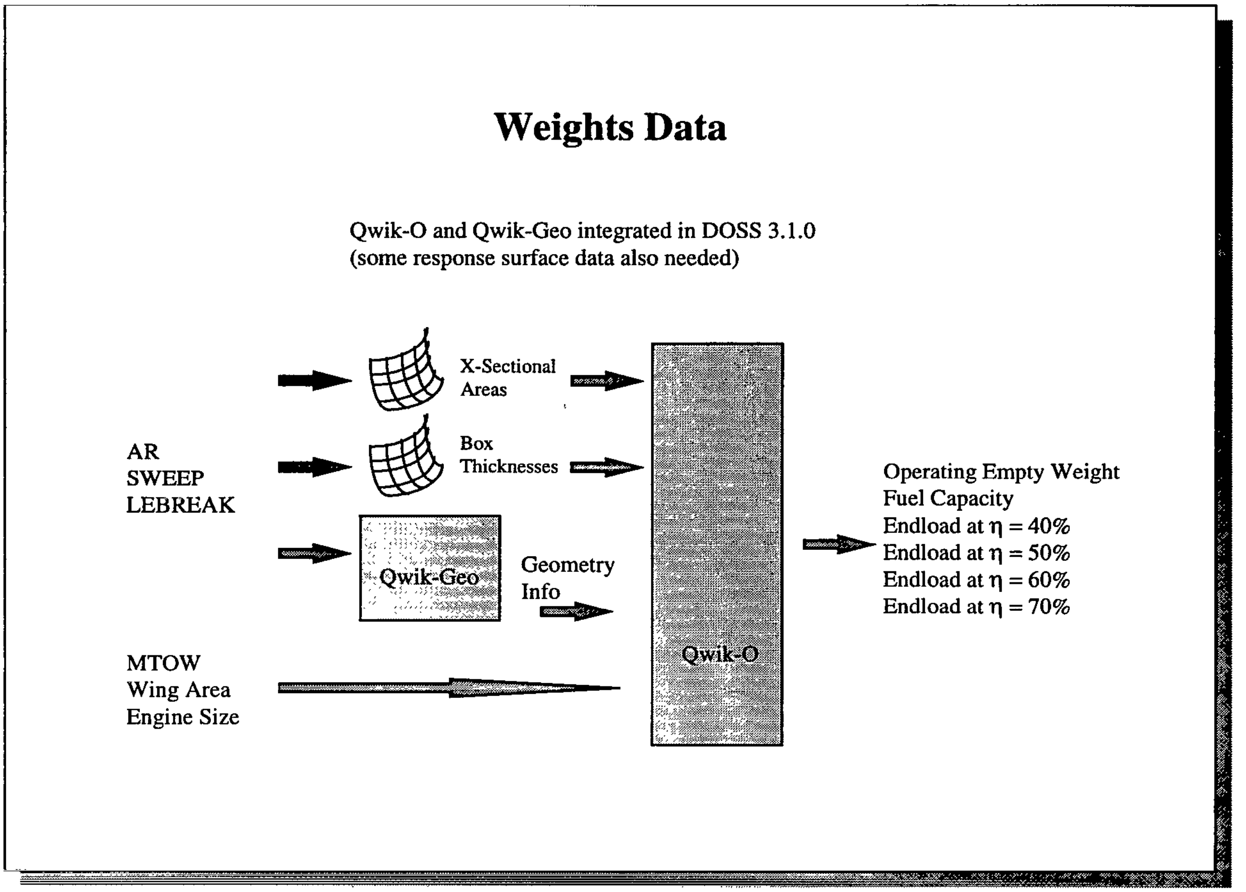

The parametric weights method currently used by all HSR partners was transcribed into a single code module by HSR weights engineering team. Given a configuration description input data file, the weights code computes operating empty weight. An add-on geometry modification routine was also developed by the weights team to provide automated configuration inputs to the weights module for any combination of outboard wing aspect ratio and sweep. Bare engine weight, length, and center of gravity data provided by the HSR engine companies was converted into a response surface which is used to provide engine-related inputs to the weights code allowing for any combination of propulsion design variable values. Taken together, the two modules and the engine response surface let the DOSS user compute operating empty weight, fuel capacity, and end load distribution for any combination of maximum takeoff weight, wing area, engine cycle and wing planform.

Mission Analysis

The FLOPS simulation code is the heart of the DOSS analysis

Inputs
Gross Weight
Wing Area
Engine Size
Planform Variables →
Engine Variables
Wing Thickness Dist.
PLR
Overspeed

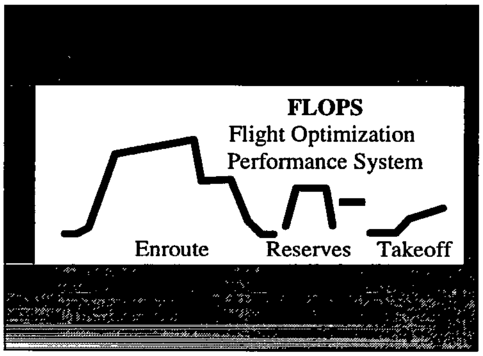

→

Outputs
Range
OEW
Field Length
Sizeline Noise
Cutback Noise
Climb Time
End Loads
Excess Fuel Cap.

The main analysis portion of DOSS consists primarily of the Flight Optimization System (FLOPS). It is responsible for computing the objective and most of the constraint values. FLOPS is a multidisciplinary system of computer programs for conceptual and preliminary design, and evaluation of advanced aircraft concepts. It consists of nine primary modules: 1) weights, 2) aerodynamics, 3) engine cycle analysis, 4) propulsion data scaling and interpolation, 5) mission performance, 6) takeoff and landing, 7) noise footprint, 8) cost analysis, and 9) program control.

For use in DOSS, only the mission performance and takeoff modules in FLOPS are utilized. All other modules are bypassed. Genie provides program control. Weights, aerodynamics, propulsion and noise calculations are performed by custom DOSS response-surface-based code modules. Capability to perform engine cycle analysis and cost analysis is not currently needed in the ACE program.

As integrated into DOSS, FLOPS is used to analyze point design cases only. All optimization and parametric variation is controlled by Genie

Mission Profile and Constraints

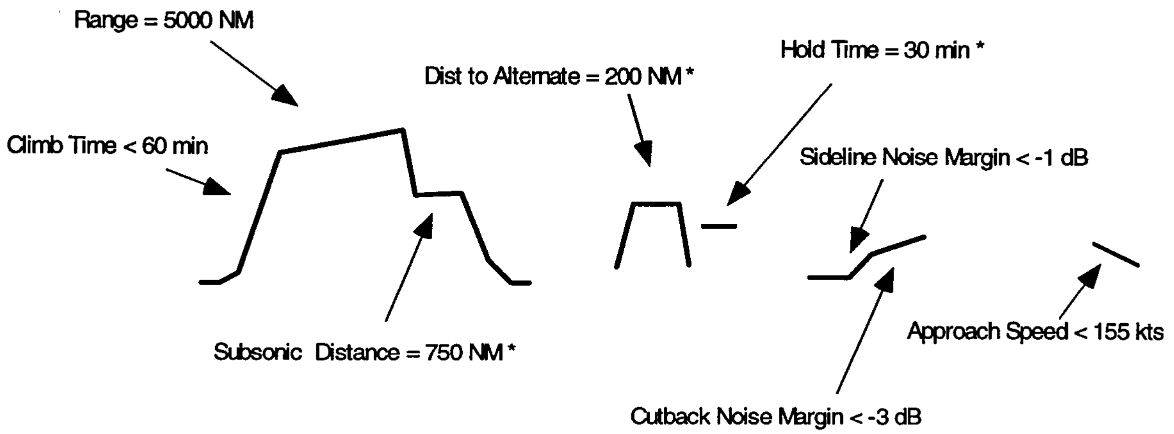

* Satisfied internally by FLOPS mission analysis

The mission profile used throughout development and validation of DOSS is the standard profile used in the High Speed Research. The enroute subprofile includes a main supersonic cruise segment as well as a shorter subsonic segment. Total range is 5000 Nautical Miles (NM), 750 NM of which consists of the subsonic cruise and the descent that follows.

The mission performance module uses the weights, aerodynamics, and propulsion system data to calculate airplane performance. A predetermined flight profile is flown to start of cruise conditions. The climbing cruise segments are flown at the optimum altitude and fixed Mach numbers. Descents are flown along constant dV/dh schedules. Reserve calculations include flight to an alternate airport and a specified hold segment.

The takeoff and landing module computes the all-engine takeoff field length. The approach speed is also calculated, and the second segment climb gradient and the missed approach climb gradient criteria are evaluated. The module also generates a detailed takeoff and climbout profile for use in calculating sideline and cutback community noise.

Minimum approach speed is calculated for a given maximum approach lift coefficient at maximum landing weight.

Optimization - Background

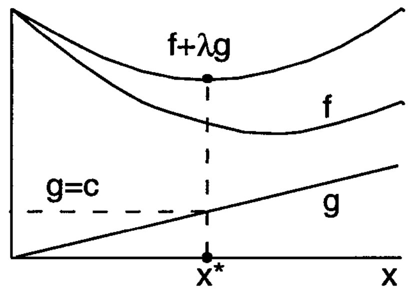

Problem:

$$\min f(x)$$
$$\text{such that } g(x) - c = 0$$

Solution:

Solve for x^* and Lagrange multiplier λ that satisfy

$$\frac{d}{dx}\left[f(x^*) + \lambda g(x^*)\right] = 0$$
$$g(x^*) - c = 0$$

Note that the augmented objective, $f + \lambda g$, has a minimum where $g = c$.

The next several pages are intended to list rules for selecting optimization parameters that affect the efficiency and reliability of the DOSS program. Some necessary background on optimization methodology is presented in the first few slides.

The optimization parameters have already been worked out for the sample problems provided as part of the DOSS package, making this section not very important in the beginning; however, as the input data and/or design problems change, this information will be crucial for obtaining converged results using optimization in DOSS.

The first background slide introduces the concept of a Lagrange multiplier that scales a constraint gradient to exactly offset the objective gradient at a point where the constraint is satisfied.

Optimization - Background

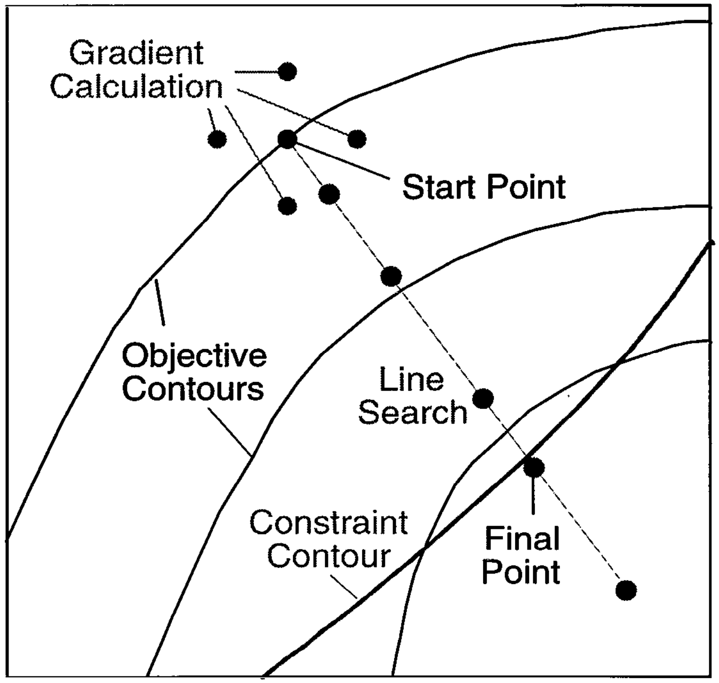

The optimization procedure samples points in the design space to find a better design.

Gradients are calculated by finite-differences, using data at points surrounding the starting point.

A direction for best improvement is calculated from the gradient information.

A line search is performed in the improvement direction: points are sampled, with the best point preserved for the next major iteration.

This completes one major iteration; the next iteration begins with a new gradient calculation.

Graphical User Interface (GUI)

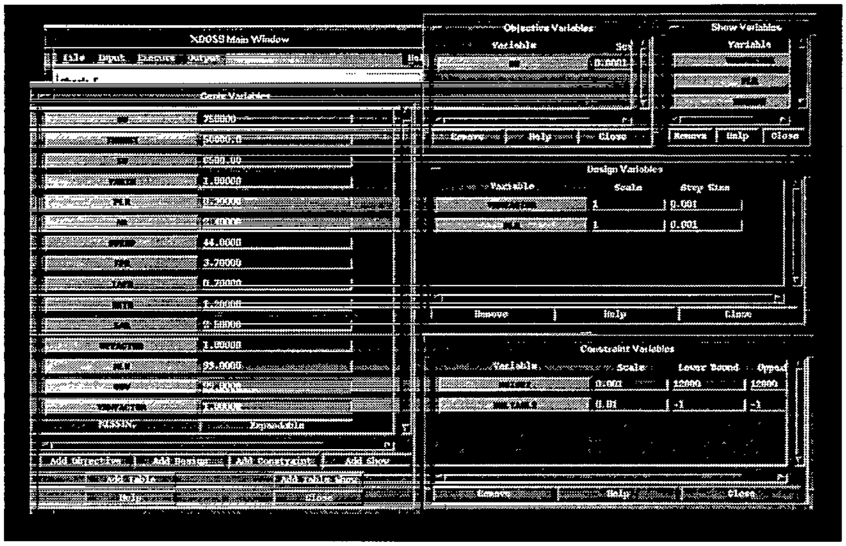

The Graphics User Interface screen is shown. The GUI allows the user to do the following in a graphical environment.

Open, modify, and save GENIE input files.

Command generation of plots of data arrays.

Set up and command optimization.

Command generation of thumbprint plots.

DOSS Visualization Program (DVP)

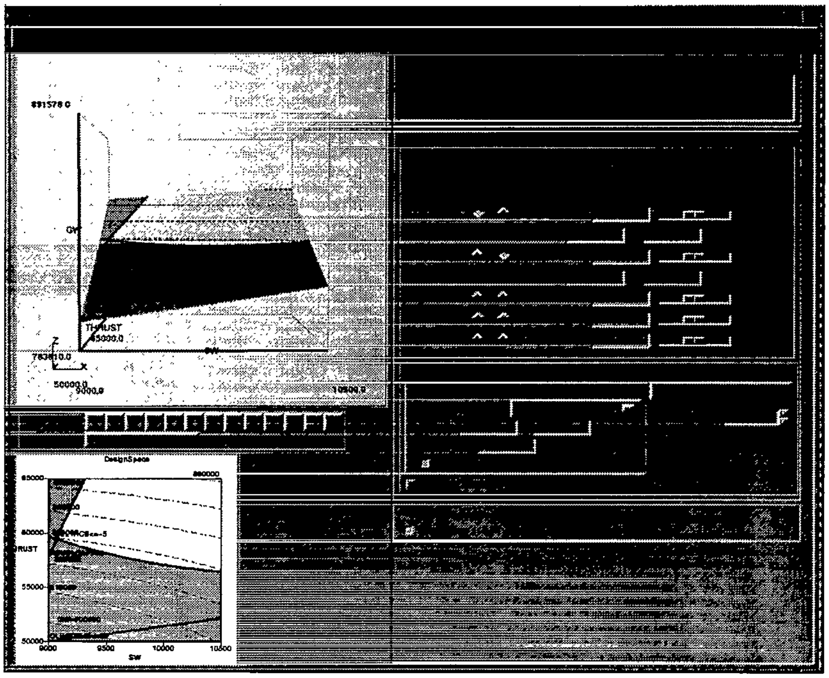

12/22/98

The DOSS Visualization Program (DVP) gives the aircraft designer a vastly improved and more powerful way to visualize the design space by offering:

- Interactive graphical visualization of independent data variables throughout the design space
- 3-dimensional Response Surface Visualization
- User-friendly interface
- High-quality hardcopy plots of graphics

DVP - Features/Dynamic Thumbprint

12/22/98

The Dynamic Thumbprint feature gives the designer the ability to fly through the design space and give them immediate visual access to the entire field of data instead of a previously chosen 2-dimensional slice of the data.

The Dynamic Thumbprint offers:

- Display of multiple levels (i.e.. contours) of independent variables at a given 2-dimensional slice through the design space.
- Interactive controls for selecting design variable levels and ranges to define the slice on which to plot.
- Display of constraint lines and greyed-out infeasible areas of plot.
- Selection and display of optimum point with associated variable values
- 3-dimensional view of objective function contour surface
- Ability to zoom, rotate and pan the 3-dimensional image

DVP - Features/Other Plot Types

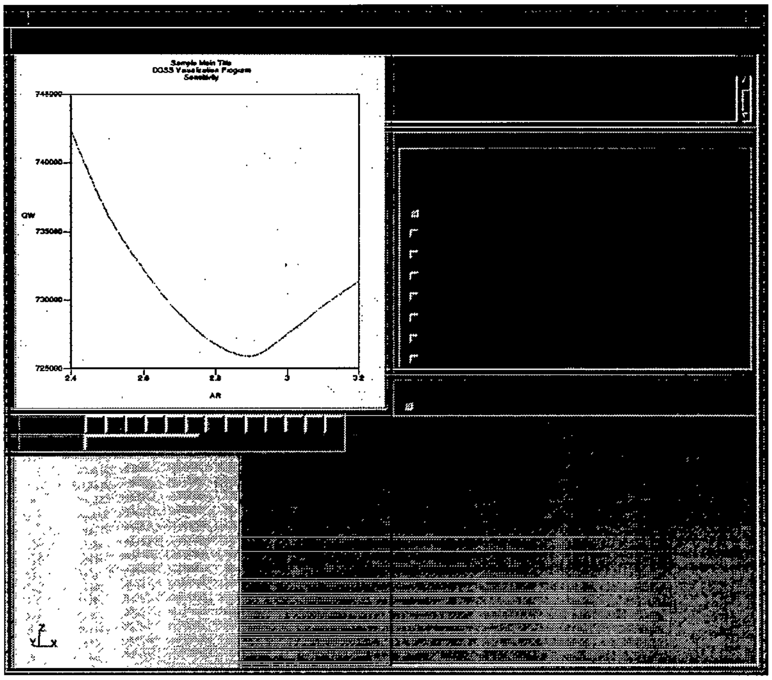

12/22/98

The DVP provides support for several additional plot types, including:

- Sensitivity
- Mission Profile
- Iteration History

The DVP is not, however, limited to these plot types. It accepts and plots any data which comes in the form of a fixed array of values (to be used as the X-axis values) plus one or more arrays of values (to be used as the Y-axis values)

DVP - General Features

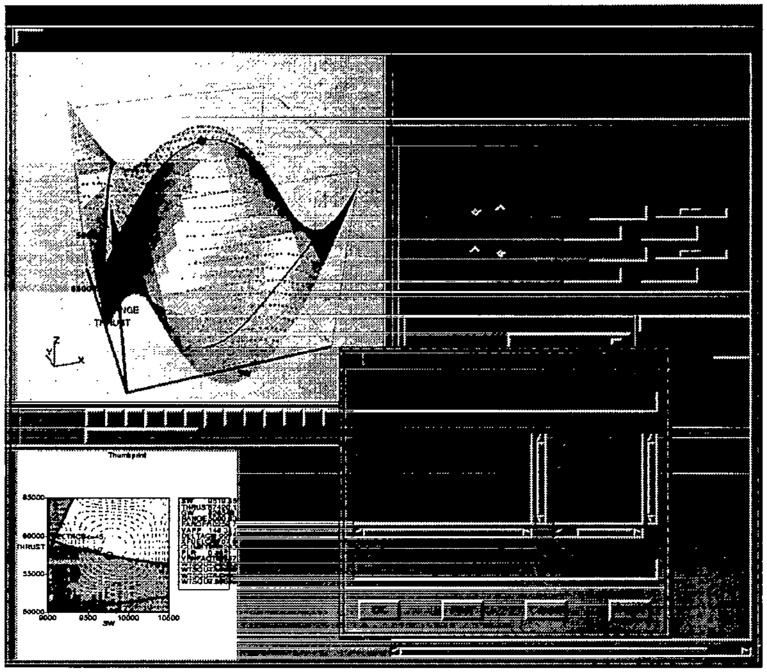

12/22/98

Additional general features of the DVP are:

- Hardcopy output
  - save images to PostScript and Encapsulated PostScript
- Platform Independent
  - current version tested on SGI, HP and SUN workstations
- Save/restore State
  - save the state of a session and restore it at a later time

DVP - New Features

- 3-dimensional viewing
- Response Surface Visualization

12/22/98

DVP - Future Plans

- Add features to Response Surface Visualization
- Add user-control of plot attributes such as color, line style, etc.

Conclusions

- DOSS is a proven MDO code with roots in the traditional sizing process.
- The GenIE architecture provides a simple, flexible, and extendable framework.
- All input data are represented using high-fidelity response surfaces.
- Additional code modules provide weight and structural end load computation capability.
- NASA's FLOPS code provides the core analysis function.
- Optimization if provided by a robust non-linear optimizer.
- The XDOSS GUI reduces errors and speeds training.
- DVP provides graphics that are simple to create and easy to understand.

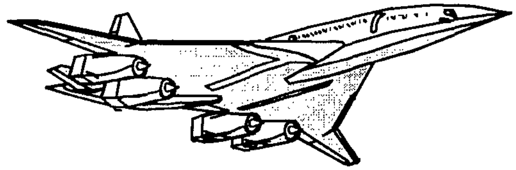

ACE Final Report

A.2 - Cutback Acoustics Module

Alan Okazaki

December 31, 1998

DOSS: ASO:001

Objectives

- Improve Noise Method Used to Assess Delayed Cutback
- Take Advantage of Altitude Gain Versus Full Power Intrusion
- Include Delayed Cutback Method Into DOSS

Approach

- Generate Performance Data at Varying Cutback Distances Using DOSS
- Evaluate Delayed Cutback Noise Benefit for the PTC
- Evaluate Configuration Sensitivity Using Briquette Data

DOSS-ASO:001

A previous parametric study of the HSCT takeoff procedure for noise certification at the takeoff monitor found that noise always decreased when the distance between the cutback initiation point and the takeoff noise monitor was decreased. The method used to conduct that study, however did not account for the impact of the full power flight segment during the engine spool-down transition period. The results were optimistic. Realizing this, a decision was made last year to continue using the conservative procedure of initiating cutback at 3,500 feet prior to the takeoff microphone.

The objectives of this task was first to improve the noise method to better account for full power intrusion (not only prior to but also during engine spool-down). Second, to evaluate any benefits to delaying the cutback (i.e. is the advantage of the additional gain in altitude greater than the disadvantage of increased noise level in the forward quadrant due to full power). And finally to include the improved cutback noise prediction method into the DOSS sizing optimization program

The approach taken was to first modify the DOSS program to generate the performance data needed by the noise method. Those modifications are discussed in this section.

Performance data generated for the PTC was then used to evaluate the noise benefit of the delayed cutback procedure for that "fixed" configuration.

The sensitivity of optimum cutback procedure to configuration parameters were then evaluated using the Briquette data.

The acoustics methodology and study results are discussed in detail in "EI TASK E11 - Optimized PTC Cutback Procedure" (ADAPT TI 14.18 "FY 98 Airframe Task E11 10/21/98")

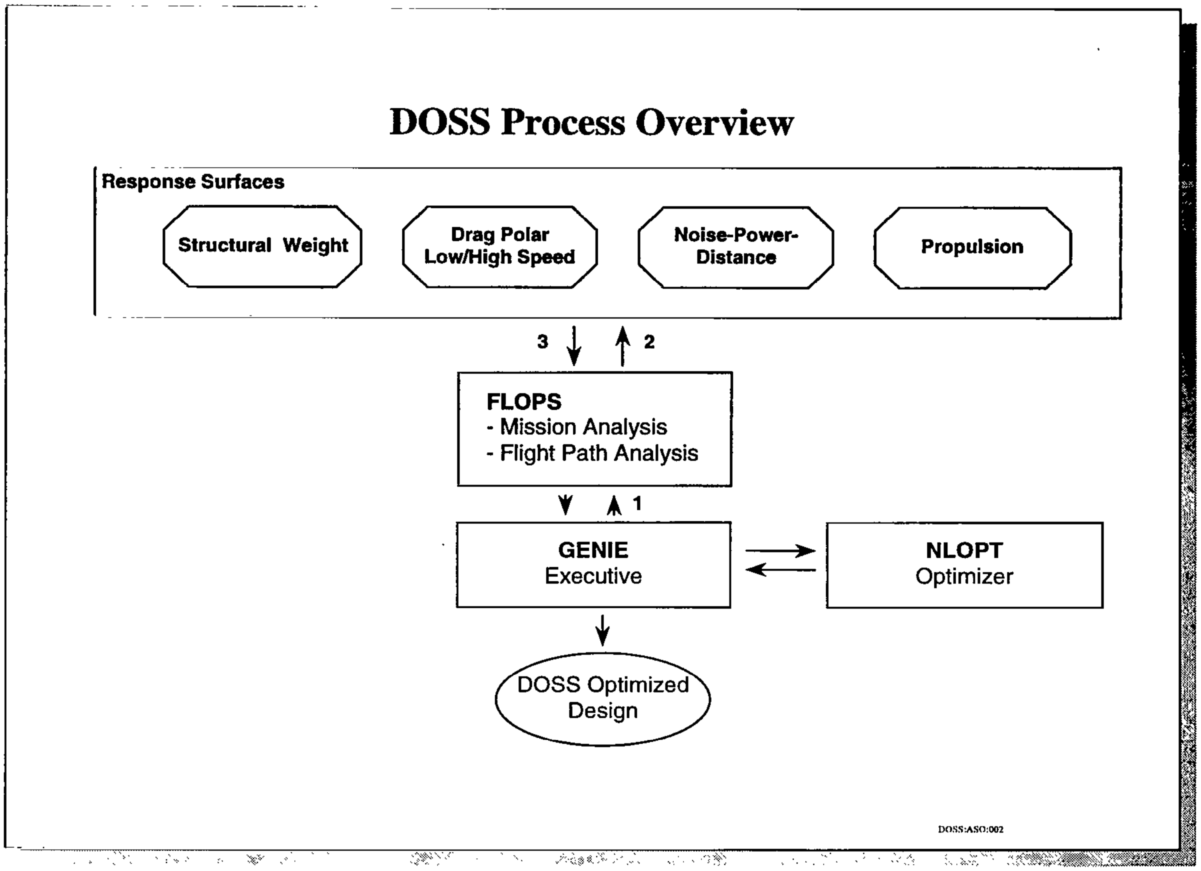

The basic operation of Design Optimization Synthesis System (DOSS) can be described as a sequence of steps as follows. First the GENeric Interface for Engineering (GENIE) executive provides the FLight OPtimization System (FLOPS), the mission analysis module, the values of the current global design variables (wing area, engine size, sweep, aspect ratio, engine parameters, thickness, etc.; arrow #1). FLOPS then initiates a mission analysis and queries the response surfaces using these global design variables given to it by GENIE plus the Mach, altitude, angle of attack, control surface deflections, throttle and distances from the noise markers required by takeoff, climb cruise, and descent of the mission analysis (arrow #2). The response surfaces furnish FLOPS with structural weight, drag, lift, moment, noise level, specific fuel consumption, engine dimensions, and weight (arrows #1,2).

The FLOPS mission module assumes a quantity of fuel, flies the mission using the response surface data, and determines the unused fuel or lack of fuel to complete the mission. A correction is made to the fuel and the process is repeated until the fuel satisfies the mission requirements. FLOPS then determines the state of the constraints such as takeoff field length, landing speed, fuel volume, etc. The flight path calculations of FLOPS are used by the acoustics module to calculate the state of the noise constraint.

This data along with fuel required and the TOGW is fed back to the GENIE executive which then provides the optimizer with properly scaled finite difference sensitivity data for the objective function (TOGW) and the constraints. The optimizer then performs a search to find the best combination of the design variables taking into account the maximum step size for each global design variable. It then sends these new values for optimum design (plus estimated TOGW) back to GENIE to check if it is a converged value. If not, GENIE repeats the whole process again and again until the TOGW converges.

Integration of Cutback Acoustics Module into DOSS

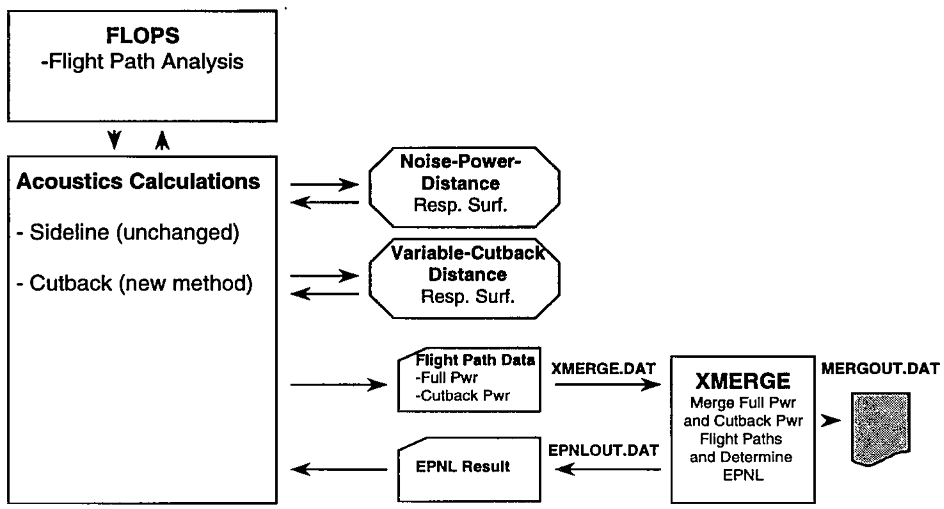

The FLOPS program first calculates the flight path prior to calling the acoustics routines. The sideline noise calculations use the existing Noise-Power-Distance response surface data. When the new cutback acoustics method is requested, DOSS is instructed to read the new format cutback response surface.

Takeoff flight Path is generated with engine thrust reduced at a user specified cutback distance. Altitude, velocity, thrust/delta, noise flag, distance, flight path angle, angle of attack data at the sideline measuring point and at the cutback noise measuring point are passed to the DOSS noise calculation routine.

The flight path data is first combined with engine data (airflow (wa), suppressor area ratio (sar), thrust lapse (tlid), fan pressure ratio (fpr)), and aircraft data (weight (mtow), aircraft pitch attitude (pae)). A spooldown time is then determined using a one degree per second rate to go from the aircraft attitude at the sideline measuring point to the attitude at the noise measuring point. The altitude at the measuring point using thrust without spooldown is also estimated. With this information, the response surface maximum fn/delta is determined using the input wa, sar, tlid, and fpr.

With the ratio of sideline to maximum thrust value, the time relative to visual overhead (TIMVRO), sound propogation distance (SPDIST), and tone corrected perceived noise level (PNLT) arrays as a function of look angle are obtained from the response surface. This process is repeated using the ratio of cutback fn/delta to maximum. The results are then written to XMERGE.DAT.

The XMERGE program is called and reads the XMERGE.DAT file. XMERGE blends the maximum thrust and cutback power flight path arrays together. The merged results, still in array form, are written out to MERGOUT.DAT for user review. The combined flight path is then integrated. The resultant cutback EPNL value is written to EPNLOUT.DAT. The file is then read by DOSS and the value is converted to cutback dB. This value is stored in the Genie database, and the program control returns to the FLOPS program. If the constraint is to meet a cutback noise level, the program will then adjust the engine values and go back through the loop until the goal is satisfied.

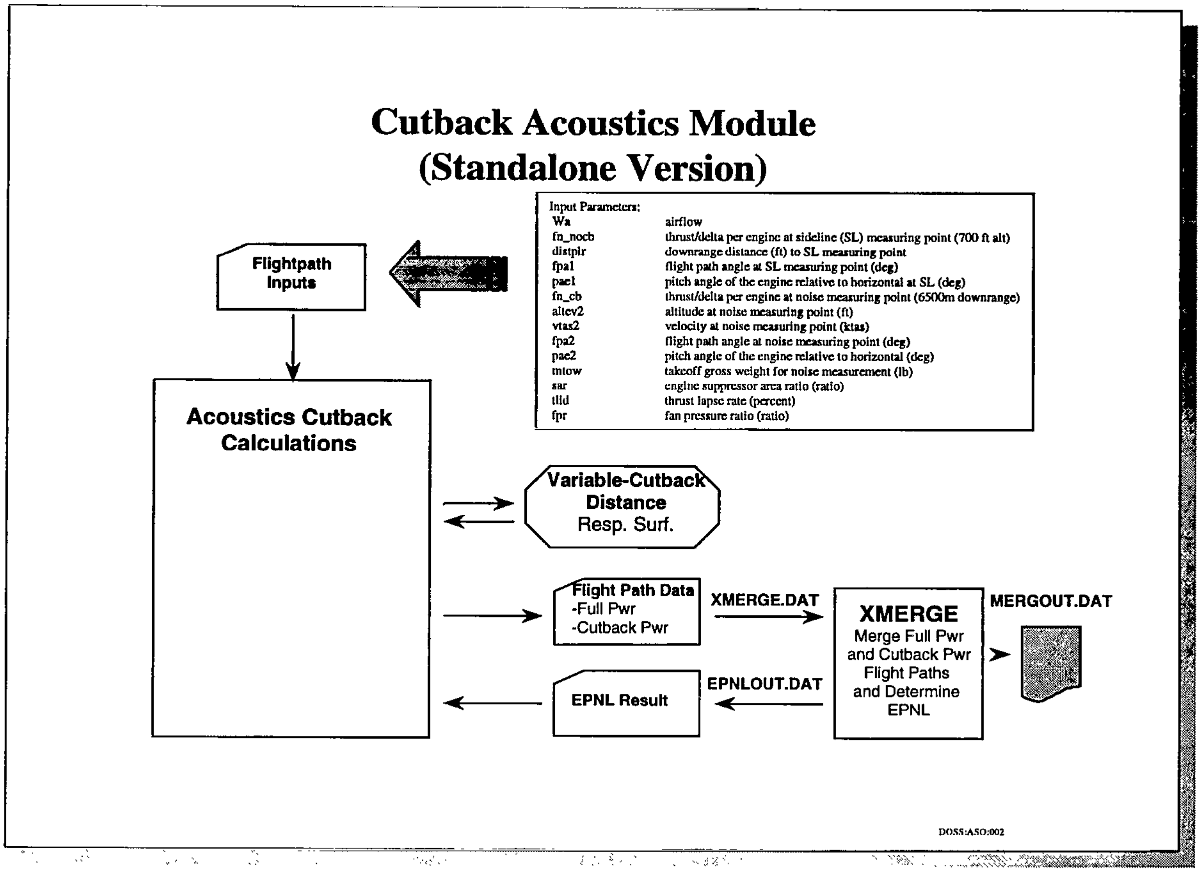

A standalone version of the cutback acoustics program was developed prior to integration into DOSS. This allows the user to check results from previous runs or from other sources independent of DOSS. It is also used to validate acoustic response surfaces.

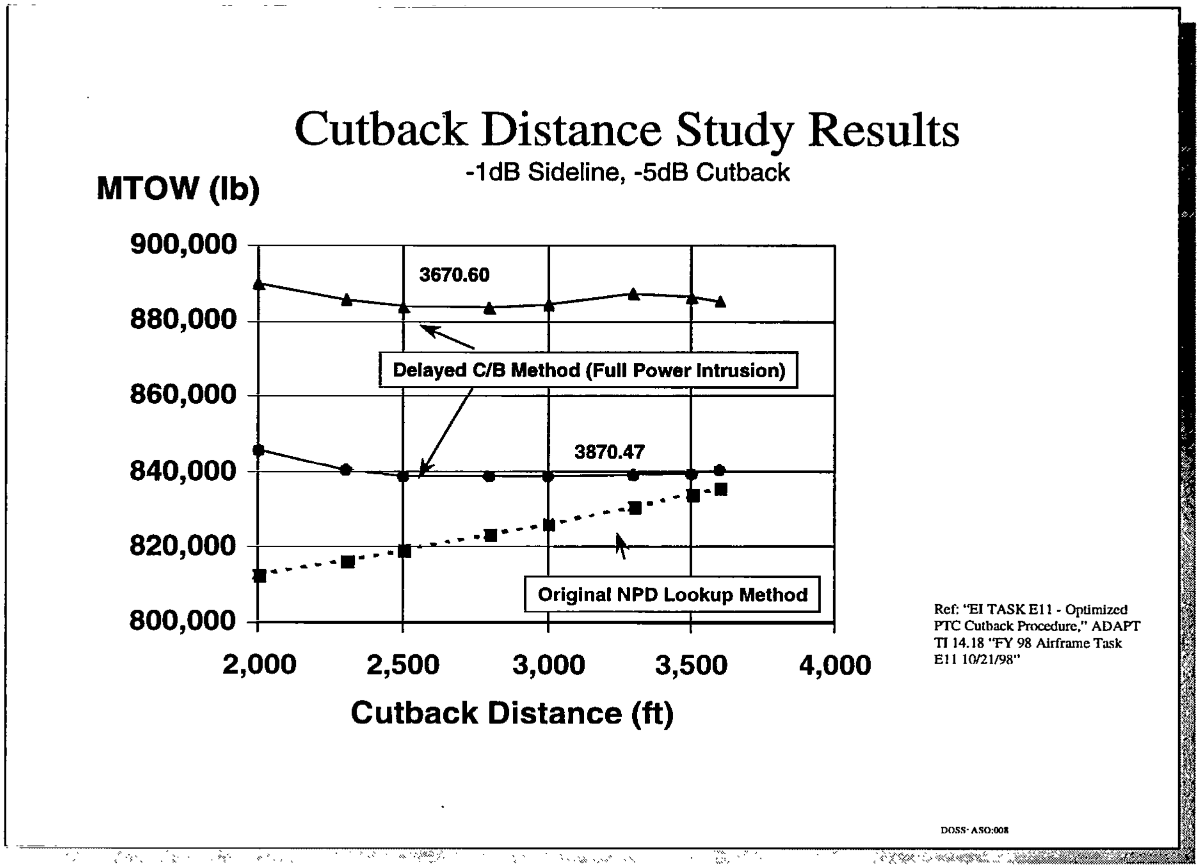

The PTC Cutback Distance Study is an example of how the DOSS cutback acoustics module was applied. The purpose of this tradestudy was to investigate if there was any benefit in delaying the cutback (ie is the advantage of the additional gain in altitude greater than the disadvantage of increased noise level in the forward quadrant due to full power the flight segment).

Configuration 1504 was sized with the M3870.47, SAR 2.7 and M3670.60 SAR 2.9 engines for (-1,-5) noise constraints. These airplanes were sized using various cutback initiation distances before the microphone (from 2,000 ft to 3,600 ft). The new noise calculation, "Delayed C/B Method", showed a flat MTOW trend for both airplanes. When the current noise method, "Original NPD Lookup Method", was used to size airplanes, the results showed an increase in MTOGW as the cutback initiation was delayed.

Note that two airplanes sized with two different engines with different Fan Pressure Ratio (FPR) showed the same flat MTOGW trend. This seems to indicate that the differences in the FPR does not make any differences in the cutback noise characteristics.

Also note that the the current noise method produces similar results as the new noise method when the cutback initiation occurs at 3,500 ft before the monitor.

Hence, the acoustics group's recommendation for the TC airplane is to use the current noise method until the inlet noise prediction method becomes more accurate and better definition of inlet noise becomes available.

Summary/Conclusions

- Cutback Acoustics Methodology was Successfully Integrated into DOSS
- Noise Study Recommendation was to Continue Sizing with the Current Cutback Procedure due to Small Payoff.
- Modifying DOSS to Determine the Optimum Cutback Distance for Minimum Cutback Noise Would Require a Significant Investment in Programming Time not Currently Justified by the Results.
- Use of the Delayed Cutback Method for Sizing Should be Re-Assessed When Improvements of Fan Noise Prediction is Available.

DOSS: ASO:001

Due to the small EPNL benefit seen for the PTC and the small changes in TOGW as a result of the delayed cutback procedure, the acoustics group's recommendation is to continue to use the less complicated and less computer intensive EPNL NPD lookup method with a conservative cutback procedure (3,500 ft) for the Briquette study and future sizing exercises.

The single caveat to this recommendation is that the Delayed Cutback Method must be reevaluated as the HSCT continues to evolve (or change radically) and as tests data, particularly fan source noise data, becomes available.

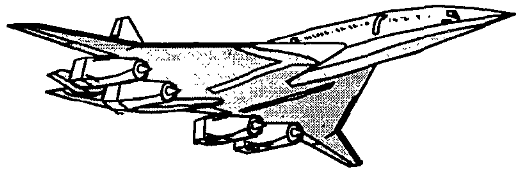

ACE Final Report

B - Aerodynamics Working Group

Chet Nelson

December 31, 1998

Appendix B, Aerodynamics Working Group

Chet Nelson
Boeing Commercial Airplane Group
P.O. Box 3707, M/S 6H-FK
Seattle, WA 98124-2207

Appendix B, Aerodynamics Working Group

- Section B.1 Linear Performance Aerodynamics
  - Boeing Commercial Aircraft
- Section B.2 Nonlinear Performance Aerodynamics
  - Boeing Phantom Works
- Section B.3 Nonlinear Performance Aerodynamics
  - NASA Langley

ACE Aero Working Group

- Introduction: ACE high speed aero process review
- OAC drag database development ("linear aero")
- Navier-Stokes planform and thickness non-linear effects
- CFD for transonic flowfield / drag level checks

The ACE Aerodynamics Working Group was responsible for several tasks related to development of the Optimized Aeroelastic Concept (OAC) airplane.

The OAC high speed drag database was created using linear potential aerodynamics methods. Higher-order Navier-Stokes methods were used for selected configurations of interest to develop linear to non-linear drag planform and thickness corrections. CFD tools were also used to evaluate the transonic flowfield and perform drag level checks.

The OAC high lift drag database was also created using linear potential methods and test to theory corrections based on the Reference H configuration.

Introduction: ACE High Speed Aero Process Review

- High speed (and high lift) performance polars :
  - Full configurations, full scale, trimmed polars, interf. scalars
  - Low aspect ratio linearized potential flow codes
  - Results for baseline config. anchored to W.T. data
  - Technology projection from baseline config. tops-down chart
- Parametric configuration Δ's individually
- Selected combinations of config. features checked for interactions
- Non-linear aero effects on configuration Δ's from selected CFD
- Database put into DOSS response surfaces

The high speed and high lift drag polars were developed by first analyzing each configuration with linearized potential flow codes. Wind tunnel test data were available for previous baseline aircraft such as the TCA to anchor the linear theory results. Non-linear aerodynamic effects were predicted for selected configurations and increments were analyzed between linear and non-linear results. The entire database was put into DOSS for sizing the OAC following the procedure developed and demonstrated on the Preliminary Aeroelastic Concept (PAC) precursor to the OAC.

OAC-Specific Drag Database Development Issues

- OAC database configurations...
  - "Prism" design space for planforms
  - Wing box thickness variations
  - Nacelle variations for matrix of engines
  - (Wing twist increments)
- "Non-linear effects" not captured in linearized potential flow code
  - Viscous effects on pressure drag across range of planforms
  - Viscous flow limits on trailing edge closure at higher t/c's
  - Differences between ACE baseline (1504) and TCA / PTC

There were several issues confronting the Aero working group regarding the task of developing the OAC drag database.

First, many different items were evaluated. These included wing planform variations (with a multi-dimensional design space known as the "Prism"), wing box thickness variations, and a matrix of propulsion systems (known as first the "Brick", and then the "Briquette"). Drag sensitivities to global twist variables which were investigated for the PAC were not applied to the OAC as the experience on the PAC showed no net configuration benefit.

Second, there were concerns that differences in non-linear effects between configurations would not be adequately captured by the linearized potential flow tools. These included viscous effects on pressure drag, viscous flow limits of large airfoil closure angles on thick wings, and differences between the ACE parametric baseline (model 1504) and the TCA/PTC airplanes.

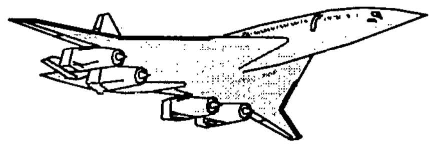

ACE Final Report

B.1 - Preliminary Design High Speed Drag

Paul Dees
Kevin Peterson
Eric Adamson
Servando Flores
Jim Fenbert

December 31, 1998

Section B.1, Linear Performance Aerodynamics

Paul Dees
Boeing Commercial Airplane Group
P.O. Box 3707, M/S 6H-FK
Seattle, WA 98124-2207

Abstract:

Linear potential methods were used to analyze 25 wing planforms, 243 thickness variations, and 12 different engine cycles to support the sizing of the Optimized Aeroelastic Concept (OAC) airplane in DOSS. Linear to non-linear analysis corrections were made to the data with CFD support provided by Boeing Phantom Works in Long Beach.

Acknowledgements:

Thanks are due to Kevin Peterson, Eric Adamson, Servando Flores from BCAG, and to Jim Fenbert at NASA Langley for contributing to this work. Thanks are also due to Chet Nelson for his technical leadership. Boeing Phantom Works (with Geojoe Kuruvila coordinating) contributed CFD support to this work which is presented in the next section.

OAC Drag and Loft Groundrules

- Keep from the PTC: Airfoils
  Structural arrangement
  OML inboard of BL 370
  Nacelles
- Assume: Loft simplifications as required for parametrics.
  Consistent tech projection for drag
  Constant LE flap effectiveness
- Restatus the PTC as the model 1504 for consistency and convienence
  (MTOGW up from 793,000 lb to 796,000 lb)
- Incorporate most current drag polar buildup process, "dragh".

A wing planform study covering a prism shaped design space was done to support OAC sizing. Global variables along the edges of the "Prism" were the buttline (WBL) of the leading edge break, aspect ratio, and outboard leading edge sweep. Twenty five different wing planforms based on the PTC were evaluated.

The structural arrangement philosophy was the same for all planforms as were the airfoil thickness forms. The wing inboard of the outboard nacelle centerline was the same as the PTC and TCA airplanes to minimize the effort needed to create finite element models for Structural evaluation. The configurations were drawn with the nacelles of the PTC's 3770.60, SAR 2.9 engine cycle. All configurations had three surfaces like the PTC with a horizontal tail sizing variation correlated by the Stability and Control and High Lift Aero groups.

Some geometric simplifications were required to easily obtain a parametric family of wing lofts. Across the range of planforms, steps were taken to assure consistent estimates of drag (e.g. constant technology projections and fixed level of leading edge flap effectiveness).

A revised parametric version of the PTC (called the model 1504) was created so there would be a consistent baseline with the other 24 planforms. A small TOGW penalty occured.

Drag was estimated using the A389 and TEA080 linear potential flow programs. The most current drag buildup program was used, known as "Dragh" (version H). It incorporated improved accuracy of nacelle skin friction drag and was better able to evaluate a three-surfaced airplane.

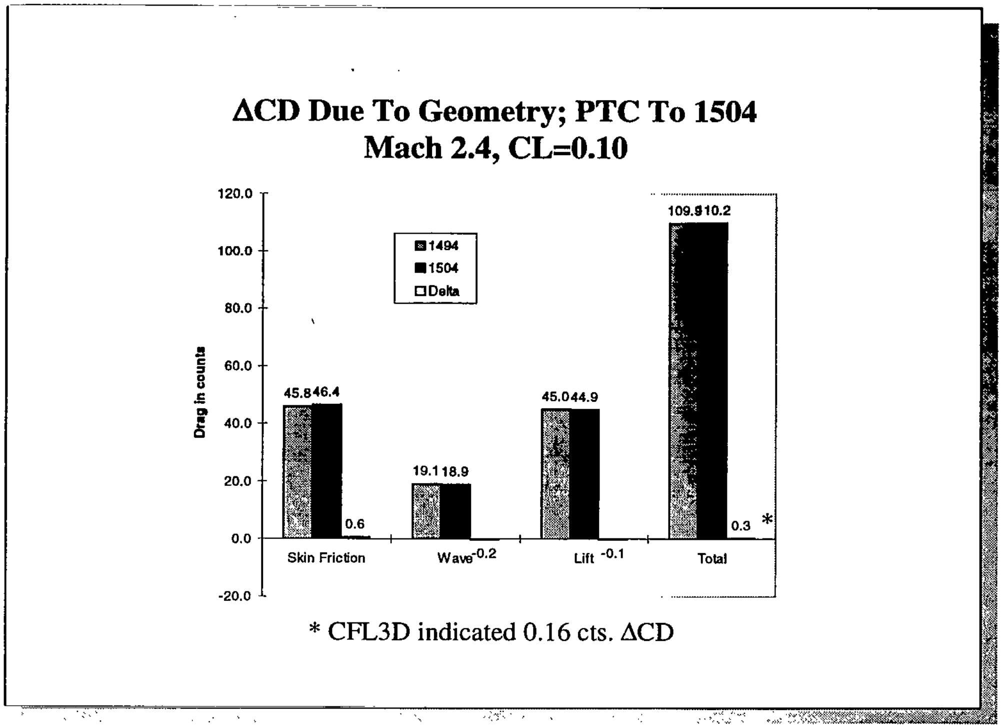

The ΔCD via the linear theory methods due to minor wing loft differences between the original PTC (model 1494) and the parametric PTC for the Prism study (model 1504) was 0.3 drag counts at the cruise condition. Navier-Stokes CFD analysis by Boeing Long Beach of just the wing-body indicated a 0.16 count difference. In both cases the 1504 had the higher drag level.

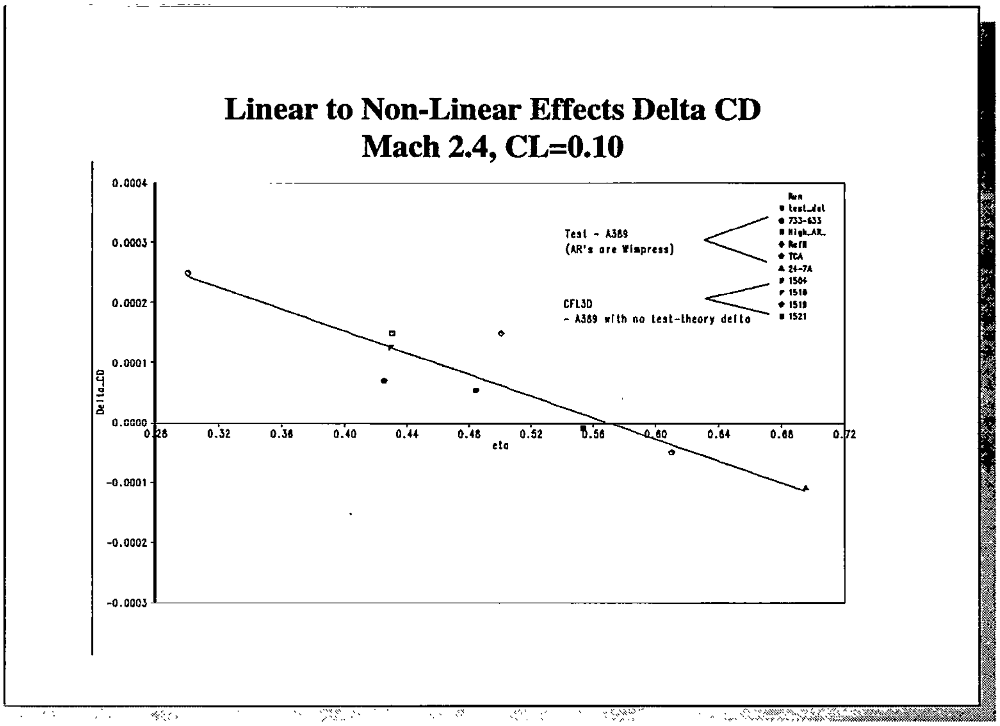

Linear theory to non-linear theory drag increments were estimated by CFL3D analysis at Boeing Long Beach for three of the Prism configurations. The increments were correlated versus a variety of different geometric parameters, some resulting in a tight fit and some with considerable scatter. The differences between CFL3D and the linear theory tool (A389) correlated well when plotted versus the semi-span location of the outboard leading edge break. They also agreed in slope with linear theory to wind tunnel test deltas for previous HSCT airplanes such as the Reference H and the TCA.

Increments for a fourth configuration analyzed later were accurately predicted by the correlation.

The linear fit through the points was shifted downward and anchored to the TCA data point at an eta of 0.61, which was considered the most accurate due to larger amounts of test data. This fit was used as the non-linear effects trend correction for the Prism planforms.

Prism Wing Planforms

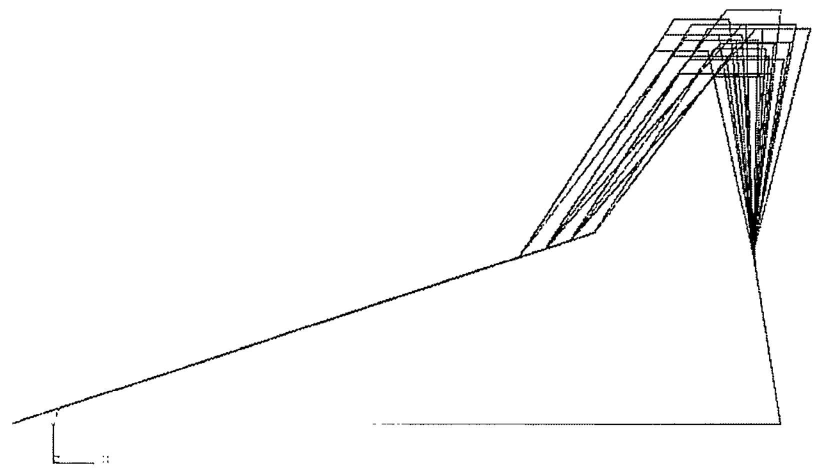

The planforms of all of the Prism planforms are shown to illustrate the common inboard wing geometry and the variety of outboard wing shapes. The four leading edge break WBL locations (nomimally 420,440, 460, and 480) and constant tip chord are also noteworthy. Wing reference area and span of the as-drawn unsized planforms were allowed to vary in order to obtain planforms with aspect ratios of 2.4, 2.56, 2.73, 2.9, or 3.06. Outboard leading edge sweeps included 32, 36, and 40 degrees.

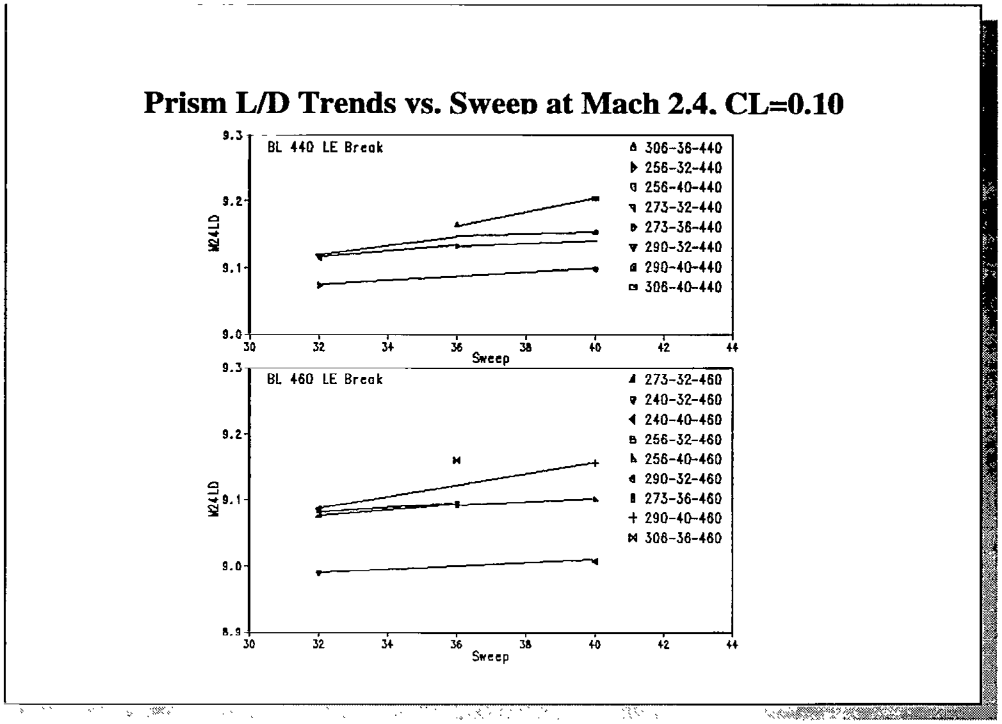

Representative high speed drag results are shown for the Prism planforms with breaks at WBL 440 and WBL 460. As expected, L/D increased as outboard sweep and aspect ratio increased. L/D at Mach 2.4 was less sensitive to those parameters since the inboard wing was not allowed to change, varying by ±1% from the 1504.

At Mach 0.9, CL=0.17 (not shown), the L/D varied ±6% from the 1504. It was sensitive primarily to aspect ratio and not at all to the outboard leading edge sweep.

These L/D's are for as-drawn rather than as-sized airplanes. During sizing the L/D may shift as the wing area changes. The sensitivity to wing area was investigated by analyzing the model 1519 (AR=3.06, O/B sweep=36 deg., WBL 440 break) with the same wing area as the 1504. The CD*Sref of the non-wing components was kept constant as the wing reference area decreased to 9200 ft2. It still had a higher L/D than the 1504, but slightly reduced from its as drawn level.

PTC Wing Thickness Variation - Drag

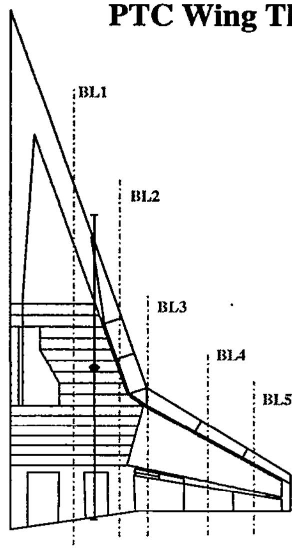

BL1	BL2	BL3	BL4	BL5	ΔCD cts.	ΔMTOW_Cd K lbs
1	1	1	1	1	4.63	67
2	2	2	2	2	11.08	161
0	1	1	0	0	2.29	33
0	2	2	0	0	5.58	81
0	1	1	1	0	3.22	47
0	2	2	2	0	7.64	111
0	2	2	1	0	6.53	95
0	1	2	2	0	5.84	85
0	0	1	0	0	0.97	14
0	0	2	0	0	2.29	33
0	0	1	1	0	1.91	28
0	0	2	2	0	4.40	65

Wing thickness variations of the model 1504 were also evaluated to support the trade of improved flutter characteristics versus increased drag. Five WBL's were chosen to have increased thickness such that a "0" meant the thickness equaled the 1504, a "2" was a full thickness increase, and a "1" was a half thickness increase. WBL's 1, 2, and 3 had a full thickness shape defined by Hicks-Henne functions and WBL's 4 and 5 had the airfoil thickness scaled up.

NASA Langley analyzed 243 different combinations of thickness increase using a linear theory code. Boeing Phantom Works also analyzed three wing-body cases using the CFL3D Navier-Stokes CFD tool (the 00000, 11111, and 22222 cases). The CFL3D results indicated a larger drag increase due to additional thickness than the linear theory, so the linear theory results were increased by 10% across the board to account for that, then provided for DOSS usage.

ΔCD due to additional thickness for several combinations of interest are shown as well as the equivalent sized airplane maximum takeoff gross weight due to the drag (not including any weight due to other factors). Any thickness increase had a significant maximum takeoff gross weight penalty.

It was assumed that these drag penalties due to additional thickness would apply equally to all the Prism planforms.

"Briquette" Engine Cycle Study

Engine cycle variations included:

- Fan Pressure Ratios = 3.6, 3.7, 3.8
- Inlet airflow ratios = 0.7
- Bypass ratios = 0.39 to 0.60 depending on FPR and extraction ratio
- SAR = 2.7, 2.9

Final OAC cycle was the 3870.47s7, which had:

FPR=3.8, IAR=0.7, BPR=0.47, SAR=2.7

Engine cycle variations were evaluated on the 1504 and assumed to be equally valid for all the Prism planforms. Originally a study known as the "Brick" was conducted involving large number of cycles (nacelle geometries), but the unacceptable propulsion impact of many of these engine options led to a new study of smaller scope known as the engine "Briquette".

Each cycle had a unique nacelle area distribution which was evaluated using A389 for nominal airflows of 700, 800, and 900 pps in order to provide nacelle interference scalars for the DOSS sizing. The engine airflow scales up or down as the airplanes sizes. Providing a range of drag as a function of engine airflow improves the accuracy of the sizing process. The drag includes nacelle skin friction drag, lift and other interference drag, and isolated nacelle wave drag.

Non-linear aerodynamic effects due to details of specific engine cycles were not assessed due to the large effort required to analyze them. Linear theory estimates were considered sufficient to provide design guidance for a preliminary design engine-airframe match.

An alpha-numeric code describes each engine cycle. DOSS indicated that the final OAC cycle should be the 3870.47s7.

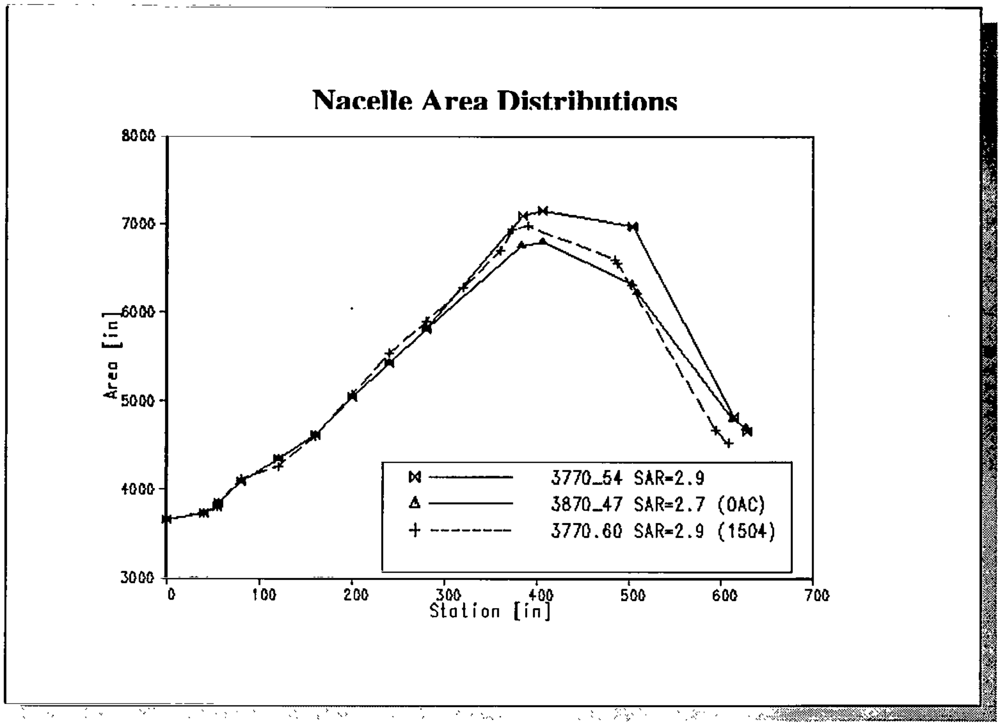

Nacelle cross sectional area distributions for two Briquette engine cycles are compared to the baseline 1504 engine cycle, the 3770.60s9. The upper line for the 3770.54s9 is the closest Briquette cycle to the baseline 1504. It had more maximum cross sectional area and therefore more drag than the 1504. Thus, the Briquette nacelle drag levels were higher for the same engine cycle than the earlier vintage PTC cycle.

The line with the triangles is for the final OAC cycle, the 3870.47s7. It had less maximum cross sectional area and less drag than the 1504/PTC.

"Briquette" Drag Results

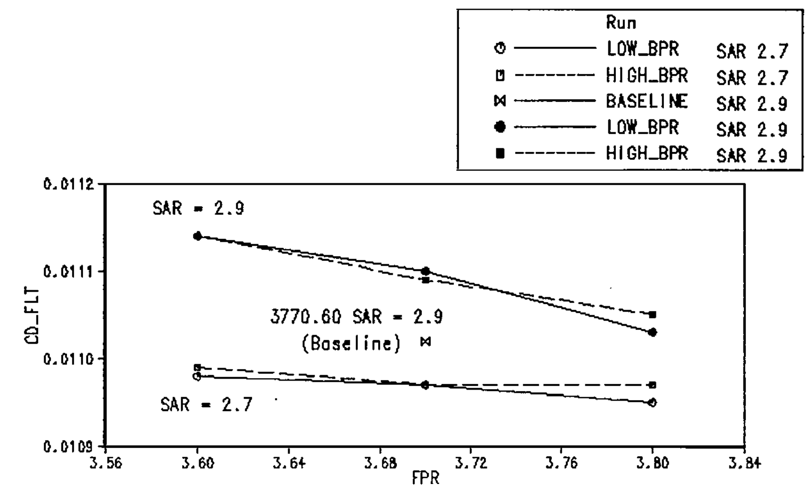

Linear theory drag results are shown for the Briquette engine cycles at Mach 2.4, CL=0.10. The 1504 baseline data point fell between the trend lines for the Briquette SAR=2.7 and 2.9 data. The SAR=2.7 data showed less drag sensitivity as fan pressure ratio increased than the SAR=2.9, and also had lower drag levels.

It was assumed that these drag trends due to engine cycle would apply equally to all the Prism planforms. The ΔCD for a given engine cycle on a given Prism planform was the difference between the cycle on this plot and the 3770.60, SAR2.9 baseline.

In Summary

- Drag increased from PTC to the parametric PTC (1504) due to improved drag accounting and geometry changes to accomodate parametric planform variations.
- (25) As-drawn configurations that vary in wing area were analyzed.
- L/D's of the "Prism" configurations vary from the 1504 by ±6% at Mach 0.9, CL=0.17, and ±1% at Mach 2.4, CL=0.1.
- High wing area and AR with > outboard LE sweep best for Mach 2.4 L/D.
- Large drag penalty for increased O/B thickness.
- Thickness trend of linear theory to NS CFD resulted in 10% increase in ΔCD.
- Configuration trend of linear theory to NS CFD consistent with previous wind tunnel data.

Several conclusions drawn from this study influenced the OAC airplane sizing. The wing planform effect helped drive the OAC toward an increased sweep outboard wing with increased wing area. The wing maximum thickness at a given WBL did not increase due to the large drag penalty. The suppressor area ratio (SAR) of the nozzle decreased from 2.9 to 2.7. Additionally, parametric drag build-ups using linear potential drag methods were improved in accuracy and ease of use.

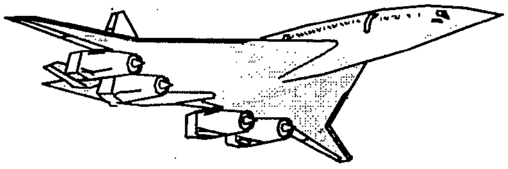

ACE Final Report

B.2 - Nonlinear Aerodynamics

Douglas E. Weigold
Suk C. Kim
Robert P. Narducci
Geojoe Kuruvila

Boeing Long Beach

December 31, 1998

Objective

- Provide Navier-Stokes aerodynamic performance data for a limited number of configurations of the OAC design space

- Establish trailing-edge closure angle limit for thickness perturbations

The primary objective of this study was to perform Navier-Stokes analyses of a limited number of configurations of the OAC design space. The performance data obtained from these analyses were used to increase the fidelity of the response surface generated from the linearized potential flow analyses of the configurations of the OAC design space.

The second objective was to determine the maximum thickness and consequently the largest trailing-edge closure angle that a PTC (1504) like configuration can have without causing flow separation at lift condition as high as 1.5g.

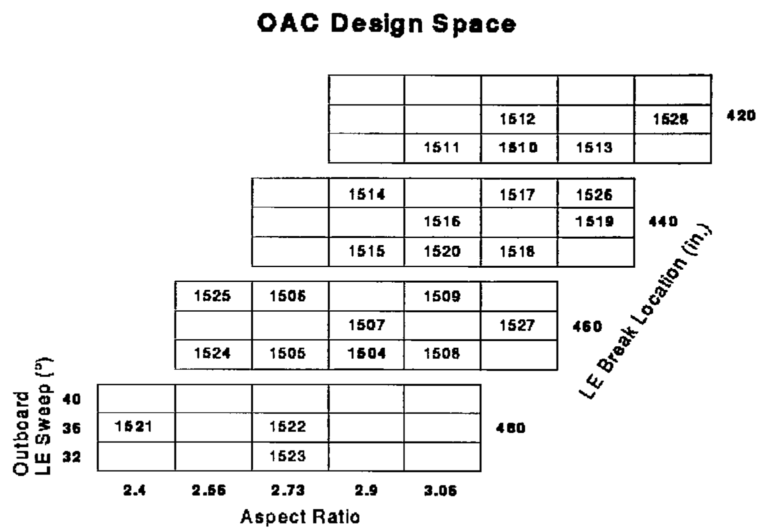

The OAC design space (also referred to as the Prism) is shown. Of the 25 configurations for which aerodynamic response surfaces were generated using a linearized potential analysis method, 4 configurations were selected for nonlinear "spot-checks". These configurations (shown in bold) are 1504, 1510, 1519 and 1521.

Prism Planforms Selected for CFD Analysis

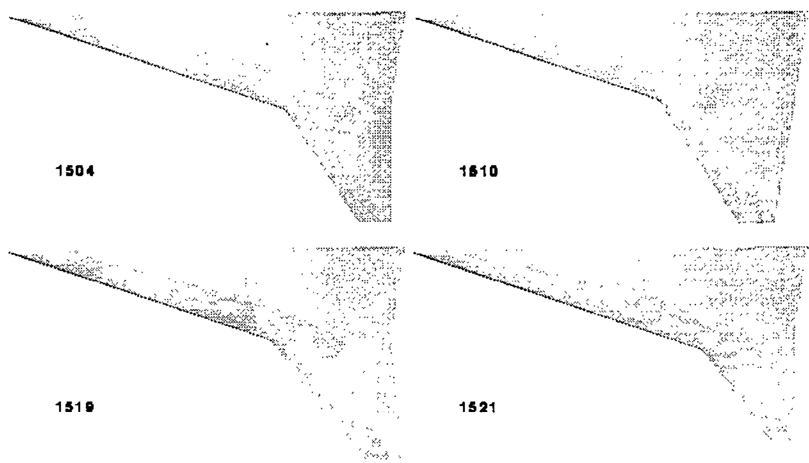

The planforms selected for CFD analysis are shown. These planforms were analyzed using CFL3D in the Navier-Stokes mode with Baldwin-Lomax turbulence model.

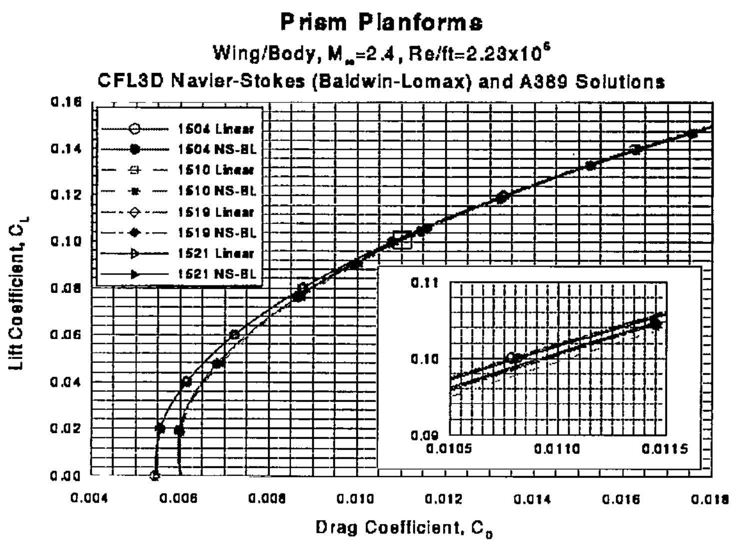

Comparison of the drag polars of 1504, 1510, 1519 and 1521 configurations, at M_∞ = 2.4 and Re/ft = 2.23x10^6, are shown. The linearized potential equation based predictions include pressure drag from the A389 panel code, viscous drag from an equivalent flat-plate method and a -1.0 count test-theory correction. The nonlinear analyses were performed using CFL3D in the Navier-Stokes mode with the Baldwin-Lomax turbulence model. Around cruise (C_L=0.1), the CFD prediction is about 0.9-2.3 counts higher than the linear-theory based values.

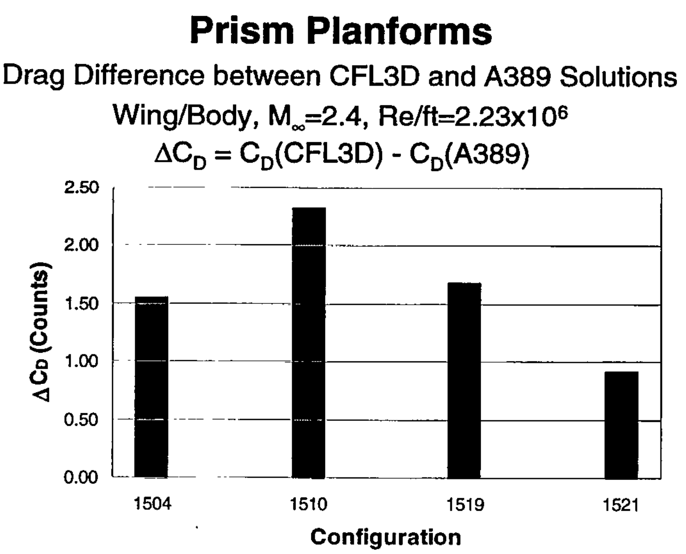

Comparison of the drag difference between CFL3D and A389 solutions for 1504, 1510, 1519 and 1521 configurations, at M_∞ 2.4, Re/ft = 2.23x10^6 and C_L =0.1, are shown. The CFD prediction is about 0.9-2.3 counts higher than the linear-theory based estimates. One count of the difference is from the test-theory correction and the rest is, mostly, due to the difference in pressure drag. These drag trends were used to correct the drag obtained from linear-theory analyses for all the prism planform configurations.

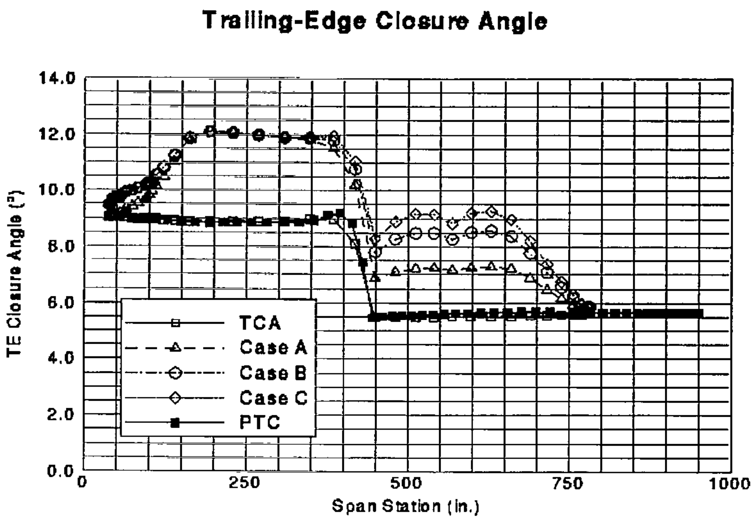

In order to improve the structural/aeroelastic viability of the OAC, it was necessary to increase the wing thickness, especially near the outboard nacelle and the outboard wing panel, without degrading the flow quality on the wing. A study was performed to determine the largest trailing-edge (TE) closure angle that the PTC (1504) configuration can have without causing flow separation at Mach 2.4, 1.5g flight condition (Re/ft = 2.23×10^6). Since the PTC OML was not available at that time, the TCA wing/body configuration was selected for this investigation.

Starting with the TCA wing/body configuration, several thicker wings were generated by perturbing the geometry at 5 span-stations. Two of these stations were on the inboard wing, one at the break and the remaining two on the outboard wing. The two inboard stations and the one at the break were perturbed using the Hicks-Henne functions and the two outboard stations were scaled up.

The figure shows the TE closure angles of TCA, PTC and three perturbed TCA configurations, namely Case A, Case B and Case C. The TE closure angles on the TCA and PTC are about 9° and 5.5° for the inboard and the outboard wing, respectively. The thickest wing, Case C, has about 12° TE closure angle on the inboard wing and about 9° on the outboard wing.

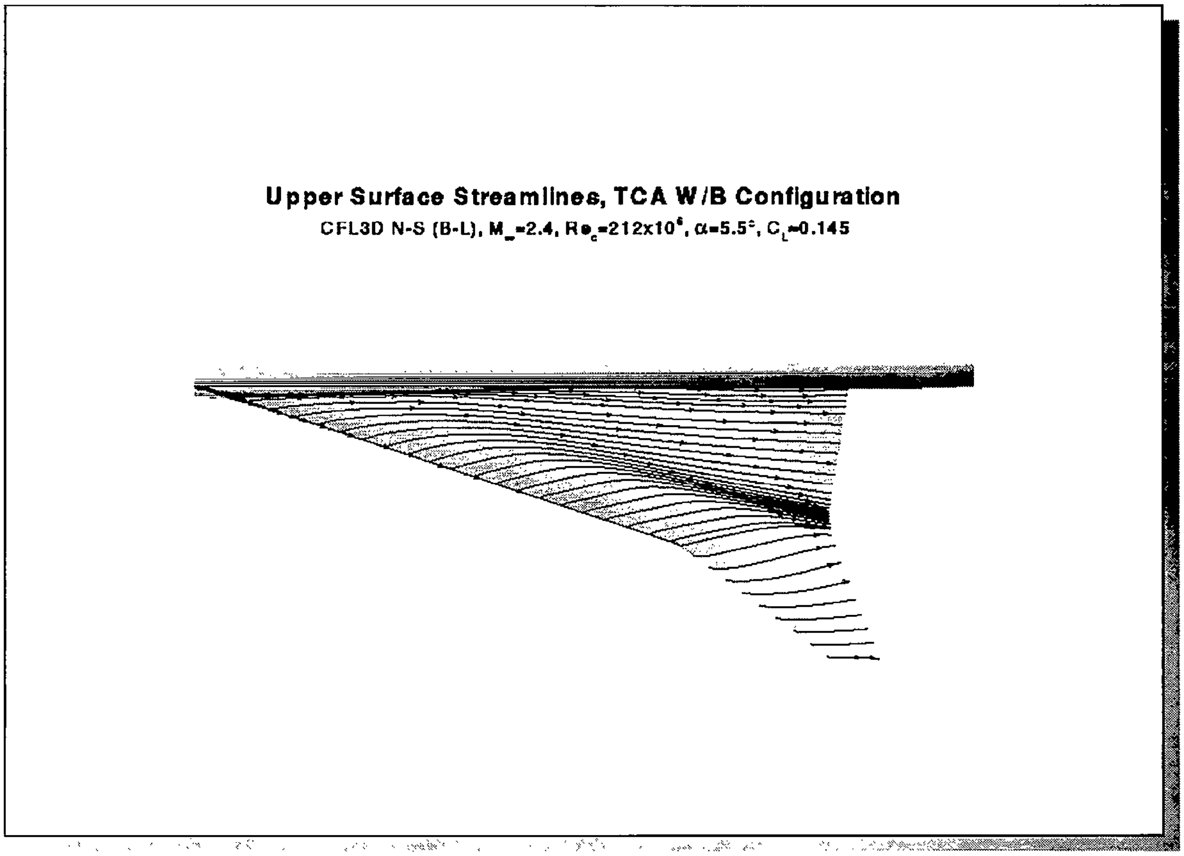

The nonlinear aerodynamic analyses at Mach 2.4, 1.5g flight condition (α=5.5°, $C_L \approx 0.145$, Re/ft = 2.23x10^6) were performed using CFL3D with the Baldwin-Lomax turbulence model. The upper surface streamlines for the TCA and Case C, presented in the next two figures, show that for both cases the flow is attached. Although the streamline patterns for both the configurations looks the same, there are subtle differences.

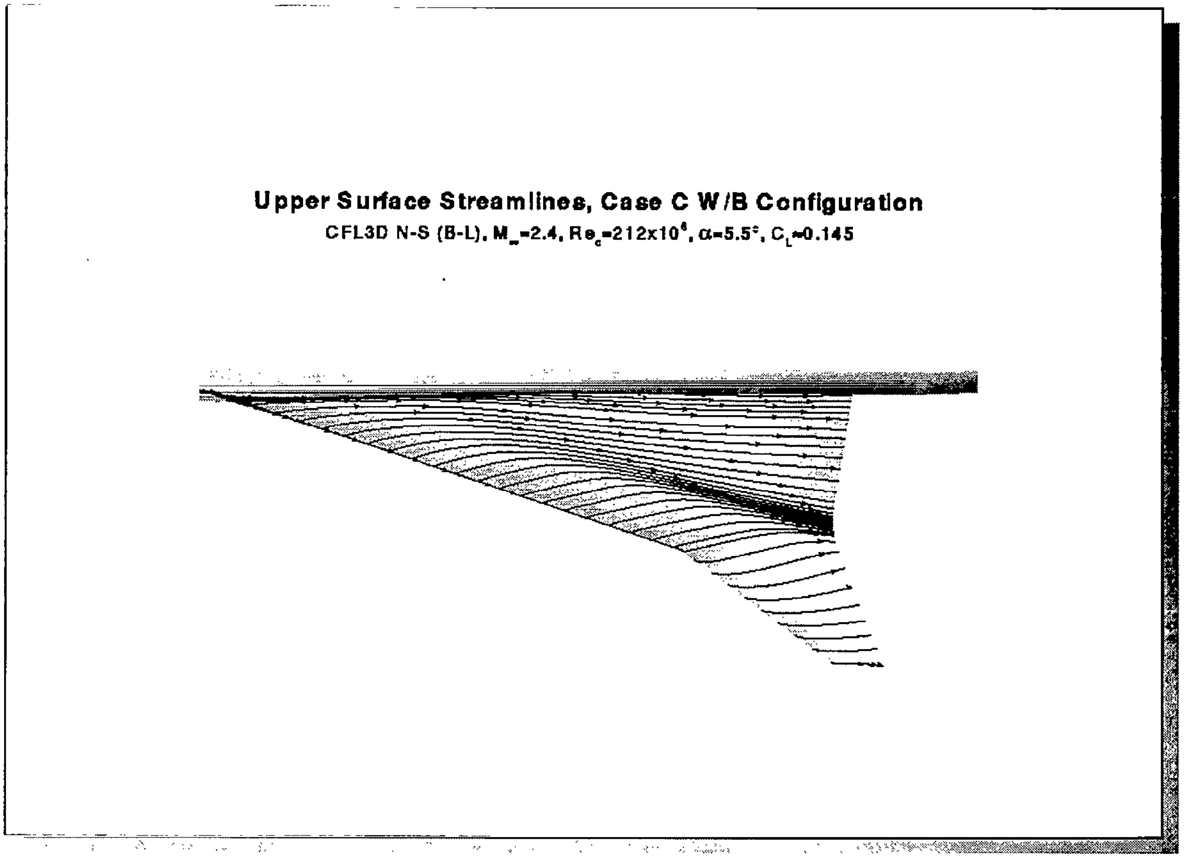
Upper Surface Streamlines, Case C W/B Configuration
CFL3D N-S (B-L), M_∞=2.4, Re_c=212x10^6, α=5.5°, C_L=0.145

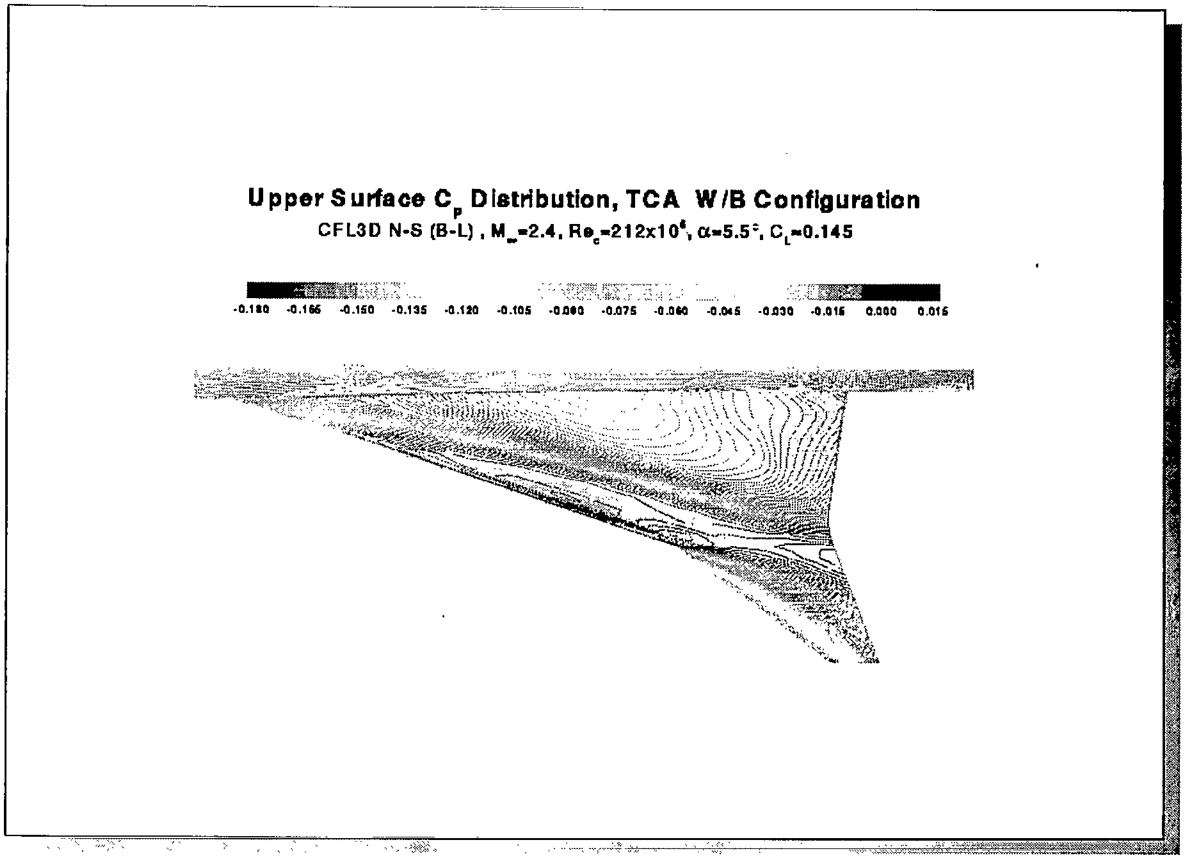

The upper surface pressure distributions for the TCA and Case C are shown in the next two figures. The 100% vacuum C_p, at Mach 2.4, is -0.248. From the surface pressure for the Case C, it can be seen that in the vicinity of the trailing-edge break-location, the C_p is about -0.186. This level of pressure, which is about 75% of the vacuum Cp, is considered to be close to the separation pressure.

Upper Surface C_p Distribution, Case C W/B Configuration

CFL3D N-S (B-L), M_∞=2.4, Re_c=212x10^6, α=5.5°, C_L=0.145

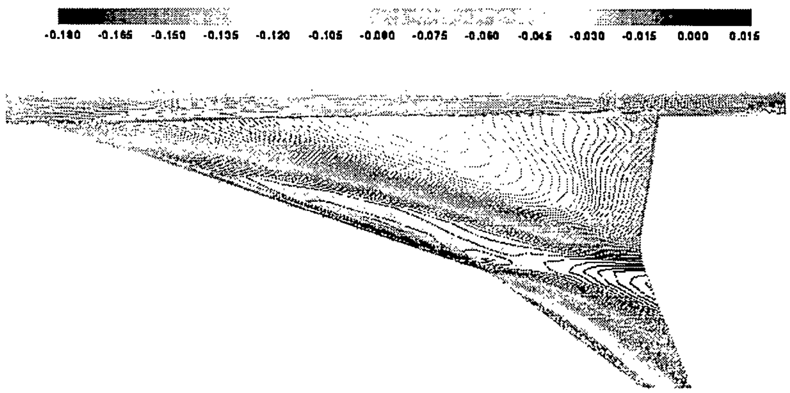

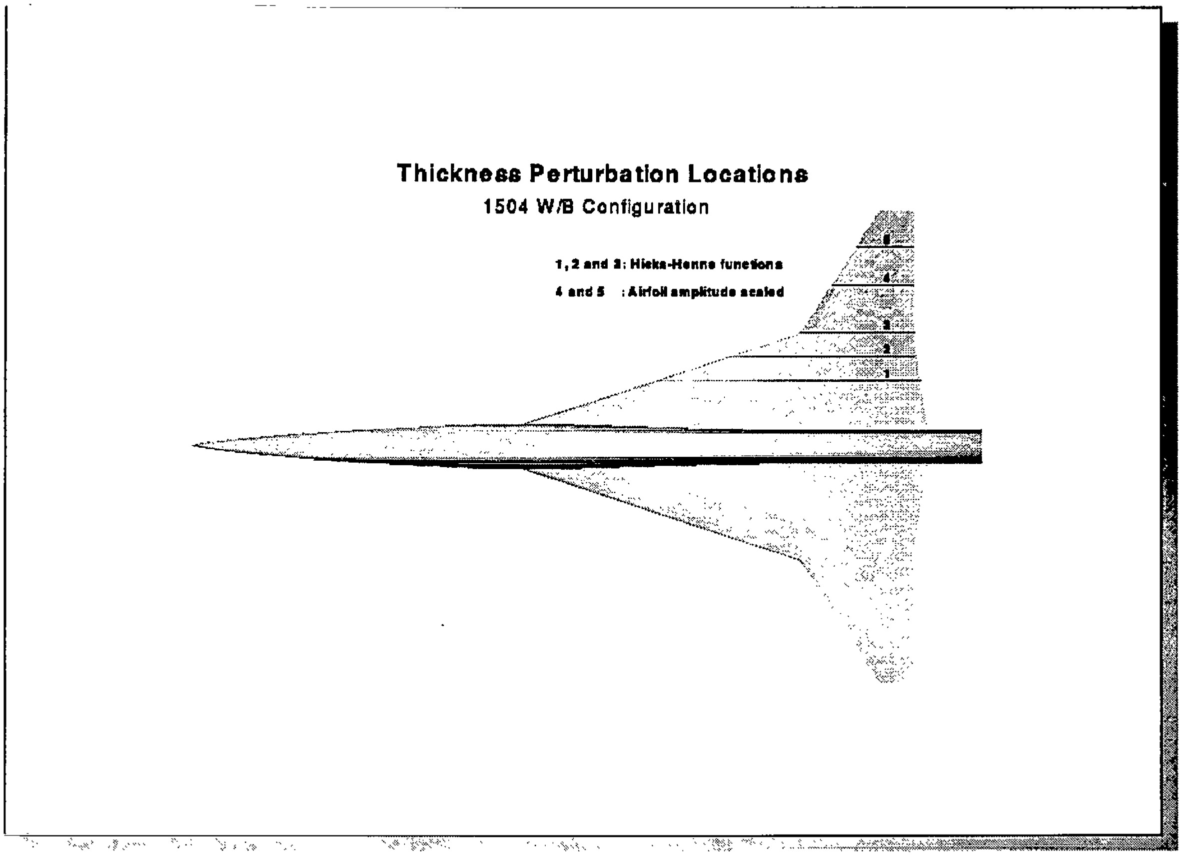

Based on the TE-angle limit study conducted on the TCA, 5 span-stations were selected on the 1504 (PTC) configuration to perturb the thickness. Stations 1 and 2 were the locations of the inboard and outboard nacelles, respectively. Station 3 was the leading-edge break location and stations 4 and 5 were on the outboard wing at BL 665 and BL 808 respectively.

Stations 1, 2 and 3 were perturbed using the Hicks-Henne functions. Stations 4 and 5 were perturbed by scaling the amplitudes of the airfoil sections.

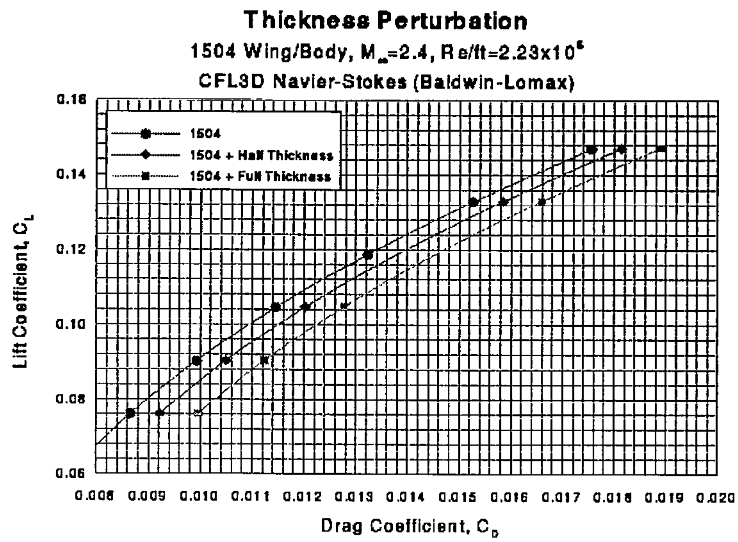

The drag polar for the 1504 configuration is compared with the drag polars for 1504 with all the thickness variables perturbed by a certain amplitude (referred to as 1504 + Half Thickness) and twice that amplitude (referred to as 1504 + Full Thickness). The maximum perturbation was such that the trailing-edge angle was limited to the maximum value established by the previous study.

The nonlinear aerodynamic analyses at Mach 2.4, 1.5g flight condition (α=5.5°, $C_L \approx 0.145$, Re/ft = 2.23×10^6) were performed using CFL3D with the Baldwin-Lomax turbulence model. As expected, when the thickness of the geometry is increased, the drag also increases. These drag trends were used to correct the drag obtained from linear-theory analyses for all the "thickness perturbed" 1504 configurations.

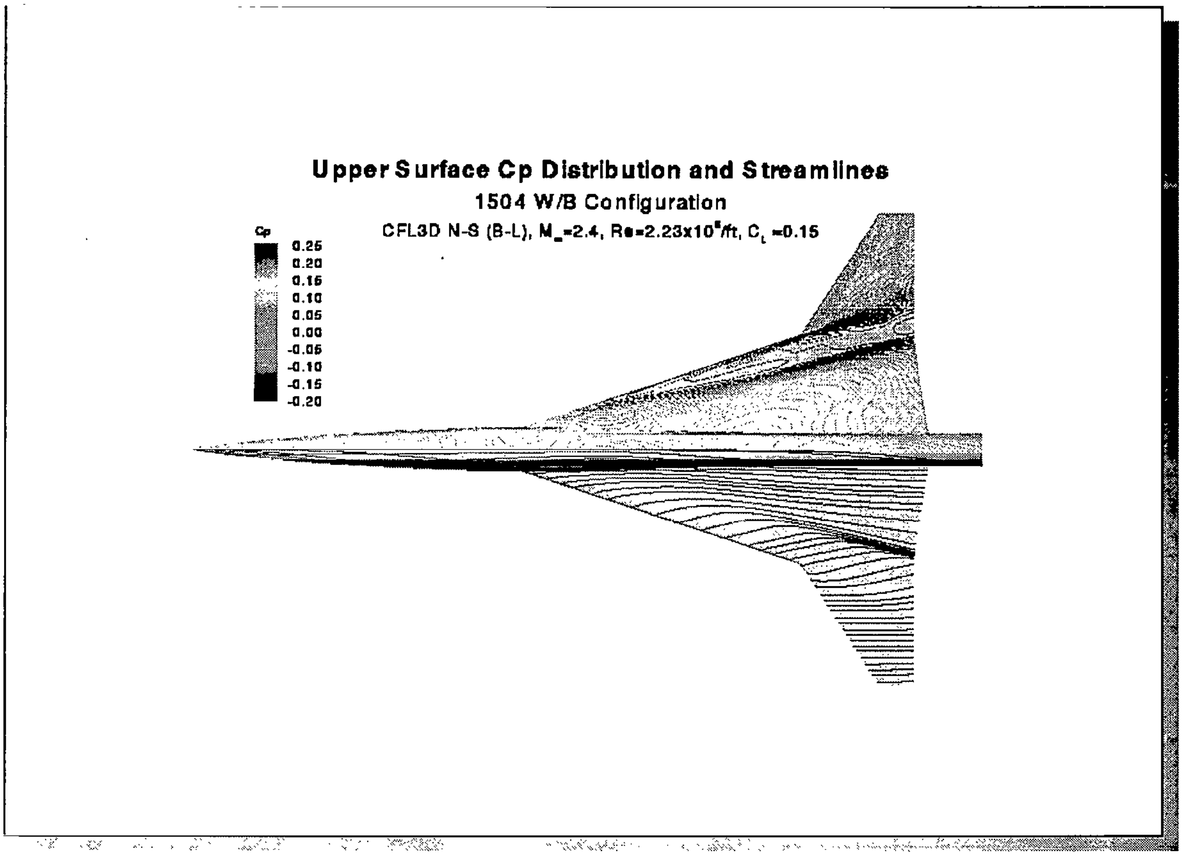

The upper-surface pressure distributions and the streamline patterns for 1504, 1504 + Half Thickness and 1504 + Full Thickness configurations are shows in the next 3 figures. At Mach 2.4, 1.5g flight condition ($C_L \approx 0.15$, Re/ft = 2.23×10^6) the flow is attached.

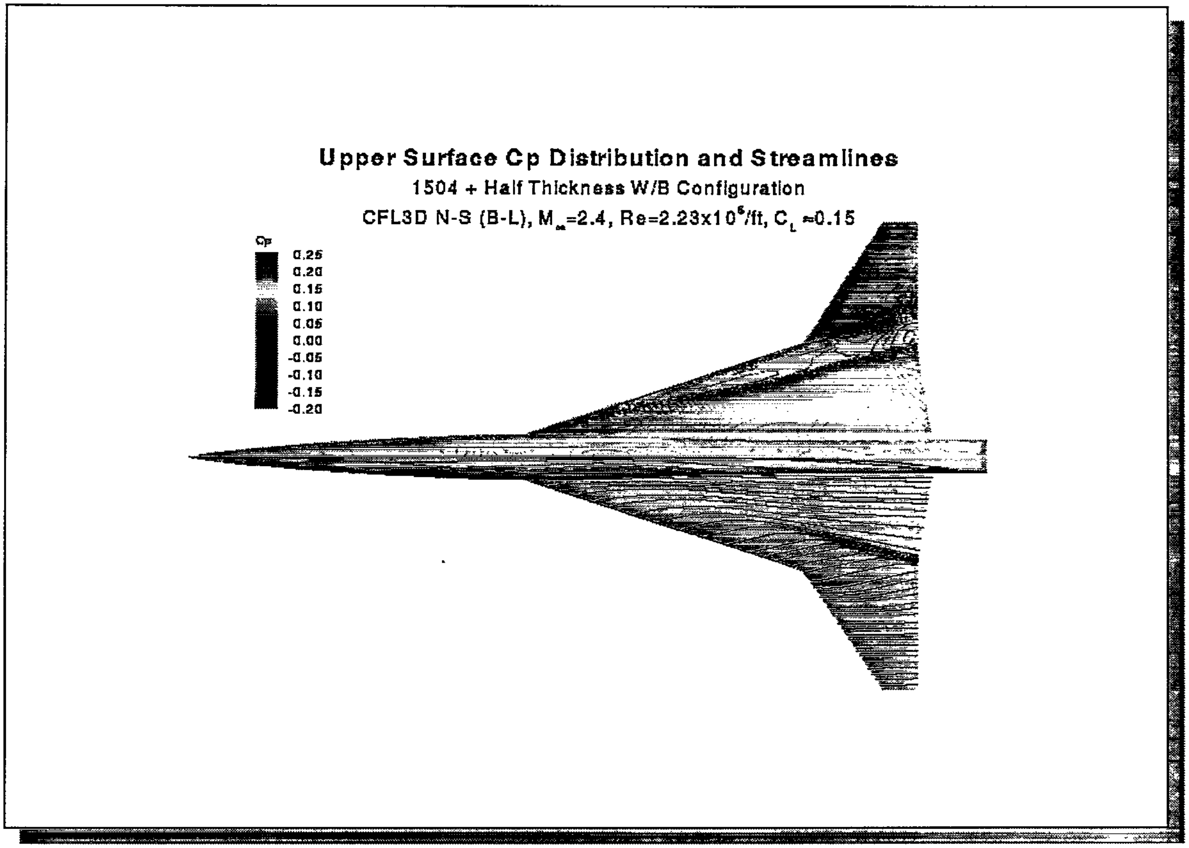
Upper Surface Cp Distribution and Streamlines
1504 + Half Thickness W/B Configuration
CFL3D N-S (B-L), M∞=2.4, Re=2.23x10⁶/ft, C_L ≈0.15
Cp
0.25
0.20
0.15
0.10
0.05
0.00
-0.05
-0.10
-0.15
-0.20

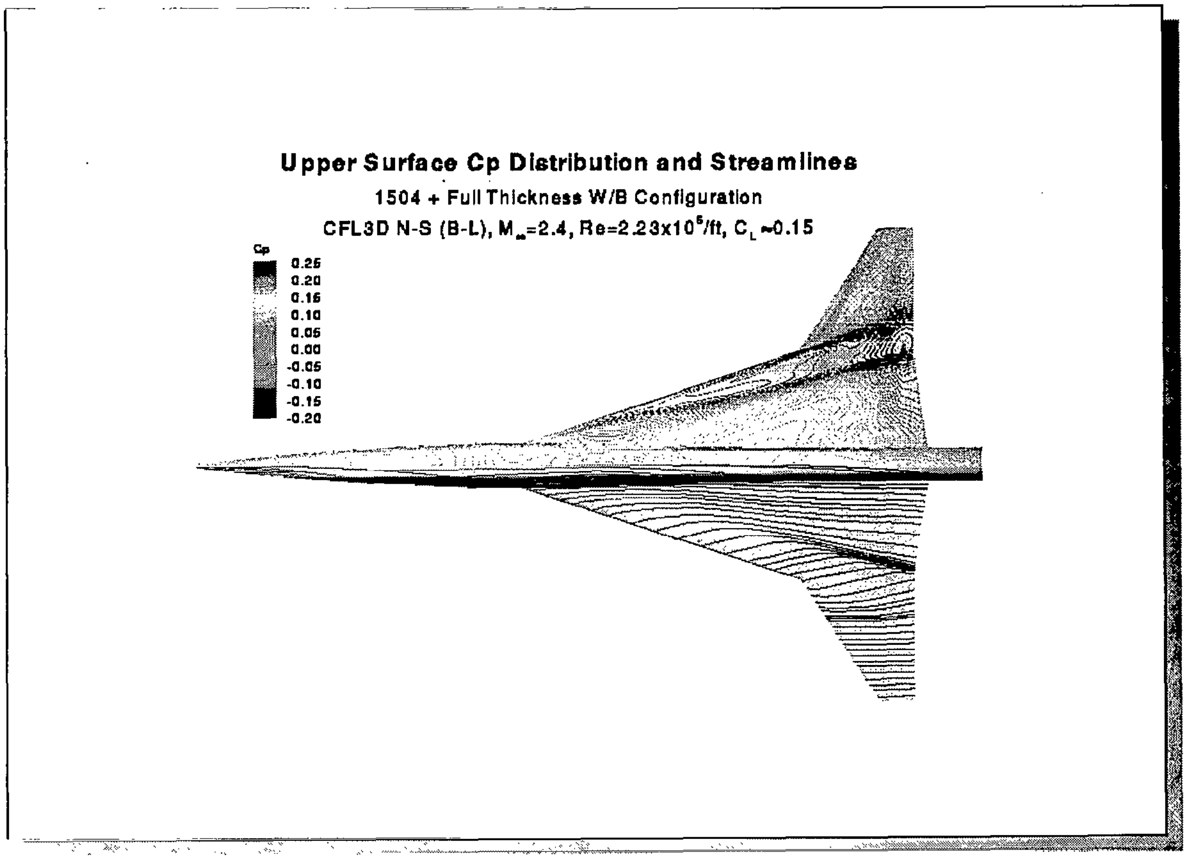
Upper Surface Cp Distribution and Streamlines
1504 + Full Thickness W/B Configuration
CFL3D N-S (B-L), M_∞=2.4, Re=2.23x10^6/ft, C_L≈0.15
Cp
0.25
0.20
0.15
0.10
0.05
0.00
-0.05
-0.10
-0.15
-0.20

Summary

- The fidelity of the aerodynamic response surface, obtained from linear-theory based method, was improved using nonlinear solutions obtained for a limited number of configurations.

- Based on the trailing-edge closure angle study, the thickness perturbations of the 1504 were constrained.

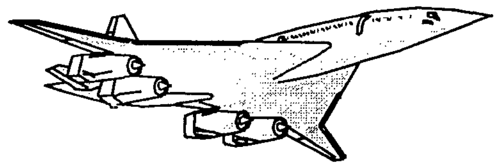

ACE Final Report

B.3 - Nonlinear Aerodynamics

Larry Green

NASA Langley

December 31, 1998

PTC Nonlinear Aerodynamics
NASA Langley Tasks

- Fund GeoLab to produce one grid for the Preliminary Technology Configuration (PTC) airplane with wing-body-nacelle-diverter-flaps (WBNDF) using the existing process by the end of May 1998 and modified grids for various flap settings and resized engines
- Green (MDOB) and Biedron (AAMB) to compute nonlinear aerodynamics with CFL3D code for PTC and selected "Prism" configurations by the end of June 1998
  - Examine transonic effects of several outboard flap settings on WBND configuration aerodynamics
  - Examine transonic effects of resized (10% larger and smaller airflow) nacelles in combination with flaps
- Fund GeoLab to develop and demonstrate automated grid modification / generation process for WBNDF configurations

In order to study nonlinear aerodynamic effects of flaps and engine airflow rates within the ACE/DOSS system, the NASA Langley Research Center Geolab was funded to create a baseline computational fluid dynamics (CFD) grid for the Preliminary Technology Configuration (PTC), wing-body-nacelle-diverter-flap (WBNDF) configuration. Geolab was also expected to construct several perturbations of the baseline grid for various flap settings and larger and smaller engines (corresponding to 10% larger and smaller engine airflow rates). Researchers from the Multidisciplinary Optimization Branch and the Aerodynamic and Acoustics Methods branch were then expected to conduct nonlinear aerodynamics studies at several transonic flight conditions (Mach, angle of attack, and flap settings) with the various grids. Similar work was previously performed during fiscal year 1997 for Technology Concept Airplane (TCA) with different engines, and without flaps, in support of the Preliminary Aeroelastic Concept airplane definition. Geolab was also funded to develop and demonstrate an automated process for grid modification / generation for WBNDF configurations.

PTC Nonlinear Aerodynamics
NASA Langley Accomplishments

- Many questions affecting the PTC WBNDF grid topology, blocking, and surface grid layout were unresolved until early in May 1998
  - Flap arrangement, location of hinge lines, and deflection schedule
  - Nacelle inlet and nozzle details
  - Ignore empenage (canard, tails, and chin fin)
- First grid (~15 million points) produced for PTC configuration produced by GeoLab by June 30, 1998
  - Determined to be too large for practical use, yet did not correctly represent important details about the nacelles
  - Subsequent discussion with ACE Aero Working Group resolved the modeling issues but required a substantial effort by GeoLab to re-grid around nacelles
- Second grid (~8 million points) produced by GeoLab by August 7, 1998
  - Essentially too late for Technology Configuration (TC) planning
  - Still some hope of getting results into the final ACE document

Discussion about the PTC gridding began in the late fall (November - December) of 1998 and continued through early May 1998, when most the questions affecting the grid topology, blocking, and surface grid layout were preliminarily resolved. The most significant questions that needed to be answered involved the details of the flaps (location of cuts and hinge line and the flap deflection schedule) and inlet / nozzle details. Until these questions could be answered in a satisfactory way, gridding could not proceed. A decision was made to ignore the emenage in this modeling, since they would only complicate the gridding process. Having resolved the questions, an initial grid of about 15 million points was produced by June 30, 1998. The grid was determined to be too large for practical use and still did not accurately represent some details about the nacelles. Subsequent discussion with the Aerodynamic Working Group satisfactorily resolved the remaining questions, while simplifying the grid structure, but required a significant regridding effort around the nacelles. A second grid of about 8 million point was delivered on August 7, 1998, which was essentially too late for CFD analyses to be included in Technology Configuration (TC) planning by early September 1998. However, there was still some hope of including nonlinear aerodynamic results in the ACE final documentation.

PTC Nonlinear Aerodynamics
NASA Langley Accomplishments (Continued)

- PTC grid characteristics
  - 34 grid blocks
  - 56 surface grid objects
  - 204 grid block faces (both point-matched and patched interfaces)
- PTC grid sizes
  - Coarse: 143,729 points; 32x55x17 = 29,920 points in largest grid block; 32x96x23 = 70,656 required maximum block dimensions
  - Medium: 1,041,374 points; 63x109x33 = 226,611 points in largest grid block; 63x191x45 = 541,485 required maximum block dimensions
  - Fine: 7,917,050 points; 125x217x65 = 1,763,125 points in largest grid block; 125x381x89 = 4,238,625 required maximum block dimensions

The second grid produced by Geolab included 34 grid blocks. There were 56 surface grid objects among the 34 blocks. The 34 grid blocks included 204 grid block faces of both point matched and patched varieties. Some grid block faces would also include several boundary condition regions or segments, as subsets of one entire grid block face. As delivered, the baseline grid included 15 degree flap deflections on the outboard wing panel, but these could easily be change to other deflection angles including zero flap deflection.

The grid delivered (fine) included 7,917,050 grid points; the largest single grid block was 125x217x65 = 1,763,125 grid points; the maximum grid block dimensions over all the grid blocks was 125x381x89 = 4,238,625 grid points. Two coarsened version of the fine grid were produced by twice removing every other point in each grid block direction. The medium grid included 1,041,374 grid points with a largest single block of 63x109x33 = 226,611 grid points, and maximum block dimensions of 63x191x45 = 541,485 grid points. The coarse grid included 143,729 grid points with a largest single block of 32x55x17 = 29,920 grid points, and maximum block dimensions of 32x96x23 = 70,656 grid points.

PTC Nonlinear Aerodynamics
NASA Langley Accomplishments (Continued)

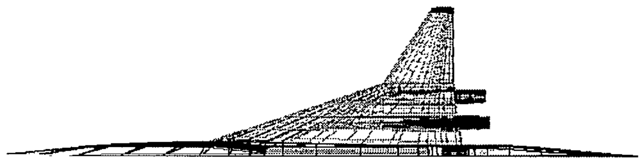

PTC planform view; colors indicate distinct surface objects; coarse grid

The figure shows a planform view of the PTC upper surfaces from the coarse grid. The colored regions represent distinct surface grid block regions. The emenange (canard, tails, and chin fin) were not represented in this grid.

PTC Nonlinear Aerodynamics
NASA Langley Accomplishments (Continued)

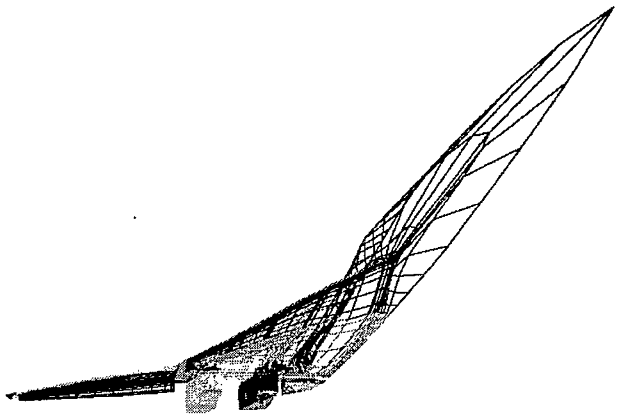

PTC underside; colors indicate distinct surface objects; coarse grid

The figure shows the PTC underside, looking downstream from the coarse grid. The colored regions represent distinct surface grid block regions. The emenange (canard, tails, and chin fin) were not represented in this grid. Deflection of the outboard flaps can be observed.

PTC Nonlinear Aerodynamics
NASA Langley Accomplishments (Continued)

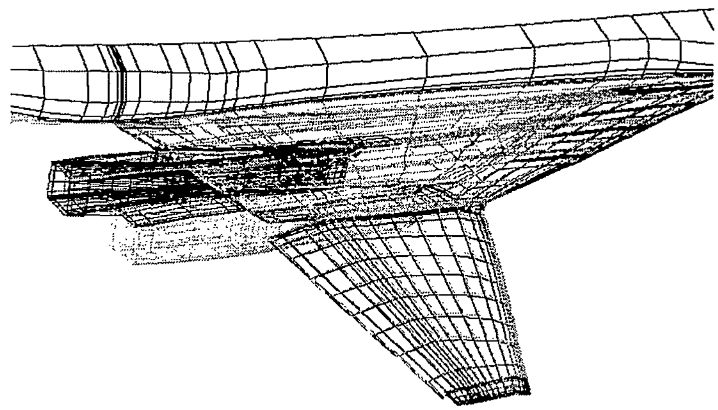

PTC wing; colors indicate distinct surface objects; coarse grid

The figure shows the PTC wing from the coarse grid. The colored regions represent distinct surface grid block regions. The emenange (canard, tails, and chin fin) were not represented in this grid. Deflection of the outboard flaps can be observed.

PTC Nonlinear Aerodynamics
NASA Langley Accomplishments (Continued)

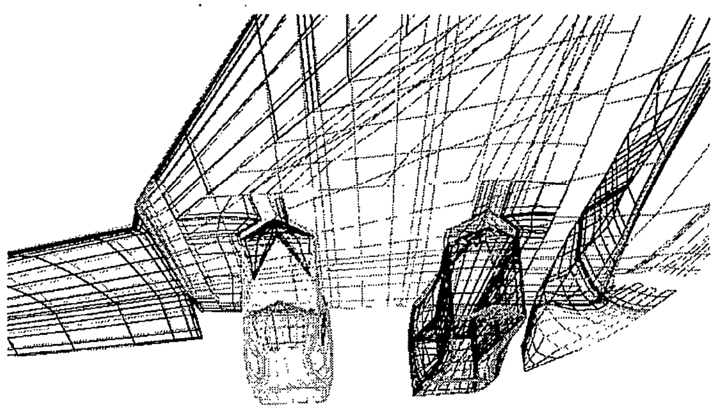

PTC nacelle detail; colors indicate distinct surface objects; coarse grid

The figure shows the PTC underside detail around the nacelles and flaps, looking downstream from the coarse grid. The colored regions represent distinct surface grid block regions. The emenange (canard, tails, and chin fin) were not represented in this grid. Deflection of the outboard flaps can be observed.

PTC Nonlinear Aerodynamics
NASA Langley Accomplishments (Continued)

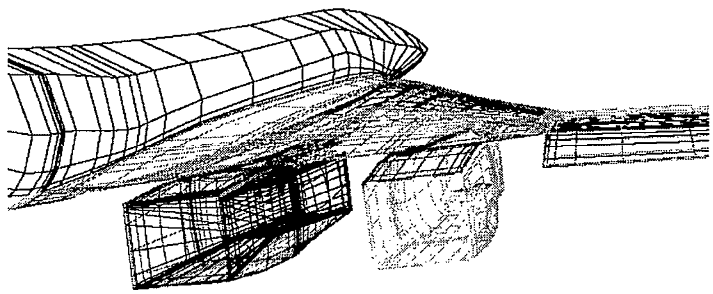

PTC nacelle aft end detail; colors indicate distinct surface objects; coarse grid

The figure shows aft end detail of the nacelles and flaps, looking upstream from the coarse grid. The colored regions represent distinct surface grid block regions. The emenange (canard, tails, and chin fin) were not represented in this grid. Deflection of the outboard flaps can be observed.

PTC Nonlinear Aerodynamics
NASA Langley Accomplishments (Concluded)

- No nonlinear aerodynamics computed
  - Lack of tools to automatically generate the input files for CFL3D and associated pre-processor codes for complex configuration grids
  - Inability to manually generate the required input files for the grid in the time available for the task
  - New task being established for Geolab to produce correct inviscid flow input files with each grid produced
- Semi-automated grid modification process (surface rubberization) developed by Geolab for WBNDF configurations
  - Assumes flap arrangements and hinge lines are known in advance or can be developed along with the surface grid
  - Assumes flaps deflect smoothly through a range of deflection angles without crossing through nacelles or gaps opening; problems to be handled manually on case by case basis
  - Assumes surface grid lines align with flap and hinge cuts or that ragged surface deformation is acceptable
  - Demonstrated but may not be without bugs
  - Similar assumptions would be required for automatic grid generation

As of this point, no nonlinear aerodynamic solutions have been computed with this set of grids for the PTC. This is due to the lack of tools to automatically generate the required input files for CFL3D and its associated pre-processor codes for complex grids. The information provided by Geolab detailing the block interface bounds was not correct and the required input files for CFL3D and the pre-processors could not be constructed manually in the time available for the task. As a result of this experience, a new task is being established to require that correct inviscid flow input files be provided with each grid produced by Geolab.

Geolab was successful in developing and demonstrating a semi-automated modification process for WBNDF grids. The process, however, makes several important assumptions about the geometry being modeled. Specifically, the process assumes: 1) that flap arrangements and hinge lines are available in advance of the process, or can be determined along with the surface grid layout, 2) that flaps deflect smoothly through a range of deflection angles without cutting through other surfaces (such as nacelles), or without opening gaps (unporting) in the surface geometry, 3) any problems encountered with respect to item 2 can be handled manually, 4) that surface grid lines align with flap cuts and hinge lines or that ragged surface deformation is acceptable. The process was demonstrated on one example and may not be without bugs. Similar assumptions would be required for any automated or semi-automated grid generation process, of which most of the pieces already exist at Geolab, but these were not specifically connected together for such purpose.

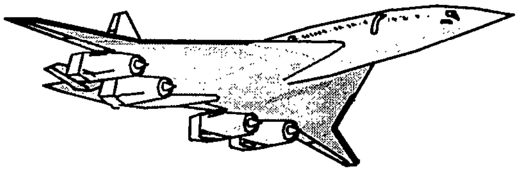

ACE Final Report

C - Nonlinear Loads

December 31, 1998

Outline for Appendix C

C.1 Nonlinear Loads Process and Results - Boeing Long Beach

- **Nonlinear Loads Process Improvements and Results**
- **Nonlinear Aerodynamic Database Generation for PTC**

C.2 Nonlinear Loads Process and Results - NASA Ames

- **Uncertainty in CFD Solutions for Loads at High-α Flow Conditions**
- **Validation Study with TCA Configuration**

In Appendix C, developments performed by the Nonlinear Loads Working Group are documented. The first part of the appendix presents work done on the nonlinear loads process and results generated at Boeing - Long Beach, including the nonlinear loads process improvements and results, and nonlinear aerodynamic database generation for the PTC configuration. In the second part of the appendix, work done on the nonlinear loads process and results obtained at NASA Ames are presented. This includes the study on uncertainty in the CFD solutions for loads at high angle-of-attack flow conditions in order to evaluate the requirements for accurately predicting the aerodynamic loads on the PTC configuration at transonic, high angle-of-attack flow conditions (which also provides an independently generated set of numerical results for comparison with CFL3D results), and the validation study with the TCA configuration.

Section C.1

Nonlinear Loads Process and Results
(Boeing - Long Beach)

High Speed Research
Aeroelastic Concept Engineering - ACE

Outline for Section C.1

- **Nonlinear Loads Process Improvements and Results**
  - **Improvements in the Nonlinear Loads Process**
  - **Application of Nonlinear Loads Process to TCA (Cont'd from FY97)**
  - **Application of Nonlinear Loads Process to PTC**
- **Nonlinear Aerodynamic Database Generation for PTC**

The first part of this section documents the improvements in the nonlinear loads process developed since the PAC, and the results generated from applying the process to the TCA and PTC configurations. The generation of the nonlinear aerodynamic database using CFD is documented in the second part of this section.

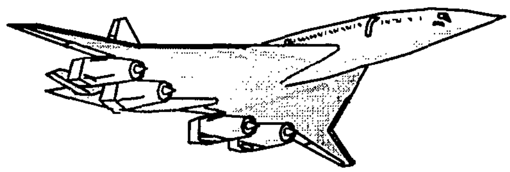

ACE Final Report

C.1.1 - Nonlinear Loads Process Improvements and Results - Boeing LB

Kuo-An Yuan
Myles Baker
Tim Allen
Patrick Goggin
Joseph Giesing

December 31, 1998

C.1.1.1 Improvements in Nonlinear Loads Process

- **Approach Used in Generating Representative Deflections**
  - **Use Appropriate Rigid-α to Replace SVD/Splining Procedure**
  - **Validation Study Performed on MDC 2.4-7A Showed Better Correlation with Aeroelastically Deflected CFD Results Using Rigid-α Approach**
  - **Significantly Simplifies Effort Required to Generate Aerodynamic Database**
- **Iteration Between Local Equivalence Corrections and Nonlinear Loads Analysis**
  - **Automate the Iteration Process Using New Capability (ISHELL) in NASTRAN Version 70.5**
    - **Save Manpower**
    - **Save Iteration Process Time (Both CPU Time and Real Time)**
    - **Minimize Computer Disk Storage Requirement During Iteration**

Since the completion of the Preliminary Aeroelastic Concept (PAC) report, several improvements were made to the nonlinear loads process. The "representative deflections", used in the the generation of the aerodynamic database, were changed to reflect a rigid aircraft at appropriate angle-of-attack. Compared to generating the "representative deflections" using the singular value decomposition (SVD) and splining procedure, this approach significantly simplifies the effort required to generate the aerodynamic database. A validation study performed on the MDC 2.4-7A configuration (which will be presented next) showed that results produced using the rigid-α approach is better than that generated from the SVD/splining procedure when they were correlated with the aeroelastically deflected CFD results.

The iteration between the local equivalence corrections and the nonlinear loads analysis was performed manually in the past. With a new capability (ISHELL) available in NASTRAN version 70.5, which allows NASTRAN to interact with user programs, this iteration process was automated using NASTRAN DMAP ALTER to make NASTRAN interact with the CORRECT program, which performs the local equivalence corrections, directly. This automated iteration process not only saves manpower and computing time, including both CPU time and real time, but also minimizes the disk storage requirement during the iterations since the process deals with one load case at a time until it finishes the requested number of iterations.

Improvements in Nonlinear Loads Process (Cont'd)

- **Computer Code for Critical Load Identification (CRLOAD)**
  - **Incorporate Dynamic Memory Allocation**
  - **Implement Design Criteria Used in TCA Configuration**
- **Computer Code for Local Equivalence Corrections (CORRECT)**
  - **Upgraded to Enable the Code Handle More Complicated Load Cases in the CFD Database for PTC Configuration (e.g., Different Control Surface Deflections at Same Mach Number but Different Angles of Attack)**

The computer code CRLOAD, which performs the critical load identification, requires large memory space at run-time. This code was upgraded to incorporate dynamic memory allocation to more efficiently manage the run-time memory space usage. In addition, the design criteria for the TCA configuration, which are much more complicated than those used for the MDC 2.4-7A, were also implemented in the CRLOAD program.

The computer code CORRECT, which performs the local equivalence corrections, was upgraded so that it can handle the more complicated load cases in the CFD database, such as different control surface deflections at the same Mach number but different angles of attack, for the PTC configuration,

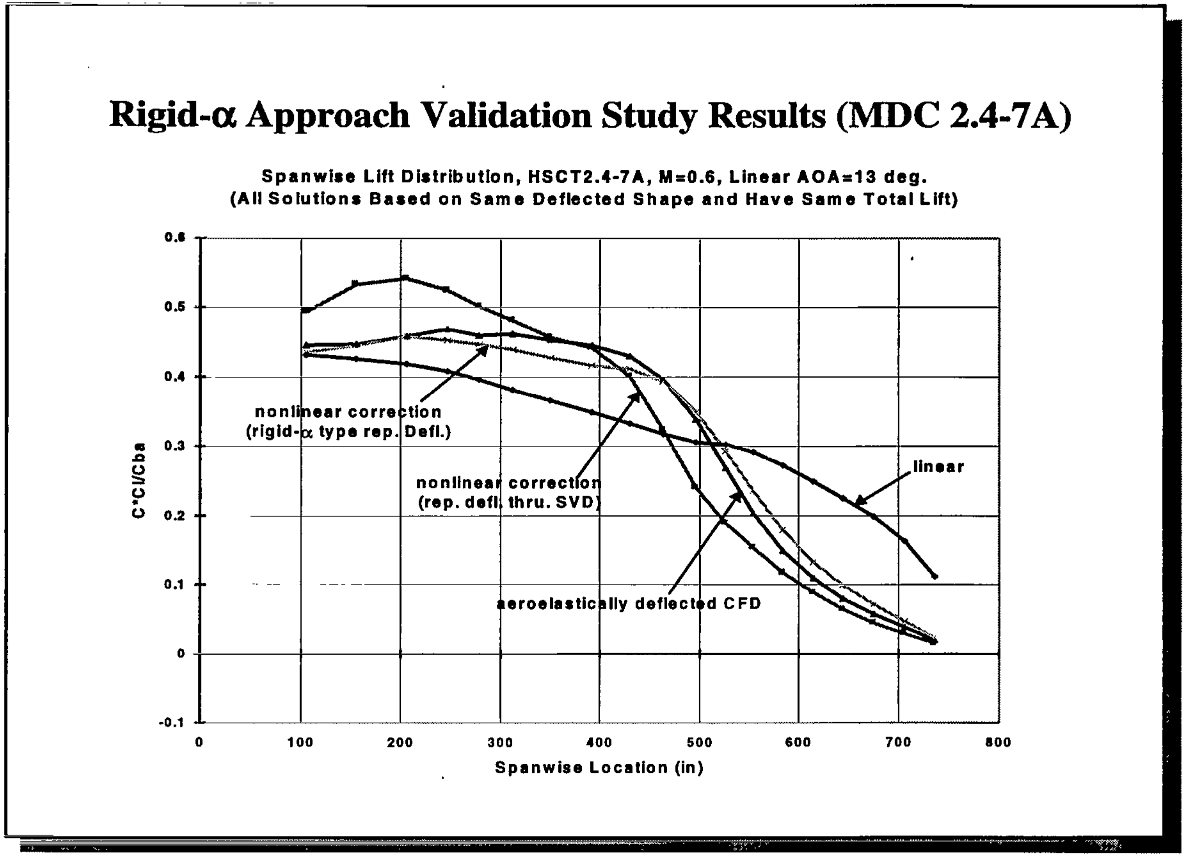

The nonlinear loads process has been improved to reflect lessons learned from process development and previous validation studies. The "representative deflections" used in the generation of the aerodynamic database are changed to reflect a rigid aircraft at appropriate angles of attack (α). This approach significantly simplifies the effort required to generate the aerodynamic database.

A validation study was performed to evaluate the fidelity of the load distribution obtained from the updated process. This study was performed on the MDC 2.4-7A configuration at Mach 0.6 and consisted of a comparison of spanwise lift distributions computed from the updated process, the previously developed process (which uses a singular value decomposition procedure to generate "representative deflections" for the aerodynamic database generation by CFD analyses), the CFD analysis on aeroelastically deflected geometry and the linear analysis. All solutions were performed based on the same deflected shape and the spanwise lift distributions obtained from these solutions has been scaled such that all approaches yield the same total lift. A new aerodynamic database, consisting of pressure distributions from three rigid-α type CFD solutions, was generated for this study. The results from this study showed that while both the updated process and the previously developed process produced spanwise lift distributions having the same trend as that obtained from the CFD analysis, it is evident that results from the updated process had a better correlation with the aeroelastically deflected CFD results.

C.1.1.2 Application of Nonlinear Loads Process to TCA (Cont'd from FY97)

- Steps Completed in FY 97
  - Linear Loads Analysis
  - Generate Representative Deflections
  - Compute CFD Solutions on Rigid Deflected Geometry to Generate Nonlinear Aerodynamic Database
- Nonlinear Loads Process on TCA is Completed with the Application of Following Steps:
  - Local Equivalence Correction
  - Nonlinear Loads Analysis
  - Iterate the Above Two Steps Until Convergence
  - Critical Load Identification

The application of the nonlinear loads process to the TCA configuration started in Fiscal Year '97. The steps in the process which were completed in Fiscal Year '97 include the linear loads analysis, the generation of representative deflections and the generation of the nonlinear aerodynamic database by computing CFD solutions on rigid deflected geometry. These completed steps have been documented in the deliverable report on Preliminary Aeroelastic Concept (PAC). The remaining steps of the nonlinear loads process for TCA include the iteration between local equivalence correction and the nonlinear loads analysis until convergence, and the critical load identification. These remaining steps for TCA have been completed and are documented in this report.

Local Equivalence Correction (TCA)

- Performed on 456 Load Cases Over 5 Mach Numbers (M=0.8, 0.95, 1.2, 1.6 and 2.0)
- Local Equivalence Correction/Nonlinear Loads Analysis Iteration
  - Used the Automated Iteration Process Developed Through the New Capability (ISHELL) in NASTRAN Version 70.5
  - 4 Iterations were Performed for Each Load Case
  - Convergence for Trim Variables were Good (Less Than 1%)

The local equivalence correction and nonlinear loads analysis were performed on 456 load cases. These load cases are candidates for critical load identification and consists of 5 Mach numbers, including 0.8, 0.95, 1.2, 1.6 and 2.0.

The iteration between the local equivalence correction and the nonlinear loads analysis was performed using the newly developed iteration process which takes advantage of the new capability (ISHELL) in NASTRAN version 70.5 to automate the iterations. For each load case, four iterations were performed and the convergence for the trim variables were good (less than 1%).

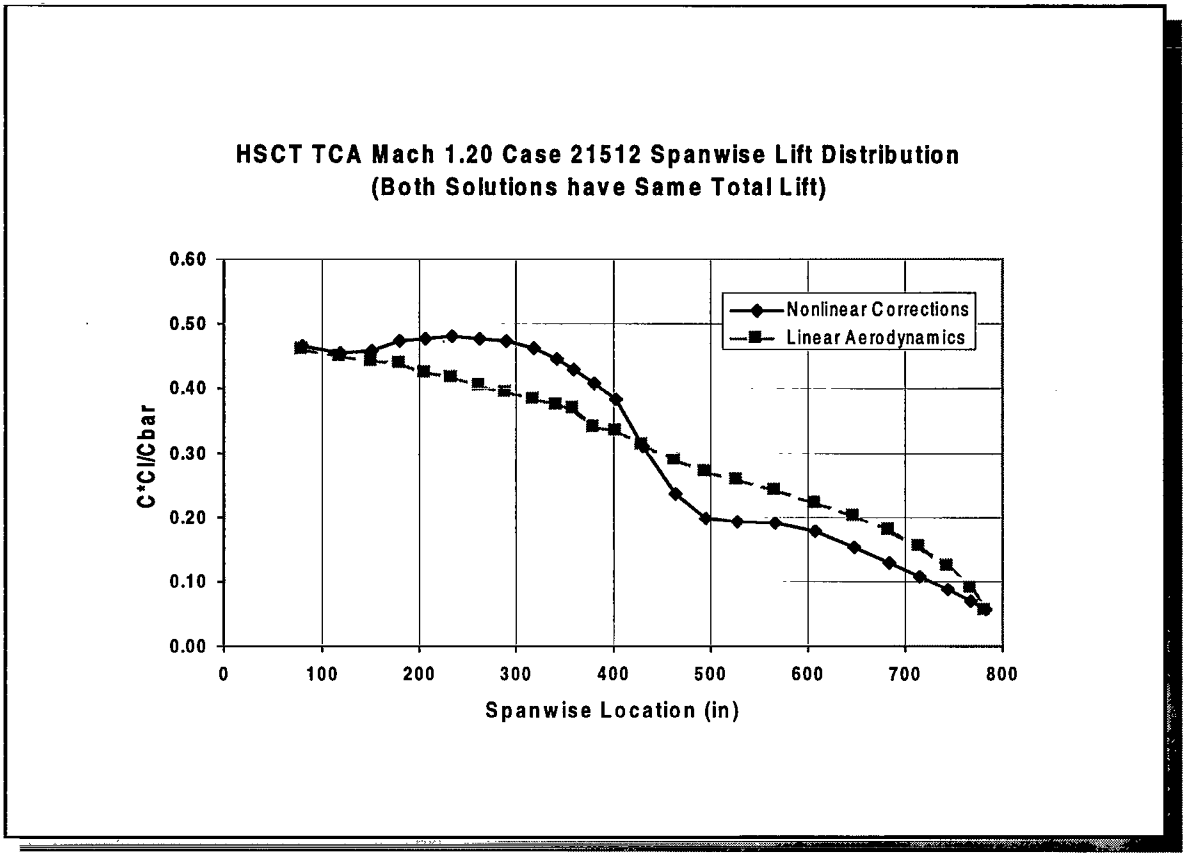

This chart shows a comparison of the spanwise lift distribution between solutions obtained using the linear (uncorrected) and nonlinear (corrected) aerodynamics at Mach 1.2 and high angle of attack with max. gross weight. This case was identified as one of the critical load conditions using linear aerodynamics in the DITS process. The spanwise lift distributions obtained from these solutions has been scaled such that both solutions yield the same total lift. The comparison shown in this chart indicates that the effect of the nonlinear aerodynamics is to shift the span load inward towards the wing root (relative to the solution based on linear aerodynamics), which is the same trend as that demonstrated with the MDC 2.4-7A configuration at Mach 0.6. This shift yields a reduction in wing root bending moment by approximately 22% and effectively eliminates this nonlinear case from being critical. However other lower angle-of-attack nonlinear cases will take its place.

Critical Load Identification - Summary of Procedure

- **Based on a Fully Stressed Design (FSD) Approach**
  - **Scale the Designed Structure to Fully Stressed State Subject to Design Upper/Lower Bounds Limitations**
    - **No Buckling or Flutter Constraints**
  - **Calculate Total Weight of Fully Stressed Design (FSD) for Each Case**
  - **The Load Case with the Highest FSD Weight is Designated as the Most Critical Case**
  - **Reset Lower Bounds of Design Variables (Thickness/Area) to FSD Level of Critical Case and Calculate Total Additional Weight (Relative to Critical Case) Required to Fully Stress for Each Remaining Load Case**
    - **The Next Critical Load Case is the One with Highest ΔW**
  - **Apply Previous Step Recursively Until Desired No. of Critical Load Cases is Obtained or No More ΔW can be Gained**
    - **Reset Lower Bounds Based on Newly Identified Critical Case**
- **Procedure Described Above is Implemented in CRLOAD Program**

A summary of the critical load identification procedure is given as follows. The critical load identification algorithm developed for the nonlinear loads process is based on a fully stressed design (FSD) approach without buckling or flutter constraints. The designed structure of the aircraft is scaled to fully stressed state (subject to design upper/lower bounds limitations) and the total weight of the FSD is calculated for each load case. The load case with the highest FSD weight is designated as the most critical case. Subsequently the lower bounds of the design variables in all design regions are reset to the FSD level of the critical case. The total additional weight (relative to the critical case) required to fully stress for each remaining load case is then computed. The next critical case is the one with the highest additional weight. The previous step for identifying additional critical cases is applied recursively, using the newly identified critical case to reset the design lower bounds, until the desired number of critical load cases is obtained or no more additional weight can be gained from this procedure. This procedure is implemented in the computer program CRLOAD.

Critical Load Identification (TCA)

- **Performed on Both Linear (Uncorrected) and Nonlinear (Corrected) Load Cases**
  - **456 Identical Cases for Both Linear and Nonlinear Loads**
  - **5 Mach Numbers Included (M=0.8, 0.95, 1.2, 1.6 and 2.0)**
- **5 Critical Cases from Linear and Nonlinear Analyses Selected**

The critical load identification procedure was performed on the TCA configuration with 456 identical load cases for both the linear (uncorrected) and nonlinear (corrected) loads. These load cases consist of 5 Mach numbers, including 0.8, 0.95, 1.2, 1.6 and 2.0. Through the critical load identification procedure, the 5 most critical cases each from linear and nonlinear analyses were identified. Results associated with these critical cases are summarized in the next chart.

Summary of Critical Loads (TCA)

❑ **From Linear Aerodynamics (Total Weight = 21778.9 lbs.)**

	Condition						FSD	
No	Weight	C.G.	L.F.	Mach	Speed	A.O.A. (deg.)	Weight (lb)	ΔW (lb)
1	MCTW	fwd.	2.5	0.95	V_{*A}	14.88	21534.6	
2	MF-1	fwd.	2.5	1.20	V_{*A}	12.45		174.7
3	MT-1	fwd.	2.5	0.80	V_{*A}	17.18		26.1
4	ML-1	fwd.	2.5	0.95	V_D	5.27		24.2
5	MCTW	fwd.	2.5	1.20	V_{*A}	13.08		8.1

❑ **Using Nonlinear Corrections (Total Weight = 20921.1 lbs.)**

	Condition						FSD	
No	Weight	C.G.	L.F.	Mach	Speed	A.O.A. (deg.)	Weight (lb)	ΔW (lb)
1	MT-1	fwd.	2.5	0.95	V_D	8.02	20796.5	
2	ML-1	fwd.	2.5	0.95	V_C	6.03		55.8
3	MCTW	fwd.	2.5	1.60	V_{*A}	11.16		27.3
4	MF-1	fwd.	2.5	0.95	V_D	7.50		19.0
5	MT-1	fwd.	2.5	0.80	V_D	7.67		13.2

This chart shows a summary of the results from the Critical Load Identification procedure which were performed on the TCA configuration for both the linear (uncorrected) and nonlinear (corrected) loads. The five most critical cases from linear and nonlinear analyses are listed above. When using linear aerodynamics, the critical cases are primarily high angle-of-attack cases. With nonlinear corrections, the critical cases are mostly lower angle-of-attack cases (at cruise or dive speed) and three of the five critical cases are at Mach 0.95. All of the critical load conditions shown in this chart have a load factor of 2.5g and forward c.g. location. The total FSD weight for the critical load conditions based on nonlinear loads is approximately 4% lower than that based on linear aerodynamics; while for the single most critical case, the nonlinear FSD weight is 3.5% lower. This trend for lower total FSD weight, when nonlinear corrected loads are used, is consistent with the results obtained with the MDC 2.4-7A configuration. This chart also illustrates the amazing fact that the most critical case accounts for about 99% of the weight. Thus really only one maneuver case may be needed.

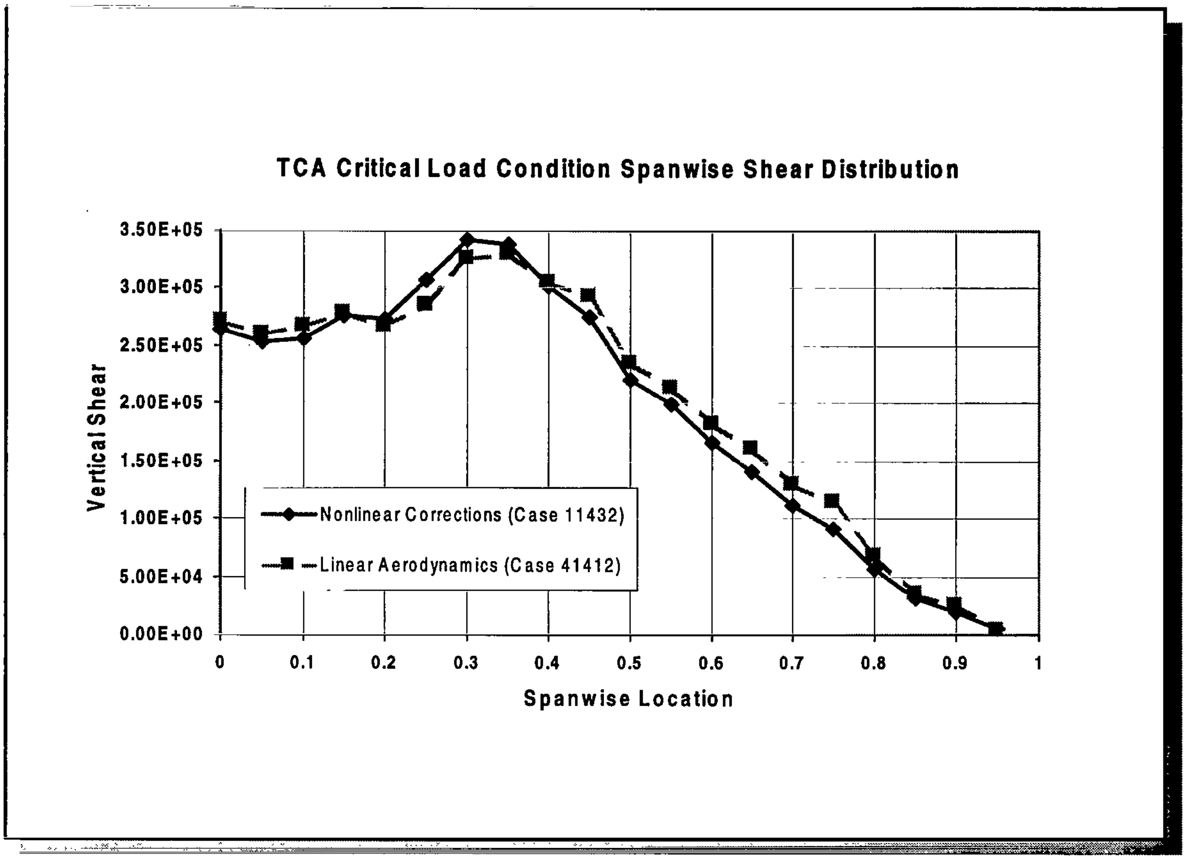

This chart shows a comparison of the spanwise vertical shear distribution between the most critical load cases based on linear and nonlinear aerodynamic loads.

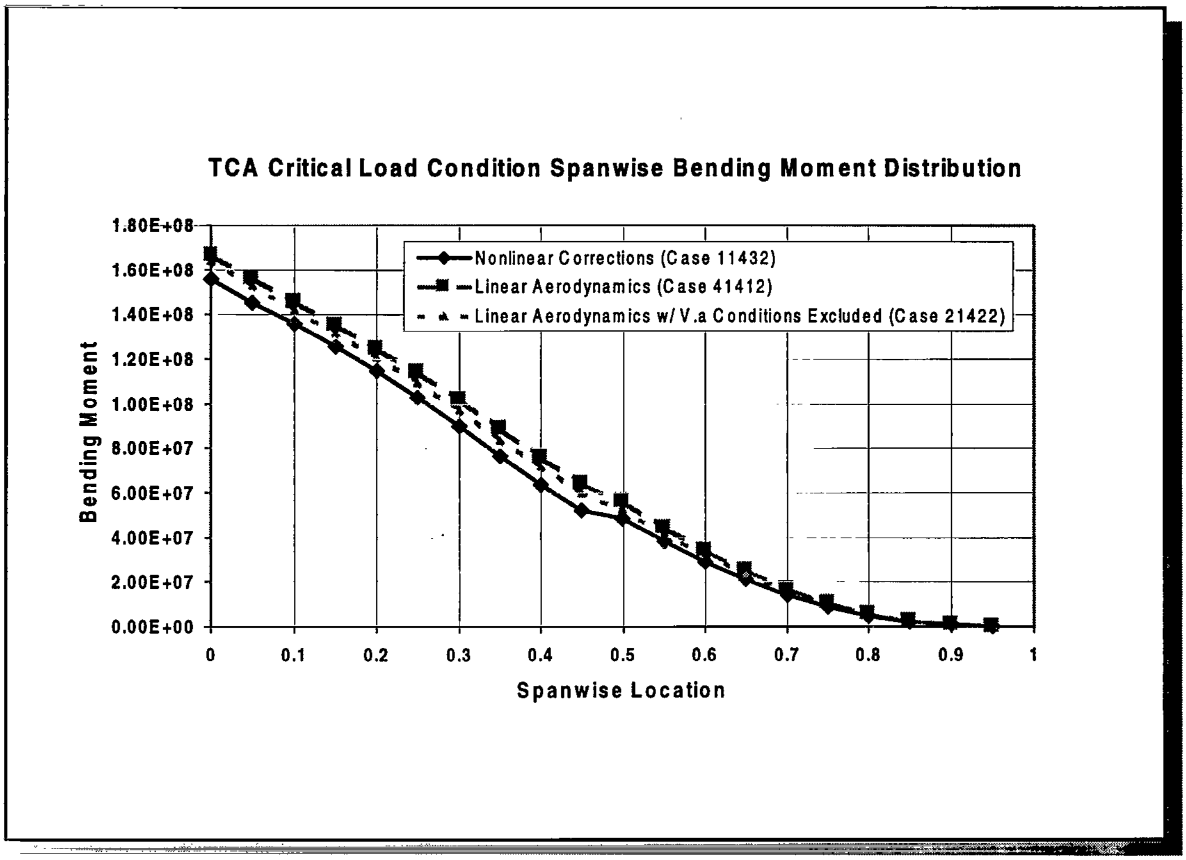

This chart shows a comparison of the spanwise bending moment distribution between the most critical load cases based on linear (long dashed line) and nonlinear (solid line) aerodynamic loads. As noted in a previous chart, high α (low speed, $V._A$) cases were eliminated from the critical list when nonlinear loads were used. It is instructive to assess if the same nonlinear results could be obtained if these high α cases were excluded from the critical load identification process using linear analysis. A third bending moment curve shown in this figure (short dashed line, corresponding to Case 21422, with mass condition MF-1 and forward c.g. location at cruise speed V_C and Mach 0.95, and having a load factor of 2.5g) presents the results of this assessment. The FSD weight reduction based on this approach is less than 20% of that when nonlinear loads are used. Therefore from the FSD point of view, this is not a good alternative to using the nonlinear loads. In the next chart, a comparison of the impact on bending moment/running loads will be discussed.

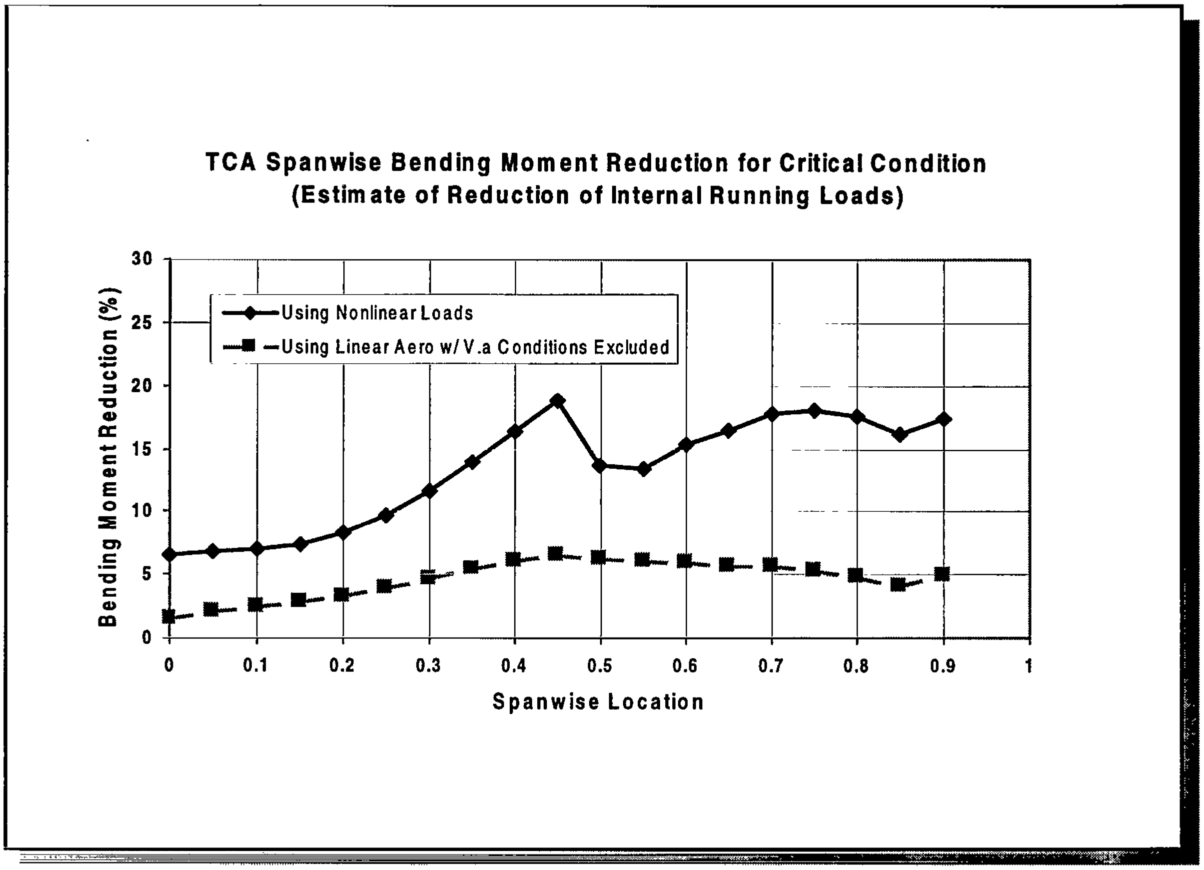

Based on the previous chart, the percentage reduction of bending moment across the semi-span of the wing from the most critical linear case (among the full set of 456 load cases), using nonlinear loads (solid line) and linear aerodynamics based on the reduced set of load cases without the $V._A$ conditions (dashed line), is shown in this chart. The internal running loads are reduced by approximately a similar amount as the bending moment. Outboard of the leading edge break (located at approximately 58% of the span), where the level of running loads is critical, the reduction due to nonlinear loads is approximately 15% to 18%; while only 5% to 6% reduction can be obtained by using linear aerodynamics with the $V._A$ conditions excluded from consideration of being critical. Therefore nonlinear loads produce a significant reduction in internal running loads for the TCA configuration, and critical load identification based on a reduced set of load cases (with $V._A$ conditions excluded) and using linear aerodynamics is not a good alternative to using nonlinear loads for internal running loads prediction.

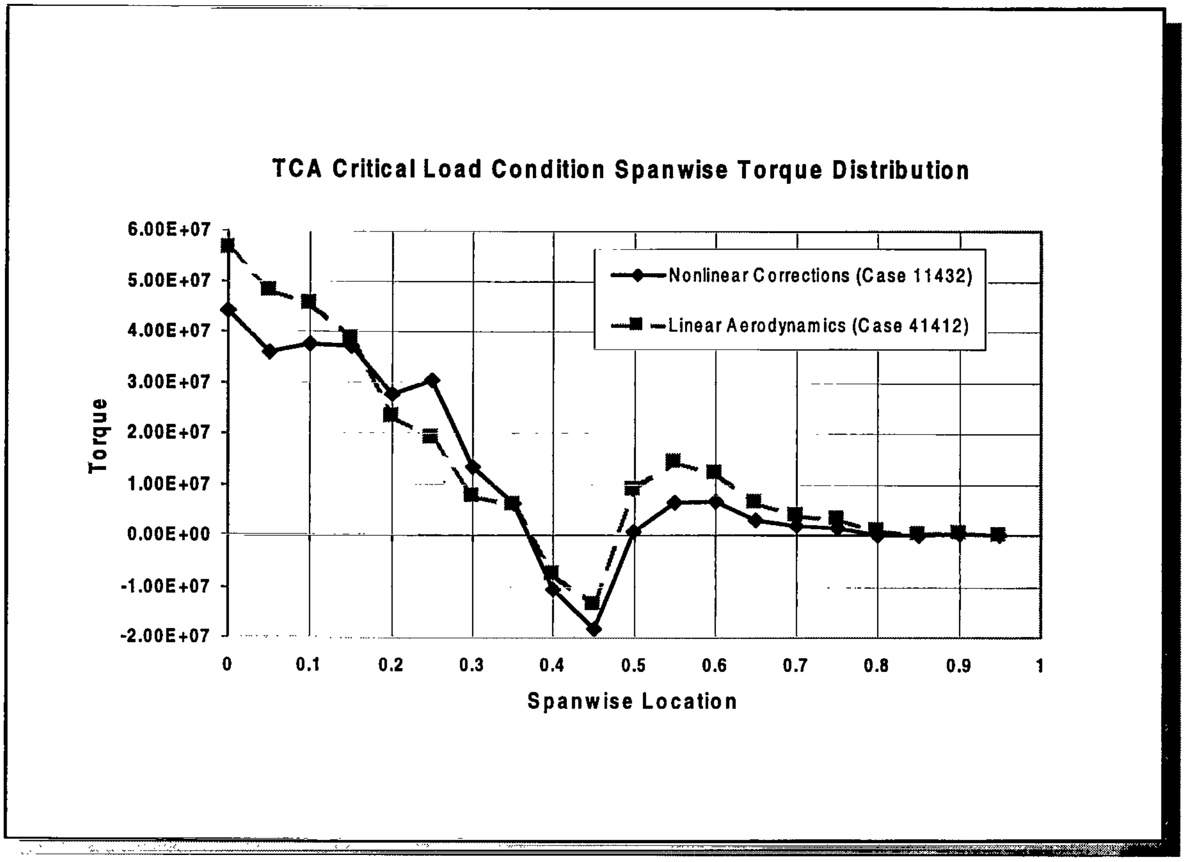

This chart shows a comparison of the spanwise torque distribution between the most critical load cases based on linear and nonlinear aerodynamic loads.

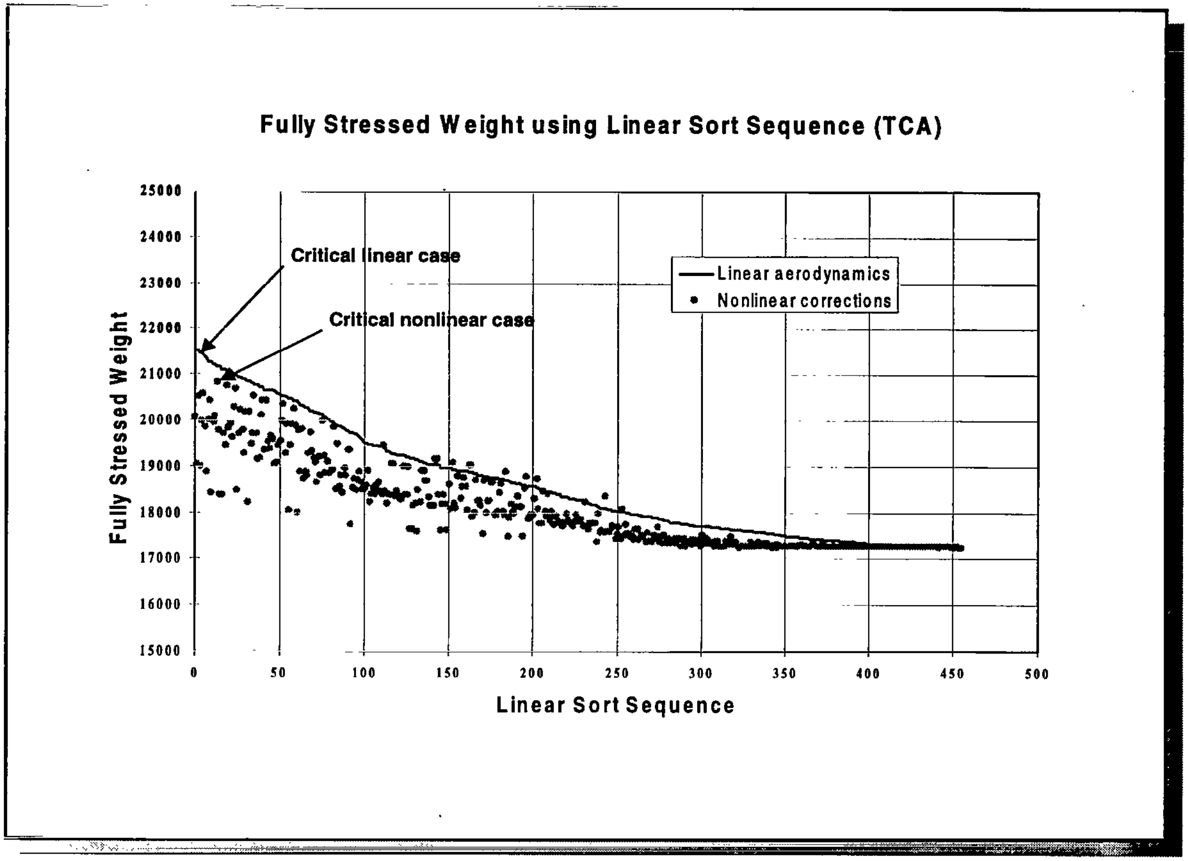

This chart shows the FSD weight of the 456 load cases for linear and nonlinear loads in the sort sequence of descending FSD weight based on linear aerodynamics. The FSD weights for the nonlinear load cases are generally lower than the corresponding linear ones except for a few cases. However the most critical case for nonlinear loads is different from that based on linear aerodynamics and it has a lower FSD weight. This chart also illustrates that when a critical load case is eliminated there is another one ready to take its place that is only slightly less critical.

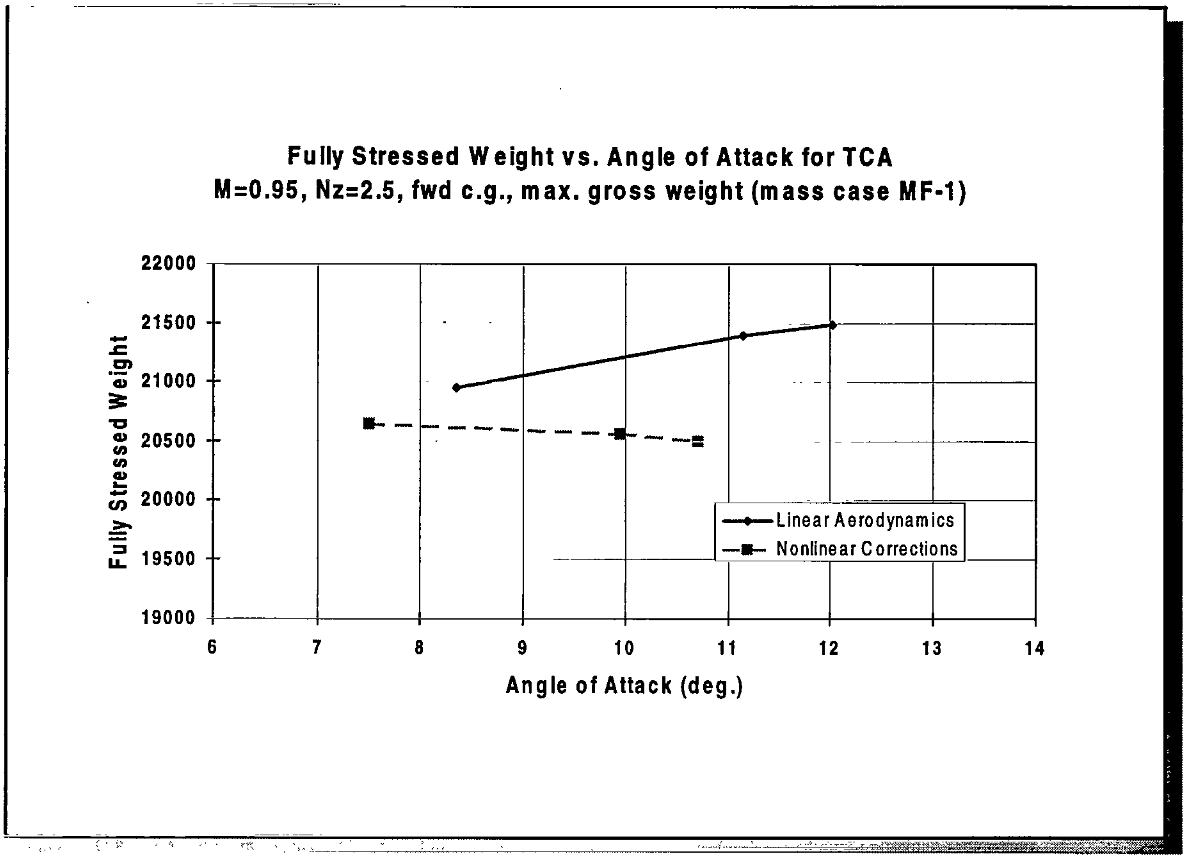

The variation of the FSD weight with angle-of-attack, for weight condition MF-1 (max. gross weight, forward c.g.) at Mach 0.95 and load factor 2.5g, is shown in this chart. The three cases shown in this chart correspond to speeds at V_D, V_C and $V._A$, respectively. When linear aerodynamics is used, the FSD weights is maximum at high angle-of-attack (low dynamic pressure, $V._A$). This is because the aeroelastic relief is minimized at low dynamic pressure and the resulting bending moments are higher. However with nonlinear corrections, the re-distribution of the aerodynamic loads due to flow separation at high angles of attack causes the FSD weights to maximize at low angle-of-attack (high dynamic pressure) and thus eliminates the low dynamic pressure $V._A$ (high angle-of-attack) cases from being critical. Note that the highest weight linear and nonlinear cases shown in this chart are not the most critical cases, thus the level and differences are not meaningful and the figure is presented only for trends.

TCA Load Conditions for Validation with NASA Ames

- **Case 1 (Condition 21512)**
  - **Mach 1.2, Mass Condition MF-1, Load Factor +2.5g**
  - **LEOB Flaps (10b, 11, 12) Deflection = 8.0°**
  - **AOA for Rigid Undeflected Configuration = 12.56°**
  - **For ENSAERO Trimmed Aeroelastic Solution**
    - **Q = 470.5042 psf (3.2647 psi)**
    - **Horizontal Tail Load (Half Airplane) = -58737 lbs (at x=3534 in.)**
- **Case 2 (Condition 21432)**
  - **Mach 0.95, Mass Condition MF-1, Load Factor +2.5g**
  - **LEOB Flaps (10b, 11, 12) Deflection = 8.0°**
  - **AOA for Rigid Undeflected Configuration = 8.36°**
  - **For ENSAERO Trimmed Aeroelastic Solution**
    - **Q = 670.3965 psf (4.6555 psi)**
    - **Horizontal Tail Load (Half Airplane) = -46484 lbs (at x=3534 in.)**
- **Trimmed Aeroelastic CFD Solution Not Completed due to Lack of Manpower at Ames**

Two load cases for the TCA configuration were selected for validation with NASA Ames using the ENSAERO code. Both cases have a mass condition MF-1 (max. gross weight, forward c.g.), load factor of +2.5g and leading edge outboard flap deflection of 8.0°.

The first case, designated as Condition 21512, is at Mach 1.2 and has an angle-of-attack of 12.56° for the rigid undeflected configuration. For the trimmed aeroelastic CFD solution, the dynamic pressure is 470.5042 psf (3.2647 psi) and the horizontal tail load for half airplane is 58737 lbs. (downward), at streamwise coordinate x=3534 in.

The second case (Condition 21432) is at Mach 0.95, with an angle-of-attack of 8.36° for the rigid undeflected configuration. At the trimmed condition, it has a dynamic pressure of 670.3965 psf (4.6555 psi) and a (downward) horizontal tail load for half airplane of 46484 lbs., also at streamwise coordinate x=3534 in. Note that the 3° aileron deflection for this condition, based on the programmed flap schedule, is neglected so that the same grid can be used for both cases.

A comparison of the spanwise lift distribution for the first case (condition 21512) obtained from both the nonlinear correction process and the linear aerodynamics has been presented in an earlier chart of this report. Similar comparison results was also obtained for the second case (condition 21432), and is not presented here. However a trimmed aeroelastic CFD solution, using the ENSAERO code, for the purpose of validation has not been obtained due to lack of manpower at NASA Ames.

C.1.1.3 Application of Nonlinear Loads Process to PTC

Goals and Objectives

- ❑ **Integrate Nonlinear Loads Process with Rapid Structural Design/Optimization Techniques (EPT)**
  - **Use Rigid-α Approach for Representative Deflections**
- ❑ **Full Study Throughout Flight Envelope**
  - **Multiple Mach Numbers**
  - **Multiple Mass Conditions**
  - **Multiple Load Factors**
  - **Multiple Altitude/Velocity Combinations**
- ❑ **Investigate Impact of Nonlinear Loads on the HSR Preliminary Technology Configuration (PTC)**
  - **Impact of canard on spanwise load distribution**
  - **Impact on Critical Conditions**
  - **Weight Impact**

The objective for applying the nonlinear loads process to the PTC configuration is to integrate the process with the rapid structural design and optimization techniques, such as the equivalent plate theory (EPT). In the generation of nonlinear aerodynamic database, the Rigid-α approach will be used for the representative deflections.

The study will demonstrate the application of the correction procedure using a comprehensive aerodynamic database at several Mach numbers, considering many mass conditions, multiple load factors, as well as multiple altitude and velocity combinations representative of a realistic design scenario. This study will also include an assessment of the impact of nonlinear aerodynamics on the critical load conditions and a preliminary impact on structural weight, as well as the impact on the spanwise load distribution due to the presence of a canard.

Structural and Aerodynamic Model (PTC)

- ❑ **Structural FEM Model (EPT)**
  - 4864 Nodes
  - 8515 Elements

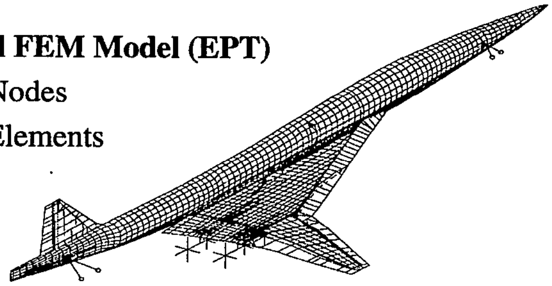

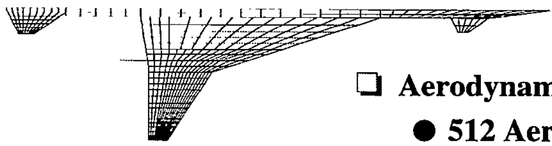

- ❑ **Aerodynamic Model**
  - **512 Aerodynamic Boxes**
  - **151 Spline Points**
  - **Panel-point Forces to Structure**

The structural and aerodynamic models of the PTC configuration, used in the NASTRAN analyses, are shown in this chart. In the structural FEM model, there are 4864 nodal points and 8515 finite elements. The wing of the structural model was generated using equivalent plate theory (EPT), while the canard and the horizontal tail were modeled as rigid bodies. The aerodynamic model (Doublet Lattice Method) has a total of 512 aerodynamic boxes, with 151 spline points between the structural and the aerodynamic models. A panel-point scheme, which maps the aerodynamic pressure into structural finite element loads and was implemented to the NASTRAN code through DMAP, was also used to improve the finite element loads distribution.

Conditions for PTC CFD Loads Analysis

Mach No.	α (deg.)	$(\delta_F)^{LEOB}$ (deg.)	$(\delta_F)^{LEIB}$ (deg.)	$(\delta_F)^{TEOB}$ (deg.)	$(\delta_F)^{TEIB}$ (4/5) (deg.)	δ_C (deg.)
0.60	-10.0	10.0	10.0	3.0	3.0	-9.74
	-4.89	10.0	10.0	3.0	3.0	-2.05
	8.22	20.08	20.08	6.04	6.04	14.0
	13.04	30.0	30.0	14.5	14.5	14.0
	17.85	42.36	42.36	23.71	23.71/12.70	14.0
0.80	-10.00	9.0	0.0	3.0	0.0	-5.03
	-1.52	9.0	0.0	3.0	0.0	0.58
	2.76	9.0	0.0	3.0	0.0	3.41
	9.57	9.0	0.0	3.0	0.0	7.91
	16.39	9.0	0.0	3.0	0.0	12.42
0.95	-10.00	7.0	0.0	2.5	0.0	-9.14
	-1.30	7.0	0.0	2.5	0.0	0.30
	2.35	7.0	0.0	2.5	0.0	4.25
	6.91	7.0	0.0	2.5	0.0	9.20
	11.46	7.0	0.0	2.5	0.0	14.0
1.20	-10.00	4.0	0.0	0.0	0.0	-15.17
	-1.28	4.0	0.0	0.0	0.0	-1.62
	2.57	4.0	0.0	0.0	0.0	4.37
	6.35	4.0	0.0	0.0	0.0	10.23
	10.12	4.0	0.0	0.0	0.0	14.0
2.00	-10.00	0.0	0.0	0.0	0.0	-10.64
	-1.73	0.0	0.0	0.0	0.0	-0.27
	3.54	0.0	0.0	0.0	0.0	6.34
	7.33	0.0	0.0	0.0	0.0	11.10
	11.12	0.0	0.0	0.0	0.0	14.0

The conditions selected for CFD loads analysis to generate the nonlinear aerodynamic database for the PTC configuration is shown in this chart. Angle-of-attack, horizontal tail, elevator and canard position were determined by solving a two degree of freedom balance on the lift and pitching moment using linear rigid PTC global aerodynamic data and elastic-to-rigid ratio from a TCA model. The balance was done with the appropriate flap deflections based on the programmed flap schedule for PTC, which is a function of Mach number and airplane C_L. The TCA elastic-to-rigid data was considered sufficient for this calculation since the results were only used to determine the conditions at which CFD data will be generated. This was done for a maximum takeoff gross weight, forward c.g. condition and load factors of -1.0g and 2.5g. The 2.5g cases were run at V_C, V_D and $V_{\cdot A}$ (C_{Lmax}), while the -1.0g cases were run at V_C and the speed to balance at -10° angle-of-attack.

Because of the time constraints and the difficulties encountered in the CFD analyses (described in Section C.1.2), it was decided that the CFD should be performed only on the middle three cases for each Mach number, based on the critical load identification results of the TCA configuration. Although the application of the process to PTC is not complete due to time constraints, the required upgrades to the process for the more complicated PTC configuration (relative to TCA and MDC 2.4-7A) have been completed and are ready to apply.

Concluding Remarks

- **Nonlinear Loads process Produces Significant Reduction in Weight and Internal Running Loads**
  - **4% Reduction in TCA Design Weight**
  - **15~18% Reduction in TCA Internal Running Loads in Critical Wing Area**
- **Nonlinear Loads process Yields Different Critical Conditions**
  - **$V._A$ Critical for Linear**
  - **V_C or V_D Critical for Nonlinear**
- **Several Improvements Made to the Nonlinear Loads Process**
  - **Use Rigid-α to Replace SVD/Splining Procedure Whenever Appropriate in Generating Representative Deflections**
  - **Iteration Between Local Equivalence Corrections and Nonlinear Loads Analysis Automated**
  - **Computer Codes CORRECT and CRLOAD Upgraded to Handle More General Conditions**
- **Integrated Nonlinear Loads Process with Rapid Structural Design/Optimization Techniques (EPT) Through PTC Configuration**

In conclusion, the results from the critical load identification, performed on the TCA configuration, showed that substantial differences in weight, loads and critical conditions may exist between the linear and nonlinear loads. The nonlinear loads process resulted in a 4% reduction in the (FSD) design weight and a 15~18% reduction in the internal running loads in the critical wing area for the TCA configuration. This process also yields critical conditions different from that obtained using the linear loads. With linear aerodynamics, the critical conditions are high α, low speed $V._A$ cases; while the critical conditions are low α, high speed V_C or V_D cases when nonlinear loads are used.

Several improvements were made to the nonlinear loads process since the completion of the Preliminary Aeroelastic Concept (PAC). The use of the rigid-α approach to replace the SVD/splining procedure significantly simplifies the effort required to generate the nonlinear aerodynamic database. Iteration between the local equivalence correction and the nonlinear loads analysis has been upgraded from a manual process to an automated process. The computer code CORRECT, which performs local equivalence corrections, and CRLOAD, which performs critical load identification, were both upgraded so that they can handle more general conditions.

Finally, the nonlinear loads process has been integrated with the rapid structural design and optimization techniques, such as equivalent plate theory (EPT), through the PTC configuration. Although the application of the process to PTC is not complete due to time constraints, the required upgrades to the process for the more complicated PTC configuration (relative to TCA and MDC 2.4-7A) have been completed and are ready to apply.

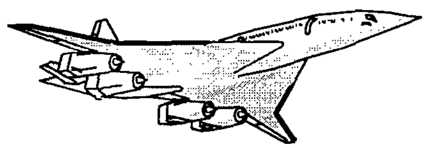

ACE Final Report

C.1.2 - CFD Data Generation Process for Nonlinear Loads on the PTC Configuration - Boeing LB

Alan Arslan
David Yeh
Todd Magee

December 31, 1998

Outline

- Objective
- CFD approach for the PTC
- Results
- Problems encountered
- Lessons learned
- Summary
- Suggested improvements

The chart above gives an outline of the following work. A discussion of the background and its relevant objectives is followed by a description of the CFD approach for the PTC configuration. Sample results from the CFD simulations are shown and the relevant problems encountered are discussed with suggestions on possible solutions and enhancements. Finally, a summary and recommendations for future work are given.

Objective

- Develop a CFD loads database for the PTC configuration for use in the non-linear loads process
  - Modify the TCA process for the inclusion of canards with gaps as well as trailing-edge flaps

In order to obtain critical loads that are realistic for an HSCT configuration higher order aerodynamics are considered. Since most of the critical loads occur in the transonic domain and at high Reynolds numbers, the best suited higher order method is believed to be Navier-Stokes-based CFD. Consequently, the current work on the PTC configuration involves applying the CFD non-linear loads process developed for the TCA configuration to the new higher aspect ratio configuration. The database generated will subsequently be used in the CORRECT program for generating non-linear loads.

Since the baseline PTC configuration involves canards, the proper CFD approach will be to model the canards and relevant gaps, since the associated generated vortices may interact with the wing flowfield and have a significant effect on the wing sectional loads.

CFD Approach for the PTC Configuration

- Configuration:
  - PTC wing/body/flaps/canard
- Geometries:
  - Obtained from rigid shapes for cases ranging from -1g to 2.5g at five angles-of-attack
- Grid-Topology:
  - C-O for wing/body/flaps, H-O for canard/gap
- Grid Generation:
  - Overset approach developed by the High-Lift group in PW-LB
- Analysis:
  - CFL3D N-S, steady flow, Baldwin-Lomax turbulence model (D-S option), Re_c= 40 million

The OAC configuration used the PTC as its baseline geometry for the CFD simulations. Since a wide range of flight conditions was considered, it was necessary to include leading and trailing-edge flaps. The canard was included for reasons mentioned in the previous chart.

Unlike the previous configuration, the nonlinear loads process did not need CFD analyses on configurations with representative deflections and only rigid shapes were used for the analyses. However, the angles-of-attack, canard, and flap settings would correspond to loading cases ranging from -1g to 2.5g at five different Mach numbers. Five angles-of-attack were used for each Mach number.

As in the previous CFD database (TCA configuration) for the nonlinear loads, a C-O topology was used around the wing/body/flap configuration. The canard is gridded with the forebody using an H-O topology.

The grid generation consisted of an overset procedure developed by the High-Lift group in Phantom Works (Long Beach).

The CFL3D code was used for the N-S analyses. The numerical scheme consisted of flux-difference splitting with multigrid acceleration. The flow was assumed to be fully turbulent and the Baldwin-Lomax algebraic turbulence model with the Degani-Schiff option was used.

Since the objective was to converge sectional loads, the Navier-Stokes clustering was relieved (roughly by a factor of 5) near the wall producing y+ values ranging from 1 to 5 at the wing trailing-edge.

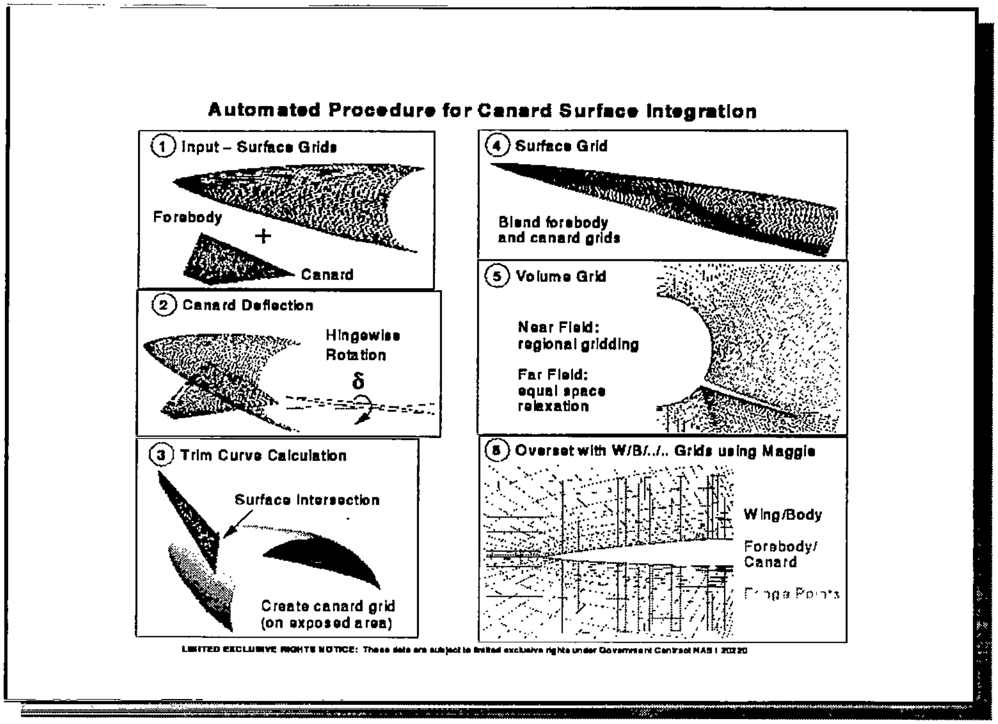

An automated grid-generation procedure was developed for the canard and applied to the PTC configuration. The procedure is briefly described in the chart above. The canard grid-generation package also allowed for elevator deflections. It was found in high-lift cases that elevator deflections did change the strength of the canard-tip vortices. Since a significant number of the cases involved high angles-of-attack for both wing and canard, it is important to model the canard gap. In fact, it is believed that the canard tip and apex vortex would interact and affect the wing flowfield and thus the relevant wing sectional loads.

The grid consisted of an H-O topology with 109 points in the streamwise direction, 161 points in the spanwise direction, and 41 point in the normal (viscous) direction.

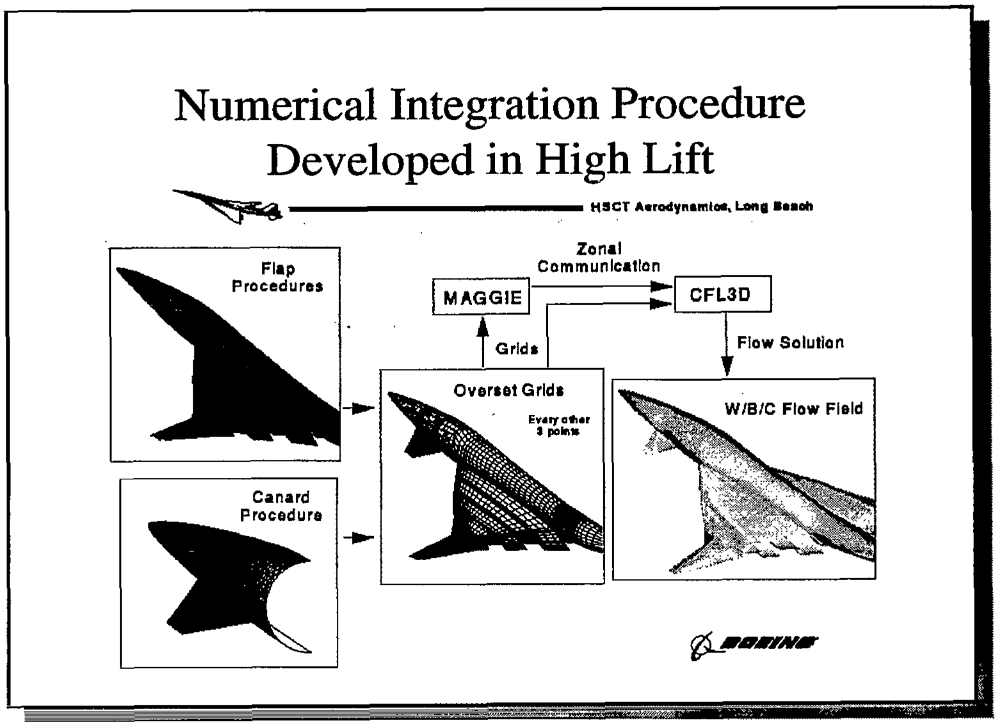

This chart shows the numerical integration procedure applied in the CFD database generation procedure for the PTC nonlinear loads. After the wing/body grid is modified for flap deflections and the canard/forebody grid is modified for the canard surface deflection, the two grids are overset with the MAGGIE code. Zonal communication data is generated and input in CFL3D for the flow solution. The wing/body/flap grids consisted of 289 points in the streamwise direction, 181 points spanwise, and 65 points in the normal (viscous) direction. The reason why the number of grid points used was so large is described in the flap deflection process of the High-Lift CFD section of last year's NASA/Industry HSR technology integration review final report.

Matrix of Cases

Mach No.	α (deg.)	$(\delta_F)^{LEOB}$ (deg.)	$(\delta_F)^{LEIB}$ (deg.)	$(\delta_F)^{TEOB}$ (deg.)	$(\delta_F)^{TEIB}$ (4/5) (deg.)	δ_C (deg.)
0.60	-10.0	10.0	10.0	3.0	3.0	-9.74
	-4.89	10.0	10.0	3.0	3.0	-2.05
	8.22	20.08	20.08	6.04	6.04	14.0
	13.04	30.0	30.0	14.5	14.5	14.0
	17.85	42.36	42.36	23.71	23.71/12.70	14.0
0.80	-10.00	9.0	0.0	3.0	0.0	-5.03
	-1.52	9.0	0.0	3.0	0.0	0.58
	2.76	9.0	0.0	3.0	0.0	3.41
	9.57	9.0	0.0	3.0	0.0	7.91
	16.39	9.0	0.0	3.0	0.0	12.42
0.95	-10.00	7.0	0.0	2.5	0.0	-9.14
	-1.30	7.0	0.0	2.5	0.0	0.30
	2.35	7.0	0.0	2.5	0.0	4.25
	6.91	7.0	0.0	2.5	0.0	9.20
	11.46	7.0	0.0	2.5	0.0	14.0
1.20	-10.00	4.0	0.0	0.0	0.0	-15.17
	-1.28	4.0	0.0	0.0	0.0	-1.62
	2.57	4.0	0.0	0.0	0.0	4.37
	6.35	4.0	0.0	0.0	0.0	10.23
	10.12	4.0	0.0	0.0	0.0	14.0
2.00	-10.00	0.0	0.0	0.0	0.0	-10.64
	-1.73	0.0	0.0	0.0	0.0	-0.27
	3.54	0.0	0.0	0.0	0.0	6.34
	7.33	0.0	0.0	0.0	0.0	11.10
	11.12	0.0	0.0	0.0	0.0	14.0

This chart shows the matrix of cases needed for CFD simulations on the PTC configuration. The two outboard trailing-edge flaps were treated as one segment. Similarly, the two inboard leading-edge flaps were treated as one and a linear transition web joins the inboard LE flap to the outboard LE flap.

Non-Linear Loads CFD Status Matrix

	AOA/FLAP/CANARD				
Mach	-HAL	-LAL	LAL	HAL	VHAL
0.6	✖	✔	•	•	✖
0.8	✖	✔	✔	✔	✖
0.95	✖	•	✔	✔	✖
1.2	✖	✔	✔	✔	✖
2.0	✖	✔	✔	✔	✖

• In Progress
✔ Completed
✖ Not started

The highest angle-of-attack (AOA) case was called +VHAL next to HAL and lowest AOA case -HAL. The low angle-of-attack cases were called -/+ LAL. Even though 23 out of the 25 grids were completed and successfully overlapped (the exceptions were the -HAL and VAL grids for Mach 0.6), only a selected number of cases could be done within the given computer budget and turn-around time. Consequently, the crosses (not started cases) in the table above indicate the cases where the solutions were not initiated. The dotted ones (in progress) indicate the cases that encountered convergence problems from a "loads" standpoint and are still being converged. Finally, the checkmarks indicate the cases that were "loads" acceptable.

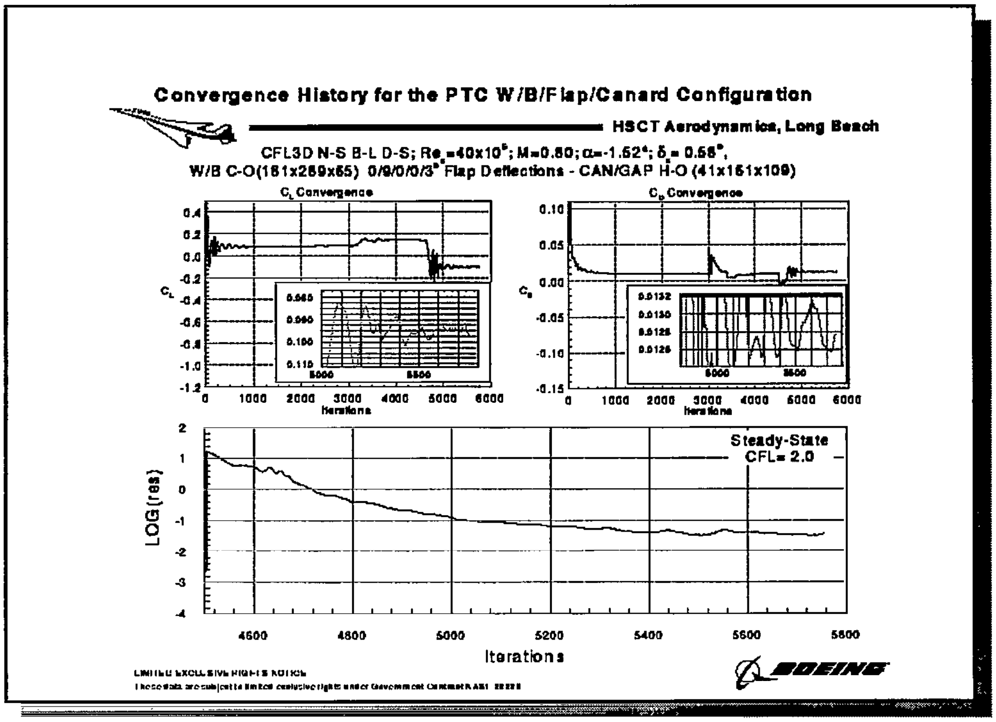

The chart above shows the convergence history for a typical low angle-of-attack case. Three orders of magnitude of residual reduction were achieved and oscillations in lift were reduced to reasonable levels (~2%).

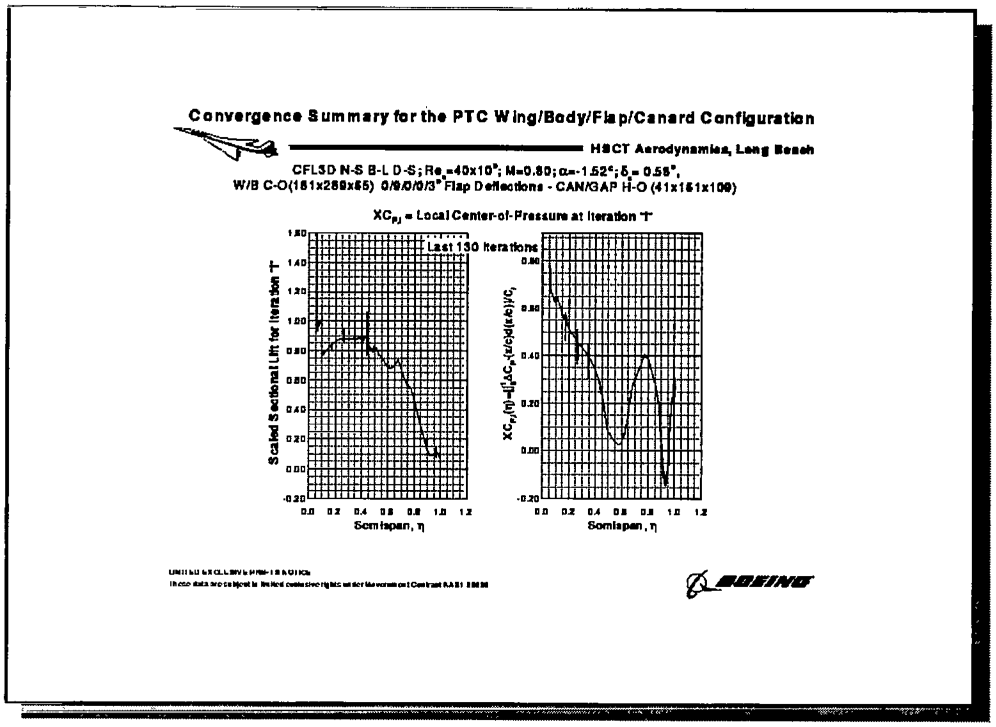

This chart shows the sectional loads of the previous case for the last 130 iterations. The narrow band observed for the scaled sectional lift indicates convergence. The spikes observed at certain span locations correspond to the gaps associated with the trailing-edge flaps. The values obtained for the first 15% span locations are not "True" sectional loads since they include grid lines that are not at the same span locations. In fact, the sectional loads are calculated by integrating along grid lines and are used here for convergence purposes only.

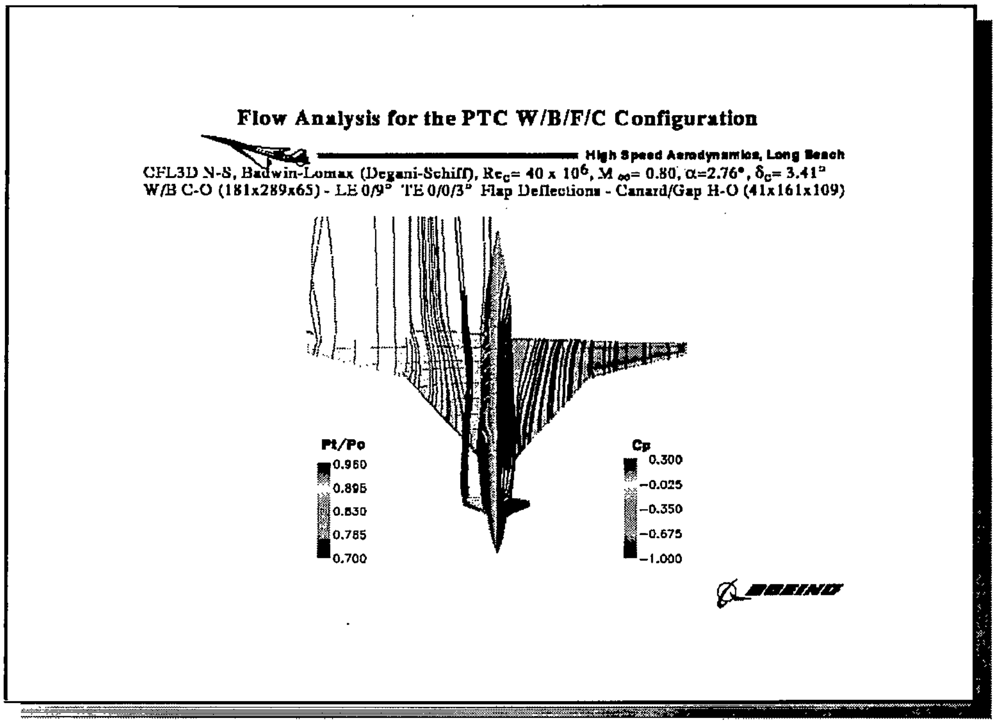

The chart above illustrates the flowfield for a typical low angle-of-attack case. The left hand side of the chart shows field streamlines with normalized total pressure cuts while the right hand side shows surface pressures and particle traces. The canard tip-field streamlines are black, the canard leading-edge streamlines are red, and the streamlines emanating from the gap are blue. The canard tip vortex is relatively weak and the flow over the wing (pink streamlines) is attached. The right side of the plot shows clearly the suction associated with the deflection of the outboard leading-edge and trailing-edge flaps. This flow is a good example of a relatively benign flowfield.

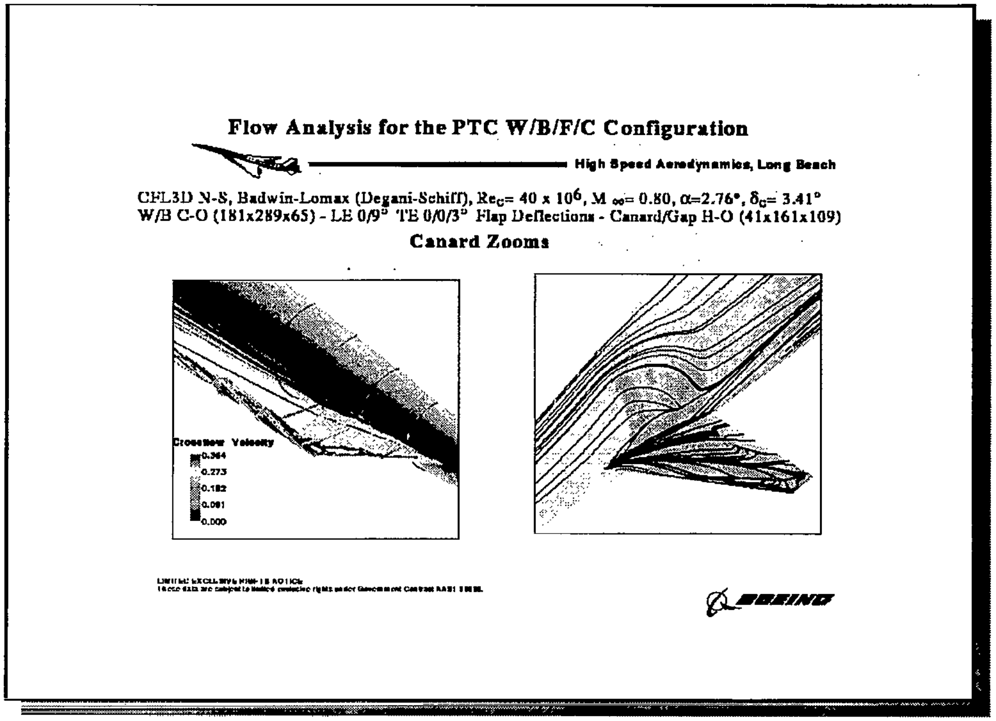

This chart shows a blow-up view of the canard flowfield. Both views indicate a mild leading-edge separation on the canard upper surface (approximately at 6.5° combined local angle-of-attack). The gap vortices remain distinct from the leading-edge and tip vortices.

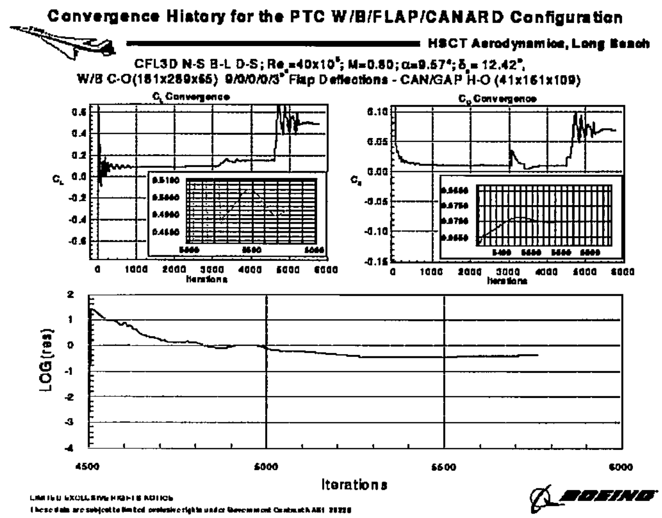

The convergence history for a typical high angle-of-attack case is shown in the chart above. After two orders of magnitude reduction the residual seems to be oscillating and the solution seems to display a periodic behavior with the lift oscillating by 4-5% about the mean. These oscillations could be eliminated or reduced with time-accurate simulations.

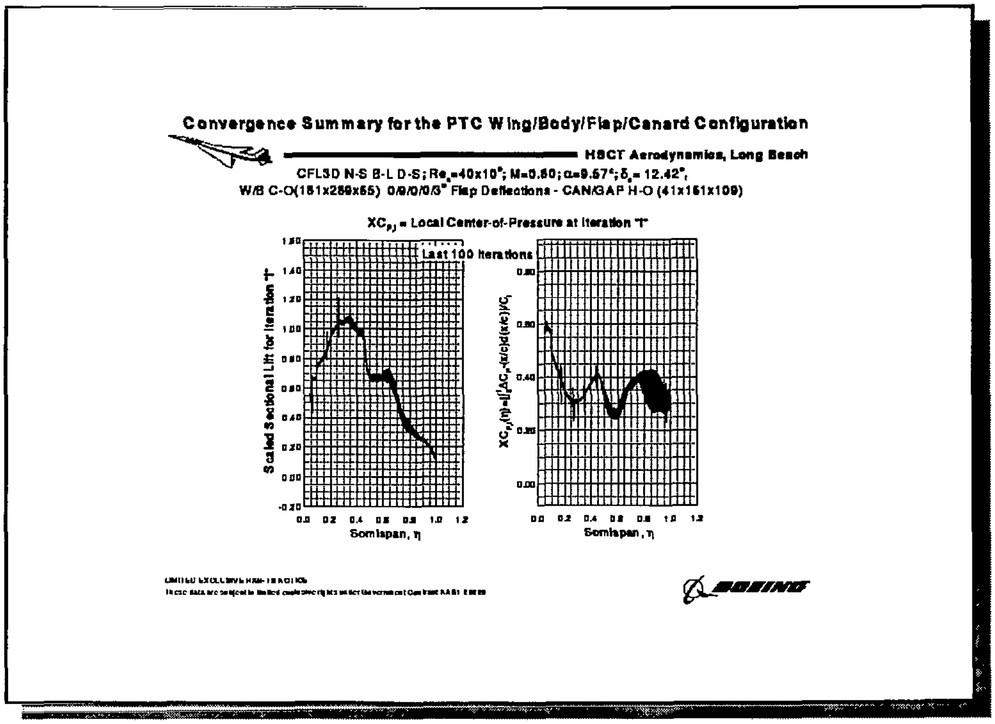

The sectional loads for the case shown in the previous residual history plot are shown in this chart. Here, the band thickness for the scaled sectional lift is larger than the low angle-of-attack case shown previously. However, the relative small percentage of variation in the scaled sectional lift values made the solution acceptable from a "loads" standpoint. The large variation in the center-of-pressure at the tip is not that significant from a loads standpoint due to the low sectional loads at the tip.

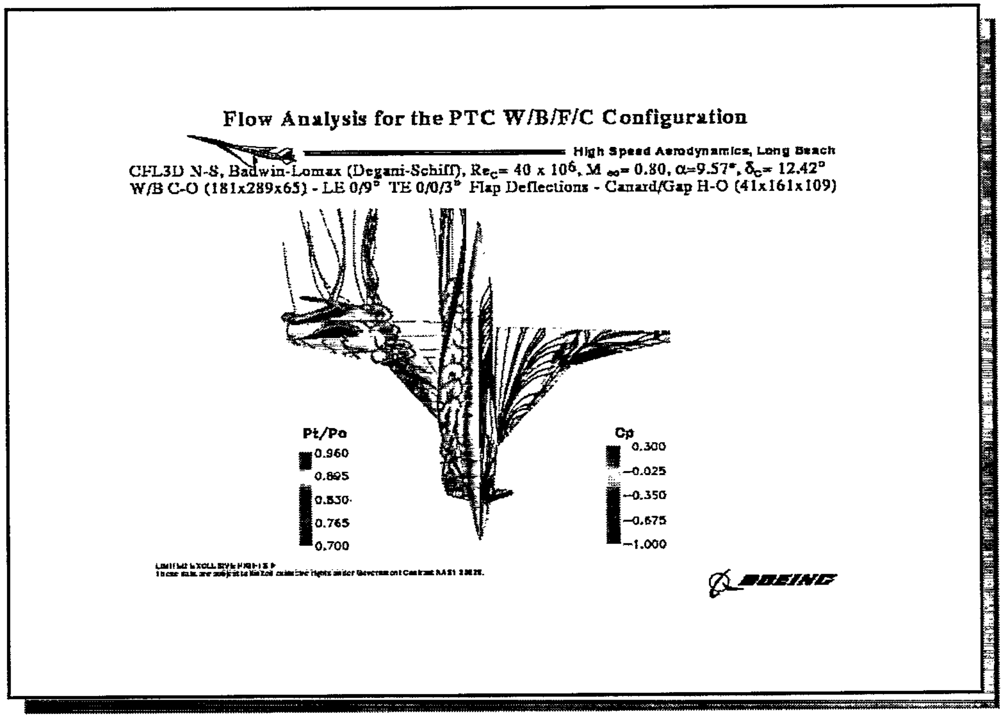

The flowfield corresponding to the convergence histories of the previous two charts is shown in the chart above. The left hand side of the chart clearly displays a strong canard vortex, wing leading-edge, and break vortices. The black streamlines (canard tip vortices) and blue ones (canard root vortices) seem to attract each other and eventually merge downstream. The leading-edge break vortex seems to be attenuated due to the flap deflection. The surface pressure and particle traces shown on the right hand side of the plot show primary and secondary separation lines on the inboard side of the wing as was observed on the TCA configuration. The absence of elastic washout does not help relieve the separated flowfield on the outboard section of this large aspect ratio wing.

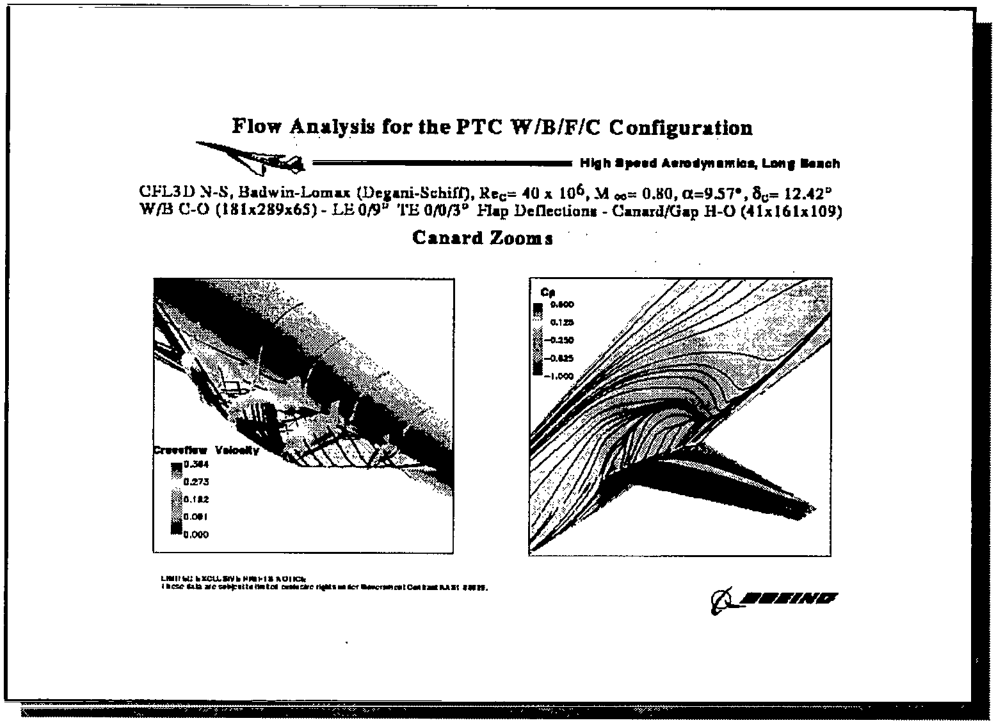

This chart shows a close-up view of the canard for the flowfield considered in the previous slide. The canard sees an angle-of-attack of about 23° and a strong vortex can be observed along the leading-edge. Regions of small cross-flow velocity values correspond to the vortex core. Another vortex is generated because of the gap (blue ribbons) and seems to be attracted to the canard tip vortex, which blends with the leading-edge separation vortex. In fact, the tip vortex and the gap vortex seem to be counter-rotating. Surface pressures and particle traces do not indicate secondary separation patterns. Finally, the strengths of the observed vortices are indicative of their significant influence on the wing flowfield and sectional loads.

Problems Encountered

- Canard grids were only obtainable for $-16° < \delta_c < 14°$
- Oversetting was not possible for coarser canard/forebody (H-O) and wing/body/flap (C-O) combinations
- Due to the large number of grid points (about 4 million per case), only a selected number of cases were run - Slow computer turn-around
- Convergence was difficult for many cases (especially at Mach 0.95) (time-accurate runs could not be initiated)

Not all cases were obtainable. Once the canard leading/trailing edge was respectively above/below the forebody, which corresponds to deflections above +14° or below -16°, the trim intersection curve with the forebody was impossible to generate and so were the corresponding grids.
Initially, coarser grids than the ones usually used for performance assessments were generated but oversetting the cell centers with MAGGIE was impossible. Consequently, it was decided to use the original grid sizes used in High-Lift (about 4 million points).
Based on the TCA simulations (about 1.8 million points), it was estimated that the CPU and labor time allotted would accommodate the 25 cases considered. However, since 4 million points was the only possible choice for the overset canard grids, only a selected number of cases were run (see following chart).
Most simulations were difficult to initiate from freestream and some "baby sitting" transitioning from Mach 0.3 and Re_c of 8 million, which were typically used for several high-lift cases, to the high-speed range was necessary.
Mach 0.95 had more convergence difficulties than the other ones. It is suspected that oversetting incompatible C-O and H-O topologies without surface grid iterative projection induced numerical noise hurting thus the convergence of the solutions at transonic conditions.
It is also suspected that the same problem rendered the time-accurate simulations impossible (crashes at the first iteration). A more systematic oversetting method where the relevant topologies and grid cell sizes are more compatible is believed to be more tailored towards the considered range of Mach numbers and angles-of-attack.

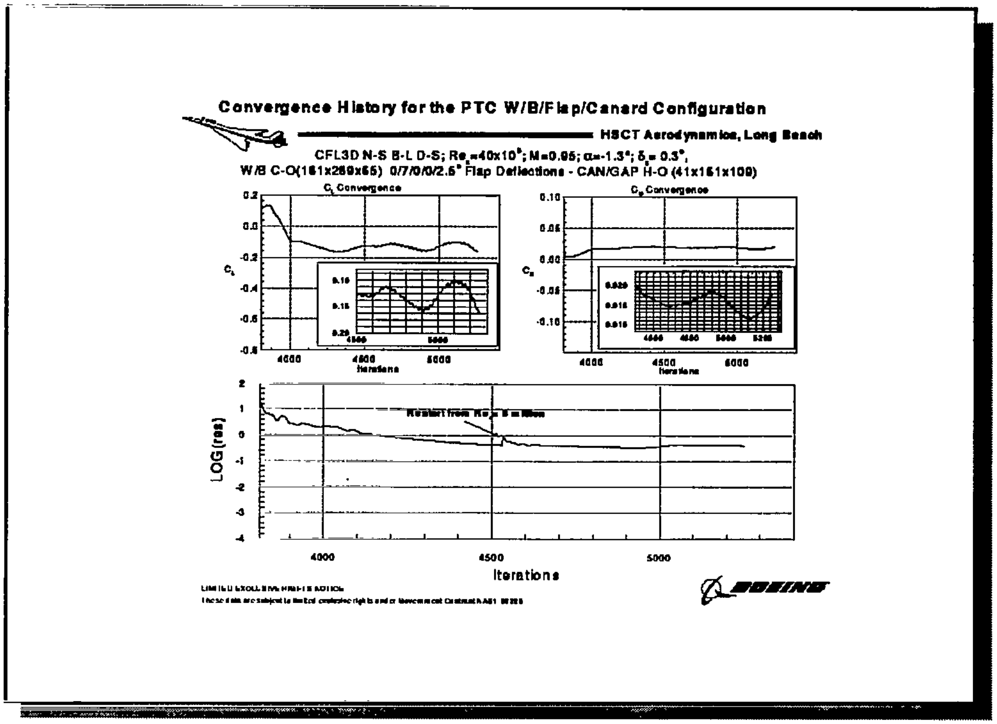

The chart above shows a case where convergence was impossible. The transonic nature of this case makes it more sensitive, even at mild conditions such as $\alpha = -1.3°$ and a canard deflection of 0.3°. Even though the solution seems to be converging at first, the oscillation amplitude of the integrated forces keeps increasing thus indicating a magnification of the instabilities. Several attempts were made to improve the convergence behavior (e.g. changing numerical schemes, flow conditions, turning-off the gap block, even restart from different conditions such as lower Reynolds number), but could not prevent the divergence observed in the integrated quantities. Because of interpolation errors due to oversetting the grids, it is suspected that such a low angle-of-attack case would be more sensitive to disturbances than other lifting cases. Consequently, oversetting the relevant grids needs to be rendered more accurate.

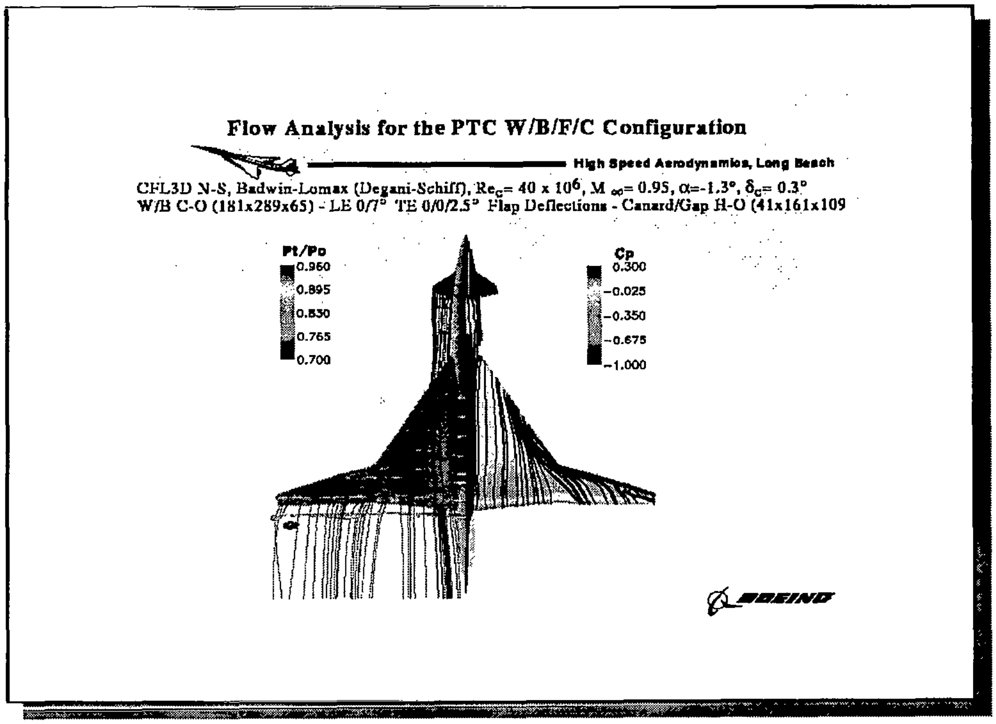

This chart describes the relatively benign flowfield described in the previous chart. In fact, no convergence problems should be expected for such a flowfield which was not the case.

Lessons Learned

- Use improved grid projection tool (PROJ provided by PW-Seattle) to fix the mismatches between incompatible overset grids - Iterations between overset surface-grid projections
- Revise overset gridding procedures to allow time-accurate runs at higher angles-of-attack

The transonic case where convergence problems were encountered was given to a Seattle division of Boeing Phantom Works for assessment. Initially, the analysis code could not converge but after using the surface grid-projection code (iterative process between surfaces of different topologies) the solution converged without any problem.
Higher angles-of-attack convergence histories and flowfields do suggest that the time-accurate approach be used for such unsteady vortical flows. Consequently, further investigations in order to get the time-accurate approach to work should be made.

Summary

- Nonlinear loads CFD runs were successfully computed and fed into the nonlinear loads database (CORRECT procedure)
- Modification to the nonlinear loads CFD data generation process were undertaken:
  - Inclusion of overset canards/gaps with available automatic grid generation capability
  - Modification of loads convergence criteria routines for multiblock grids

In spite of the larger scale of the simulated cases for the PTC (4 million points - canards with gaps and gapped trailing-edge flaps) CFD solutions were "loads" converged and input into the nonlinear loads database.

The CFD process for the nonlinear loads was modified to incorporate trailing-edge flaps and overset canards. The use of an automated grid generation procedure for canards and gaps allowed faster turn-around of the relevant grids. Changes to the CFL3D routines that monitor convergence of sectional loads were implemented to accommodate flaps with gaps and multiblock grids. Some minor code modifications were made to allow variable pseudo-time CFL numbers for the τ-TS time-accurate method. This option is very useful when dealing with high Mach and high Reynolds number cases.

Suggested Improvements

- Overset of coarser wing/body grids is recommended
- Enhancement of the current overset process (grids suitable for time-accurate runs) is needed
- Investigation of the sensitivity of wing loads to canard vortex strength is useful (with and without gaps) ⇒ May not need to model the canard/gap for all cases
- Parallelization of the relevant codes is needed to enhance turn-around time

Oversetting the C-O wing/body and H-O canard/body topologies dictated the use of fine grids For better turn-around time, the use of coarser grids is necessary and should be pursued once the surface grid projection capability is streamlined. In fact, the high resolution along flap edges is not needed for sectional loads and fewer streamwise and spanwise stations may be used on both wings and canards.

Investigations concerning the effect of the canard vortex on the wing loading still need to be undertaken. The results may indicate a low level of wing-canard interaction on loads and thus a lack of sensitivity for a given range of flight conditions and consequent savings in the computational effort.

Since most of the CFD jobs were high memory jobs (above 180 MW on the C90) the turn-around time was very slow. This time can be significantly reduced if the ACE loads routines were incorporated in CFL3Dhp, which would allow the cases to run in a parallel environment.

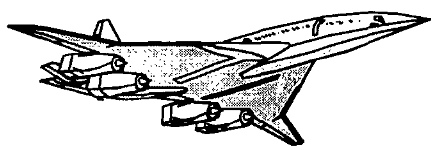

ACE Final Report

C.2.1 - Uncertainty in CFD Solutions for Loads at High-Alpha Flow Conditions - NASA Ames

Scott Murman
Neal Chaderjian

December 31, 1998

GOALS AND OBJECTIVES

- Utilize NASA Ames Research Center's computational fluid dynamic (CFD) experience with high angle of attack (AOA) flows to evaluate the Boeing Long Beach (BLB) CFD loads prediction process for the PTC geometry at high AOA
- High AOA flow conditions correspond to a 2.5-g load, which is used to size the vehicle
- Various numerical issues that effect the computational accuracy for the PTC geometry are examined
  - Geometry modeling
  - Grid density
  - Turbulence models
- The effect of different turbulence models for predicting vortical loads on simple geometries at high AOA are quantified with experimental data

Boeing Long Beach (BLB) has developed an efficient nonlinear loads prediction process, which coupled with their structural deflection code, is used to size the PTC geometry. The vehicle sizing is based on a 2.5 g load requirement, which is achieved using high angle of attack (AOA) flow conditions. Boeing Long Beach is also using the CFL3D computational fluid dynamic (CFD) code to calibrateed by vorticesmethods that work well for low AOA cruise conditions must be modified to accurately predict the complex flow features found at high AOA. NASA Ames has extensive experience with computing high AOA flows with high-fidelity Navier-Stokes codes. The purpose of this analysis is to evaluate the requirements for accurately predicting the aerodynamic loads (lift) on the PTC configuration at transonic, high AOA flow conditions, and also provide an independently generated set of numerical simulations for comparison with the BLB CFL3D results, in lieu of experimental data. The BLB loads group uses a single-zone grid topology to model the PTC wing and fuselage, and separate grid to model the canard. The current analysis uses the OVERFLOW CFD code, and the fuselage-wing-canard PTC geometry is modeled with an overset, multi-zone, grid system. This different gridding strategy allows for a higher degree of geometry resolution and grid refinement. The effect of different turbulence models on the PTC loads are examined. Computations for simple geometries at high AOA are also carried out, where the effects of different turbulencecomputed vortical loads can be quantified by comparison with experimental data.

APPROACH

- PTC wing-body-canard configuration at transonic, high AOA flow conditions
- Investigate parametric effects on integrated lift, wing sectional lift, and wing sectional center-of-pressure
  - Turbulence model implementation
  - Off-surface grid refinement of the canard vortex and wing leading-edge vortices
- Utilize the OVERFLOW code and an overset grid system to compute the flow using the Reynolds-averaged Navier-Stokes (RANS) equations
  - Use additional refined overset grids to resolve the off-surface vortices
  - Turbulence model (AIAA Paper 98-4519)
    - Simplified Baldwin-Lomax/Degani-Schiff algebraic model (similar to CFL3D used by BLB)
    - Complete Baldwin-Lomax/Degani-Schiff algebraic model from the NASA High-Alpha Technology Program
    - Spalart-Allmaras one-equation model

The CFD loads analysis was carried out on a wing-body-canard PTC configuration. The flow conditions for all computed results are 11.5 degrees angle of attack, Mach number of 0.95, and Reynolds number of 40 million. A CAD file was provided by BLB, and an overset grid system was developed that modeled the geometry, including deflected flap settings. The wing inboard flaps were all undeflected, the wing leading-edge outboard flap was deflected 7 degrees down, and the wing trailing-edge outboard flap was deflected 2.5 degrees down. The relative canard AOA was 14 degrees (a total AOA of 25.5 degrees), from schedules provided by BLB. The overset grid system consists of 6 viscous zones and 1 Euler zone, forming 2.3 million viscous points, and 400k Euler points for a half-body geometry. The OVERFLOW finite-difference RANS code was utilized for all computations. This code has been used extensively for computations on overset grid systems in the past at NASA Ames, with good results.

Due to the lack of experimental data for the PTC at high AOA, a precise assessment of the accuracy of the computations isn't possible. However, the effect of each parametric effect, as well as the cumulative effects, can be quantified as a percent change relative to a baseline. For this study, the wing-body-canard geometry using a turbulence model similar to that used by BLB in CFL3D was chosen as the baseline configuration. This turbulence model is a simplified form of the Baldwin-Lomax/Degani-Schiff (B-L/D-S) turbulence model for crossflow separation. The complete B-L/D-S turbulence model, as developed for the NASA High-Alpha Technology program was also utilized, as was the Spalart-Allmaras one-equation model for some simplified geometries. The effects of the different turbulence models, and the resolution of the off-body canard vortex and wing leading-edge vortices, were examined against the baseline configuration.

RESULTS
Effect of Canard on Wing Flowfield
$M_\infty = 0.95, \alpha = 11.5^\circ, Re = 40 \times 10^6$

- The canard vortex does not strike the wing, but has a significant influence on the wing loading

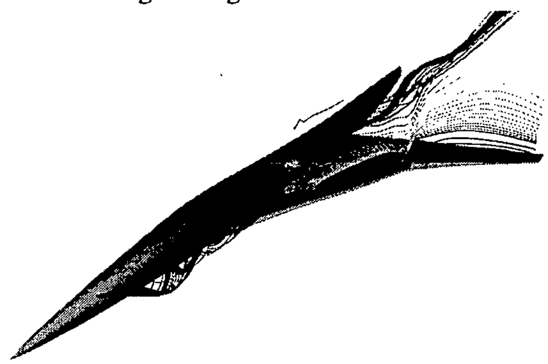

The angle-of-attack for the current configuration is 11.5 degrees. The canard is inclined 14 degrees relative to the fuselage, so that the total angle of attack of the canard is 25.5 degrees. This results in the formation of a strong canard vortex, which convects downstream (cf. Fig.). The canard vortex does not strike the wing, however it passes sufficiently close to the wing surface to effect the wing loading, especially on the inboard section of the wing. Sufficient grid resolution of the canard vortex formation and convection downstream is needed to accurately compute the influence of this vortex on the wing loading. The effect of adding a refined, embedded Cartesian

RESULTS
Effect of Turbulence Model
$$M_\infty = 0.95, \alpha = 11.5^\circ, Re = 40 \times 10^6$$

- Different turbulence models effect the surface-flow patterns on the leeward side of the wing, resulting in a slight difference in the loads

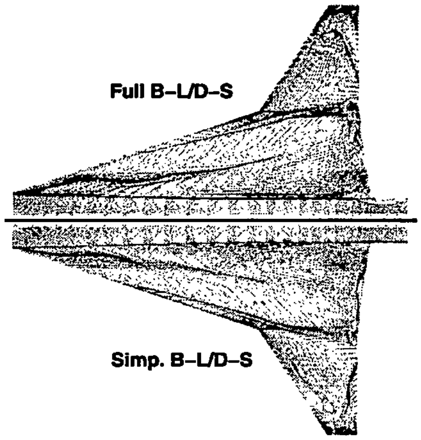

The two turbulence models predict similar surface-flow patterns on the leeward side of the PTC wing, with most of the differences occurringorming a primary vortex. This vortex is of sufficient strength to form secondary and tertiary vortices, along with their associated separation/reattachmentrd of the simplified B-L/D-S model. Both models predict inboard separation and reattachment lines due to a complex interaction between the primary and canard vortices.

Both turbulence models predict different separation patterns near the wing trailing-edge. The simplified B-L/D-S model predicts a shock-induced separation line near the wing trailing edge, consistent with the 0.95 freestream Mach number. There is also a shock/vortex surface-flow interaction. The full B-L/D-S model predicts a very complex surface flow topology that is difficult to physically justify. The additional crossflow logic in the full model was not designed for streamwise separation.

On the outboard section of the wing, the flow separates downwind of the deflected leading-edge flap hinge line. The surface-flow patterns near the wing tip are very complex due to the interaction of the hinge-line separation and the wing-tip vortex.

The loads predicted by these two models differ only slightly, as described in the next slide.

RESULTS
Summary of Loads due to Turbulence Model and Vortex Grid Refinement
$M_\infty = 0.95, \alpha = 11.5°, Re = 40 \times 10^6$

Case	C_L	$(C_L)_{wing}$	C_D	C_L/C_D
Simplified D-S	0.725	0.637	0.145	5.0
Full D-S	0.713	0.635	0.143	5.0
Refined Grid	0.715	0.625	0.143	5.0

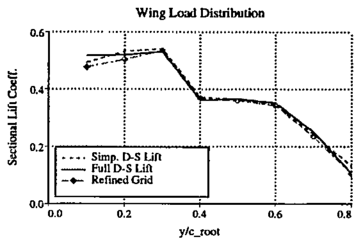

It is often necessary to refine the grid in the off-surface vortex core region in order to accurately capture the high core velocities and resulting suction peak on the wing surface. A Cartesiane canard vortex. This grid begins near the canard trailing-edge and extends downstream past the wing trailing-edge, roughly following the path of the canard vortex. A similar approach was not feasible for the wing leading-edge vortices, due to their close proximity to the upper wing surface. Embedding such a grid so close to the boundary layer would be problematic. Instead, the wing grid was refined in both the chordwise, and body-normal directions, to better resolve these vortices. The area of refinement roughly corresponds to the location of the primary vortex core.

Computations for this refined grid system used the Simplified B-L/D-S model. Overall, the difference in loads was very slight, with the refined grid having a slightly smaller sectional lift, especially near the wing/fuselage region. The canard vortex, for the refined grid, may be displaced slightly higher above the wing surface than in the unrefined grid case. These results indicate that the baseline grid was suitable for resolving the loads due to off-surface vortices.

The loads for the simplified B-L/D-S model were slightly higher than with the full B-L/D-S model.

RESULTS
Effect of Turbulence Model on a 65° Sweep Delta Wing
$M_\infty = 0.27, \alpha = 15^\circ, Re = 3.67 \times 10^6$

- Surface pressures predicted by the Simplified and Full B-L/D-S turbulence models compare well with experiment
- The S-A turbulence model significantly underpredicts the vortex suction peak, even when the production term is reduced for vortical flows

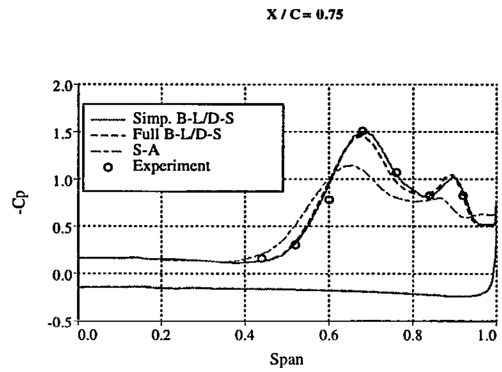

The relative effects of turbulence model on the loads for the PTC geometry have been demonstrated; however, there is no experimental data to quantify the accuracy of these models. We therefore investigated the effect of turbulence model on high AOA vortical flows for two simple geometries, a tangent-ojive cylinder and a 65 degree sweep delta wing, which had experimental surface-flow and surface-pressure data. The former geometry represents forebody shapes while the latter represents swept wings. Only the delta wing is briefly discussed here, due to space limitations. Further details about the results for both geometries are described in AIAA Paper 98-4519.

Computations for the delta wing were carried out with a 0.27 freestream Mach number, 15 degrees AOA, and 3.67 million Reynolds number based on the wing root chord. Three turbulence models were included in this study, the simplified and full B-L/D-S models, and the Spalart-Allamaras (S-A) model. The latter was investigated last year with the TCA geometry, and is more suitable for general grid topologies and shock-induced separation common to high Mach number flows.

Both the simple and full B-L/D-S models give near identical results, and compare well with the experimental surface pressures. The primary suction peak is well predicted. The S-A model, however, significantly underpredicts the vortex suction peak. This is a well known problem with this model, and other investigators have suggested modifying the production term by replacing the vorticity magnitude with the strain rate in the off-surface vortex core region. We implementedent in the predicted suction peak. Further investigation showed that the S-A model predicts turbulent eddy viscosities that are 2-3 times greater than either B-L/D-S model. A more fundamental change is needed for the S-A model within the boundary layer. The baseline S-A model is not recommended for predicting high AOA vortical flows, and their resulting loads.

CONCLUSIONS

- Different flowfield regions are dominated by different physical phenomenaion, which place difficult requirements on a single turbulence model
  - The simplified B-L/D-S model performed best for predicting loads for the present high AOA flow conditions
- The canard vortex influences the wing flowfield and loading
  - Baseline grid is adequate
- Outboard flap deflections prevented leading-edge vortex formation, however, streamwise separation occurs downwind of the hinge line.
- Improved resolution of the wing-tip geometry for the PTC using overset grids eliminated turbulence model differences found last year with a single-grid TCA geometry
- Computations were carried out for a delta wing at high AOA
  - The simplified and full B-L/D-S models accurately predicted the primary suction peak
  - The S-A model significantly underpredicted the primary suction peak, even with modifications to the production term

Different regions of the flowfield are dominated by different flow phenomena, e.g., crossflow separation (vortices), streamwise separation, shock-induced separation, and complex interactions between two or more vortices. All of these features were present on the PTC geometry under the present high AOA flow conditions, which are difficult to model with a single turbulence model. The simplified B-L/D-S turbulence model seemed to perform best, compared to the full B-L/D-S model, for predicting the wing loads.

The canard vortex does influence the wing loading and the surface-flow patterns near the wing/fuselage juncture, the latter due to an interaction between the canard vortex and the inboard leading-edge vortex. The outboard flaps were deflected with a sheared grid, i.e., spanwise gaps were not modeled. This flap deflection eliminated the flap vortex, as expected, however there was a streamwise separation just aft of the flap hinge line. High AOA computations on the TCA geometry last year showed unsteady flow and different surface-flow topologies with different turbulence models. It was felt that the single-zone grid provided by Boeing was inadequate to properly model the wing-tip geometry, and may be responsible for these differences. There were no such differences found for the present computations on the PTC, where additional overset grids were used to properly model the wing-tip geometry. We remark, however, that the PTC computations were at a lower angle of attack than the TCA computations.

Computations for a delta wing were compared with experimental data, which helped quantify the the effect of turbulence model on predicting the primary vortex suction peak. The simplified and full B-L/D-S models accurately predicted this suction peak, while the S-A model significantly underpredicted the suction peak, even when the production term was modified in the off-surface vortex-core region. We do not recommend the baseline S-A model for predicting vortex dominated loads.

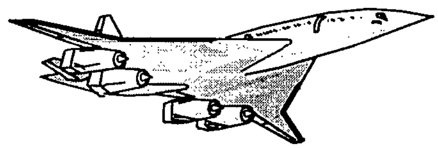

ACE Final Report

C.2.2 - ACE Non-Linear Loads Validation Process

Mehrdad Farhangnia - NASA Ames
Guru P. Guruswamy- NASA Ames
Pat Goggin - Boeing LB
Kuo-An Youn- Boeing LB

December 31, 1998

OBJECTIVES

COMPUTE NON-LINEAR LOADS USING NAVIER-STOKES FLOW EQUATIONS FULLY COUPLED WITH STRUCTURAL EQUATIONS

VALIDATE AND CALIBRATE ACE NON-LINEAR LOADS PROCESS BASED ON NS COMPUTATIONS OVER RIGID CONFIGURATIONS

ACE NON-LINEAR LOADS PROCESS

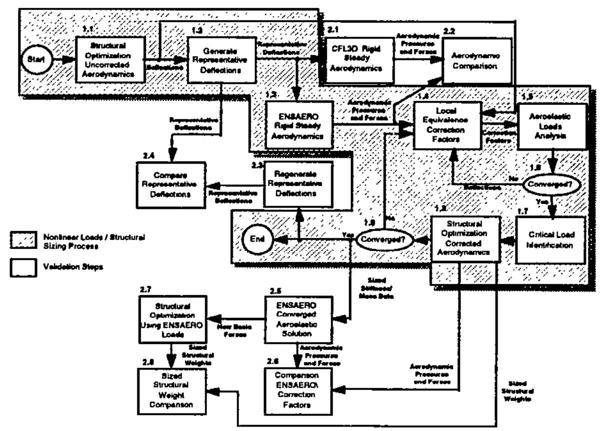

HPCCP ENSAERO_MPI DEVELOPMENTS AND HSR APPLICATIONS

- A CONCURRENT 3-LEVEL MULTIDISCIPLINARY ENSAERO PROCESS IS COMPLETED USING MPIRUN UTILITY BASED ON IEEE MPI STANDARDS
  - PARALLELIZATION WITHIN DISCIPLINES (FLUIDS, STRUCTURES, CONTROLS)
  - DISCIPLINE TO DISCIPLINE PARALLELIZATION
  - MULTIPLE CASES WITH DIFFERENT FLOW PARAMETERS IN PARALLEL

- THIS NEW CAPABILITY IS APPLIED TO COMPUTE ACCURATE NON-LINEAR LOADS FOR TCA-6 W-B WITH TAIL LOADS FOR CALIBRATING ACE NON-LINEAR LOADS PROCESS
  - STRUCTURES ARE MODELED USING MODAL APPROACH
  - GIVEN TAIL TRIM LOADS ARE APPLIED AS GENERALIZED MODAL FORCES

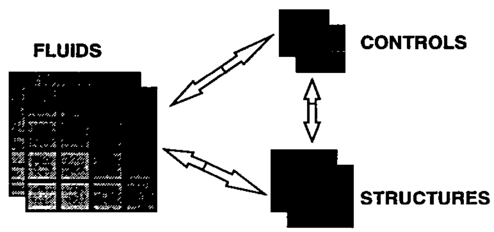

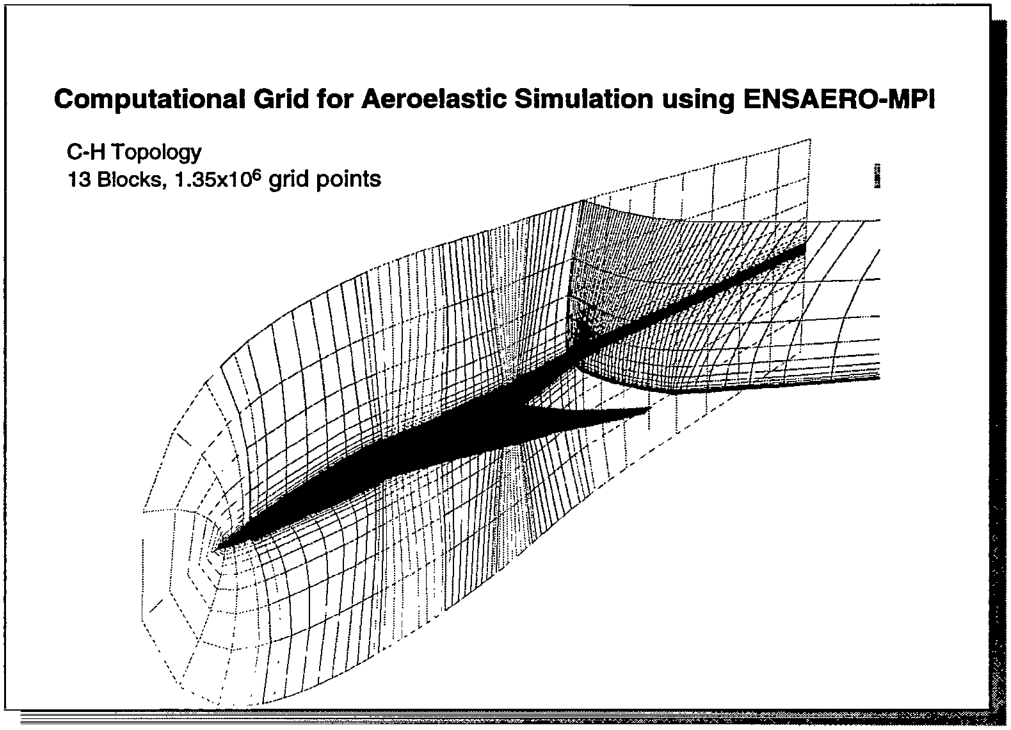

The surface grid used for the above configuration was derived from a CFD grid obtained from Boeing Long Beach using GRIDGEN, maintaining the same C-H topology. The surface grid was resized to be 217 points in the streamwise direction and 112 points in the spanwise. The volume grid was developed using a hyperbollic grid generator called LE GRID, with 55 points in the body-normal direction. The final grid was split into 13 nearly equal sized blocks in the streamwise direction with a one cell overlap. The uniform sizing of each block greatly improves the load balancing of processors on parallel platforms, where computations are performed. The total grid size is 1.35×10^6, while each block is approximately 1.11×10^5.

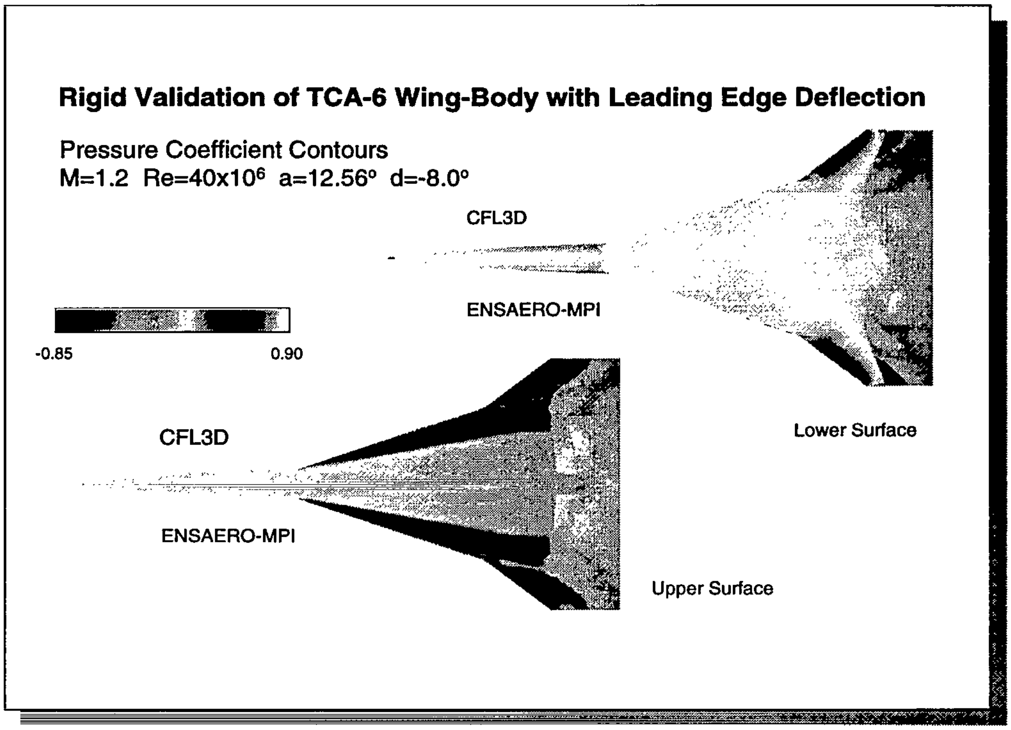

This slide shows the pressure coefficients on the upper and lower surfaces of the ACE geometry at $M=1.2$, $Re=40\times10^6$, $\alpha=12.56°$ and $\delta=-8.0°$. These calculations were computed by ENSAERO-MPI using the rigid conficuration and compared directly with the results from CFL3D generated at Boeing Long Beach. The comparisons agree well in both magnitude and location of the lifting vortex on the upper surface. The CFL3D result has a higher pressure peak through the core of the vortex, creating a slight increase in overall Cl. It should be noted that the grid used in the ENSAERO-MPI calculation is coarser (1.35×10^6 points) relative to the grid used for the CFL3D calculations (1.83×10^6 points), particularly in the body normal direction (69 vs. 55 points).

ENSAERO-MPI Aeroelastic Simulation TCA-6 Wing-Body with Leading Edge Deflection

Flexible: Shown with Pressure Contours M=1.2 Re=40x10^{6} a=12.56° d=-8.0°

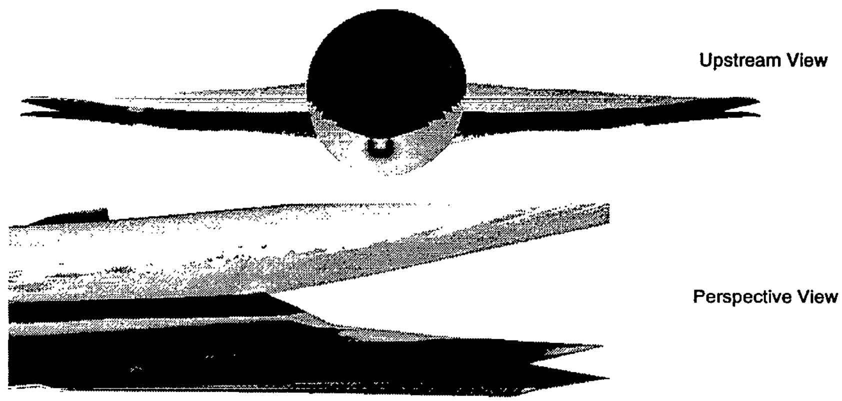

This slide shows the result of the static aeroelastic computations using ENSAERO-MPI on the flexible ACE configuration. The above result is generated by coupling the Navier-Stokes and modal equations on the structures side at each time step, until the deflections at the tip coverge. This process is accelerated by including the dynamic terms in the equations of motion with large damping coefficients. Six mode shapes are included in this simulation to capture bending and torsional effects.

The results show deflections mostly due to bending, particularly on the outboard portion of the wing. The magnitude of the bending at the tip is less than 3 percent of the root chord. As expected, the fuselage is much more stiff, with only slight nose-down bending at the nose (top figure).

CONCLUSIONS

- AN ACCURATE AND EFFICIENT PROCEDURE IS DEVELOPED ON PARALLEL COMPUTERS TO COMPUTE STATIC AEROELASTICITY OF FULL HSR CONFIGURATION
- A PROCEDURE IS DEVELOPED TO APPLY EXTERNAL TAIL TRIM LOADS DURING COUPLED ANALYSIS
- STATIC DEFLECTIONS AND LOADS ARE COMPUTED FOR TCA-6 WING-BODY CONFIGURATION TO VALIDATE ACE NON-LINEAR LOADS PROCESS WHICH IS BASED ON NAVIER-STOKES COMPUTATIONS OVER RIGID MODELS

There was delay in delivering data from this work due to delays in obtaining profer resources from ACE and branch.

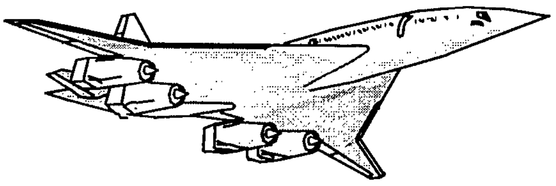

ACE Final Report

D.1 - PTC Variant Strength Sized Structural FEM Data Package - Boeing/Elfini Process

December 31, 1998

Contents

Contents

PTC Variant Weights

PTC Variant FEM Weight vs.
PTC Variant Weight Allocation

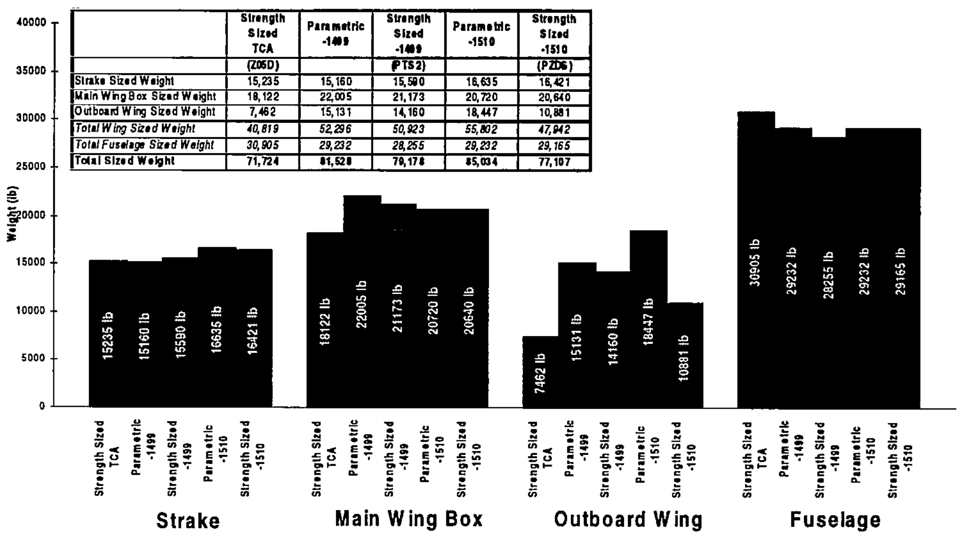

	Strength Sized TCA	Parametric -1499	Strength Sized -1499	Parametric -1510	Strength Sized -1510
	(Z05D)		(PTS2)		(PZD6)
Strake Sized Weight	15,235	15,160	15,590	16,635	16,421
Main Wing Box Sized Weight	18,122	22,005	21,173	20,720	20,640
Outboard Wing Sized Weight	7,462	15,131	14,160	18,447	10,881
Total Wing Sized Weight	*40,819*	*52,296*	*50,923*	*55,802*	*47,942*
Total Fuselage Sized Weight	*30,905*	*29,232*	*28,255*	*29,232*	*29,165*
Total Sized Weight	71,724	81,528	79,178	85,034	77,107

Note: the PTS2 is the PTC Strength Sized mesh with Variable Allowables and Discretization.

PTC Variant vs. PTC Variant FEM Weight

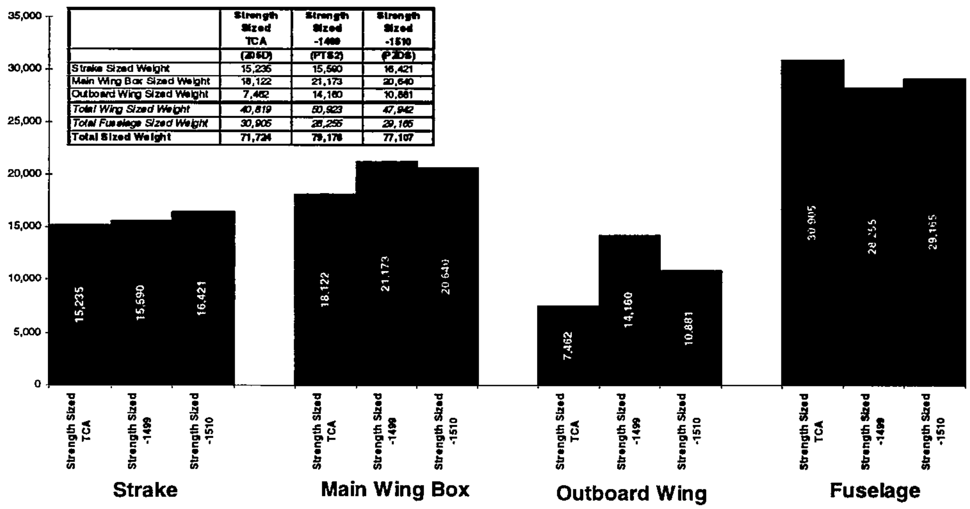

	Strength Sized TCA	Strength Sized -1499	Strength Sized -1510
	(205D)	(PTS2)	(P2D8)
Strake Sized Weight	15,235	15,590	16,421
Main Wing Box Sized Weight	18,122	21,173	20,640
Outboard Wing Sized Weight	7,462	14,160	10,881
Total Wing Sized Weight	*40,819*	*50,923*	*47,942*
Total Fuselage Sized Weight	*30,905*	*28,255*	*29,165*
Total Sized Weight	**71,724**	**79,176**	**77,107**

Note: the PTS2 is the PTC Strength Sized mesh with Variable Allowables and Discretization.

PTC Variant Strength-only Fuselage Structure Weight

Fuselage Structure Weight	Strength Sized TCA (740K) (Z05D model)		Strength Sized -1499 (788K) (PTS2 model)		Strength Sized -1510 (788K) (PZSD model)	
	Weight (lb)	Unit Weight (lb/ft^2)	Weight (lb)	Unit Weight (lb/ft^2)	Weight (lb)	Unit Weight (lb/ft^2)
FUSELAGE STRUCTURE	**44,796**	**4.05**	**43,506**	**3.94**	**44,426**	**4.02**
Weighed Structure	**30,905**	**2.80**	**28,255**	**2.56**	**29,165**	**2.64**
Semi-Monocoque	27,079		25,920		26,548	
Skin Panels	19,400		18,753		19,386	
Frames	7,679		7,167		7,162	
Keel Beam	3,472		1,975		2,257	
Lightning Protection	355		360		360	
Fixed Weight Structure	**13,891**	**1.26**	**15,251**	**1.38**	**15,261**	**1.38**
Bulkheads	2,123		3,041		3,051	
Nose Gear Wheel Well	400		450		450	
Empennage Support	315		315		315	
Windows	1,090		1,120		1,120	
Passenger Windows						
Cockpit Windows						
Doors	3,241		2,911		2,911	
Pressurized						
Unpressurized						
Main Deck Floor	3,146		3,146		3,146	
Seat Tracks	713		713		713	
Other Items	1,082		2,049		2,049	
Tail Skid						
Seam, Seal, & Finish						
Forebody Controls						
Chines						
Fairings						
Miscellaneous	1,781		1,506		1,506	

PTC Variant Strength-only Wing Structure Weight

Wing Structure Weight	Strength Sized TCA (740K) (Z05D model)		Strength Sized -1499 (788K) (PTS2 model)		Strength Sized -1510 (788K) (PZSD model)	
	Weight (lb)	Unit Weight (lb/ft^2)	Weight (lb)	Unit Weight (lb/ft^2)	Weight (lb)	Unit Weight (lb/ft^2)
TOTAL WING STRUCTURE	**67,228**	**7.9**	**80,434**	**8.7**	**78,167**	**8.1**
TOTAL WEIGHED STRUCTURE	40,819	4.8	50,923	5.5	47,942	5.0
TOTAL FIXED WEIGHT	26,409	3.1	29,511	3.2	30,225	3.1
Strake	**21,765**	**7.80**	**22,238**	**7.95**	**23,219**	**7.74**
Weighed Structure	15,235	5.46	15,590	5.57	16,421	5.48
Fixed Weight	6,530	2.34	6,648	2.38	6,798	2.27
FORWARD STRAKE	7,727	8.59	7,812	7.58	7,607	7.44
Weighed Structure	6,332	7.04	6,287	6.10	6,048	5.92
Bending Material (Skin Panels & Spar Caps)	4,292		4,927		4,718	
Shear Material (Spar Webs & Ribs)	1,944		1,286		1,258	
Lightning Protection	96		74		71	
Fixed Weight	1,395	1.55	1,525	1.48	1,559	1.53
Access Doors	645		714		708	
Wing/Fuselage Attachment	600		649		681	
Actuator Attachment	150		162		170	
MID/GEAR BOX	14,039	7.42	14,426	8.16	15,612	7.90
Weighed Structure	8,904	4.71	9,303	5.26	10,373	5.25
Bending Material (Skin Panels & Spar Caps)	6,859		6,950		7,864	
Shear Material (Spar Webs & Ribs)	1,947		2,226		2,370	
Lightning Protection	98		127		138	
Fixed Weight	5,135	2.71	5,123	2.90	5,239	2.65
Access Doors	815		762		852	
Wing/Fuselage Attachment	400		433		454	
Actuator Attachment	100		108		113	
MLG Doors & Jam/Attachment	3,820		3,820		3,820	
Main Wing Box	**20,192**	**16.90**	**23,314**	**19.14**	**22,764**	**18.71**
Weighed Structure	18,122	15.16	21,173	17.38	20,640	16.96
Bending Material (Skin Panels & Spar Caps)	14,371		17,227		16,198	
Shear Material (Spar Webs & Ribs)	3,751		3,858		4,357	
Lightning Protection	0		88		85	
Fixed Weight	2,070	1.73	2,141	1.76	2,124	1.75
Access Doors	920		897		819	
Wing/Fuselage Attachment	950		1,028		1,078	
Actuator Attachment	200		216		227	
Outboard Wing Box	**8,443**	**13.34**	**15,273**	**15.32**	**12,127**	**9.61**
Weighed Structure	7,462	11.79	14,160	14.20	10,881	8.62
Bending Material (Skin Panels & Spar Caps)	6,923		12,814		9,995	
Shear Material (Spar Webs & Ribs)	489		1,275		798	
Lightning Protection	49		72		88	
Fixed Weight	981	1.55	1,113	1.12	1,246	0.99
Access Doors	631		734		849	
Actuator Attachment	350		379		397	
Leading Edge (Fixed Weight)	7,036		7,028		7,285	
Trailing Edge (Fixed Weight)	7,792		9,370		9,679	
Fairings (Fixed Weight)	800		832		852	
Miscellaneous (Fixed Weight)	1,200		2,379		2,241	

Running Loads

PTC Variant Strength Only Upper Outboard Wing Running Loads (Spar Direction)

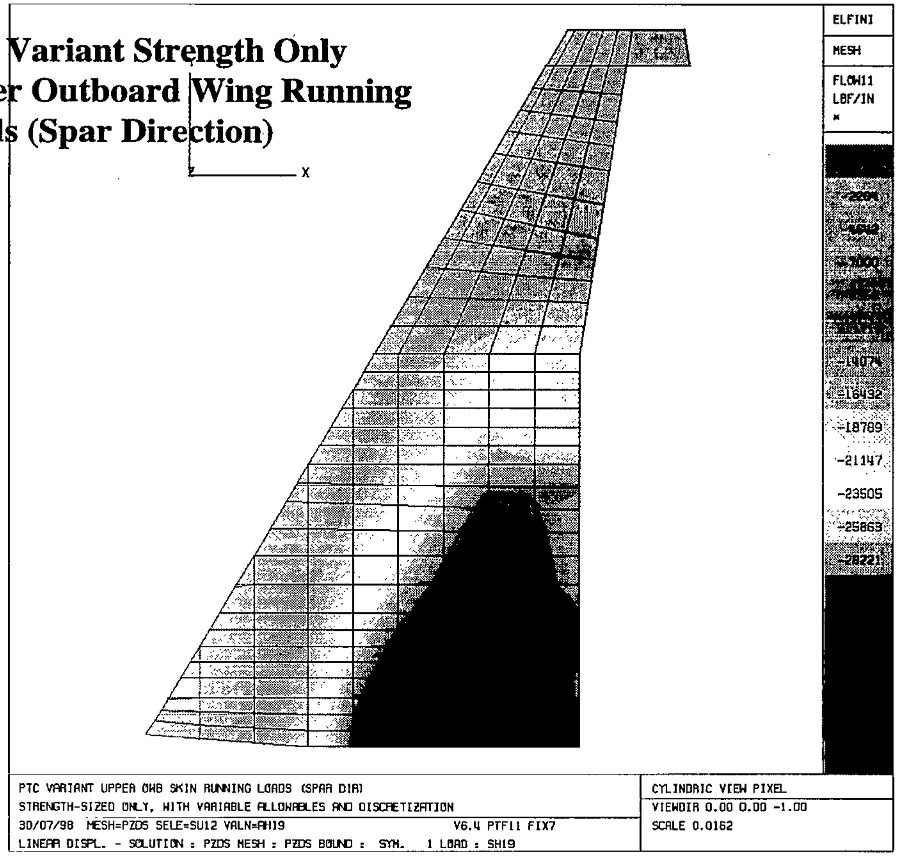

PTC Variant Strength Only Upper Outboard Wing Running Loads (Transverse)

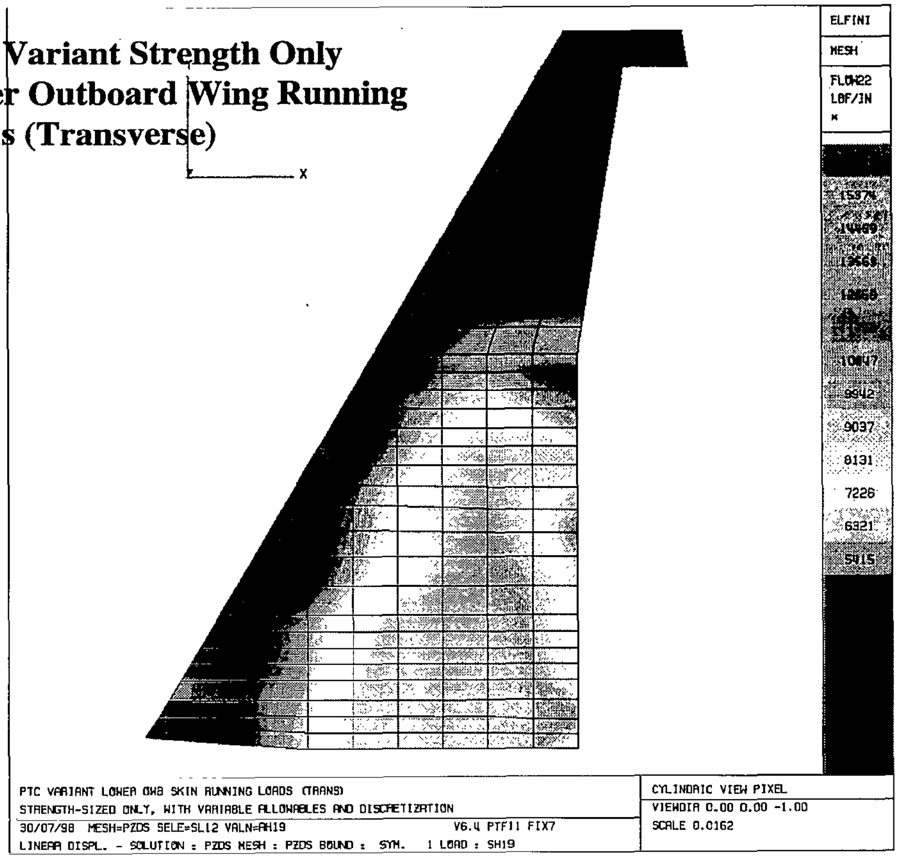

PTC Variant Strength Only Upper Outboard Wing Running Loads (Shear)

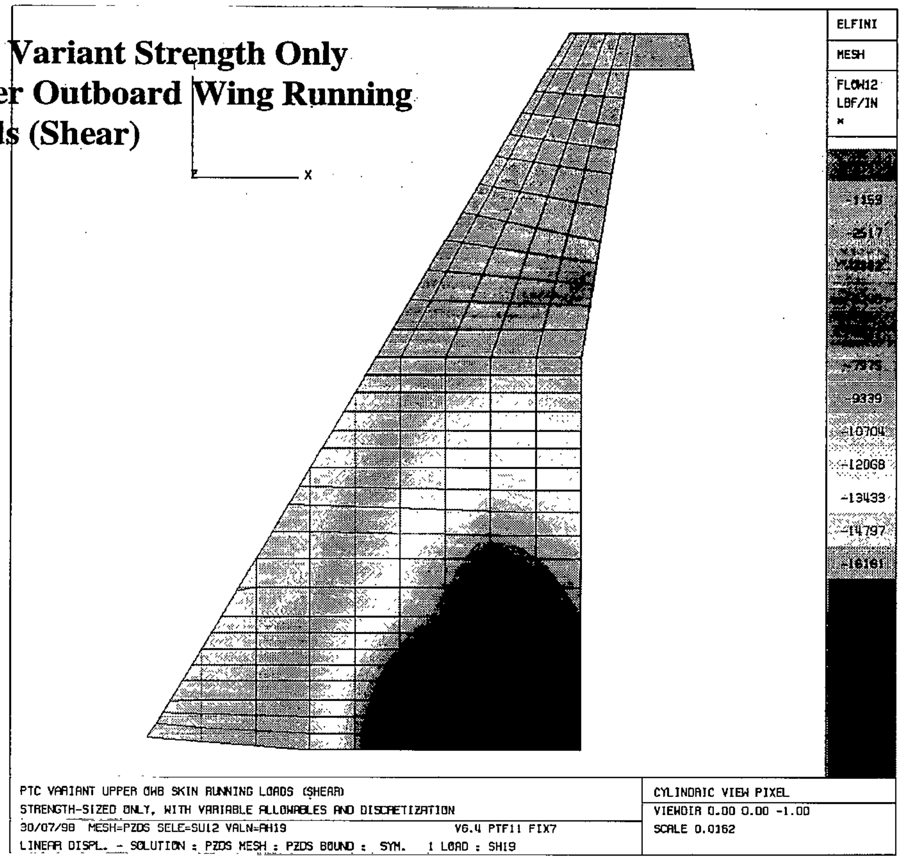

**PTC Variant Strength Only
Upper MWB Running Loads
(Spar Direction)**

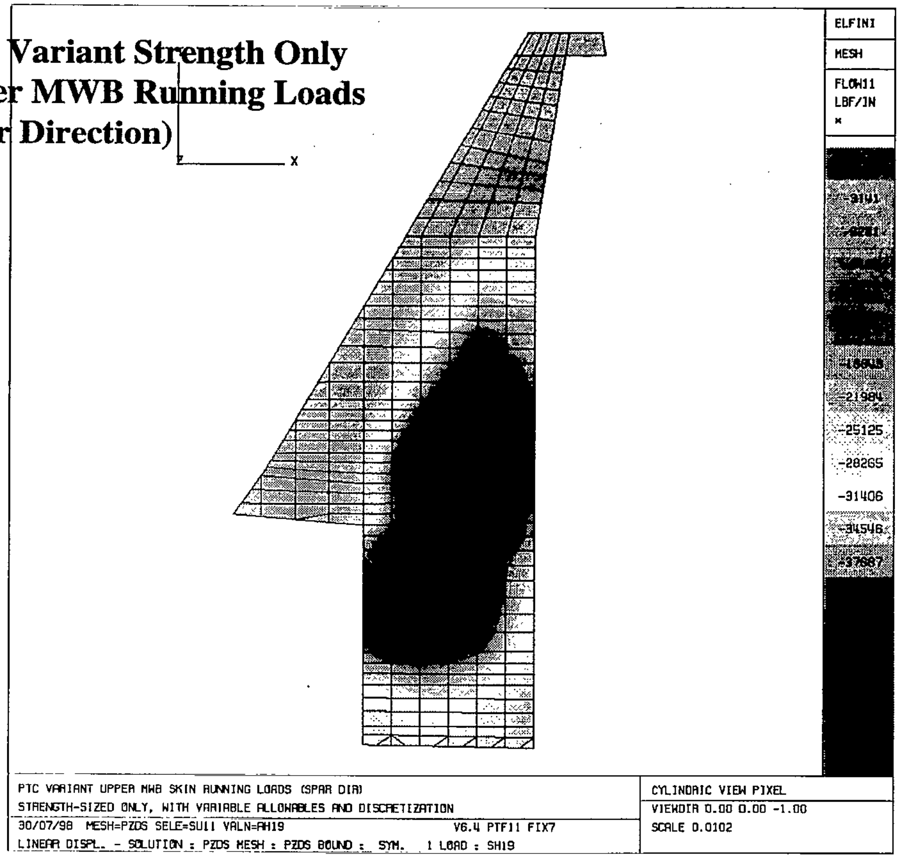

PTC Variant Strength Only Upper MWB Running Loads (Transverse)

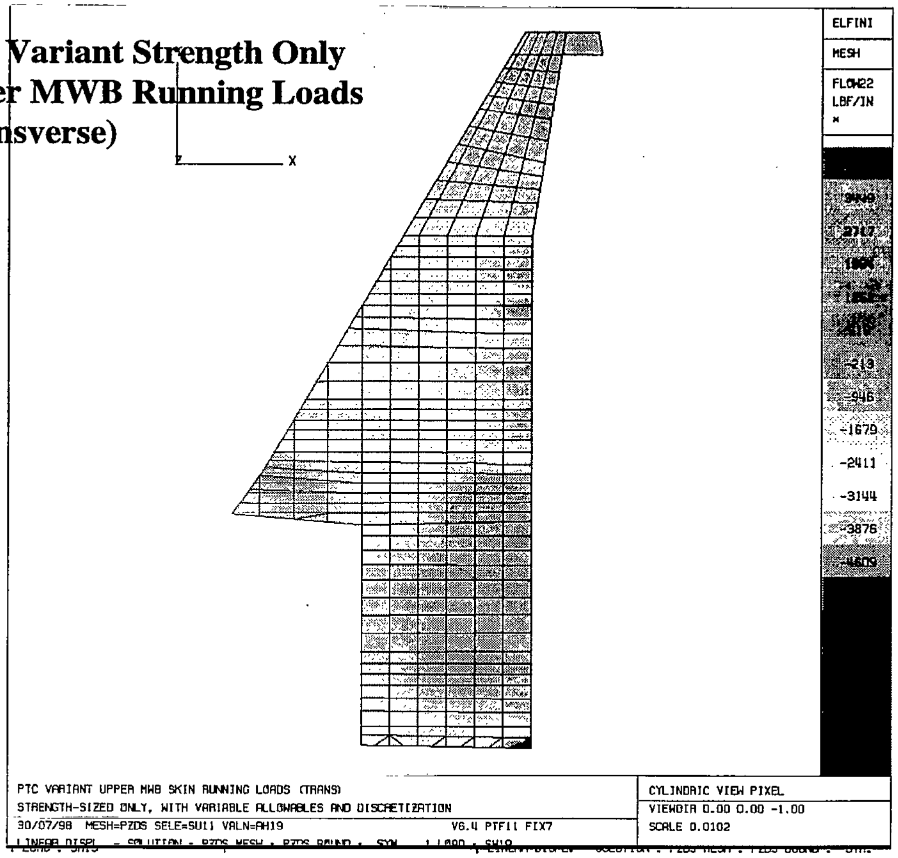

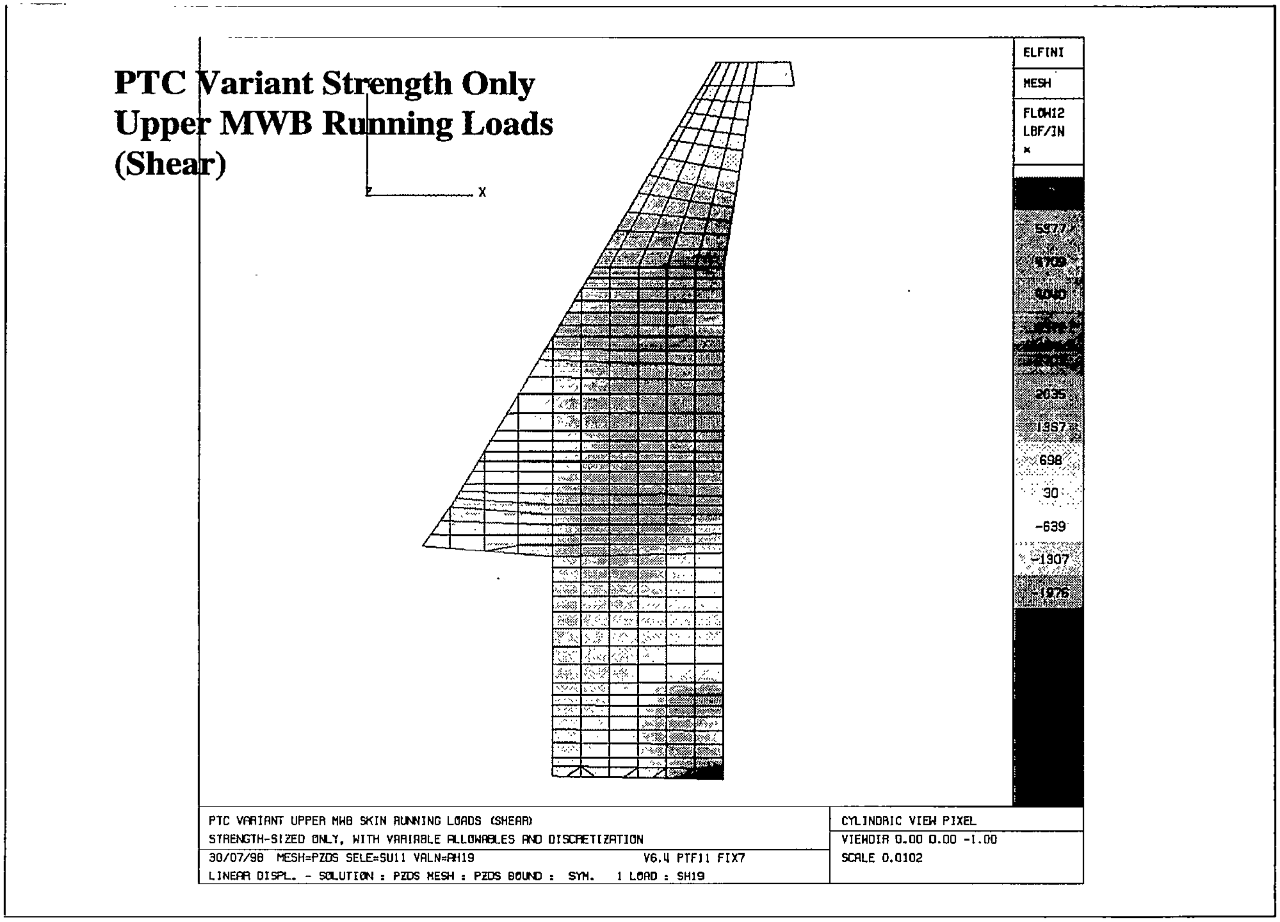
PTC Variant Strength Only
Upper MWB Running Loads
(Shear)
X
ELFINI
MESH
FLOW12
LBF/IN
2035
1357
698
30
-639
-1307
PTC VARIANT UPPER MWB SKIN RUNNING LOADS (SHEAR)
STRENGTH-SIZED ONLY, WITH VARIABLE ALLOWABLES AND DISCRETIZATION
30/07/98 MESH=PZDS SELE=SU11 VALN=AH19
V6.4 PTF11 FIX7
LINEAR DISPL. - SOLUTION : PZDS MESH : PZDS BOUND : SYM. 1 LOAD : SH19
CYLINDRIC VIEW PIXEL
VIEWDIR 0.00 0.00 -1.00
SCALE 0.0102

PTC Variant Strength Only
Upper Strake Running Loads
(Spar Direction)

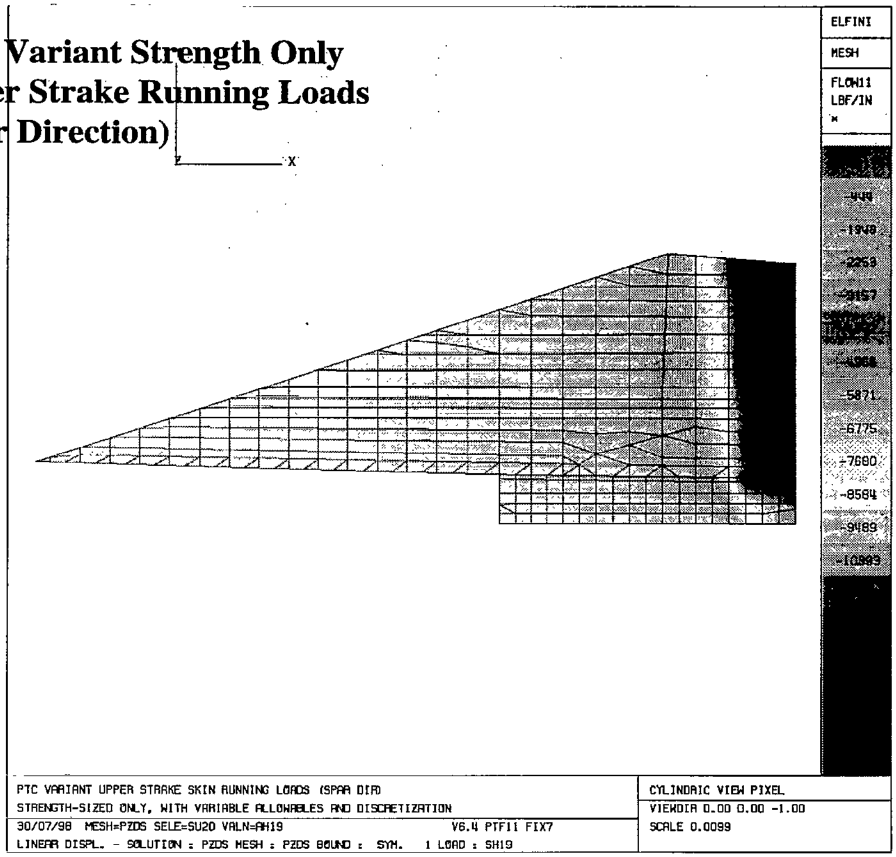

PTC Variant Strength Only Upper Strake Running Loads (Transverse)

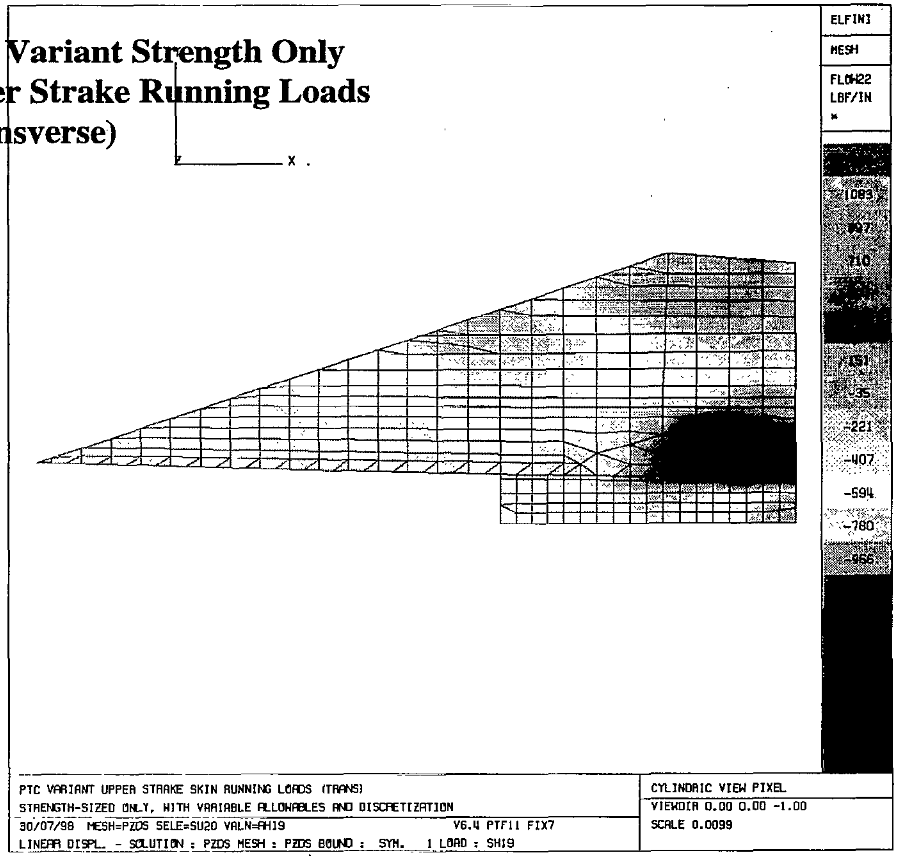

PTC Variant Strength Only Upper Strake Running Loads (Shear)

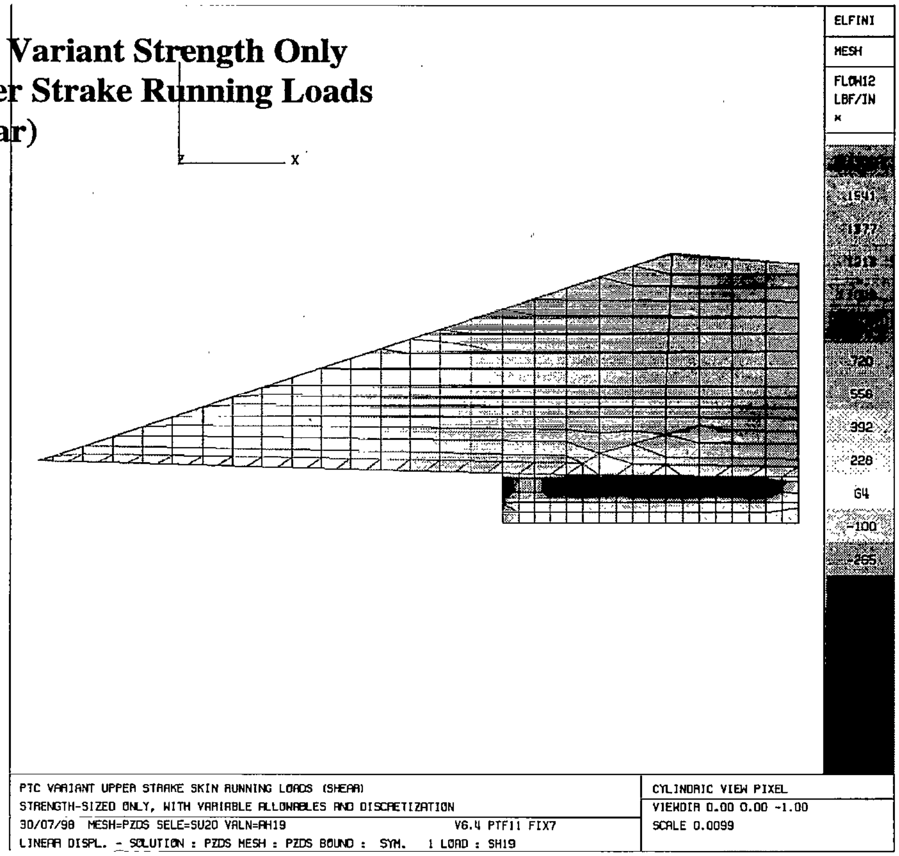

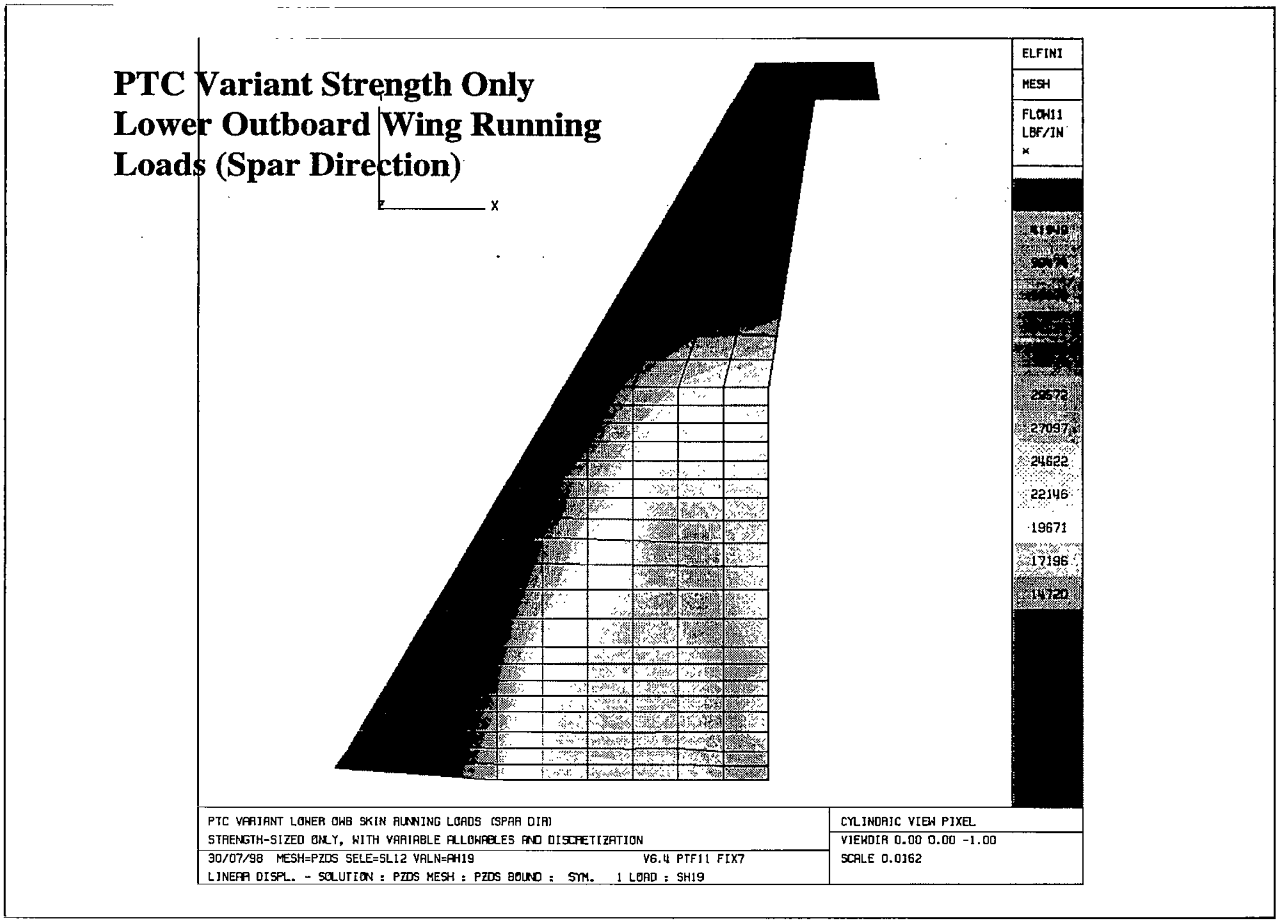
PTC Variant Strength Only
Lower Outboard Wing Running
Loads (Spar Direction)
X
ELFINI
MESH
FLOW11
LBF/IN
27097
24622
22146
19671
17196
14720
PTC VARIANT LOWER OWB SKIN RUNNING LOADS (SPAR DIR)
STRENGTH-SIZED ONLY, WITH VARIABLE ALLOWABLES AND DISCRETIZATION
30/07/98 MESH=PZDS SELE=SL12 VALN=AH19 V6.4 PTF11 FIX7
LINEAR DISPL. - SOLUTION : PZDS MESH : PZDS BOUND : SYM. 1 LOAD : SH19
CYLINDRIC VIEW PIXEL
VIEWDIR 0.00 0.00 -1.00
SCALE 0.0162

PTC Variant Strength Only Lower Outboard Wing Running Loads (Transverse)

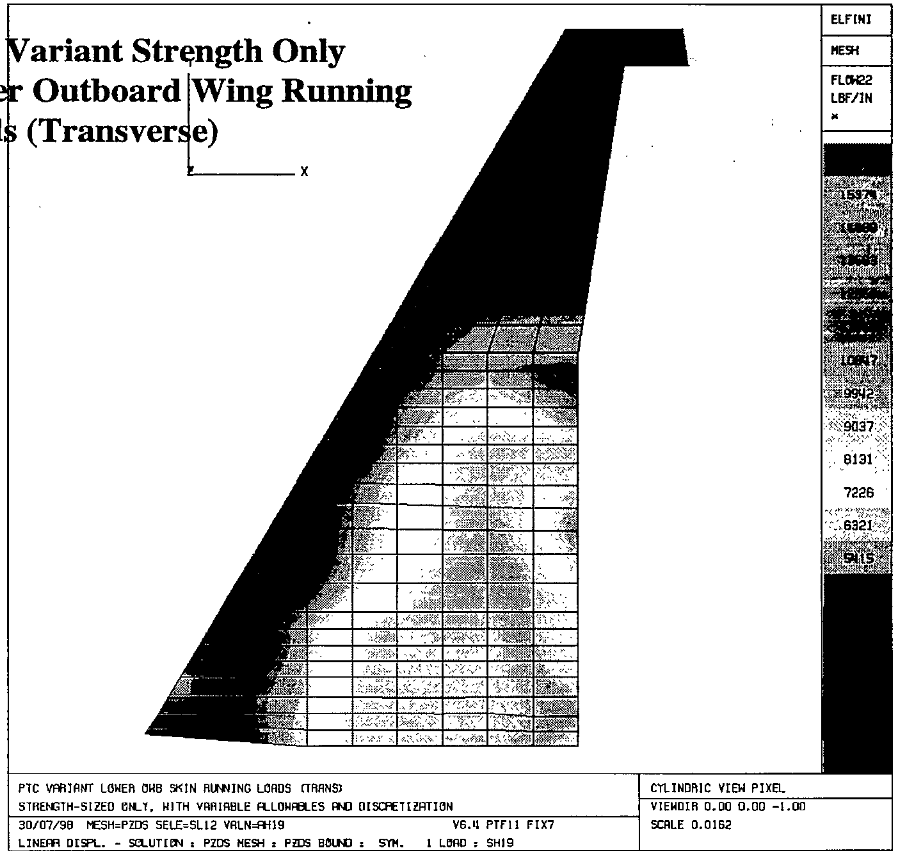

PTC Variant Strength Only Lower Outboard Wing Running Loads (Shear)

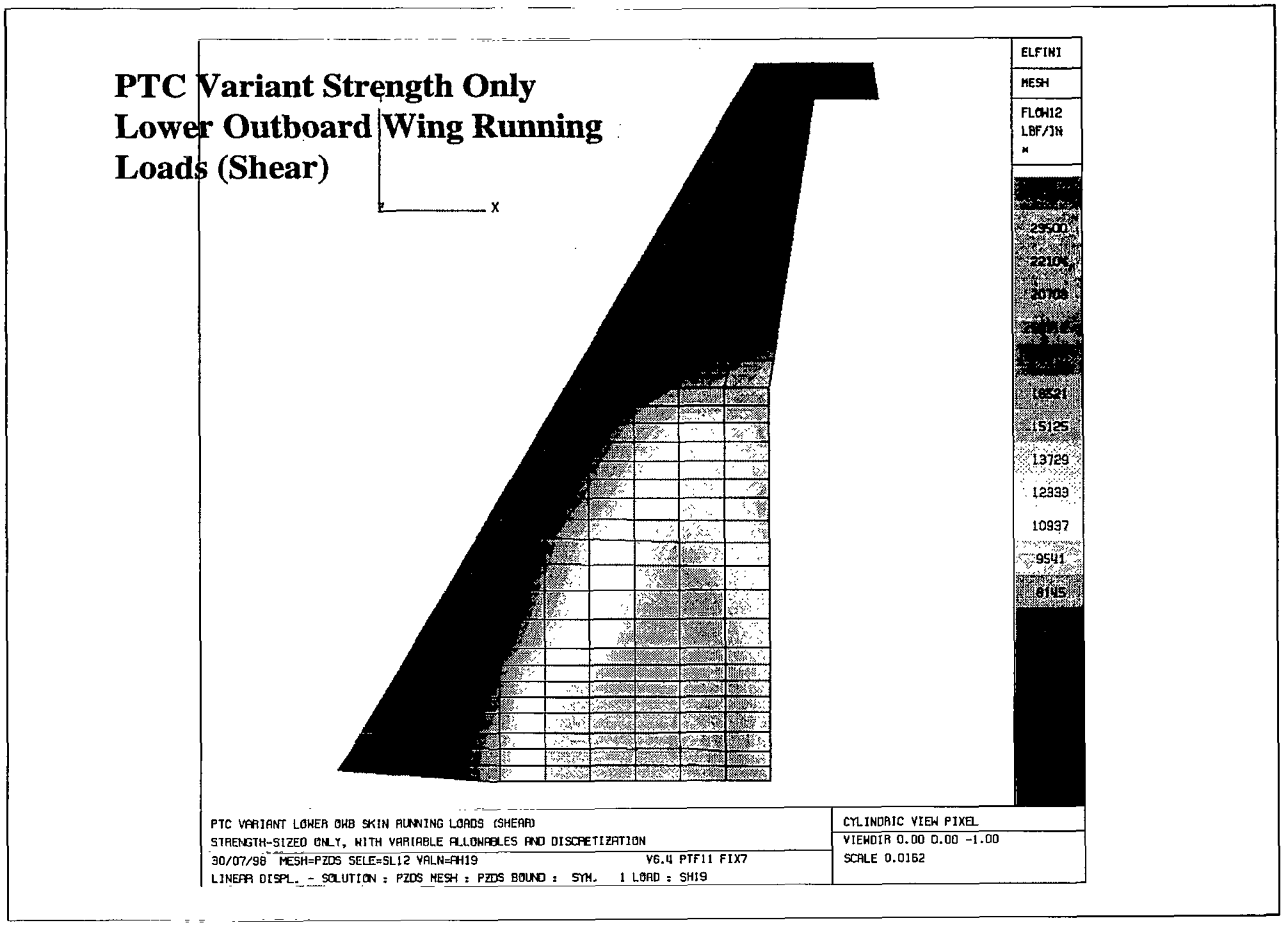

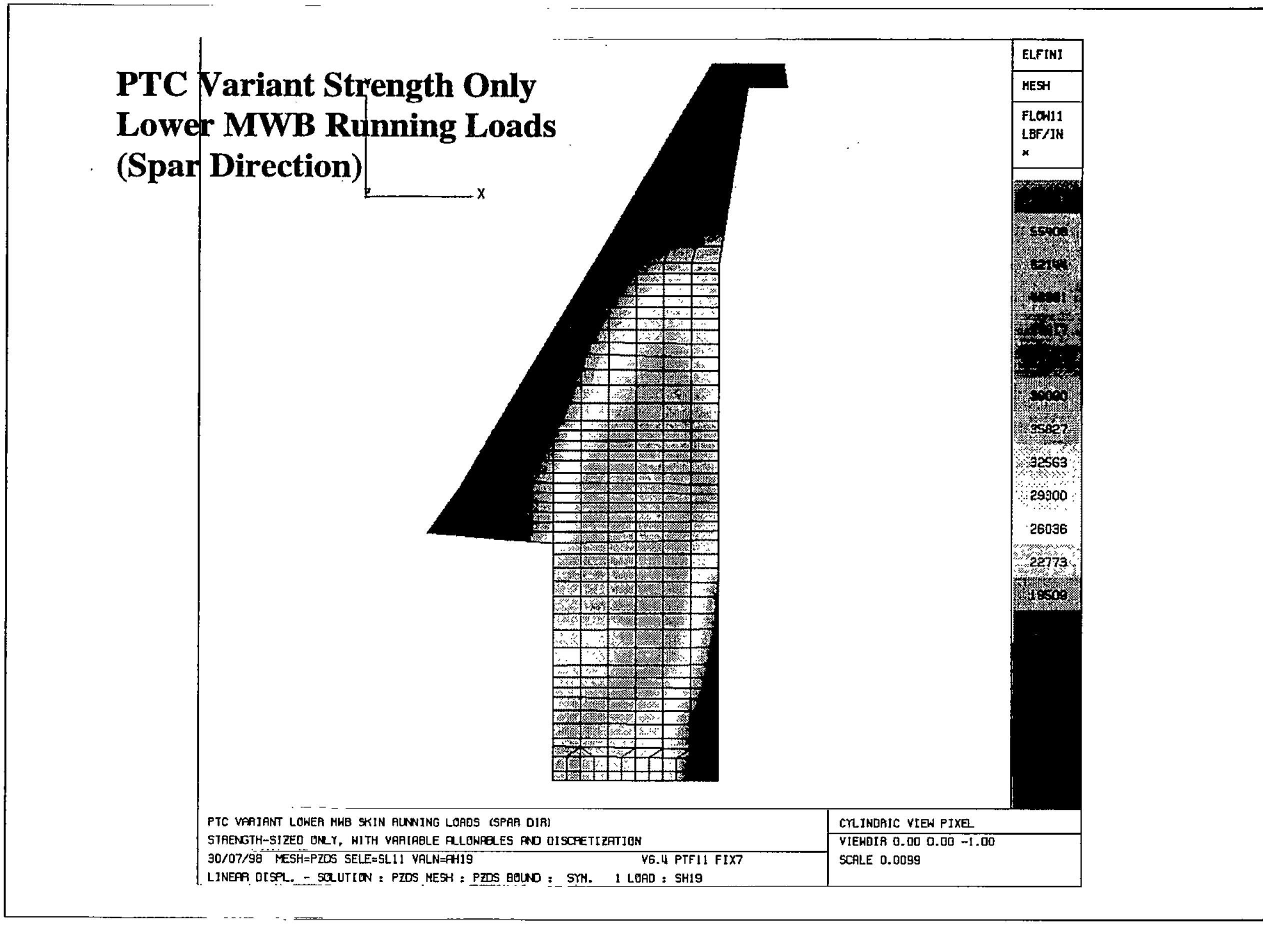
PTC Variant Strength Only
Lower MWB Running Loads
(Spar Direction)
X
ELFINI
MESH
FLOW11
LBF/IN
35827
32563
29300
26036
22773
19509
PTC VARIANT LOWER MWB SKIN RUNNING LOADS (SPAR DIR)
STRENGTH-SIZED ONLY, WITH VARIABLE ALLOWABLES AND DISCRETIZATION
30/07/98 MESH=PZDS SELE=SL11 VALN=AH19
V6.4 PTF11 FIX7
LINEAR DISPL. - SOLUTION : PZDS MESH : PZDS BOUND : SYM. 1 LOAD : SH19
CYLINDRIC VIEW PIXEL
VIEWDIR 0.00 0.00 -1.00
SCALE 0.0099

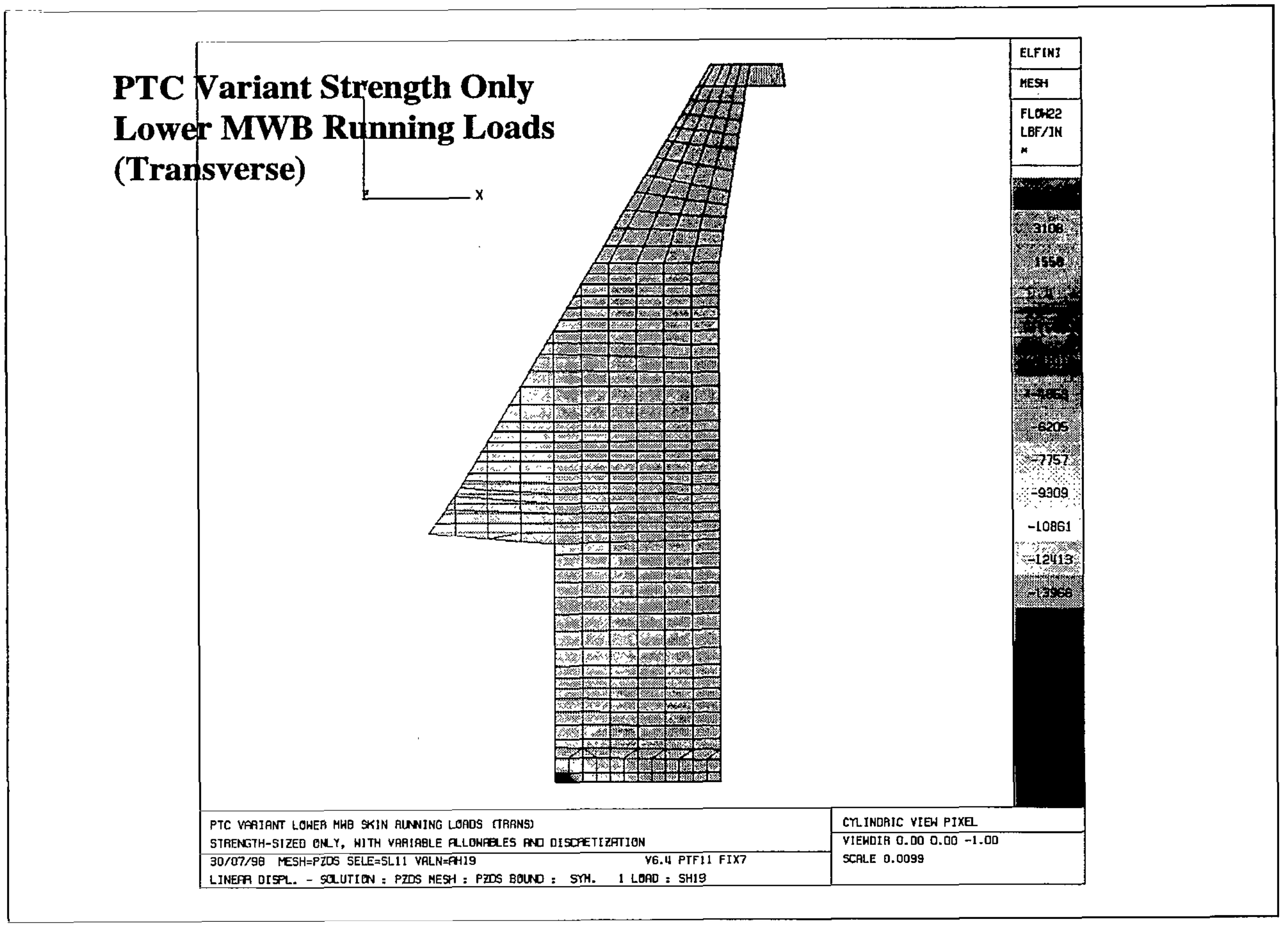
PTC Variant Strength Only
Lower MWB Running Loads
(Transverse)
X
ELFINI
MESH
FLOW22
LBF/IN
3108
1556
-6205
-7757
-9309
-10861
-12413
PTC VARIANT LOWER MWB SKIN RUNNING LOADS (TRANS)
STRENGTH-SIZED ONLY, WITH VARIABLE ALLOWABLES AND DISCRETIZATION
30/07/98 MESH=PZDS SELE=SL11 VALN=AH19
V6.4 PTF11 FIX7
LINEAR DISPL. - SOLUTION : PZDS MESH : PZDS BOUND : SYM. 1 LOAD : SH19
CYLINDRIC VIEW PIXEL
VIEWDIR 0.00 0.00 -1.00
SCALE 0.0099

**PTC Variant Strength Only
Lower MWB Running Loads
(Shear)**

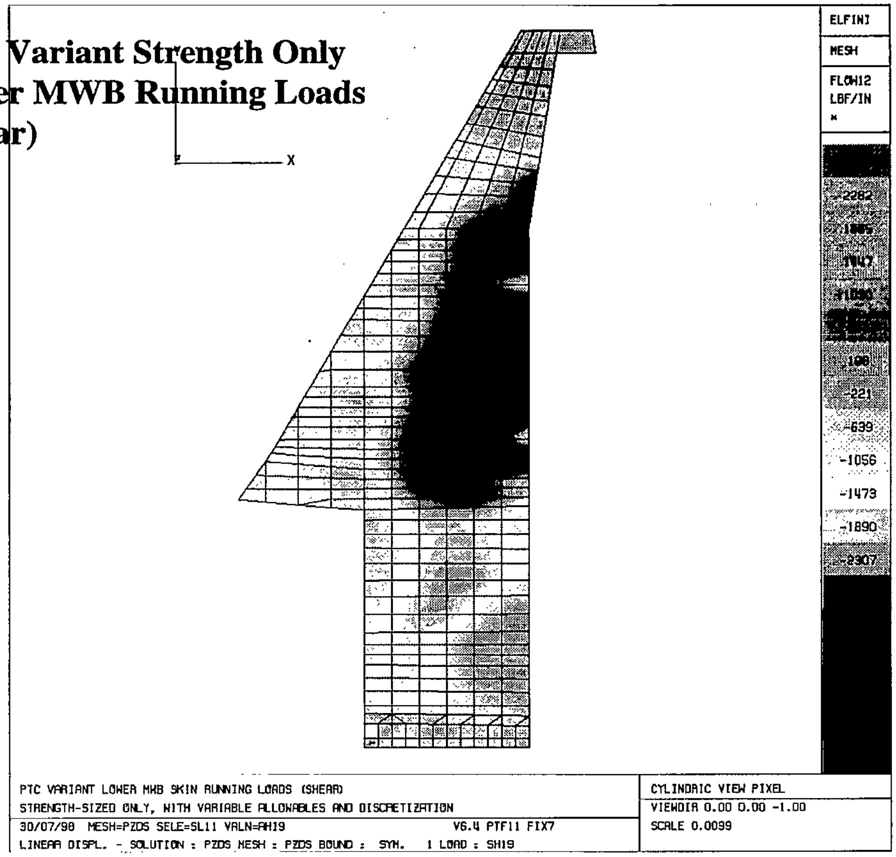

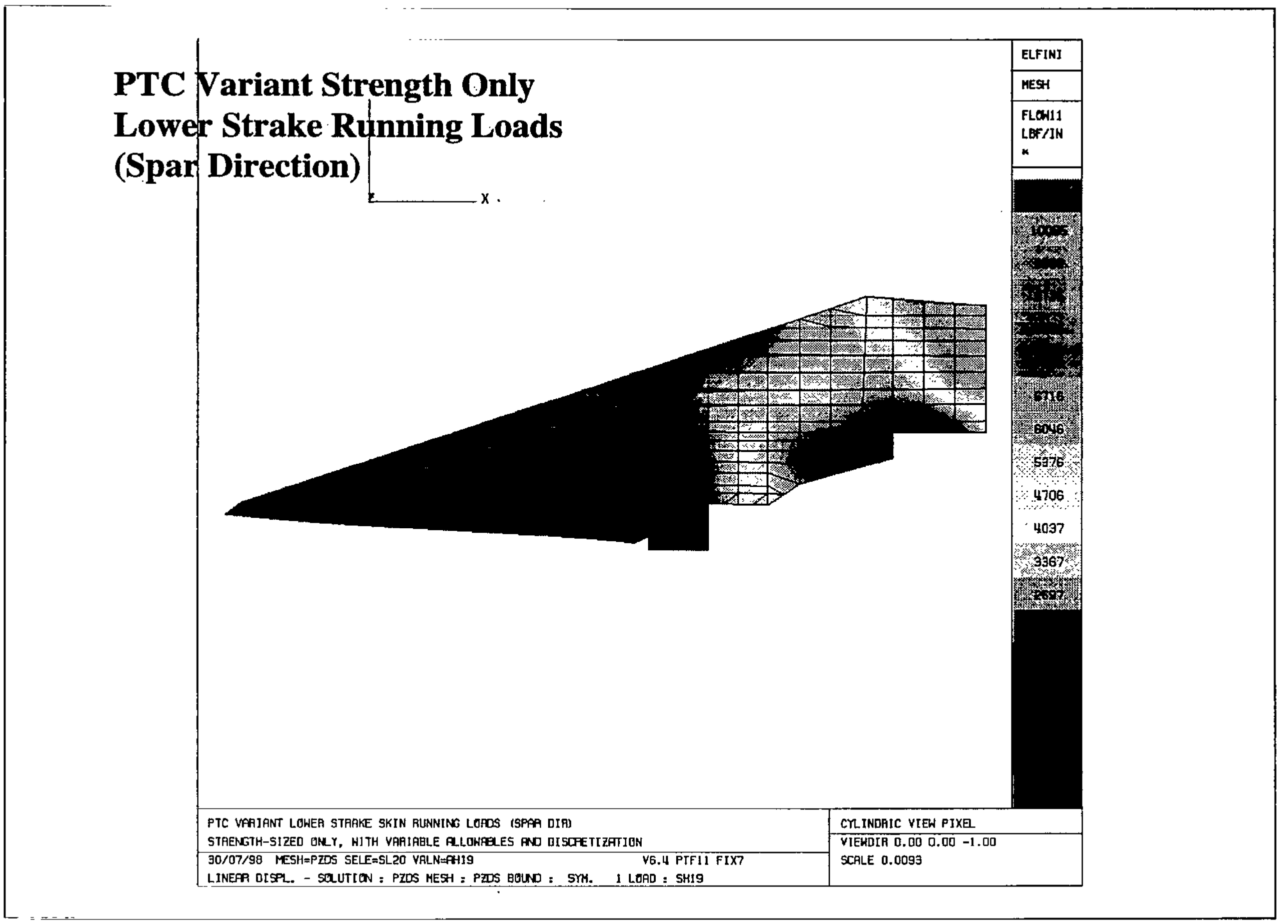
PTC Variant Strength Only
Lower Strake Running Loads
(Spar Direction)
ELFINI
MESH
FLOW11
LBF/IN
6716
6046
5376
4706
4037
3367
PTC VARIANT LOWER STRAKE SKIN RUNNING LOADS (SPAR DIR)
STRENGTH-SIZED ONLY, WITH VARIABLE ALLOWABLES AND DISCRETIZATION
30/07/98 MESH=PZDS SELE=SL20 VALN=AH19
V6.4 PTF11 FIX7
LINEAR DISPL. - SOLUTION : PZDS MESH : PZDS BOUND : SYM. 1 LOAD : SH19
CYLINDRIC VIEW PIXEL
VIEWDIR 0.00 0.00 -1.00
SCALE 0.0093

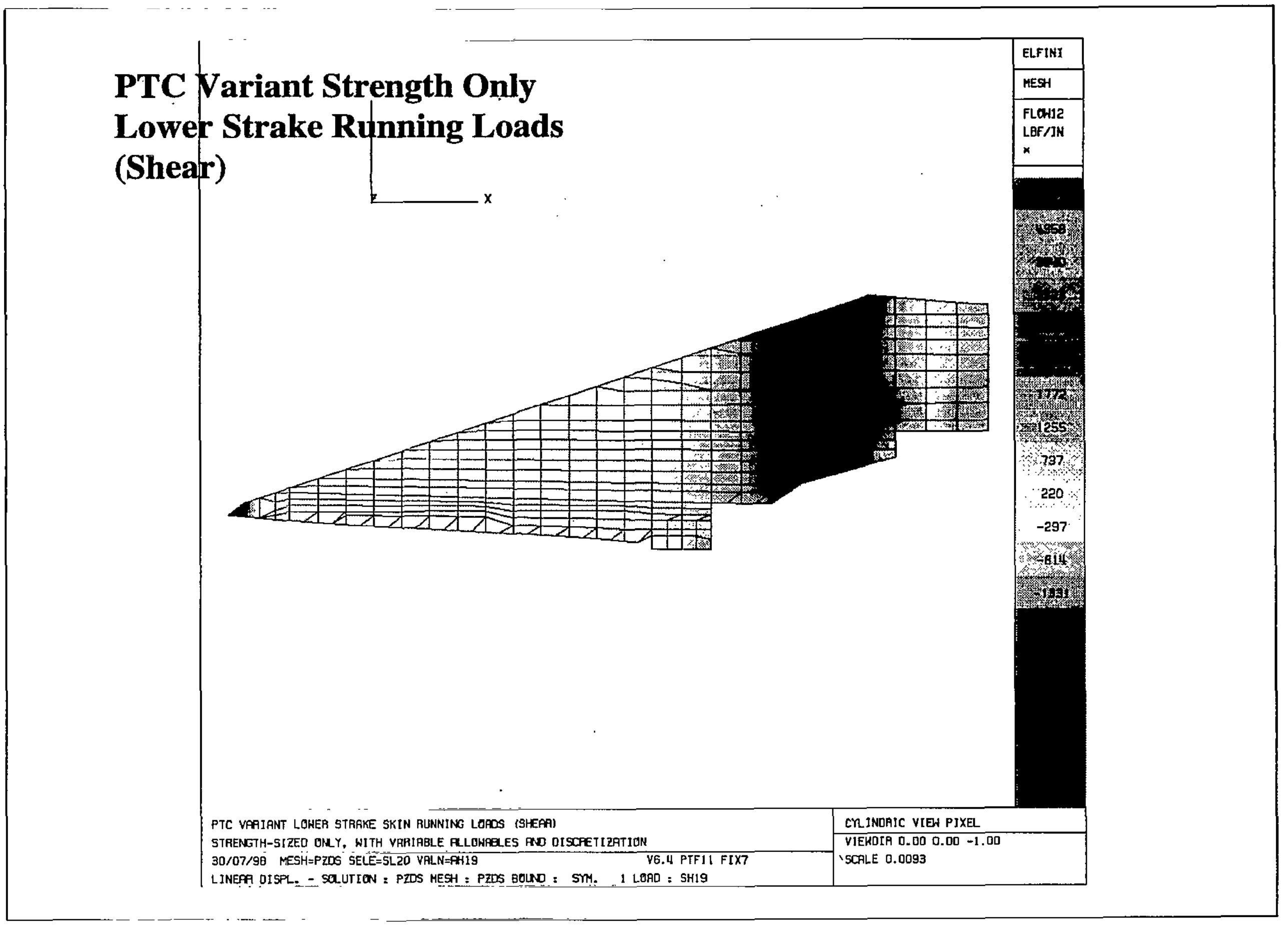
PTC Variant Strength Only
Lower Strake Running Loads
(Shear)
X
ELFINI
MESH
FLOW12
LBF/IN
1772
1255
797
220
-297
-814
-1331
PTC VARIANT LOWER STRAKE SKIN RUNNING LOADS (SHEAR)
STRENGTH-SIZED ONLY, WITH VARIABLE ALLOWABLES AND DISCRETIZATION
30/07/98 MESH=PZDS SELE=SL20 VALN=AH19 V6.4 PTF11 FIX7
LINEAR DISPL. - SOLUTION : PZDS MESH : PZDS BOUND : SYM. 1 LOAD : SH19
CYLINDRIC VIEW PIXEL
VIEWDIR 0.00 0.00 -1.00
SCALE 0.0093

PTC Variant Strength Only Wing Substructure Running Loads (Transverse)

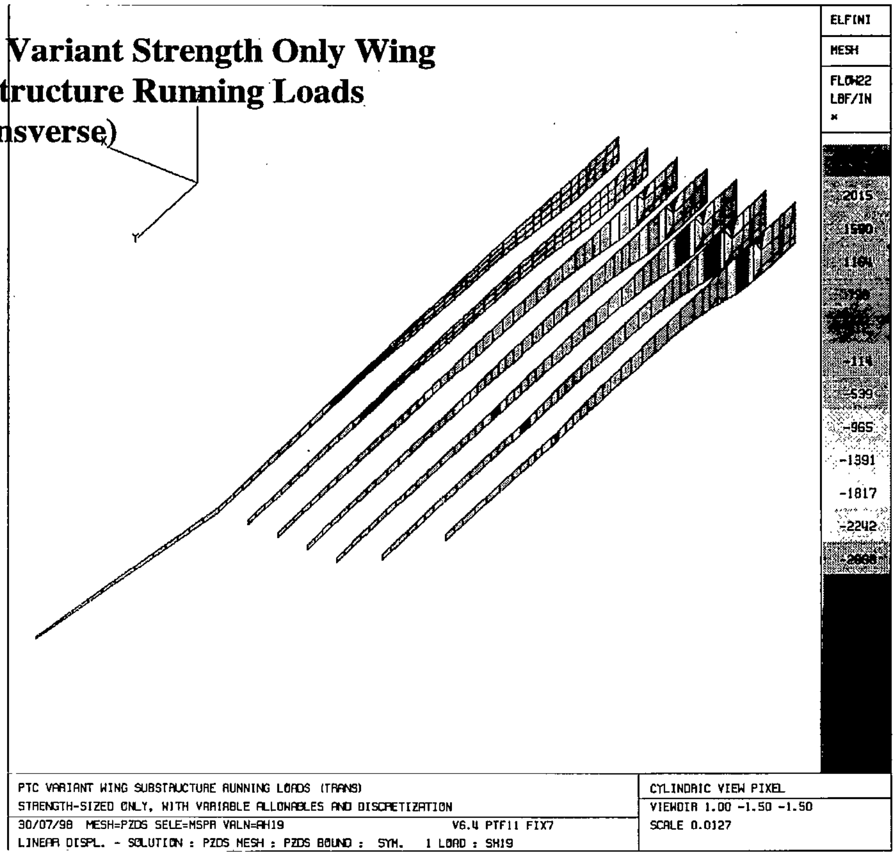

PTC Variant Strength Only Wing Substructure Running Loads (Spar Direction)

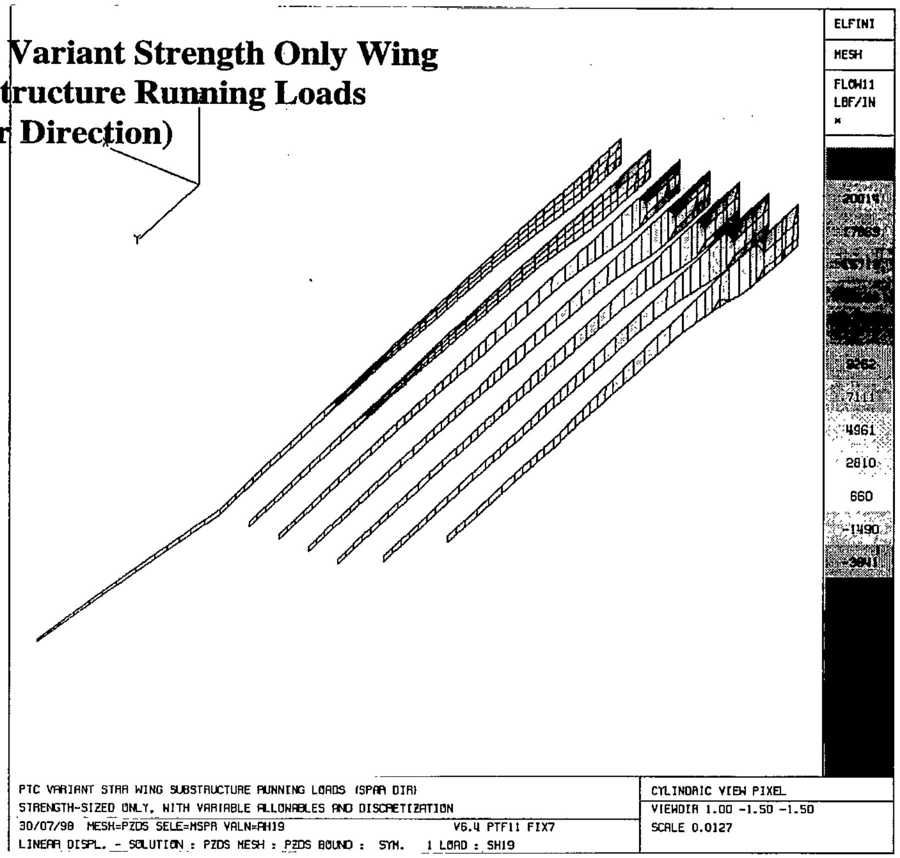

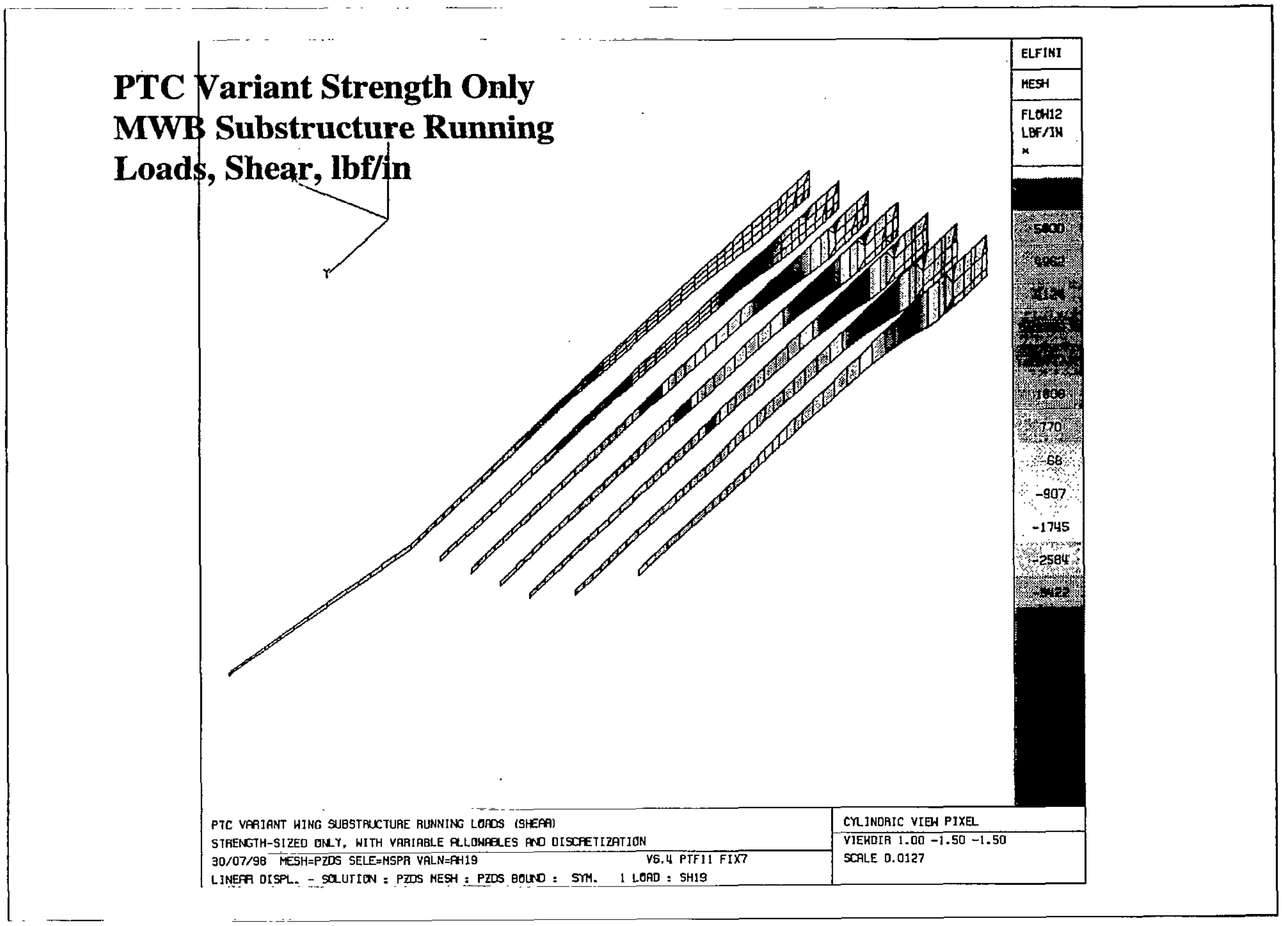
PTC Variant Strength Only
MWB Substructure Running
Loads, Shear, lbf/in
ELFINI
MESH
FLOW12
LBF/IN
5800
770
-68
-907
-1745
-2584
PTC VARIANT WING SUBSTRUCTURE RUNNING LOADS (SHEAR)
STRENGTH-SIZED ONLY, WITH VARIABLE ALLOWABLES AND DISCRETIZATION
30/07/98 MESH=PZDS SELE=NSPR VALN=AH19
V6.4 PTF11 FIX7
LINEAR DISPL. - SOLUTION : PZDS MESH : PZDS BOUND : SYM. 1 LOAD : SH19
CYLINDRIC VIEW PIXEL
VIEWDIR 1.00 -1.50 -1.50
SCALE 0.0127

PTC Variant Strength Only Section 41, 43, & 44 Running Loads, Fore/Aft, w/pressure, lbf/in

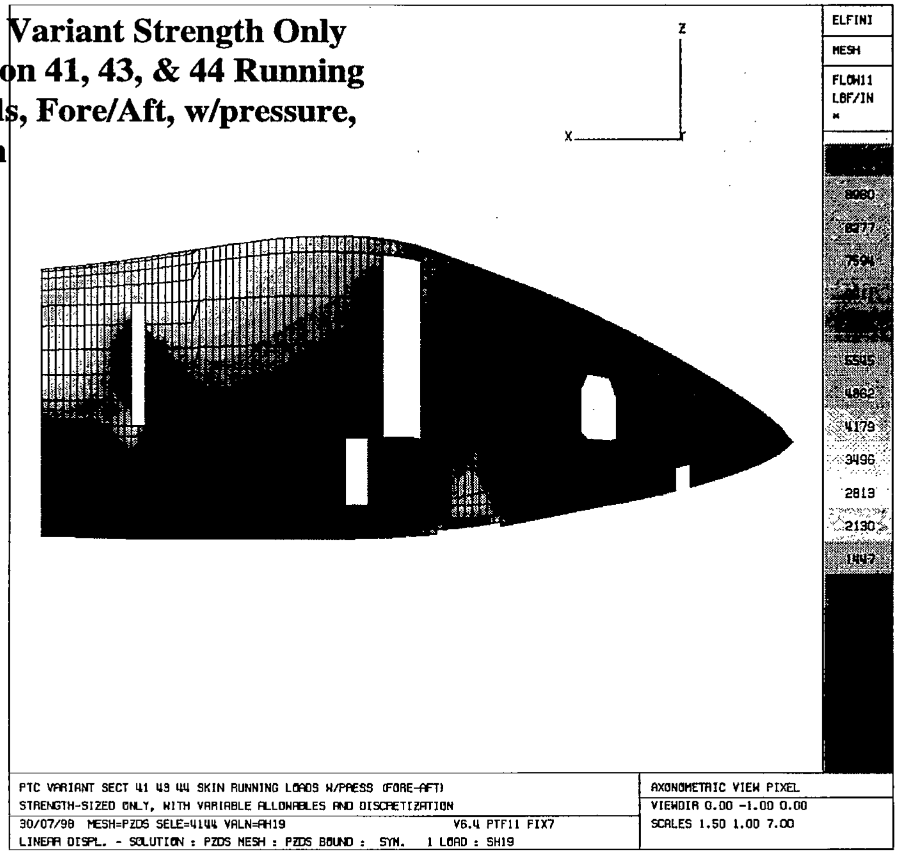

PTC Variant Strength Only Section 45 & 46 Running Loads, Fore/Aft, w/pressure, lbf/in

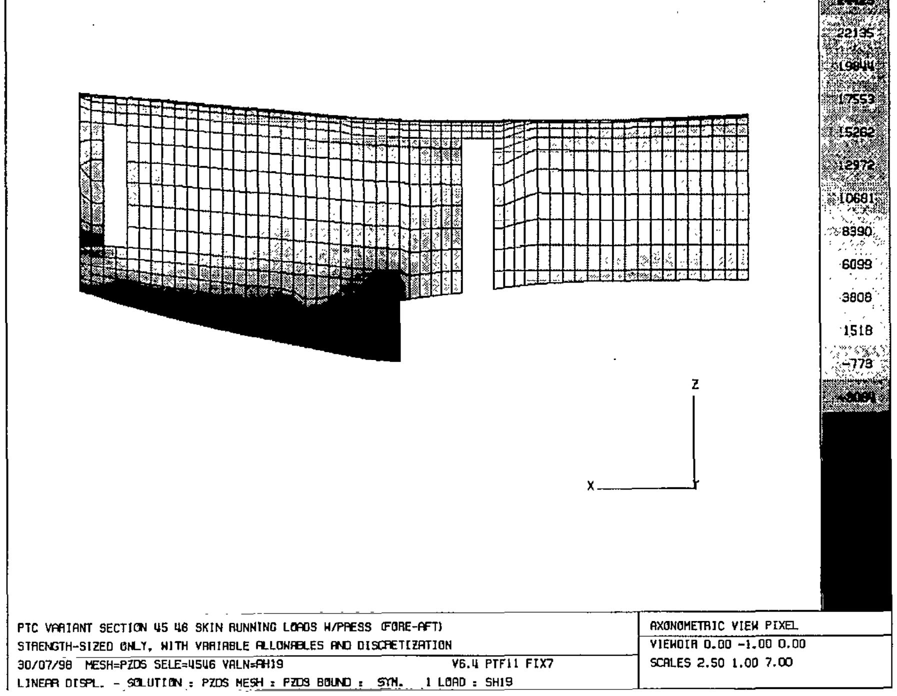

PTC Variant Strength Only Section 45 & 46 Running Loads, Circumferential, w/pressure, lbf/in

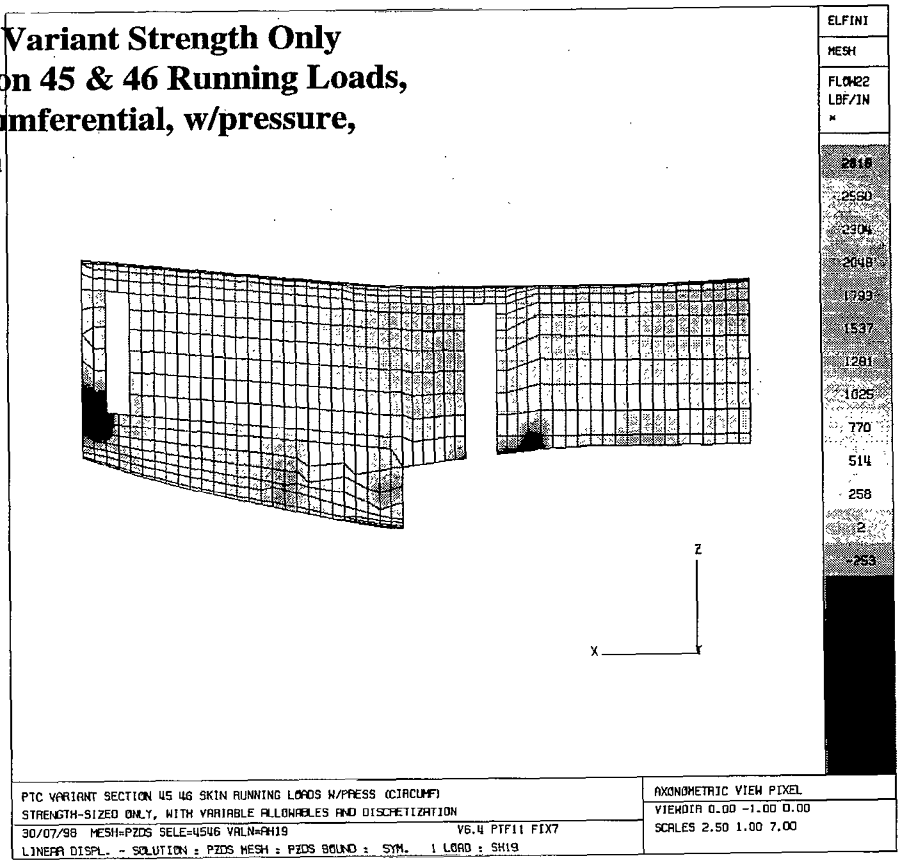

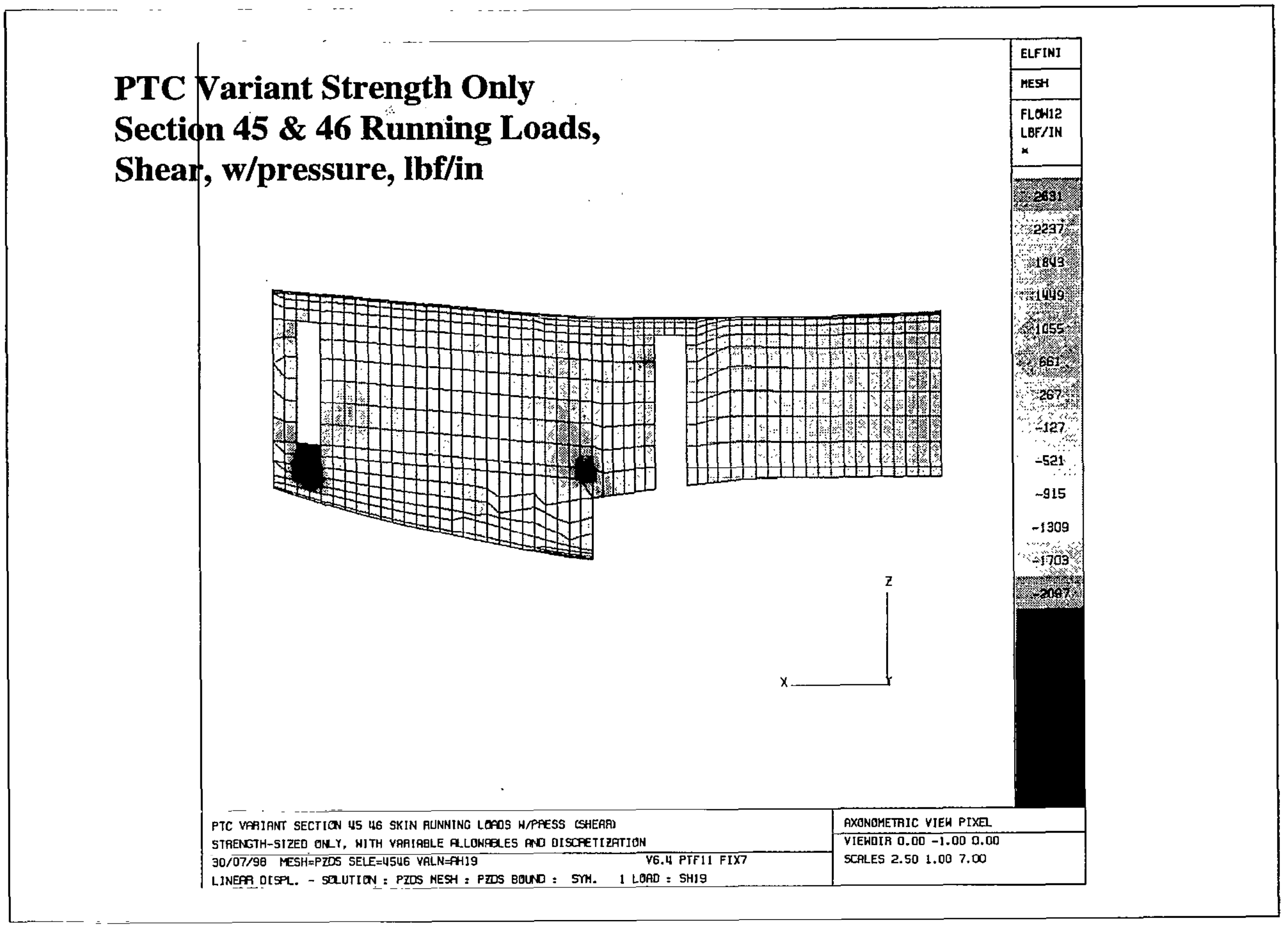
PTC Variant Strength Only
Section 45 & 46 Running Loads,
Shear, w/pressure, lbf/in
ELFINI
MESH
FLOW12
LBF/IN
2631
2237
1843
1449
1055
661
267
-127
-521
-915
-1309
-1703
-2097
Z
X
PTC VARIANT SECTION 45 46 SKIN RUNNING LOADS W/PRESS (SHEAR)
STRENGTH-SIZED ONLY, WITH VARIABLE ALLOWABLES AND DISCRETIZATION
30/07/98 MESH=PZDS SELE=4546 VALN=AH19
V6.4 PTF11 FIX7
LINEAR DISPL. - SOLUTION : PZDS MESH : PZDS BOUND : SYM. 1 LOAD : SH19
AXONOMETRIC VIEW PIXEL
VIEWDIR 0.00 -1.00 0.00
SCALES 2.50 1.00 7.00

**PTC Variant Strength Only
Section 48 Running Loads,
Fore/Aft, w/pressure, lbf/in**

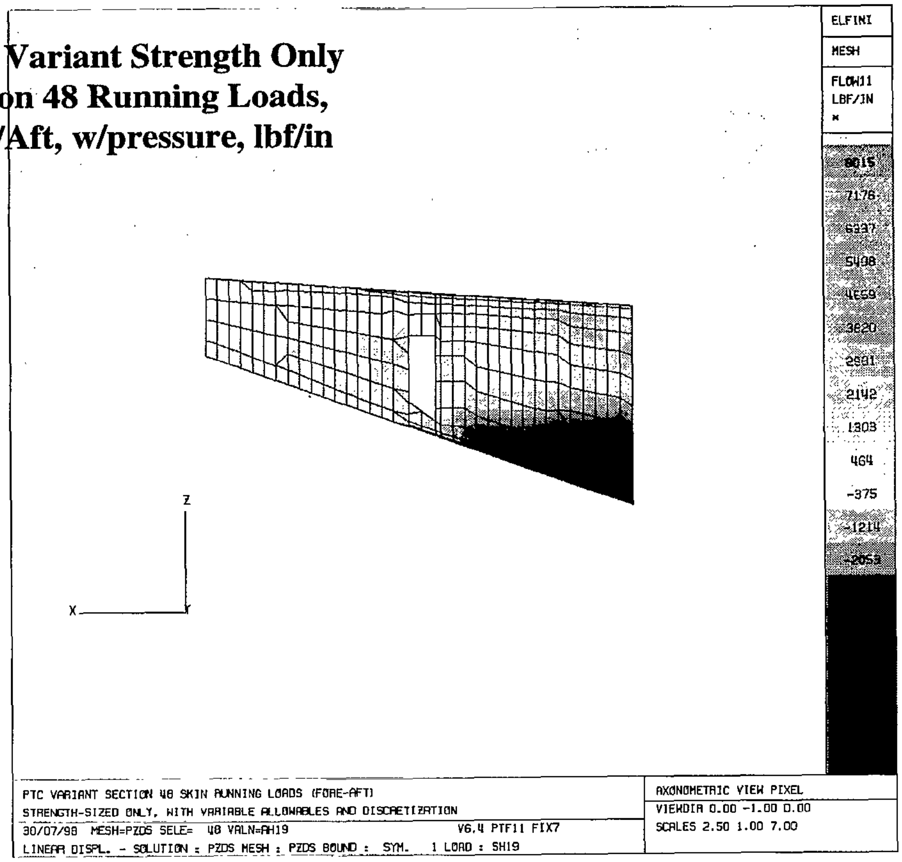

PTC Variant Strength Only Section 48 Running Loads, Circumferential, w/pressure, lbf/in

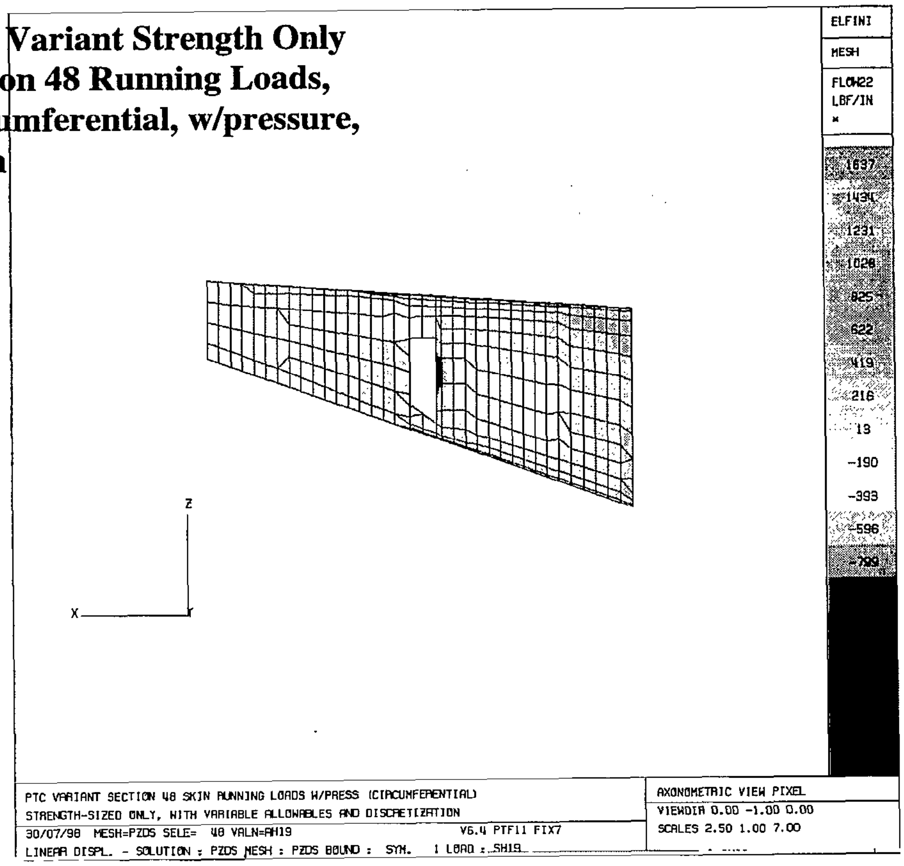

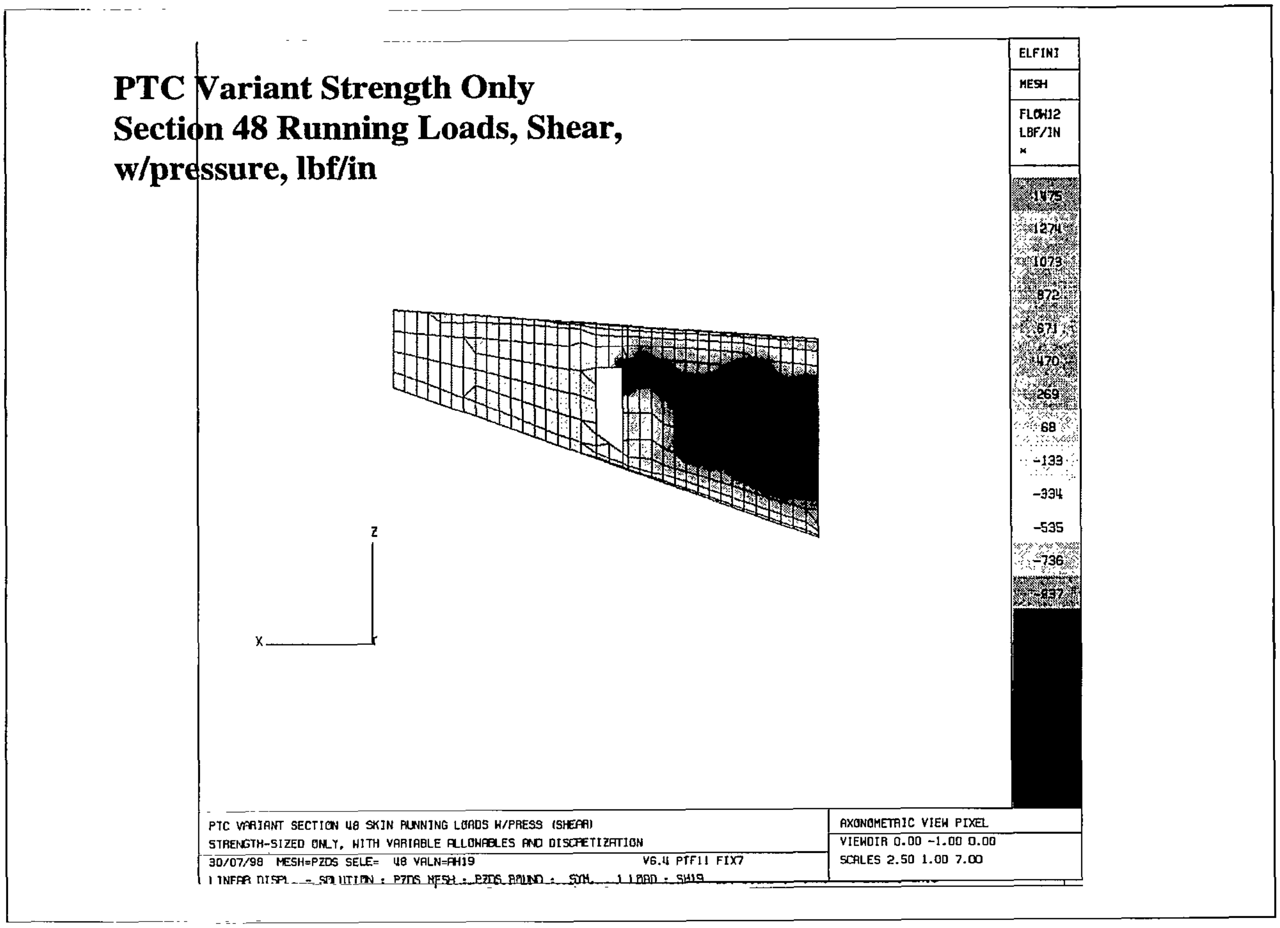
PTC Variant Strength Only
Section 48 Running Loads, Shear,
w/pressure, lbf/in
ELFINI
MESH
FLOW12
LBF/IN
1475
1274
1073
872
671
470
269
68
-133
-334
-535
-736
-937
Z
X
PTC VARIANT SECTION 48 SKIN RUNNING LOADS W/PRESS (SHEAR)
STRENGTH-SIZED ONLY, WITH VARIABLE ALLOWABLES AND DISCRETIZATION
30/07/98 MESH=PZDS SELE= 48 VALN=AH19
V6.4 PTF11 FIX7
AXONOMETRIC VIEW PIXEL
VIEWDIR 0.00 -1.00 0.00
SCALES 2.50 1.00 7.00

PTC Variant Strength Only Section 41, 43, & 44 Running Loads, Fore/Aft, lbf/in

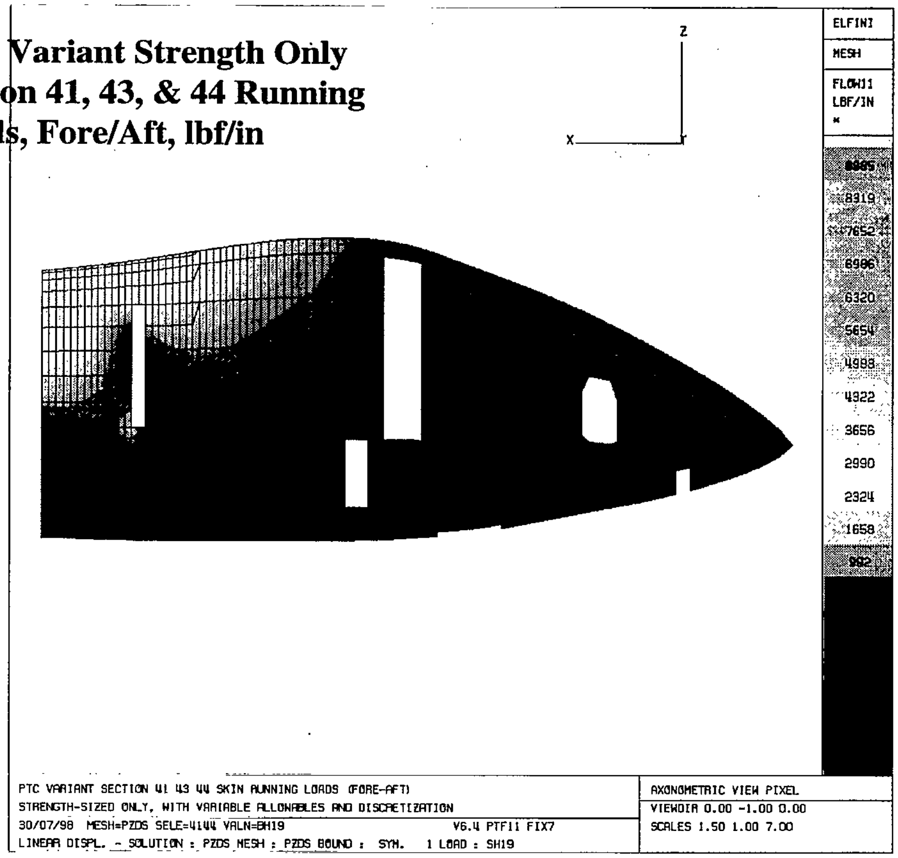

**PTC Variant Strength Only
Section 41, 43, & 44 Running
Loads, Circumferential, lbf/in**

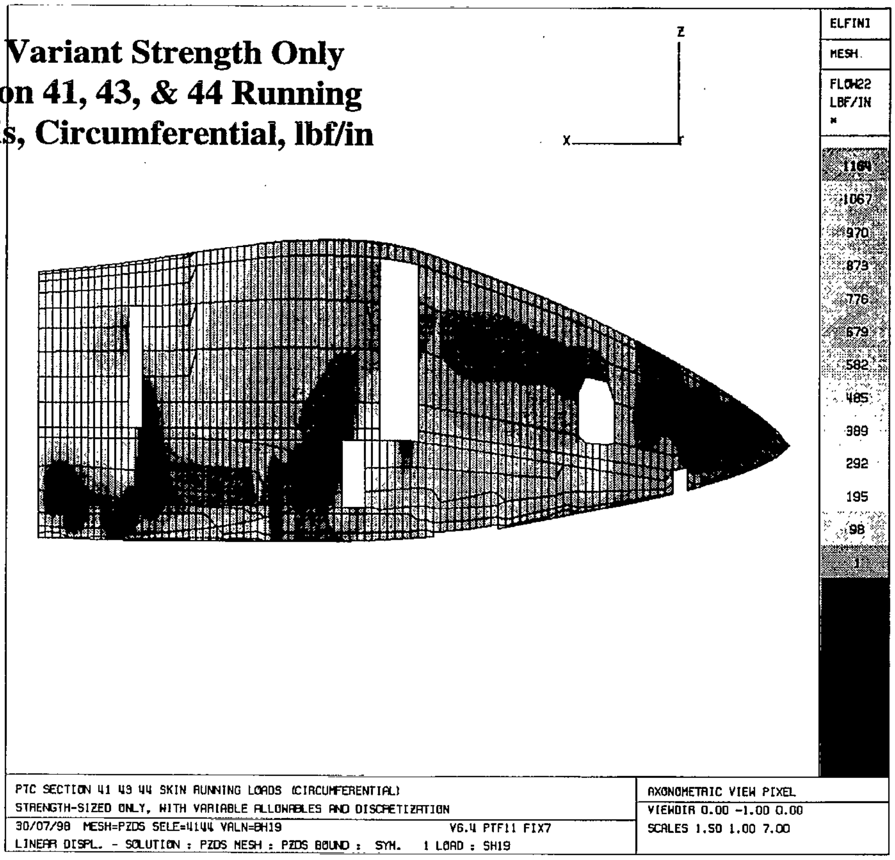

PTC Variant Strength Only Section 41, 43, & 44 Running Loads, Shear, lbf/in

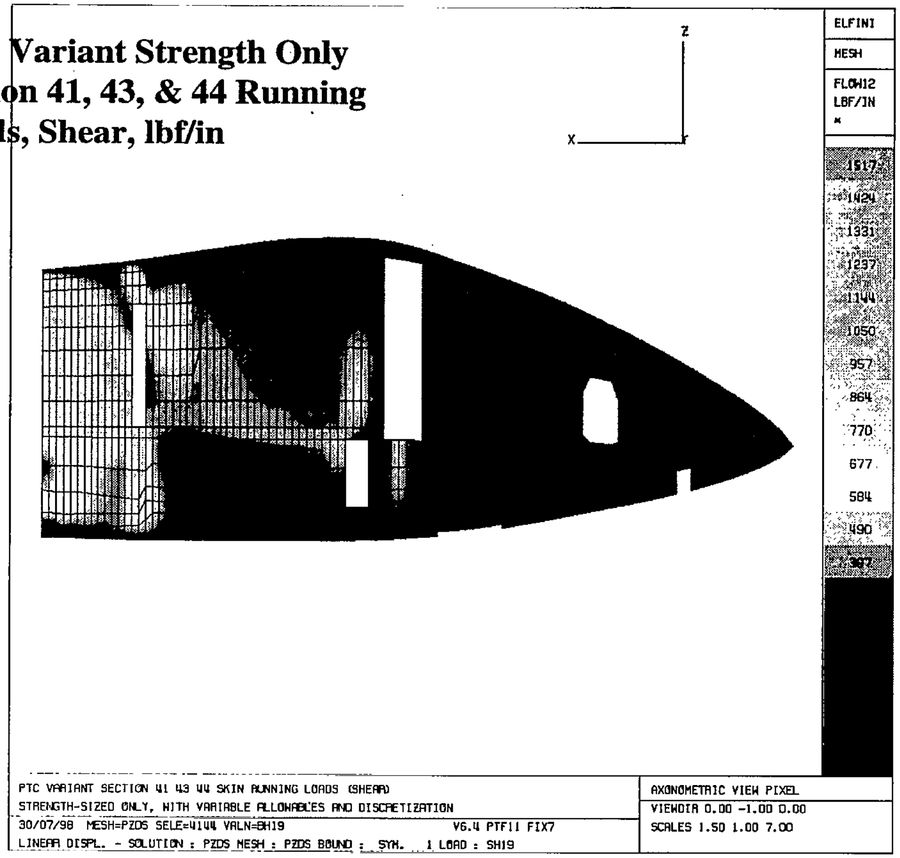

PTC Variant Strength Only Section 45 & 46 Running Loads, Fore/Aft, lbf/in

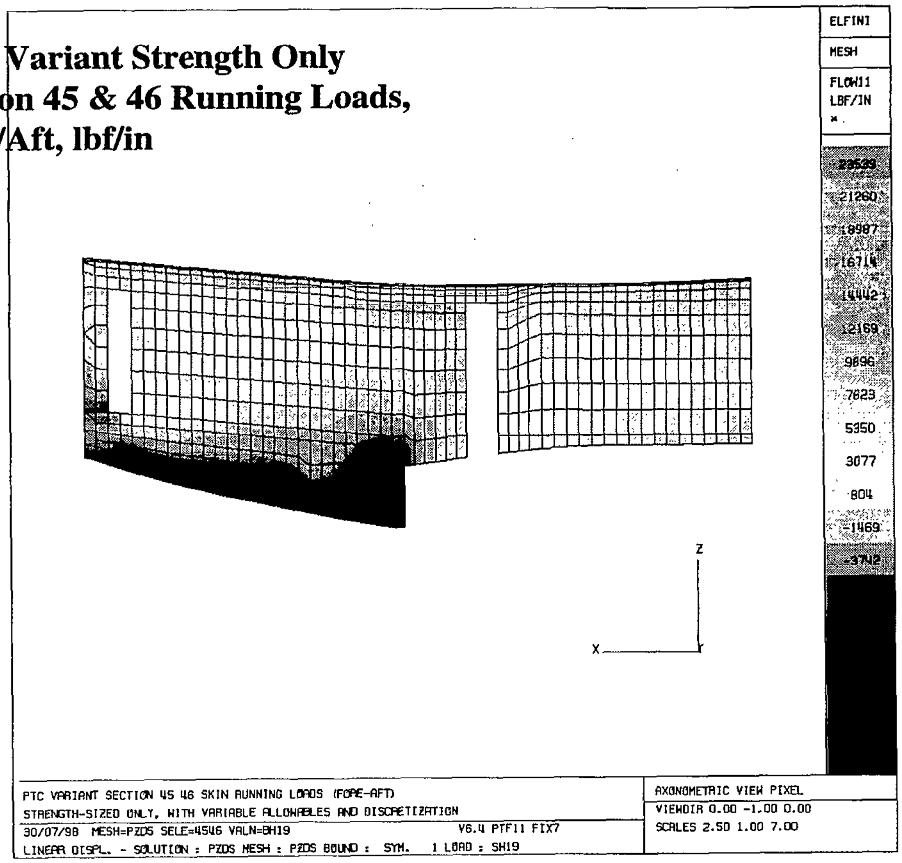

PTC Variant Strength Only Section 45 & 46 Running Loads, Circumferential, lbf/in

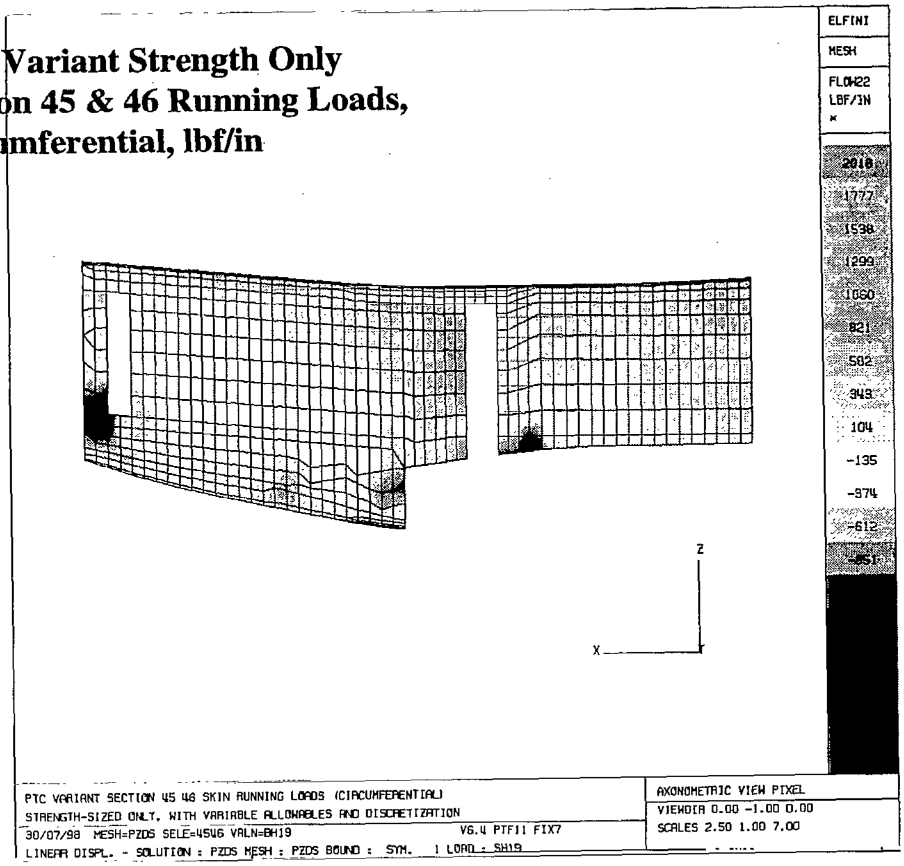

PTC Variant Strength Only
Section 45 & 46 Running Loads,
Shear, lbf/in

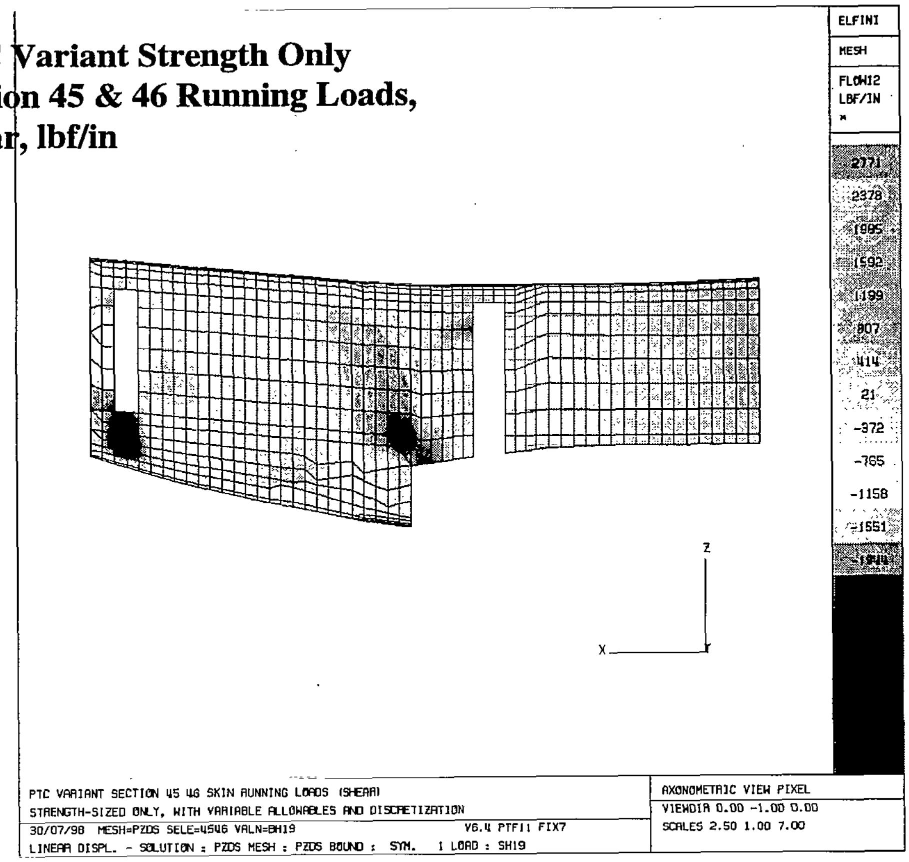

PTC Variant Strength Only Section 48 Running Loads, Fore/Aft, lbf/in

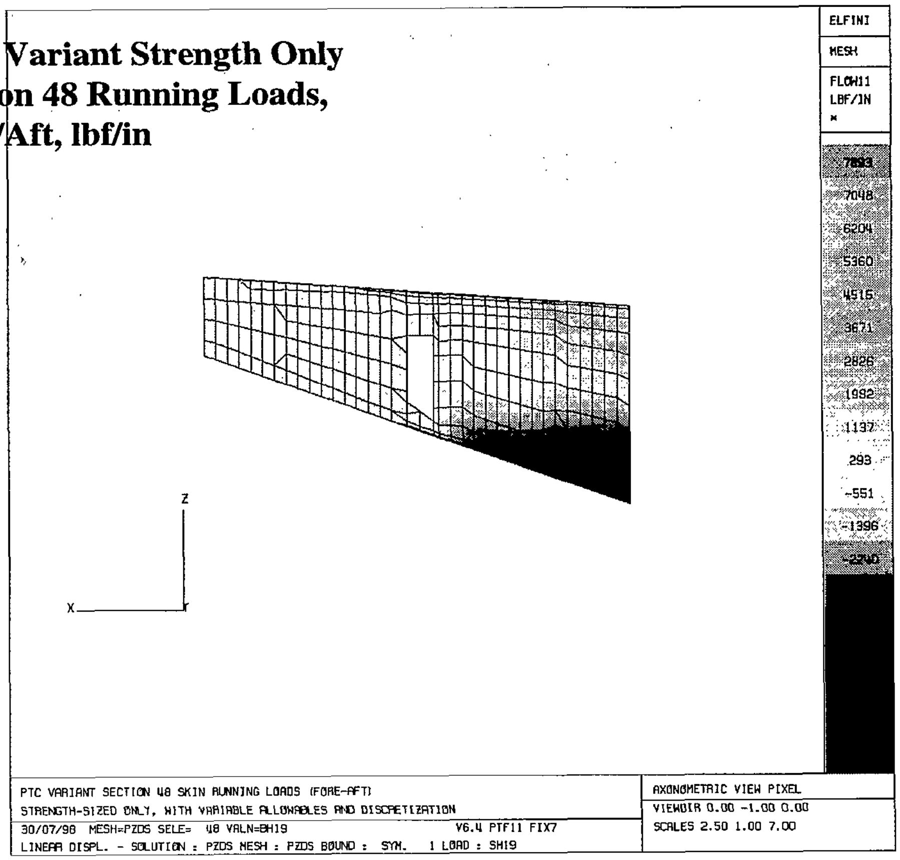

**PTC Variant Strength Only
Section 48 Running Loads,
Circumferential, lbf/in**

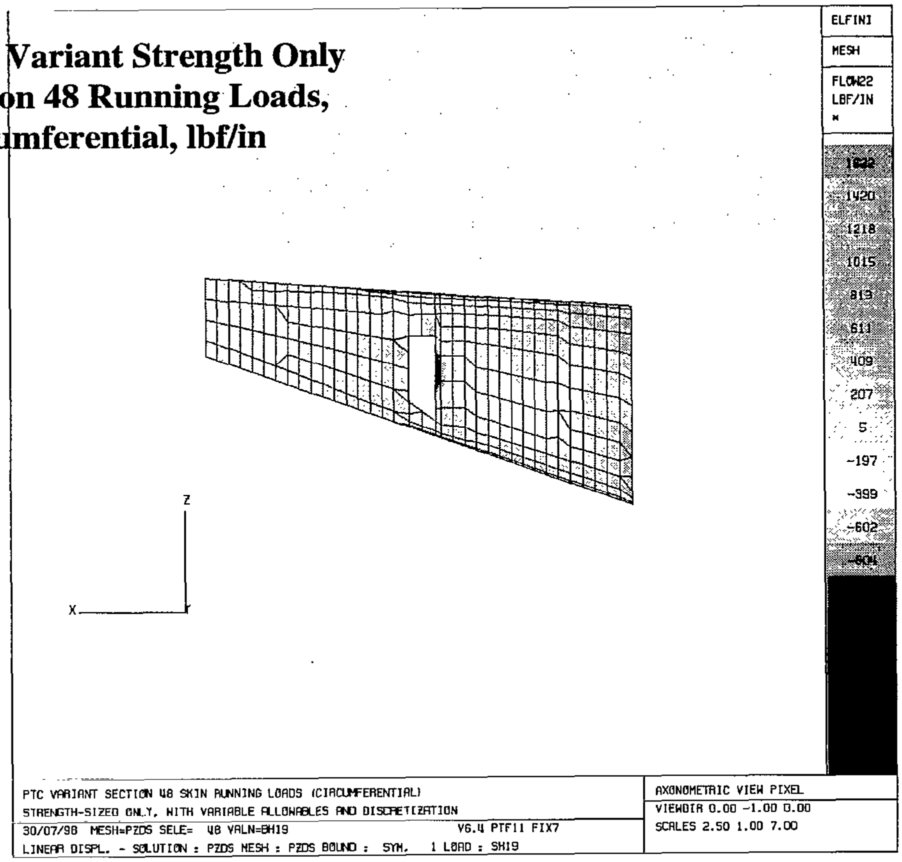

PTC Variant Strength Only Section 48 Running Loads, Shear, lbf/in

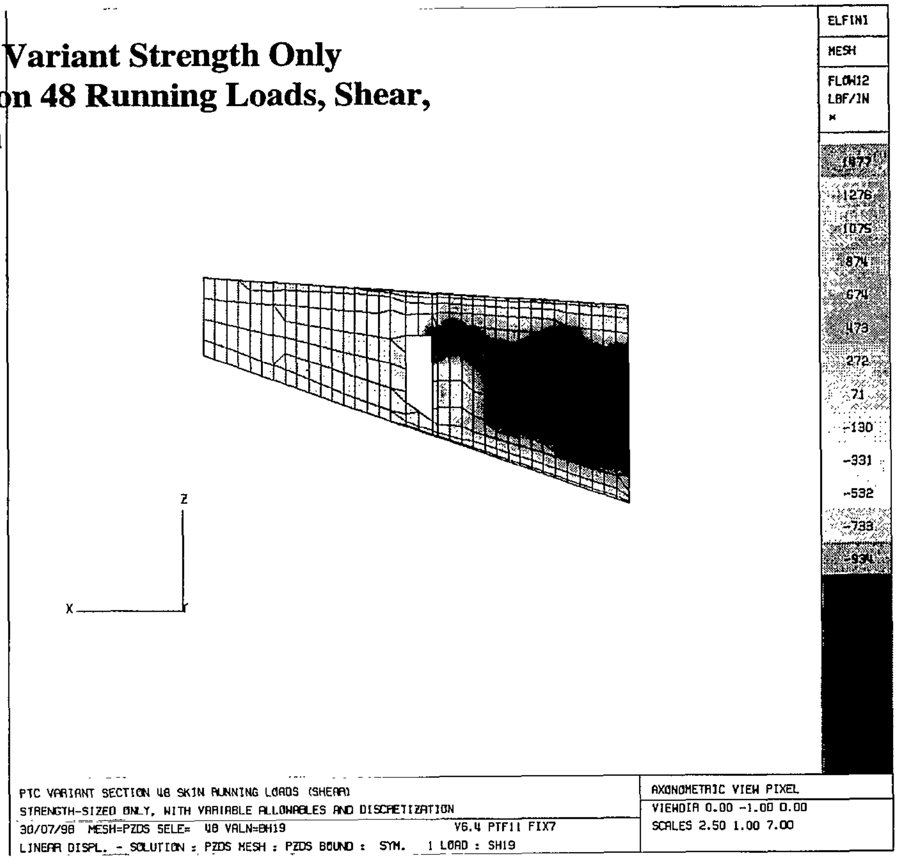

Total Element Thickness

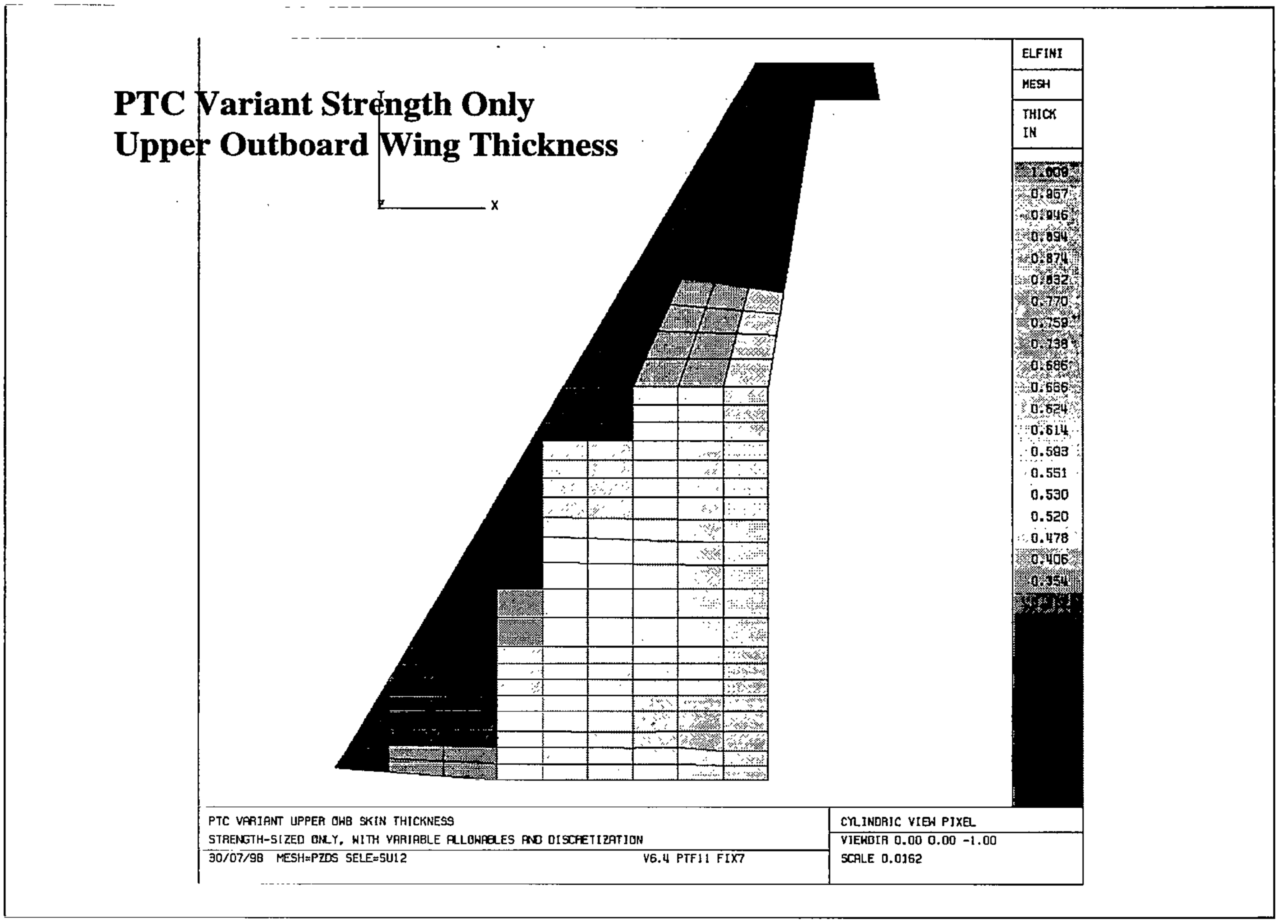
PTC Variant Strength Only
Upper Outboard Wing Thickness
X
ELFINI
MESH
THICK
IN
1.000
0.967
0.946
0.894
0.874
0.832
0.770
0.759
0.738
0.686
0.666
0.624
0.614
0.593
0.551
0.530
0.520
0.478
0.406
0.354
PTC VARIANT UPPER OWB SKIN THICKNESS
STRENGTH-SIZED ONLY, WITH VARIABLE ALLOWABLES AND DISCRETIZATION
30/07/98 MESH=PZDS SELE=SU12
V6.4 PTF11 FIX7
CYLINDRIC VIEW PIXEL
VIEWDIR 0.00 0.00 -1.00
SCALE 0.0162

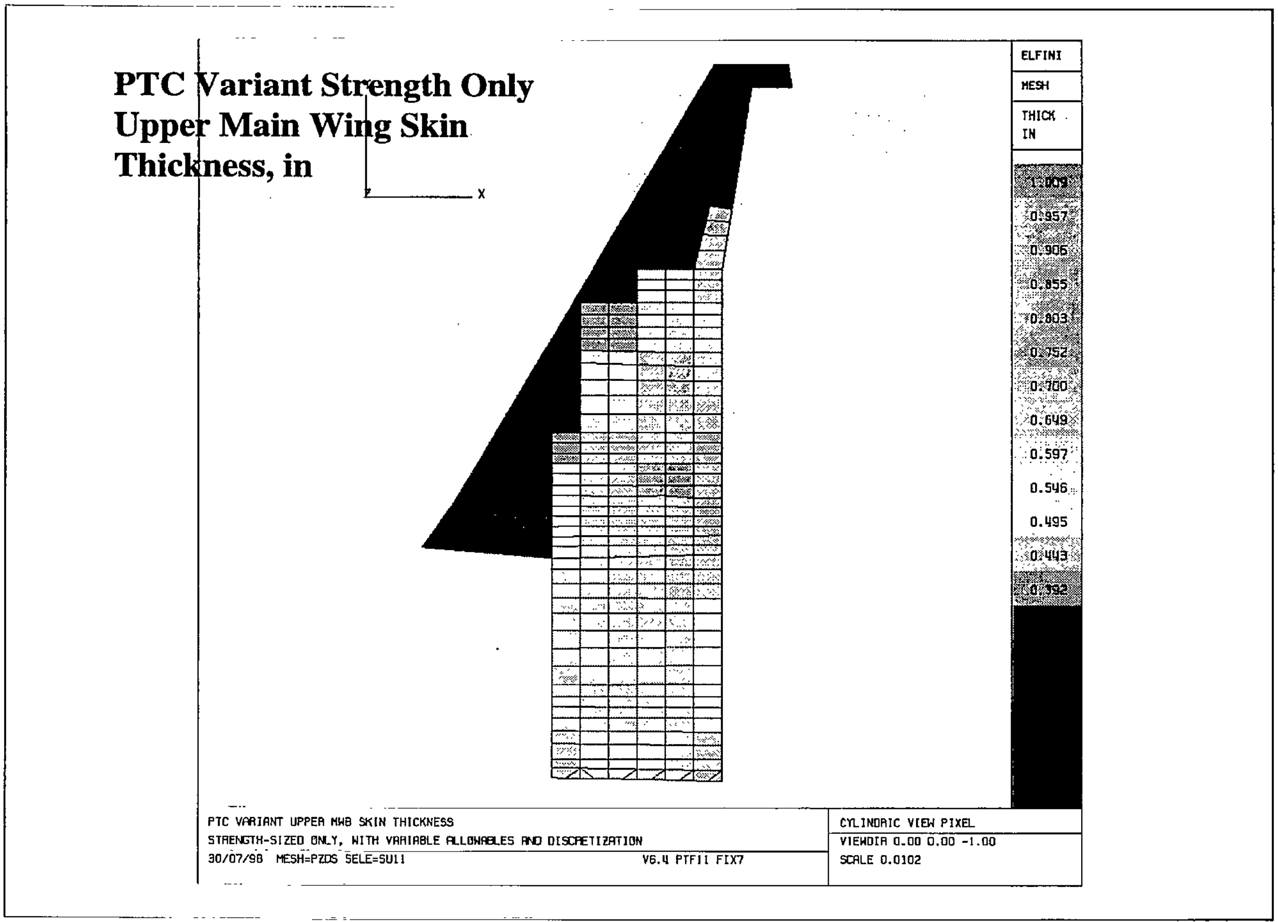
PTC Variant Strength Only
Upper Main Wing Skin
Thickness, in
X
ELFINI
MESH
THICK
IN
1.009
0.957
0.906
0.855
0.803
0.752
0.700
0.649
0.597
0.546
0.495
0.443
0.392
PTC VARIANT UPPER MWB SKIN THICKNESS
STRENGTH-SIZED ONLY, WITH VARIABLE ALLOWABLES AND DISCRETIZATION
30/07/98 MESH=PZDS SELE=SU11
V6.4 PTF11 FIX7
CYLINDRIC VIEW PIXEL
VIEWDIR 0.00 0.00 -1.00
SCALE 0.0102

PTC Variant Strength Only Upper Strake Thickness, Both Face Sheets

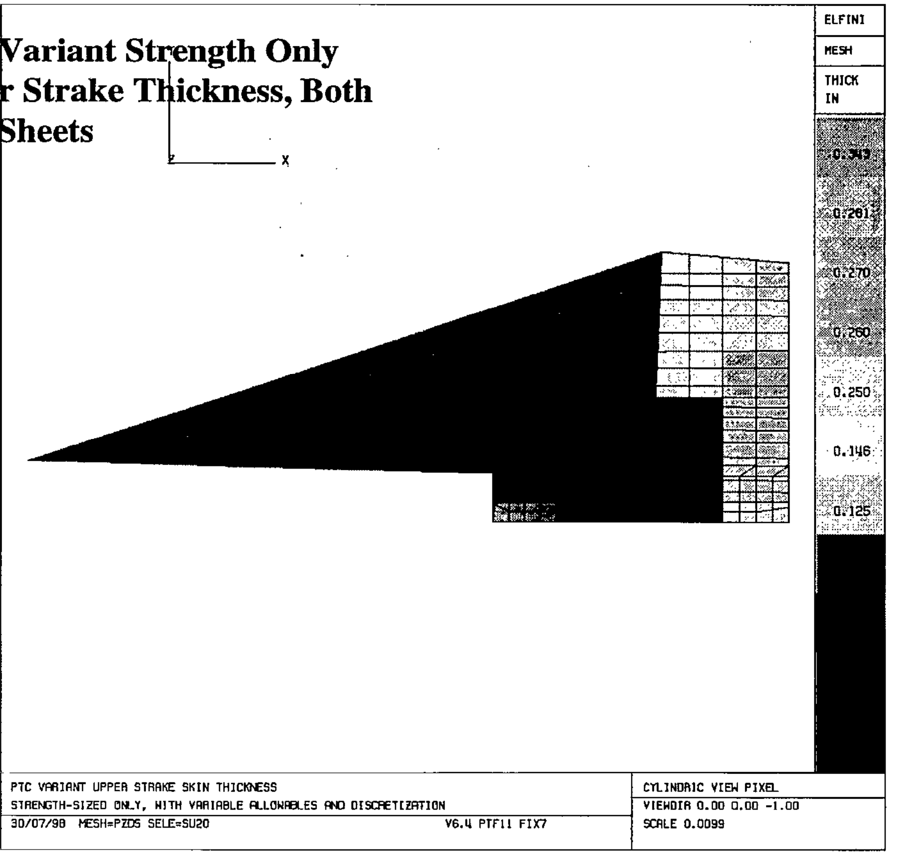

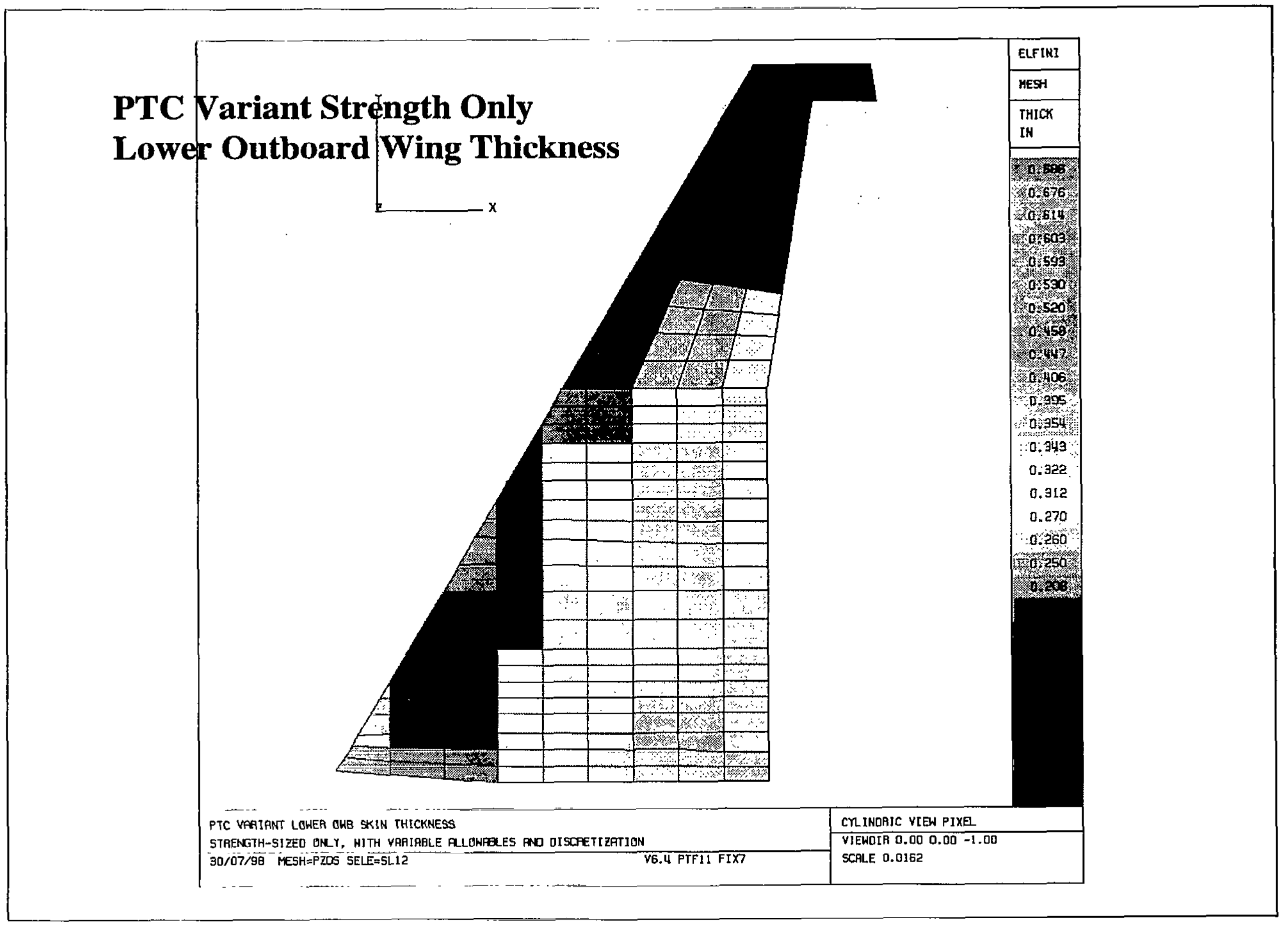
PTC Variant Strength Only
Lower Outboard Wing Thickness
X
ELFINI
MESH
THICK
IN
0.676
0.614
0.603
0.593
0.530
0.520
0.458
0.447
0.406
0.395
0.354
0.343
0.322
0.312
0.270
0.260
0.250
PTC VARIANT LOWER OWB SKIN THICKNESS
STRENGTH-SIZED ONLY, WITH VARIABLE ALLOWABLES AND DISCRETIZATION
30/07/98 MESH=PZOS SELE=SL12
V6.4 PTF11 FIX7
CYLINDRIC VIEW PIXEL
VIEWDIR 0.00 0.00 -1.00
SCALE 0.0162

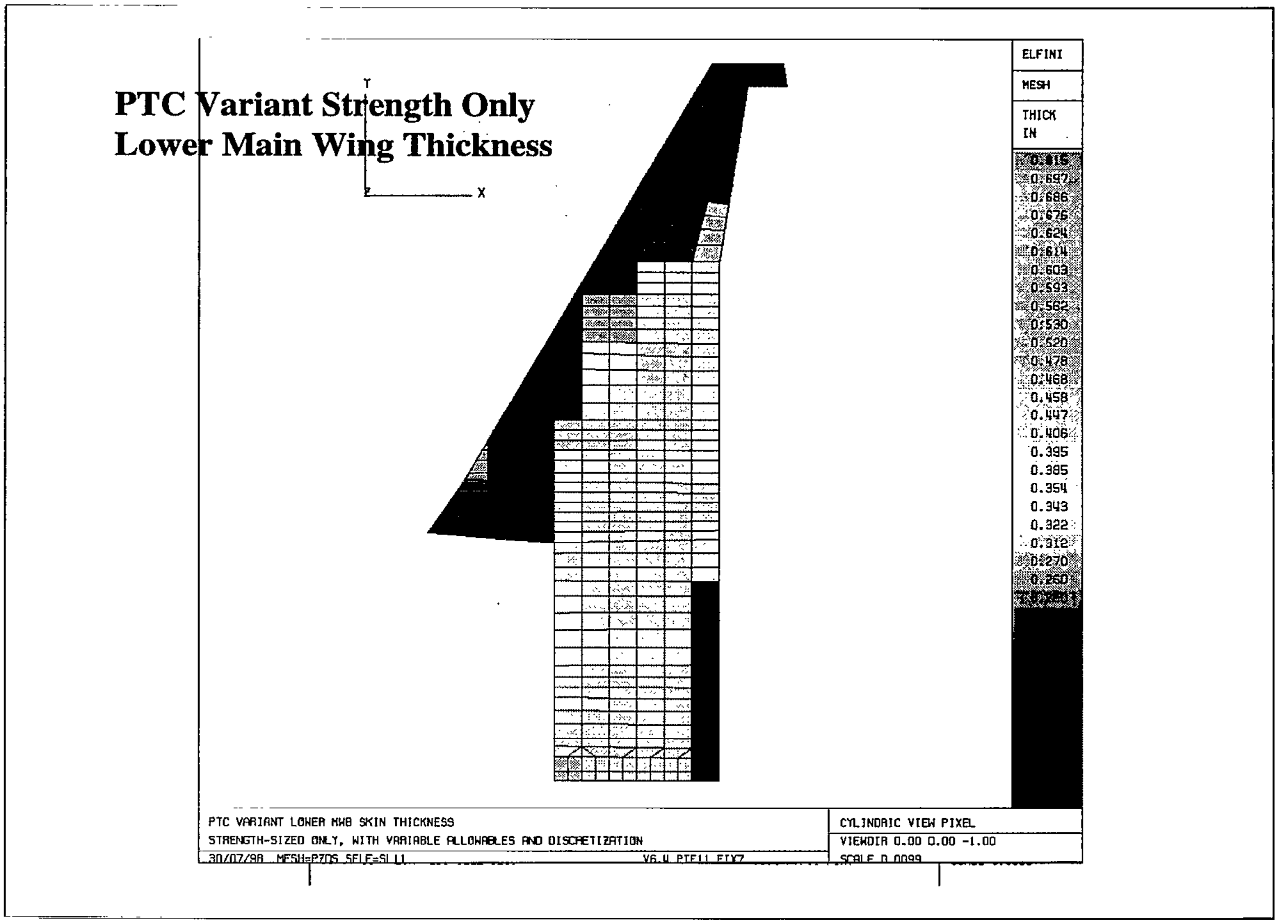
PTC Variant Strength Only
Lower Main Wing Thickness
Y
X
ELFINI
MESH
THICK
IN
0.697
0.686
0.676
0.624
0.614
0.603
0.593
0.562
0.530
0.520
0.478
0.468
0.458
0.447
0.406
0.395
0.385
0.354
0.343
0.322
0.312
0.270
0.260
PTC VARIANT LOWER MWB SKIN THICKNESS
STRENGTH-SIZED ONLY, WITH VARIABLE ALLOWABLES AND DISCRETIZATION
CYLINDRIC VIEW PIXEL
VIEWDIR 0.00 0.00 -1.00

PTC Variant Strength Only Lower Strake Thickness, Both Face Sheets

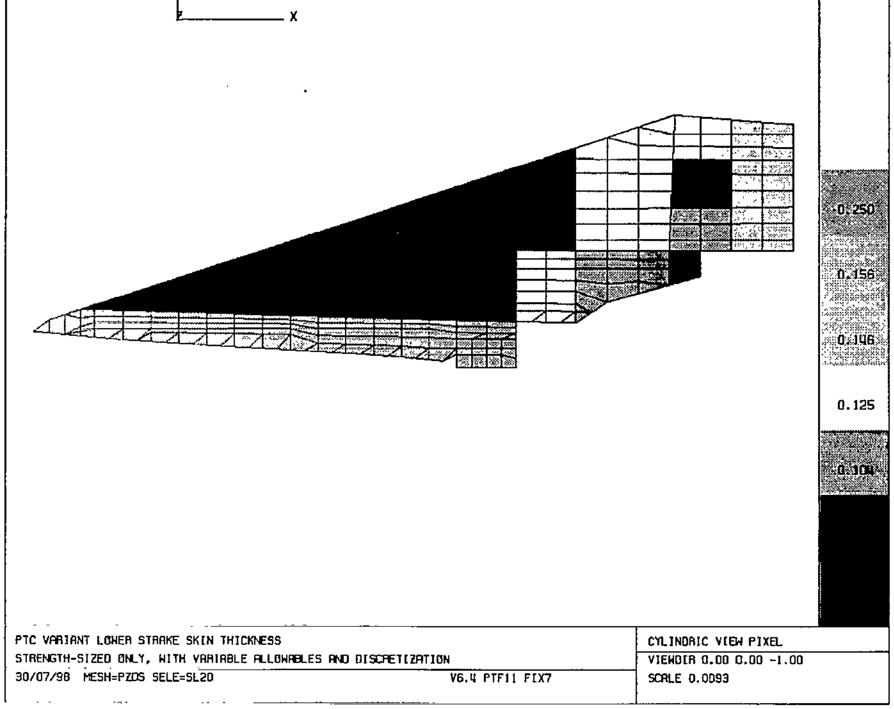

PTC Variant Strength Only Main Wing Substructure Thickness

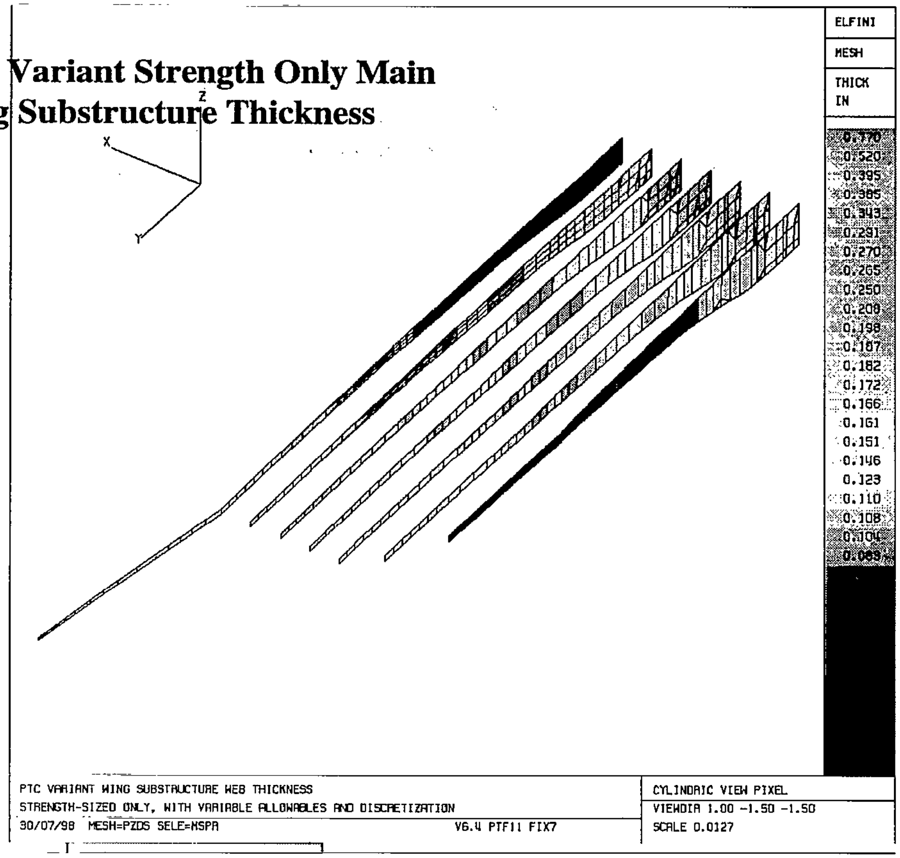

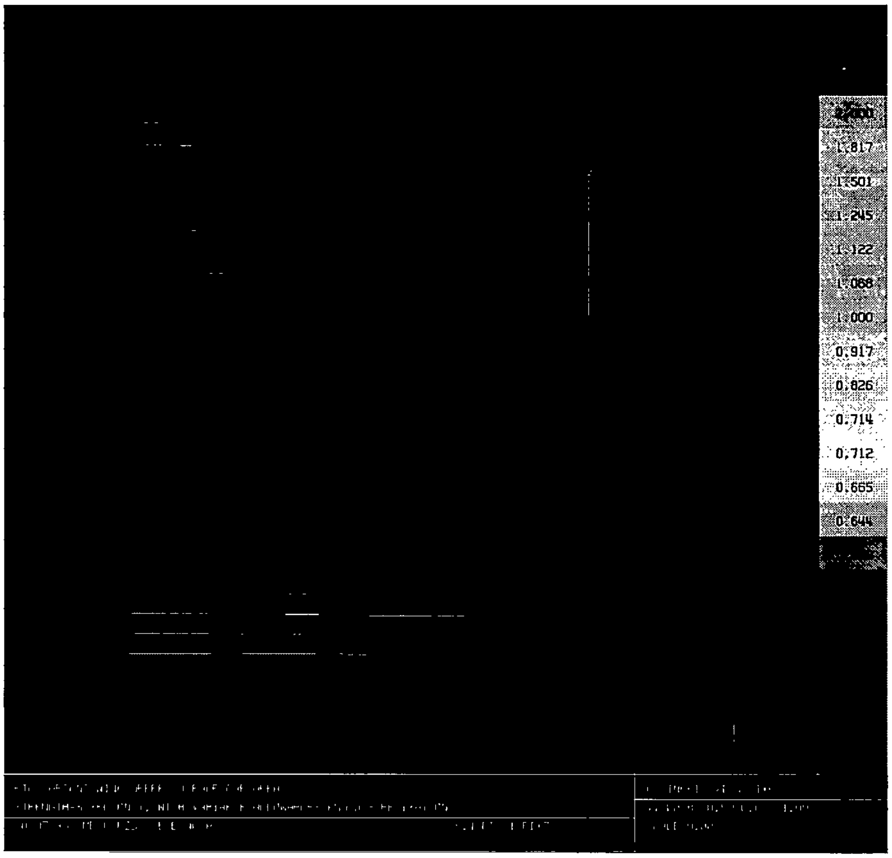
1.817
1.501
1.245
1.122
1.068
1.000
0.917
0.826
0.714
0.712
0.665
0.644

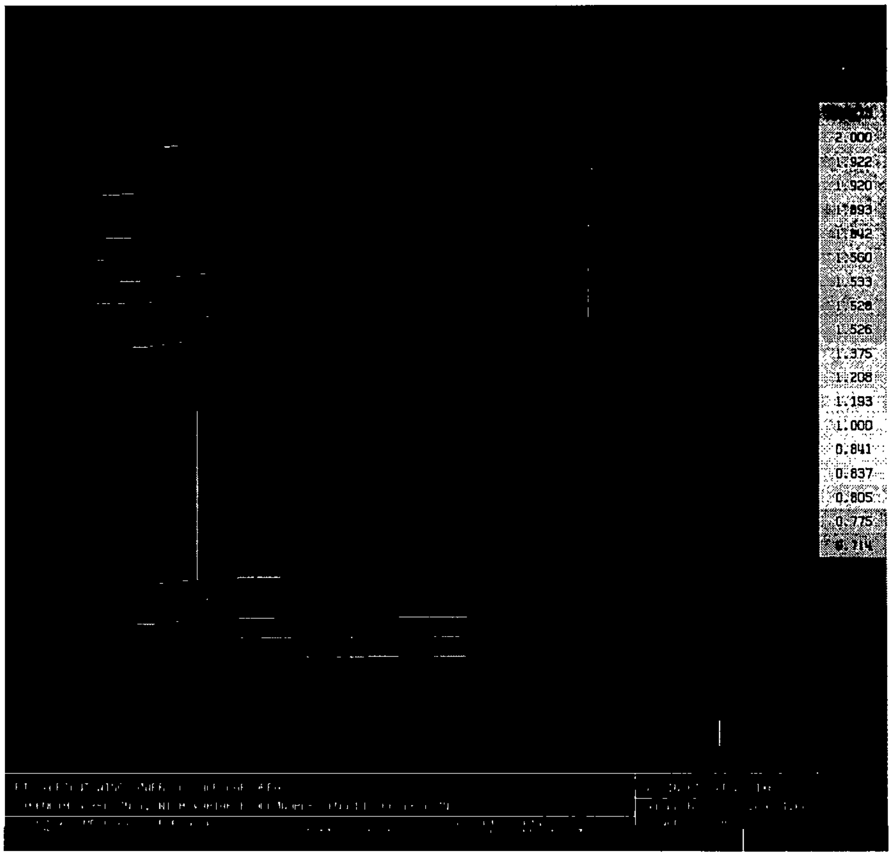
2.000
1.922
1.920
1.893
1.842
1.560
1.533
1.528
1.526
1.375
1.208
1.193
1.000
0.841
0.837
0.805
0.775
0.714

PTC Variant Strength Only Section 41, 43, & 44 Skin + Stringer Thickness

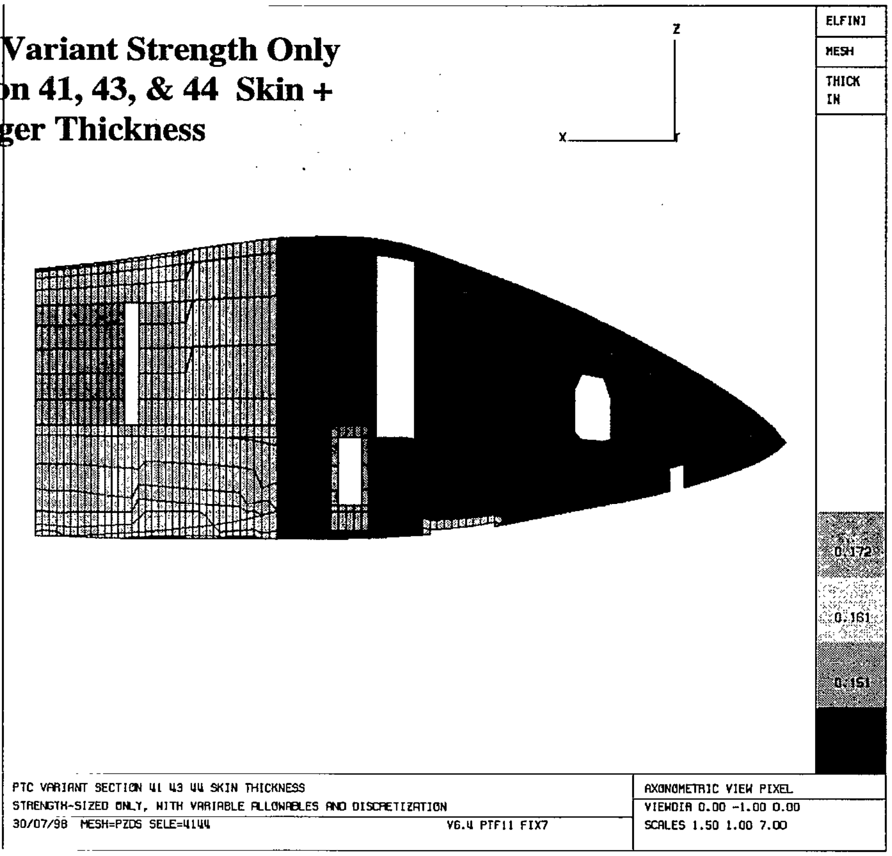

PTC Variant Strength Only Section 45 & 46 Skin + Stringer Thickness

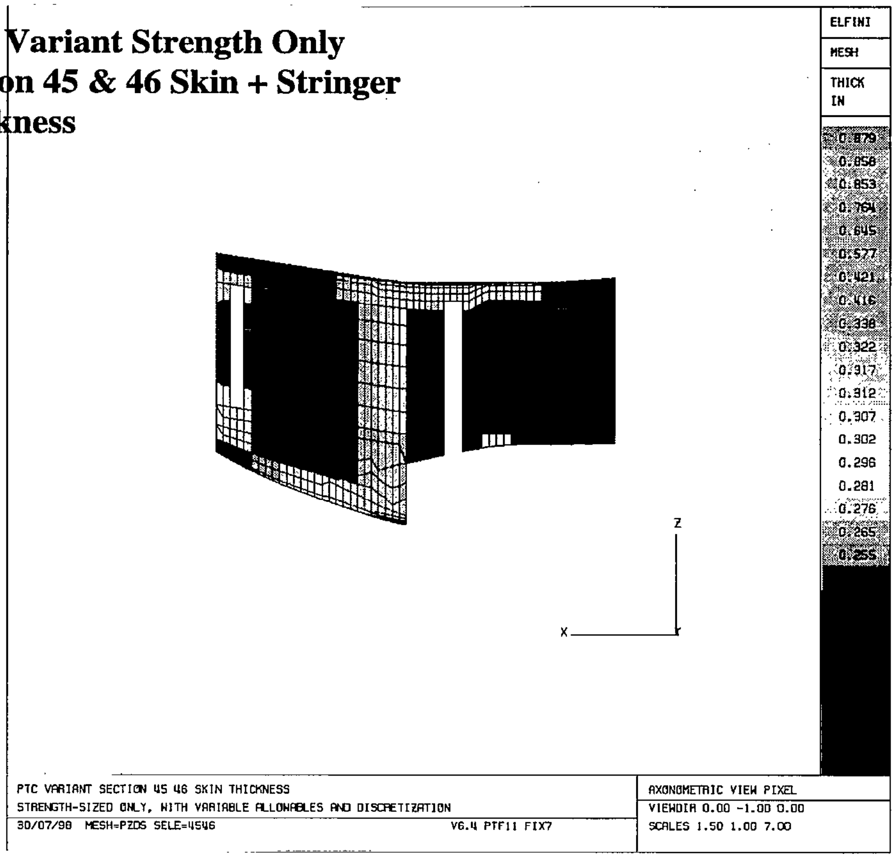

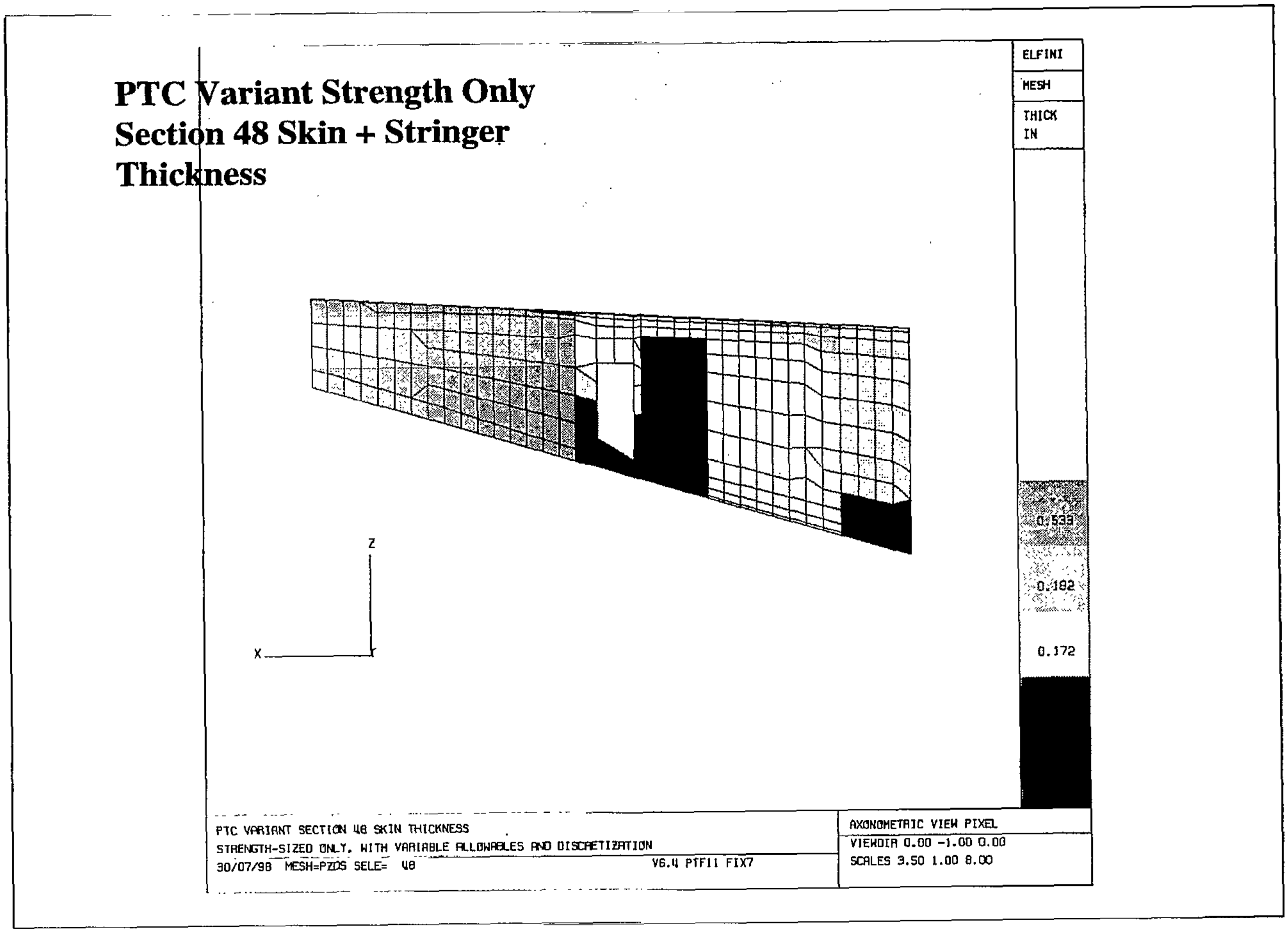
PTC Variant Strength Only
Section 48 Skin + Stringer
Thickness
ELFINI
MESH
THICK
IN
0.539
0.182
0.172
Z
X
PTC VARIANT SECTION 48 SKIN THICKNESS
STRENGTH-SIZED ONLY, WITH VARIABLE ALLOWABLES AND DISCRETIZATION
30/07/98 MESH=PZOS SELE= 48
V6.4 PTF11 FIX7
AXONOMETRIC VIEW PIXEL
VIEWDIR 0.00 -1.00 0.00
SCALES 3.50 1.00 8.00

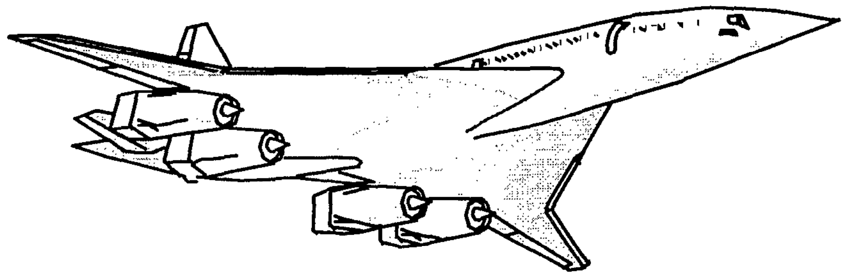

ACE Final Report

D.2 - Wing Span Study

Starr Parker
Steve Sergev
Brad Becker
Steve Stone

December 31, 1998

The following individuals contributed to this report:

Starr Parker - Aerodynamics and Loads

Steve Sergev - Sizing

Brad Becker - Weights

Steve Stone - Flutter

Study Motivation

Weights engineering expressed an interest to assess the effects of changing wing span on airplane weight. The ground rules for this study were to use the PTC Variant as a baseline and to change only the outboard wing. Changes were to stay within the existing planform and conform to the loft and were done by projecting all nodes inboard, proportionally, toward the inboard-outboard wing joint along spars they were attached to. It was acknowledged that his change would also change wing area, but this was judged to be acceptable for the study.

Analysis Model

Two wing planforms were created that reduced the span of the outboard wing by approximately 1/3 and 2/3; these are referenced in this report by the percentage of outboard wing remaining relative to the Variant. The 1/3 reduction is known as the .69 wing and the 2/3 reduction is known as the .37 wing. The planforms are compared to the PTC Variant in Figure 1.

Analysis Approach

The analysis was designed to make maximum use of existing processes, procedures, and files. In the finite element model, all nodes in the PTC Variant model were preserved using the proportional projection approach. Thus all subsequent files that worked with the Variant would work with this study. This facilitated rapid turn around for both loads (overnight) and weights (one-half day) calculations.

Sizing Process

Sizing was done by using the final strength sized gages from the Variant as the initial gages for both models. Initial loads were from the Variant, as well. After four global iterations, new masses and new loads were calculated for each model. Four additional global iterations led to the final reported weights. Convergence histories are shown in Figure 2. Shear, moment, and torsion plots are shown in Figures 3 - 7.

Weights Results

This study was initiated in order to provide the Weight Engineering group with a consistent set of data with which to validate and/or re-calibrate their parametric weight prediction methodology with respect to wing span. The following table presents the weight results (for the sized structure) of the 3 wings in this study from both the finite element model (FEM) as well as the common HSR Weight Methodology (Parametric Results).

	PTC Variant	Delta	.69 Wing	Delta	.37 Wing
Wing Semispan	944 in	-82 in	861 in	-82 in	779 in
FEM Results	47,940 lb	-5,390 lb	42,550 lb	-7,910 lb	34,640 lb
Parametric Results	50,900 lb	-5,930 lb	44,970 lb	-5,200 lb	39,770 lb

Wing Sized Structure Weight Results

The FEM results and the Parametric results both give similar trends with decreasing span; i.e. decreasing weight with decreasing span as expected. However, the rate of weight change with span change does not agree very well between the two methods. The HSR Weight Methodology will be updated to reflect the trends as seen in the FEM results. Note, that the absolute values between the FEM and the Parametrics do not currently agree here. The Parametrics are currently being updated and correlated with the FEM results from the PTC (1080-1499) as well as the PTC Variant.

The fuselage weight results are somewhat surprising. The following table presents the weight results (for the sized structure) of the fuselages corresponding to 3 wings in this study from both the finite element model (FEM) as well as the common HSR Weight Methodology (Parametric Results).

	PTC Variant	Delta	.69 Wing	Delta	.37 Wing
FEM Results	+29,170 lb	-360 lb	+28,810 lb	-1,980 lb	+26,830 lb
Parametric Results	+28,260 lb	+0 lb	+28,260 lb	+0 lb	+28,260 lb

Fuselage Sized Structure Weight Results

The fuselage magnitude of the weight sensitivity to wing span as determined by the FEM results is larger than expected. Currently, the Parametric methods do not have any sensitivity to wing span in the fuselage weight estimation since this effect was assumed to be small. This discrepancy will be addressed in a future update to the parametrics.

Weights are summarized in Figures 8 and 9.

Flutter Assessment

A flutter assessment (not flutter sizing) was performed and is described below.

PTC Variant with clipped tip planform data

Wing	Area sq.ft.	Span ft.	Tip chord in.	MAC in.	Ybar in.	LEMAC in.
PTC Variant	9642.9	162.25	129.895	1058.96	300.90	735.31
Clipped Variant 1	9458.0	148.54	193.855	1076.46	288.61	719.69
Clipped Variant 2	9200.0	134.83	257.815	1100.27	272.92	698.28

Note: LEMAC measured from wing apex

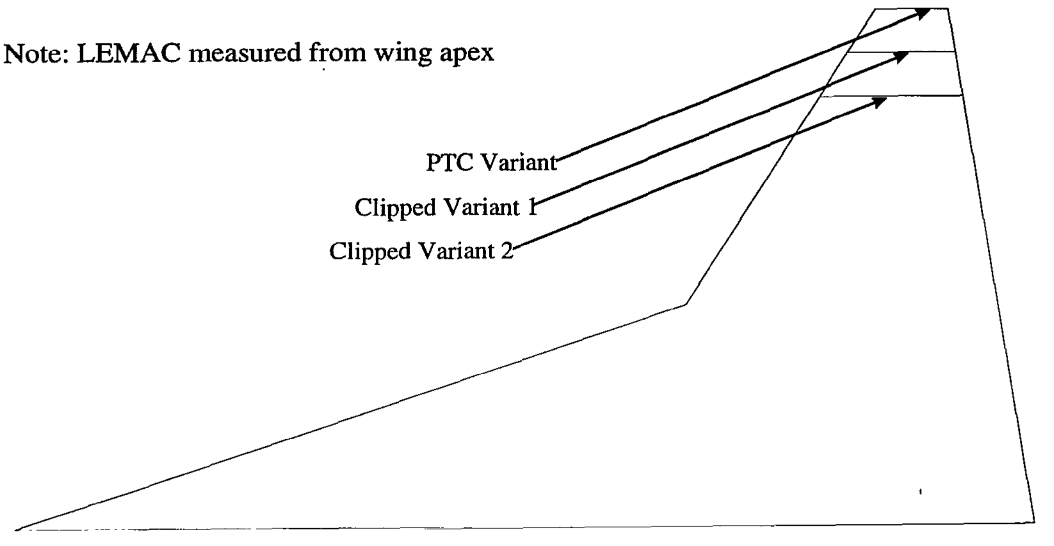

Figure 1 Planform Comparison

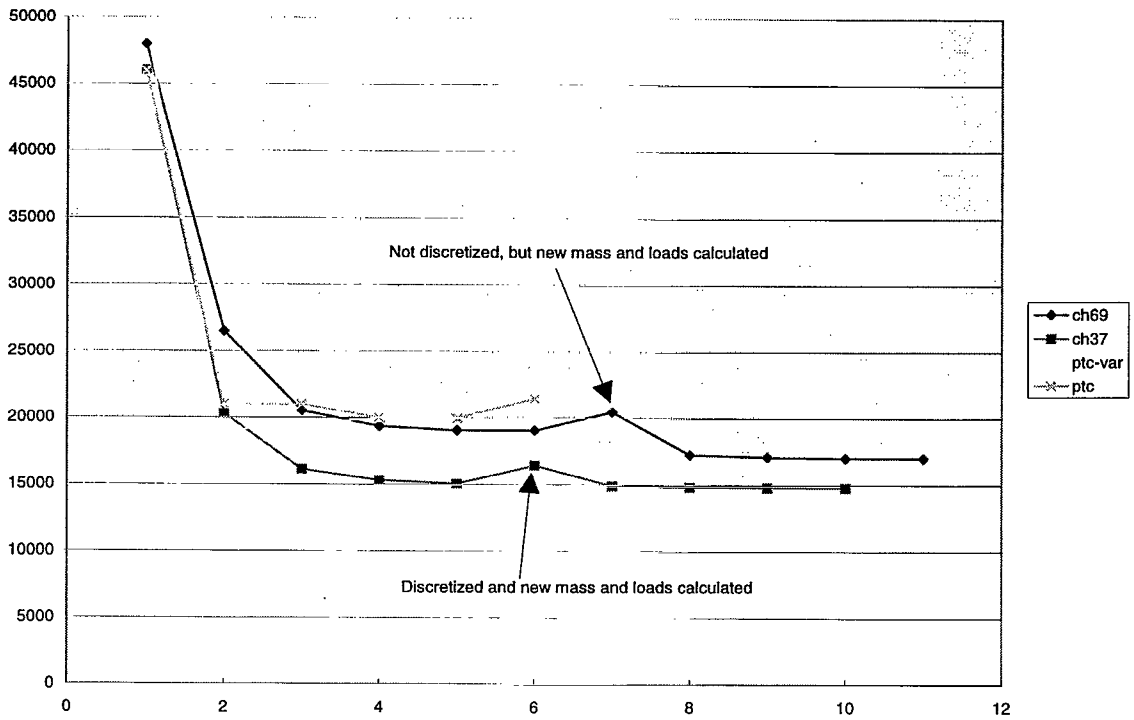

Figure 2. Convergence History

Loads Results

Results appear on the following pages.

Wing Shear Comparison

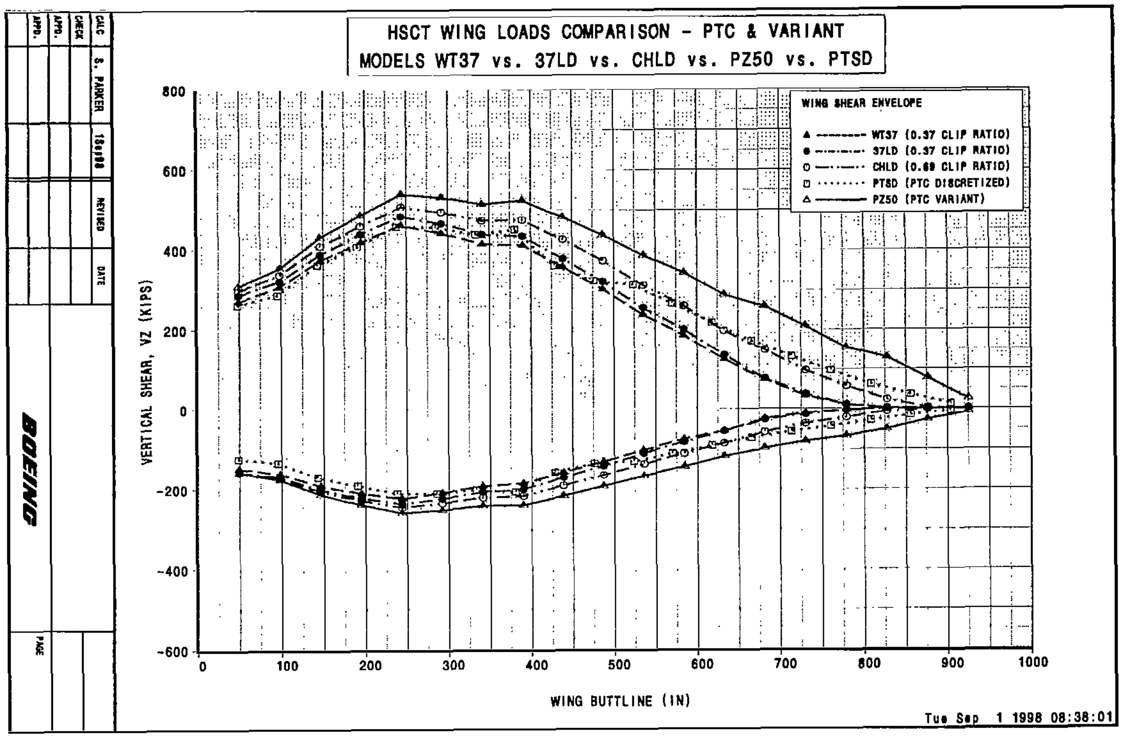

Figure 3

Wing Moment Comparison

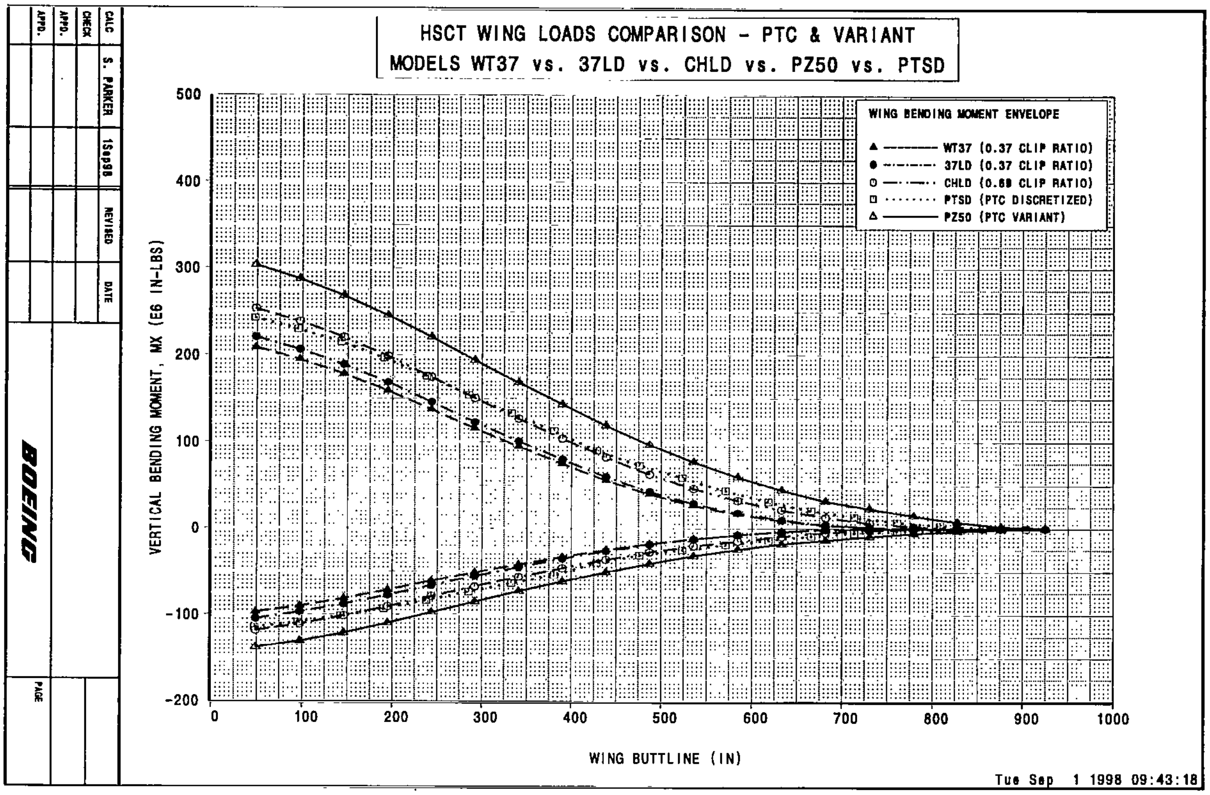

Figure 4

Wing Torsion Comparison

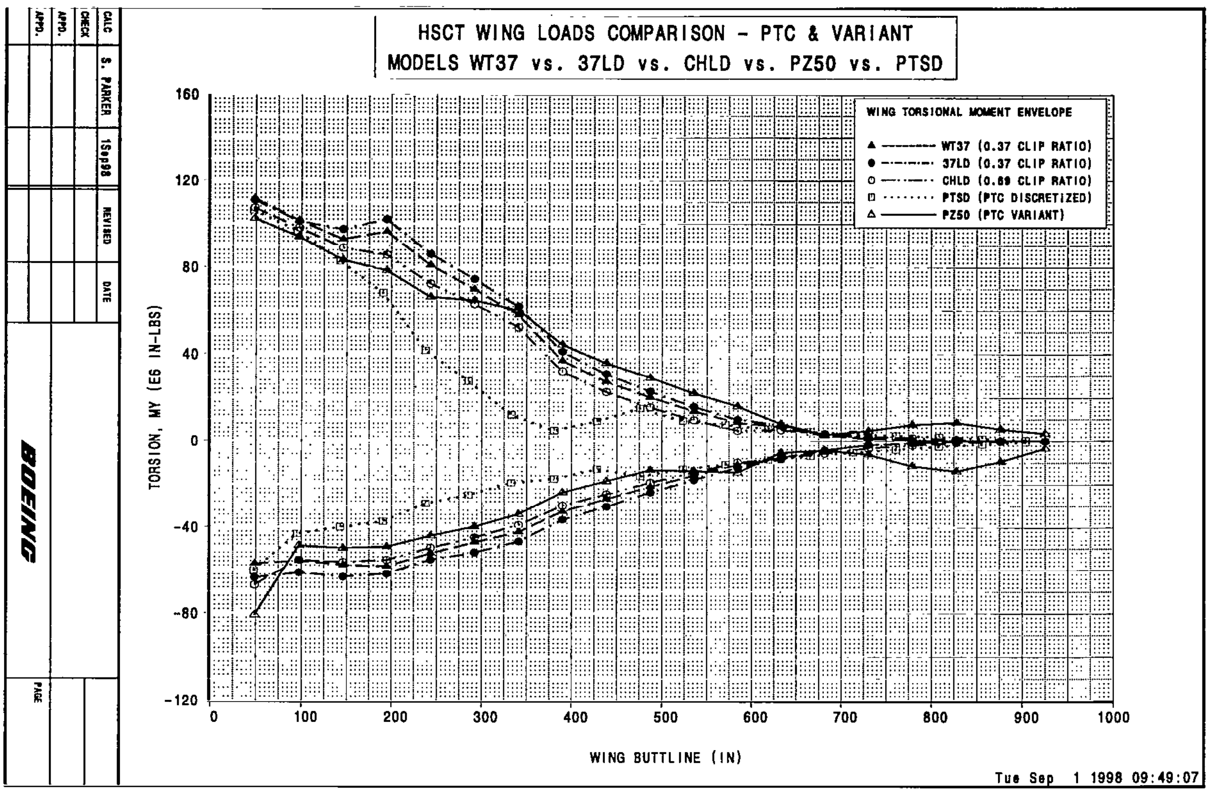

Figure 5

Fuselage Shear Comparison

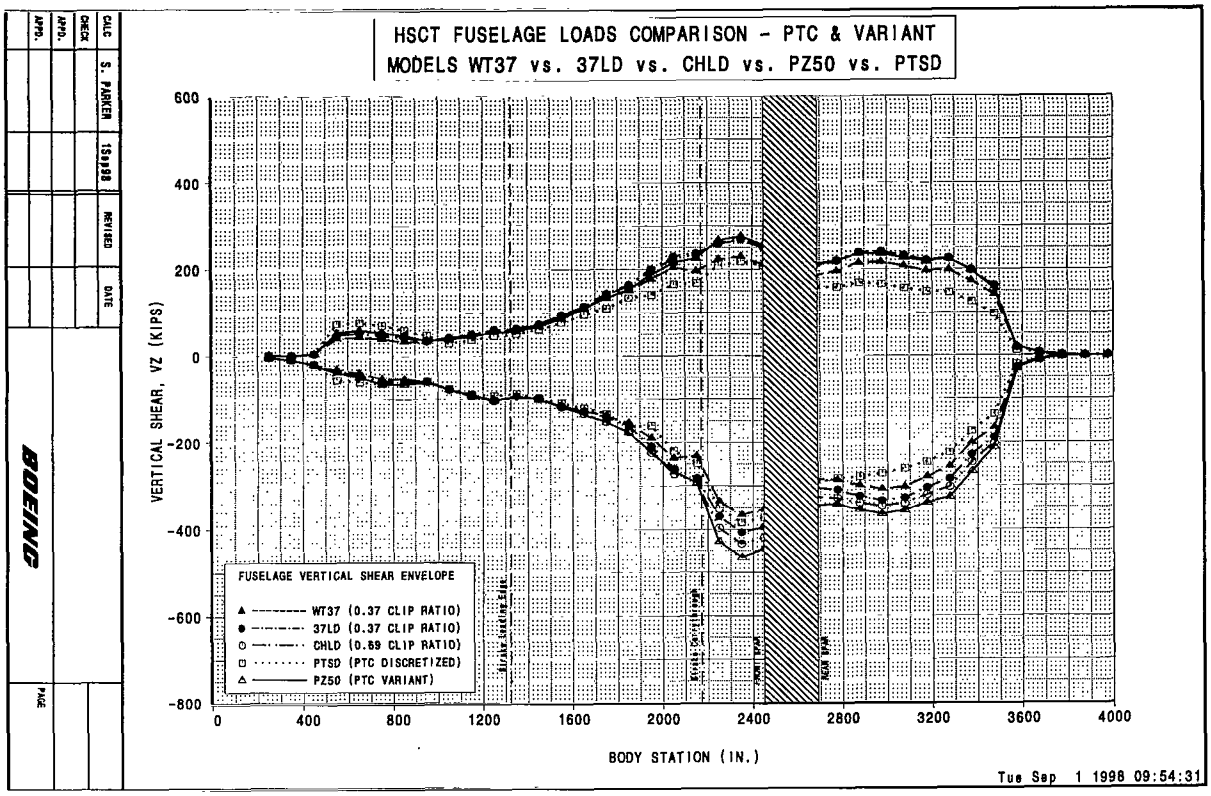

Figure 6

Fuselage Moment Comparison

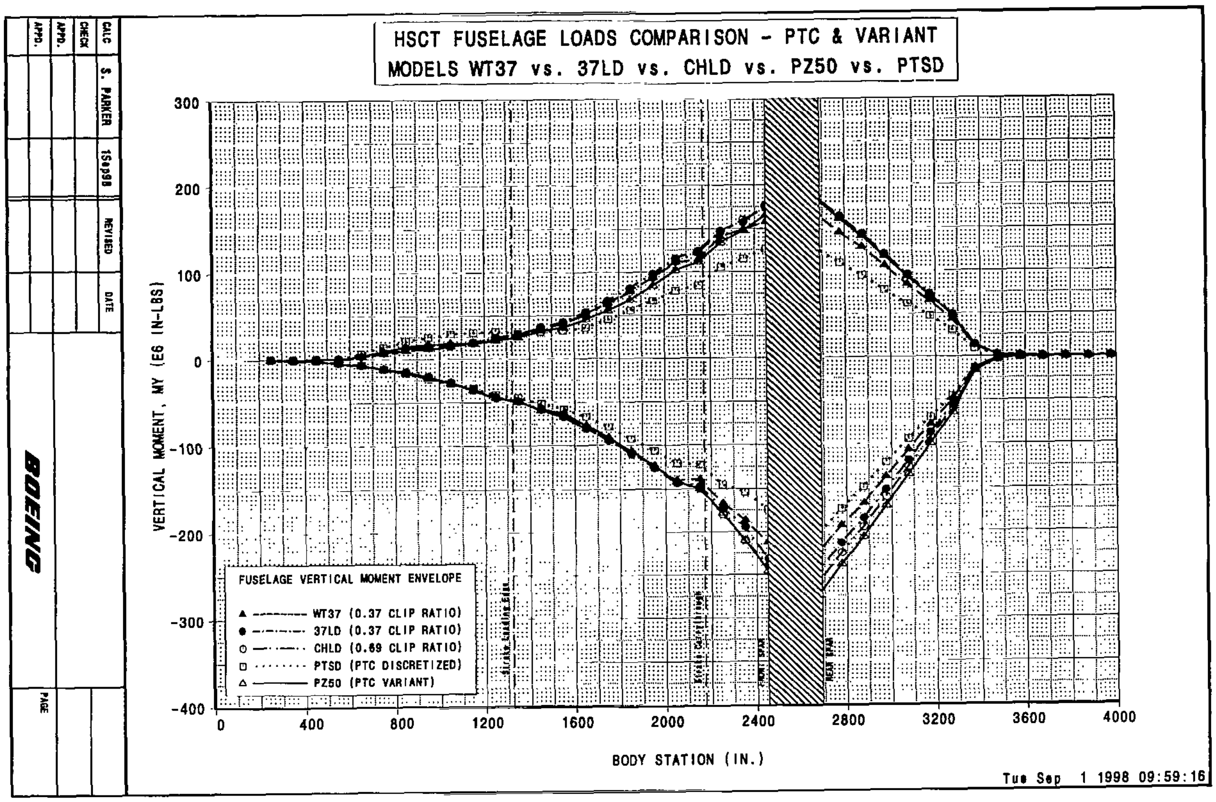

Figure 7

Wing Structure Weight	Strength Sized -1510 (788K) (PZSD model)		Strength Sized - 69 Chop (67WT model)		Strength Sized -37 Chop (37WT model)	
	Weight (lb)	Unit Weight (lb/ft^2)	Weight (lb)	Unit Weight (lb/ft^2)	Weight (lb)	Unit Weight (lb/ft^2)
TOTAL WING STRUCTURE	78,167	8.1	71,570	7.6	62,983	6.8
TOTAL WEIGHED STRUCTURE	47,942	5.0	42,548	4.5	34,643	3.8
TOTAL FIXED WEIGHT	30,225	3.1	29,022	3.1	28,340	3.1
Strake	23,219	7.74	23,895	7.97	22,928	7.65
Weighed Structure	16,421	5.48	17,097	5.70	16,130	5.38
Fixed Weight	6,798	2.27	6,798	2.27	6,798	2.27
FORWARD STRAKE	7,607	7.44	7,607	7.44	7,607	7.44
Weighed Structure	6,048	5.92	6,048	5.92	6,048	5.92
Bending Material (Skin Panels & Spar Caps)	4,718		4,717		4,717	
Shear Material (Spar Webs & Ribs)	1,258		1,258		1,258	
Lightning Protection	71		72		72	
Fixed Weight	1,559	1.53	1,559	1.53	1,559	1.53
Access Doors	708		708		708	
Wing/Fuselage Attachment	681		681		681	
Actuator Attachment	170		170		170	
MID/GEAR BOX	15,612	7.90	16,288	8.24	15,321	7.75
Weighed Structure	10,373	5.25	11,049	5.59	10,082	5.10
Bending Material (Skin Panels & Spar Caps)	7,864		8,336		7,500	
Shear Material (Spar Webs & Ribs)	2,370		2,574		2,442	
Lightning Protection	138		140		140	
Fixed Weight	5,239	2.65	5,239	2.65	5,239	2.65
Access Doors	852		852		852	
Wing/Fuselage Attachment	454		454		454	
Actuator Attachment	113		113		113	
MLG Doors & Jam/Attachment	3,820		3,820		3,820	
Main Wing Box	22,764	18.71	19,784	16.26	16,059	13.20
Weighed Structure	20,640	16.96	17,660	14.51	13,935	11.45
Bending Material (Skin Panels & Spar Caps)	16,198		13,655		10,620	
Shear Material (Spar Webs & Ribs)	4,357		3,919		3,229	
Lightning Protection	85		86		86	
Fixed Weight	2,124	1.75	2,124	1.75	2,124	1.75
Access Doors	819		819		819	
Wing/Fuselage Attachment	1,078		1,078		1,078	
Actuator Attachment	227		227		227	
Outboard Wing Box	12,127	9.61	8,883	8.01	5,640	5.76
Weighed Structure	10,881	8.62	7,791	7.02	4,578	4.68
Bending Material (Skin Panels & Spar Caps)	9,995		6,948		3,839	
Shear Material (Spar Webs & Ribs)	798		764		670	
Lightning Protection	88		79		69	
Fixed Weight	1,246	0.99	1,092	0.98	1,062	1.08
Access Doors	849		720		700	
Actuator Attachment	397		372		362	
Leading Edge (Fixed Weight)	7,285		6,929		6,740	
Trailing Edge (Fixed Weight)	9,679		9,278		9,022	
Fairings (Fixed Weight)	852		852		852	
Miscellaneous (Fixed Weight)	2,241		1,949		1,742	

Figure 9

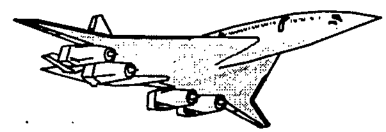

ACE Final Report

D.3 - Engine Trade Study

Steven C. Stone - Boeing Seattle

December 31, 1998

A trade study was performed to try and understand the relationships between engine mass, fence height, and flutter. The goal was to estimate the weight penalty for correcting flutter in a TCA configuration that was a product of strength and some flutter optimizing.

In performing the study, the nominal TCA engine mass flow (800 lb/sec) was varied by 10%. This roughly corresponded to a 10% change in weight of the 18350 lb combined inlet, engine, and nozzle. For the fence, configurations were investigated that had no fence as well as 25", 30", and 35" fences.

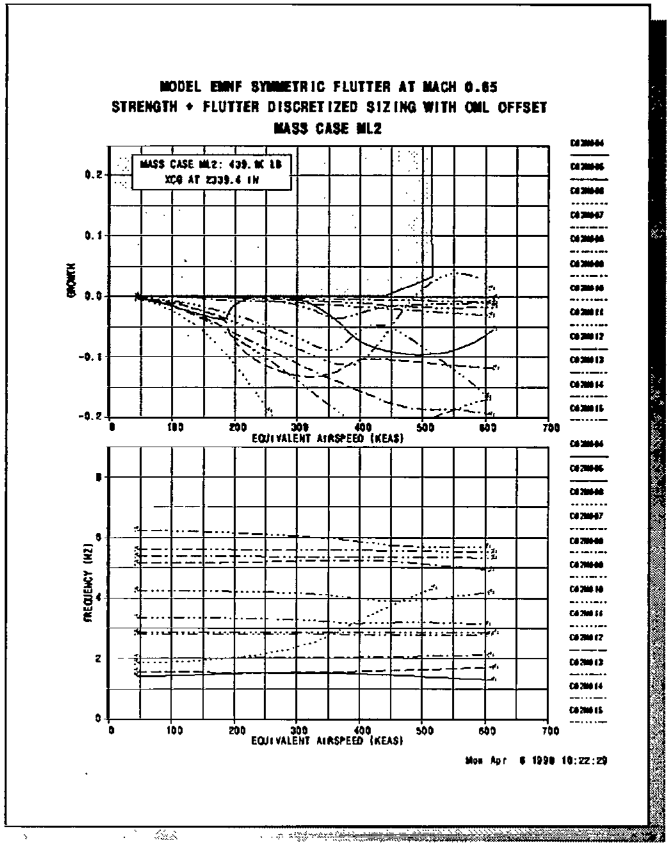

Shown above are the results of the flutter analysis for the light engine (nominal engine -10%) aircraft without a fence for the ML2 mass case at Mach 0.65 (ML2 and MT2 are often the most critical mass cases) Note that all of the flutter modes remain damped for this case.

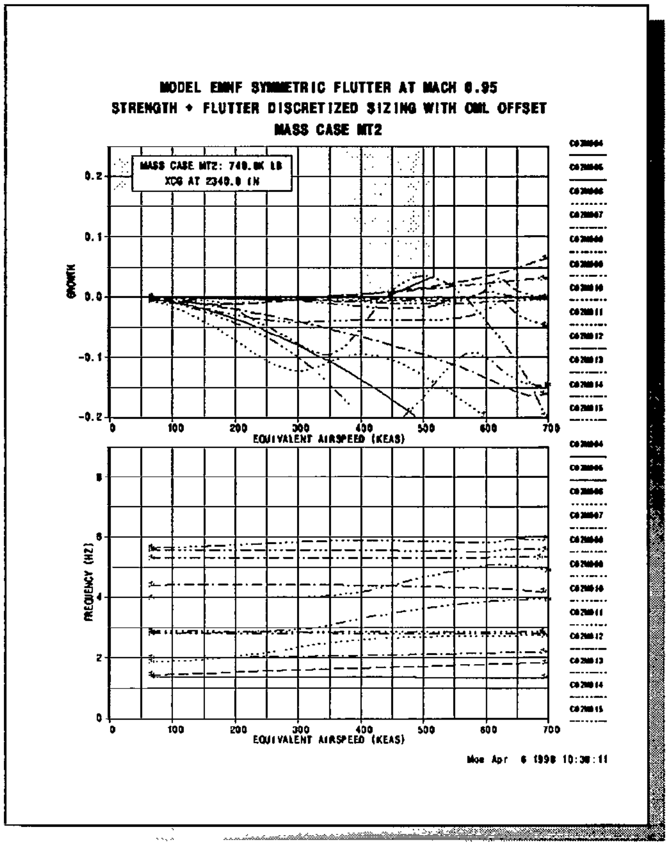

The same configuration was investigated for MT2 at Mach 0.95. Here, the low frequency second mode does not satisfy the flutter requirements as can be seen by the dashed line cutting the corner of the gray flutter clearance boundary.

The higher frequency (3-dot dash line) that is in violation is an outboard wing mode that is of less concern here. The TCA model with additional flutter optimization would satisfy this violation without much additional weight.

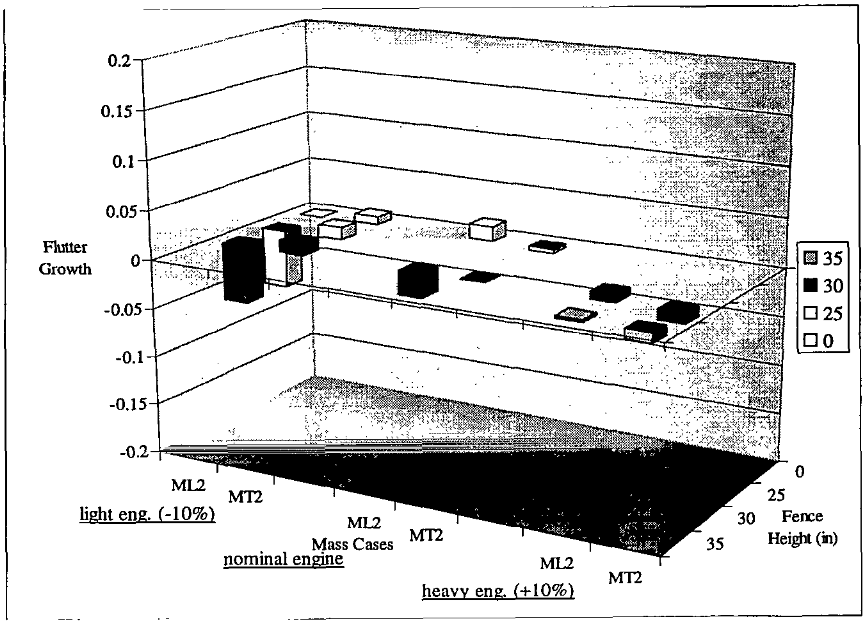

Similar analyses were performed on a variety of cases. To help in understanding the sensitivities, the bar graph above shows the variation of flutter growth with engine weight and fence height. The scale of the flutter growth is the same as that seen in the previous flutter plots. Even though it is not a complete set of data in relation to all of the variables, there is enough information to see important trends.

In this chart, the ML2 critical flutter growth values for the low frequency mode 1 were taken at the speed where the mode had the greatest value. For MT2, values for the second mode were taken at Vd (445 KEAS). Thus, the two previous plots each contribute a single value to the chart above for the "0" fence height, light engine category.

Generally, as the weight of the engine is increased, the ML2 case transitions from non-critical to critical in flutter. Opposite to this, the MT2 case transitions from critical with the light engine to non-critical with the heavy engine.

The change in fence height has a more dramatic reduction of flutter tendencies for the ML2 case. For the most part, the change in the fence has little effect on MT2. Also, the lighter engine is more sensitive to the increase in height than the heavy engine

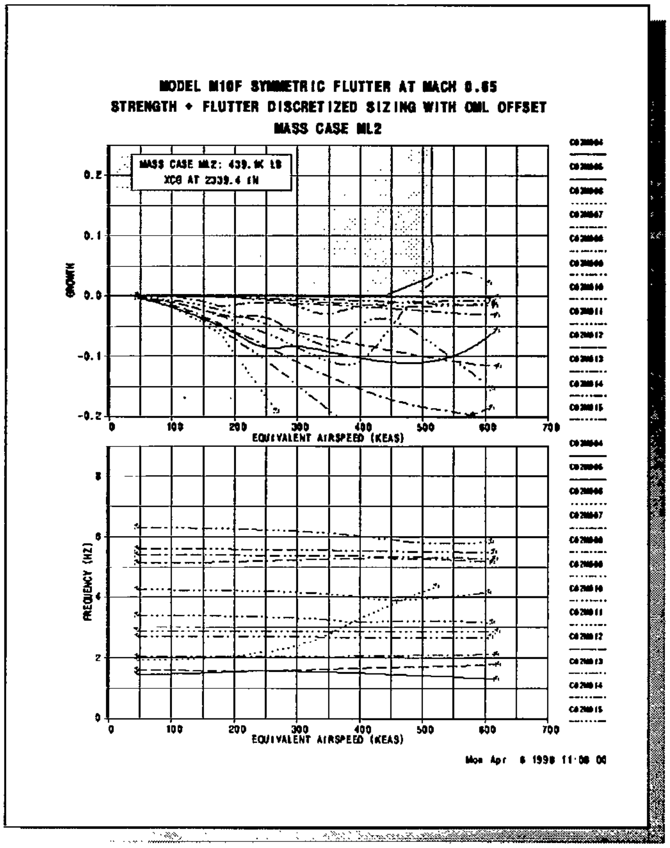

From the bar graph, it was clear that the light engine MT2 case was the violated constraint that would have to be satisfied by additional means. The addition of the fence would keep the flutter under control for the configuration with heavier engines.

With this in mind, stiffness was added to select portions of the wing structure to see the effect on the 2nd mode for the MT2 case. The result was positive since it indicated a small reduction in flutter growth. However, the slight improvement was unacceptable in light of the amount of stiffness (weight) that was added to obtain the results.

Instead, a decision was made to try a mass balance approach. This consisted of adding 600 lb to the aft end of the outboard engine (when viewing the flutter results from Elfini, it was this engine that appeared to be the driving mechanism).

Shown above are the flutter results of this mass balancing for the ML2 case for the light engine case with a 30 inch fence. Just as before, the flutter modes remain well damped.

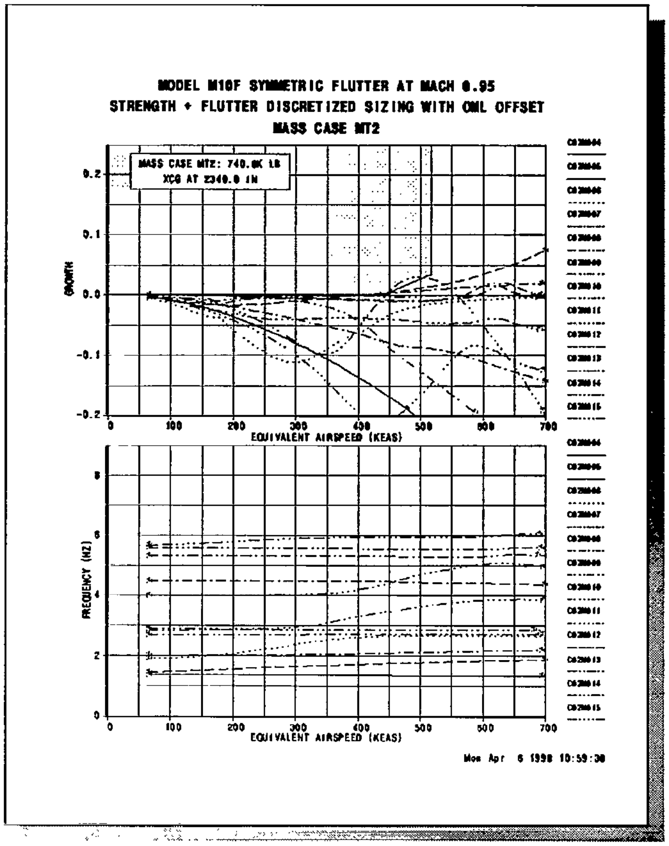

Presented here are the improved results for the MT2 mass case for the same configuration. Notice how the second mode has now dropped down to where it is barely clipping the corner of the unacceptable region.

Eleven different flutter analyses were accomplished on models with various engine mass and fence configurations. For a heavier engine aircraft, the addition of a fence was enough to satisfy flutter requirements. For aircraft with lighter engines, the engine fence plus additional mass balancing provided a solution. For the TCA configuration studied, a weight of approximately 600 lb per outboard engine proved to be adequate in helping the concerned mass cases clear the flutter requirements.

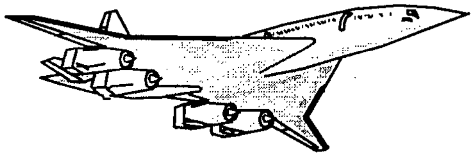

ACE Final Report

D.4 - Nastran EPT Process and Results

Derek Barkey
Michael Shih
Joseph Giesing
Gilles DeBrouwer
Boeing PW - Long Beach

December 31, 1998

D.4.1 EPT Validation with TCA

The Need for Vehicle Structural Sizing

- **Vehicle structural sizing is performed for several reasons:**
  - **To support Airplane Configuration Trade Studies**
  - **To support Material and Structures Trade Studies**
  - **To support Detailed Weight Estimates**
- **Why a FEM based approach?**
  - **FEM structural analysis is required to address flutter, loads, unconventional configurations, and new materials and structural concepts which cannot be captured by conventional statistically based parametric weight equations.**

For the purposes of ACE, rapid structural sizing is required to develop weight sensitivities to configuration variables, including wing planform, multiple surfaces, engine locations, etc. A finite element approach is required, rather than a parametric weight estimate, because parametric equations for unconventional configurations and materials do not exist. Also, flutter can have a significant impact on aircraft weight. That weight impact cannot be determined without an accurate representation of stiffness, mass, and aerodynamics.

Vehicle Structural Sizing for HSR

- **Vehicle structural sizing techniques with a very high level of detail have been developed in Seattle and Long Beach for the HSR Design Integration Trade Study (DITS) task.**
- **Developing a FEM, design information, loads data, mass properties algorithms, etc. is a very time consuming and expensive process, at least five months are required for a configuration.**

Cycle Time Reduction

- **HSR recognized cycle time as an issue in 1996, and Boeing-Seattle, Boeing-Long Beach, and NASA-Langley began developing more efficient methods with a goal of 5% the weight of a full FEM model.**
- **Long Beach approach was to use a simpler modeling technique:**
  - **Analogous to using a beam representation for a high aspect ratio wing**
  - **Use existing process and tools as much as possible**
  - **Allow variable levels of detail**

The critical issue is to reduce cycle time to generate sensitivities of weight with respect to global design variables. This can be done at the expense of weight accuracy, as long as the sensitivities are captured accurately.

Assessing the accuracy of sensitivities would require sizing several different configuration variations using both the full sizing process and the rapid process. Since this would be prohibitively time consuming, a more rigorous goal of matching vehicle weight was chose, which would require only one or two analyses for validation.

FEM Structural Sizing Process

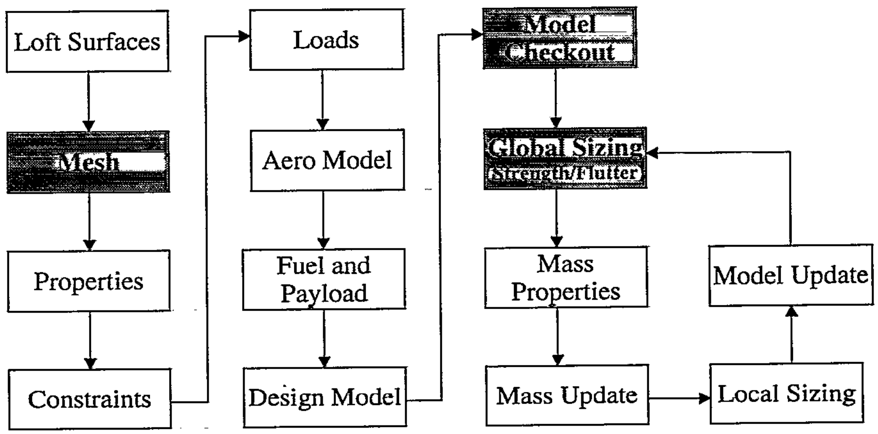

This figure is a simplified illustration of the sizing process. Those boxes which are shaded indicate the stages which are addressed by an equivalent plate representation of the wing. Note that these steps are not necessarily performed serially, nor do they all require the same level of time to complete. The three boxes, "Mesh", "Model Checkout" and "Global Sizing" are the most time consuming steps, which was why the EPT approach was selected to address the issue of span time.

HSR TCA Configuration with Plate Wing

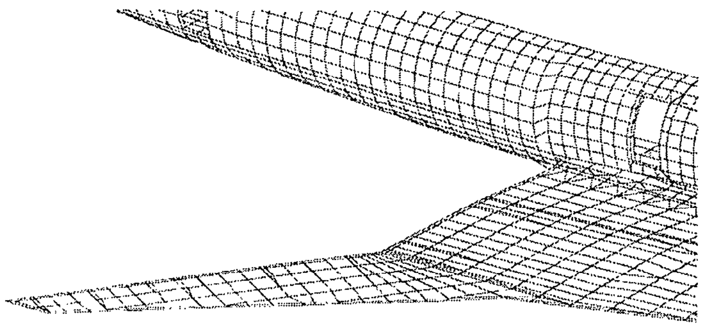

Conceptually equivalent to a beam representation of a high aspect ratio wing

Cross Section Through EPT Wing Structure

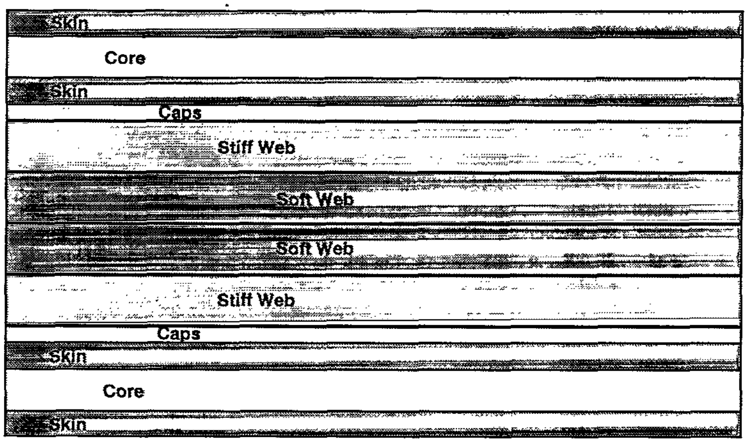

This figure schematically illustrates the representation of a wing box as layers, each layer representing a different structural component. In this case, the top three and bottom three layers represent sandwich skin panels. The four center layers represent the stiffness of spar and rib layers. By varying the ratio of thickness between the "soft" layers and the "stiff" layers, the stiffness impact of changing the web thicknesses can be simulated.

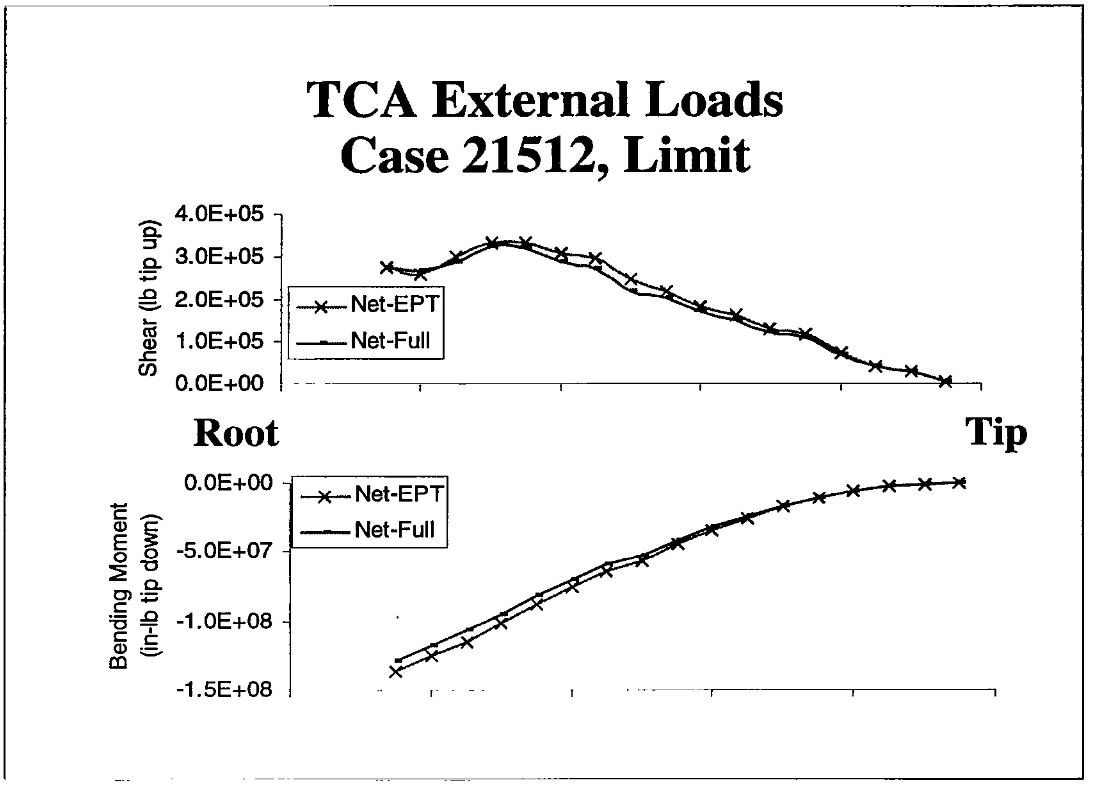

This figure illustrates the correlation of external loads for a representative mass and load case between a full FEM representation of the HSR TCA configuration and a simplified EPT representation.

Z-Deflections
Case 21512, Limit

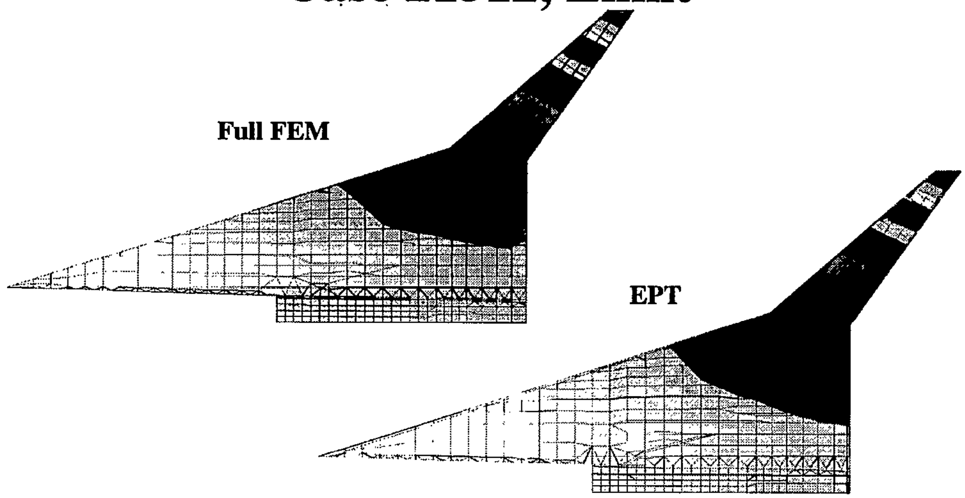

This figure illustrates the correlation of vertical displacements for a representative mass and load case between a full FEM representation of the HSR TCA configuration and a simplified EPT representation.

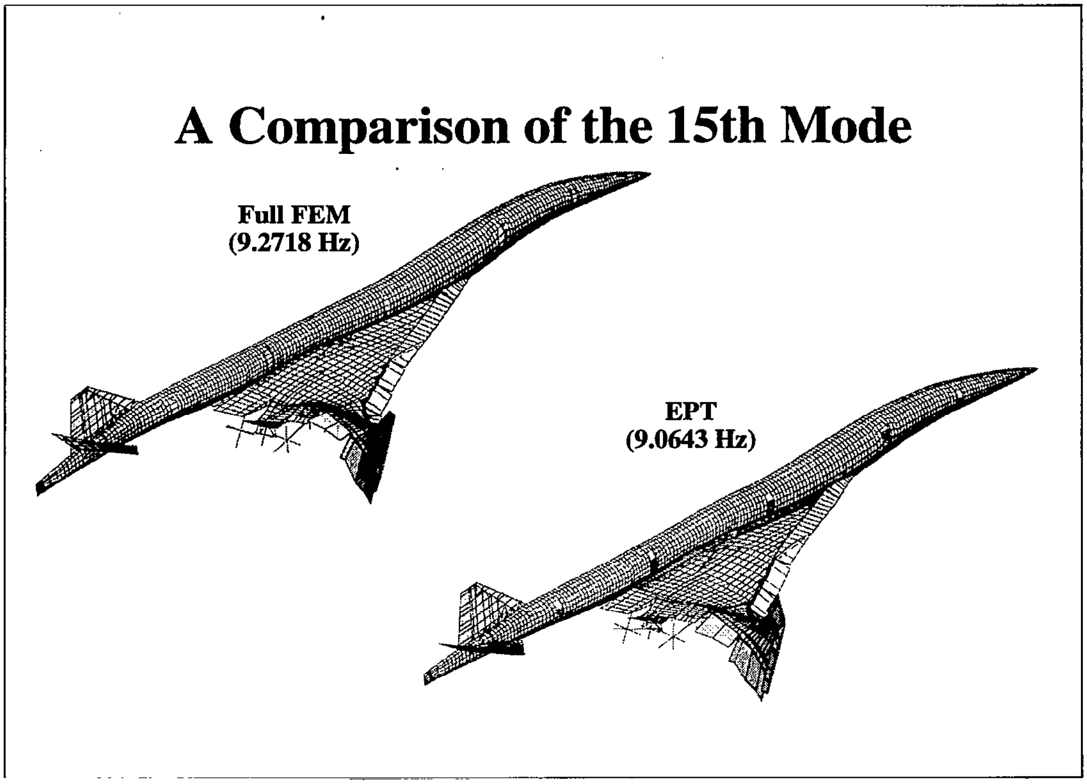

This figure illustrates the correlation of a higher order mode for a representative mass case between a full FEM representation of the HSR TCA configuration and a simplified EPT representation.

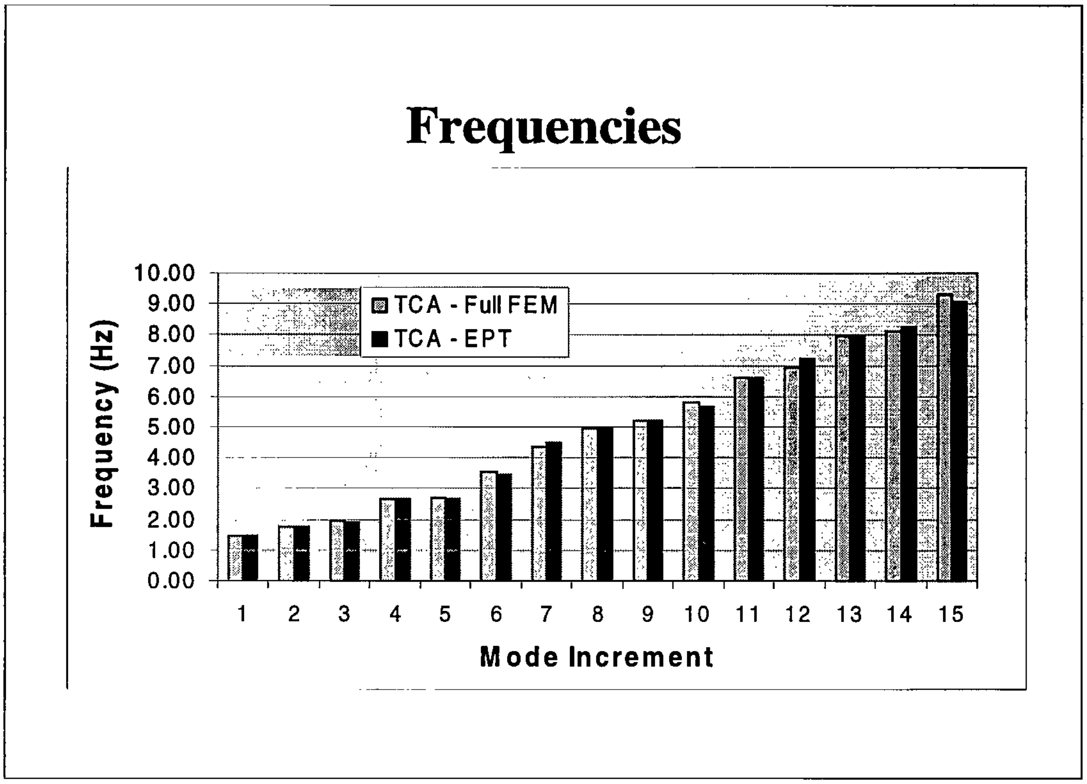

This figure illustrates the correlation of the first fifteen frequencies for a representative mass case between a full FEM representation of the HSR TCA configuration and a simplified EPT representation.

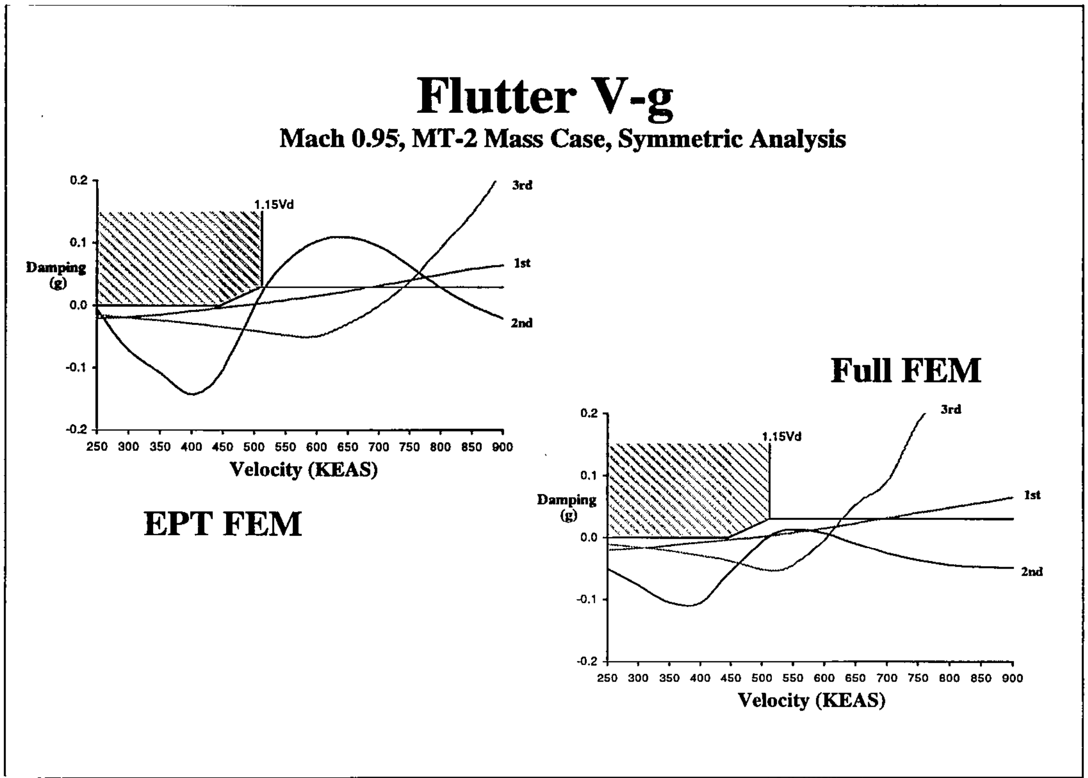

This figure illustrates the correlation of flutter for a representative mass case between a full FEM representation of the HSR TCA configuration and a simplified EPT representation. The shaded region indicates the critical area of the envelope for flutter. The first two modes are virtually identical. The shape of the third mode is identical in both cases, although the amplitude is larger for the EPT representation. Differences between the two results are in part due to slightly different optimized designs.

Inboard Wing Skin Critical Running Loads

Mach 1.2, Alt. 36350 ft, 2.5g pull-up, MF-1 Mass Condition (Subcase 21512, Limit)

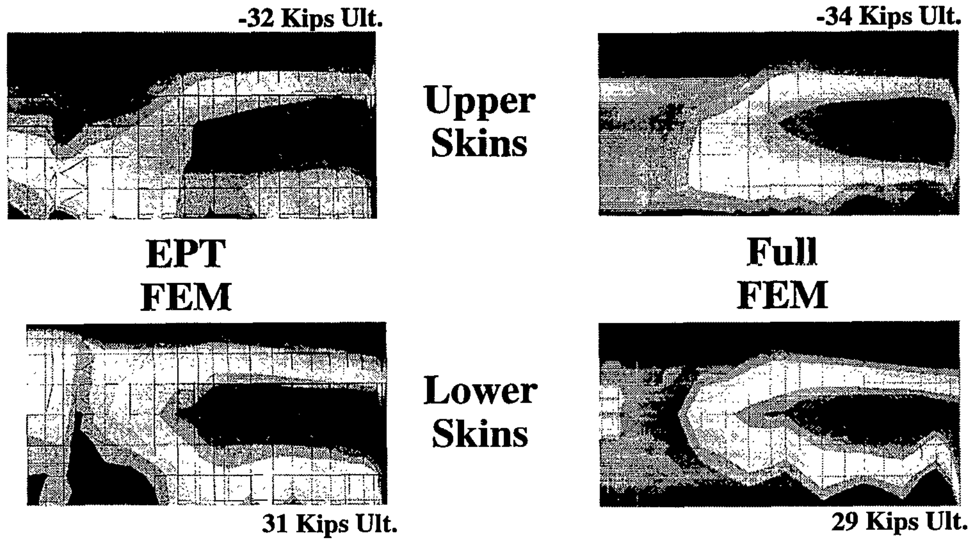

This figure illustrates the correlation of spanwise internal loads for a representative mass and load case between a full FEM representation of the HSR TCA configuration and a simplified EPT representation. The area illustrated is the main wing box area inboard of the wing break and aft of the landing gear well. For the upper skin, cool colors indicate greater magnitude; for the lower skin, warm colors indicate greater magnitude.

In the case of the EPT representation, the caps of the substructure are inset from the loft surface by a distance equal to the depth of the skin panels. As a result, the skin panels carry more of the wing bending load in the EPT representation than in the full representation, where both the caps and skin panels are modeled at the loft surface.

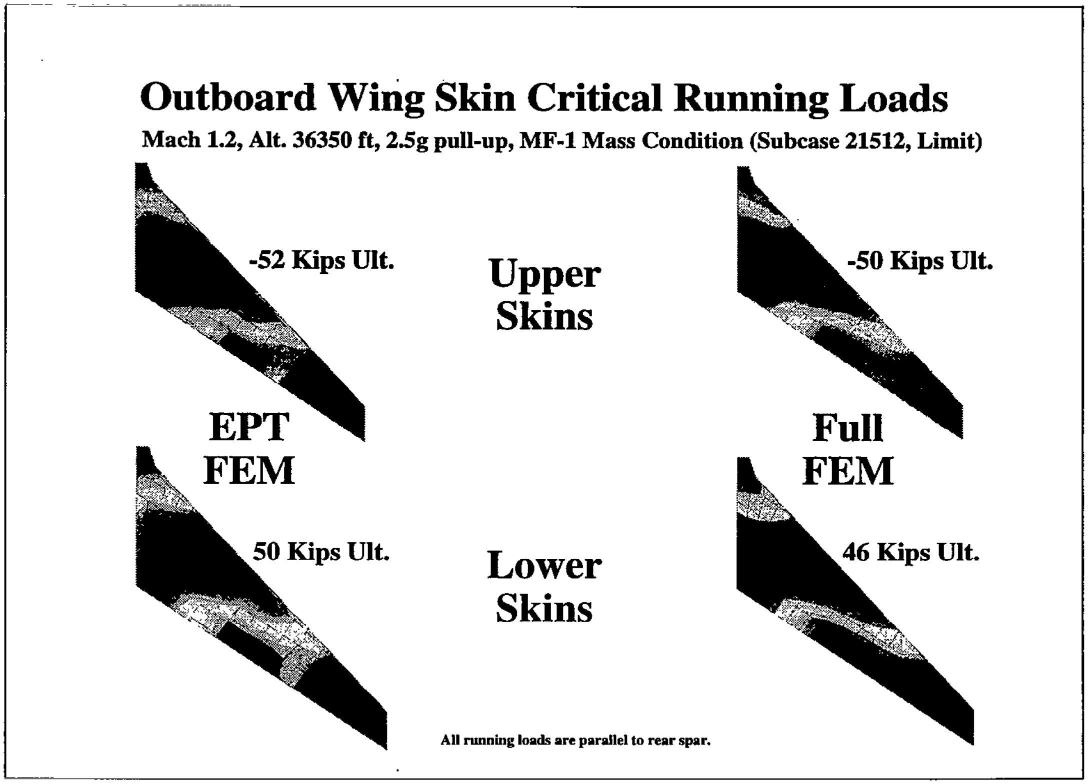

This figure illustrates the correlation of spanwise internal loads for a representative mass and load case between a full FEM representation of the HSR TCA configuration and a simplified EPT representation. The area illustrated is the wing box outboard of the wing break. For the upper skin, cool colors indicate greater magnitude; for the lower skin, warm colors indicate greater magnitude.

In the case of the EPT representation, the caps of the substructure are inset from the loft surface by a distance equal to the depth of the skin panels. As a result, the skin panels carry more of the wing bending load in the EPT representation than in the full representation, where both the caps and skin panels are modeled at the loft surface.

Strake Skin Critical Running Loads

Mach 1.2, Alt. 36350 ft, 2.5g pull-up, MF-1 Mass Condition (Subcase 21512, Limit)

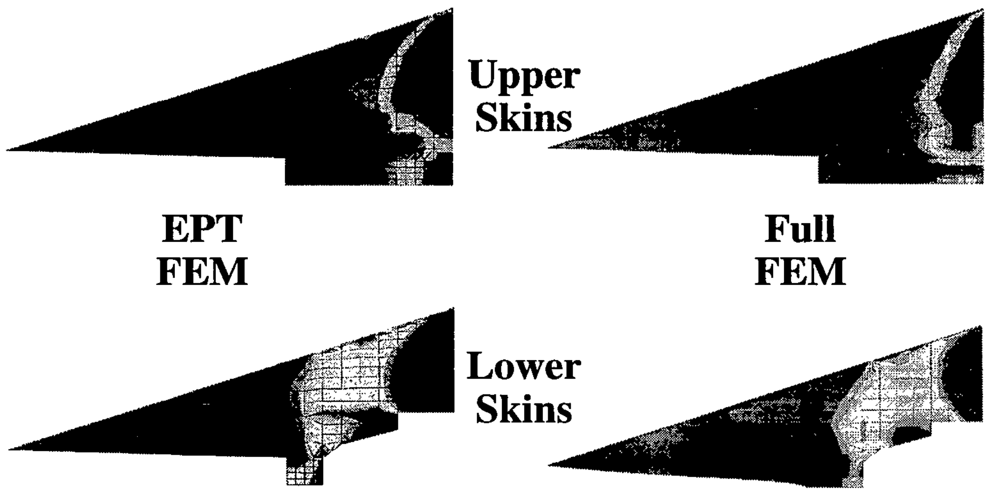

All running loads are spanwise.

This figure illustrates the correlation of spanwise internal loads for a representative mass and load case between a full FEM representation of the HSR TCA configuration and a simplified EPT representation. The area illustrated is the wing strake. For the upper skin, cool colors indicate greater magnitude; for the lower skin, warm colors indicate greater magnitude.

In the case of the EPT representation, the caps of the substructure are inset from the loft surface by a distance equal to the depth of the skin panels. As a result, the skin panels carry more of the wing bending load in the EPT representation than in the full representation, where both the caps and skin panels are modeled at the loft surface.

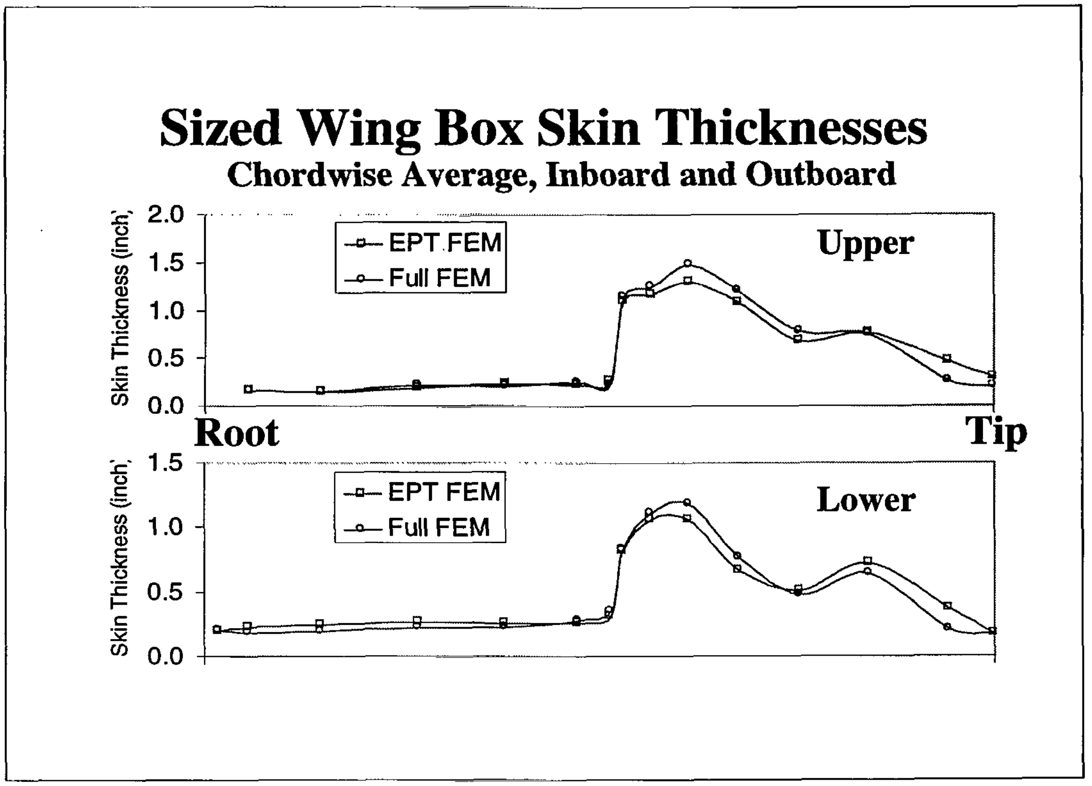

This figure illustrates average thickness for the upper and lower skins from the centerline to the wing tip along the main wing box. This is for models which have been sized for both strength and flutter requirements.

Sized Aircraft Weights

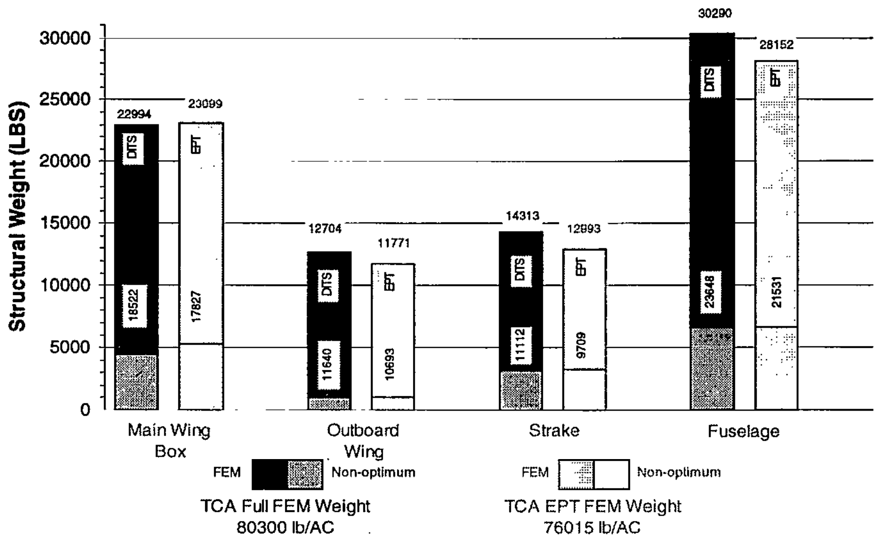

This figure illustrates the correlation in weight between the full model and the simplified EPT model. The solid regions are algorithmic weight to account for non-modeled features, such as joints and cut outs. The shaded regions are actual FEM weights. The EPT model is 95% of the weight of the full model, for sizing for both strength and flutter requirements.

D.4.2 PTC and Variants

Differences Between PTC and TCA EPT Models

- A coarser fuselage mesh with a revised keel
- Revised outboard wing mesh
- Horizontal stabilizer and canard modeled with a concentrated mass
- Outboard movable leading/trailing edges modeled with simple bars
- Reduced and redefined fuselage design variables
- Reduced and redefined wing design variables
- No flutter sizing for PTC

PTC EPT Model

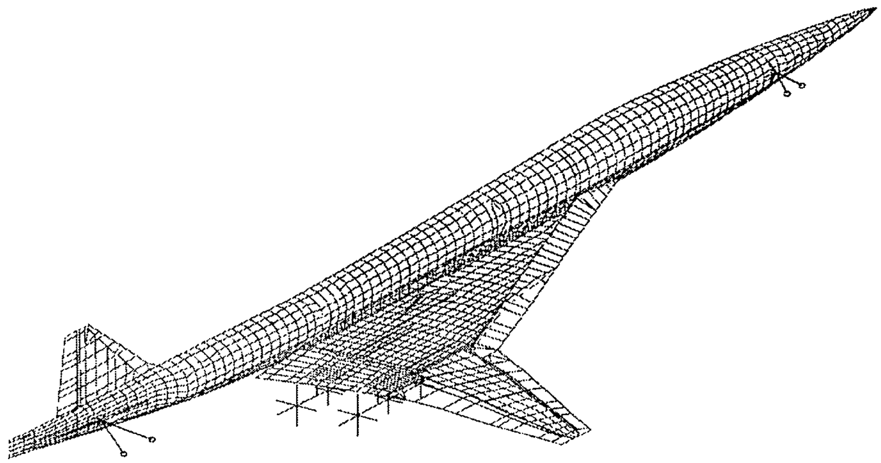

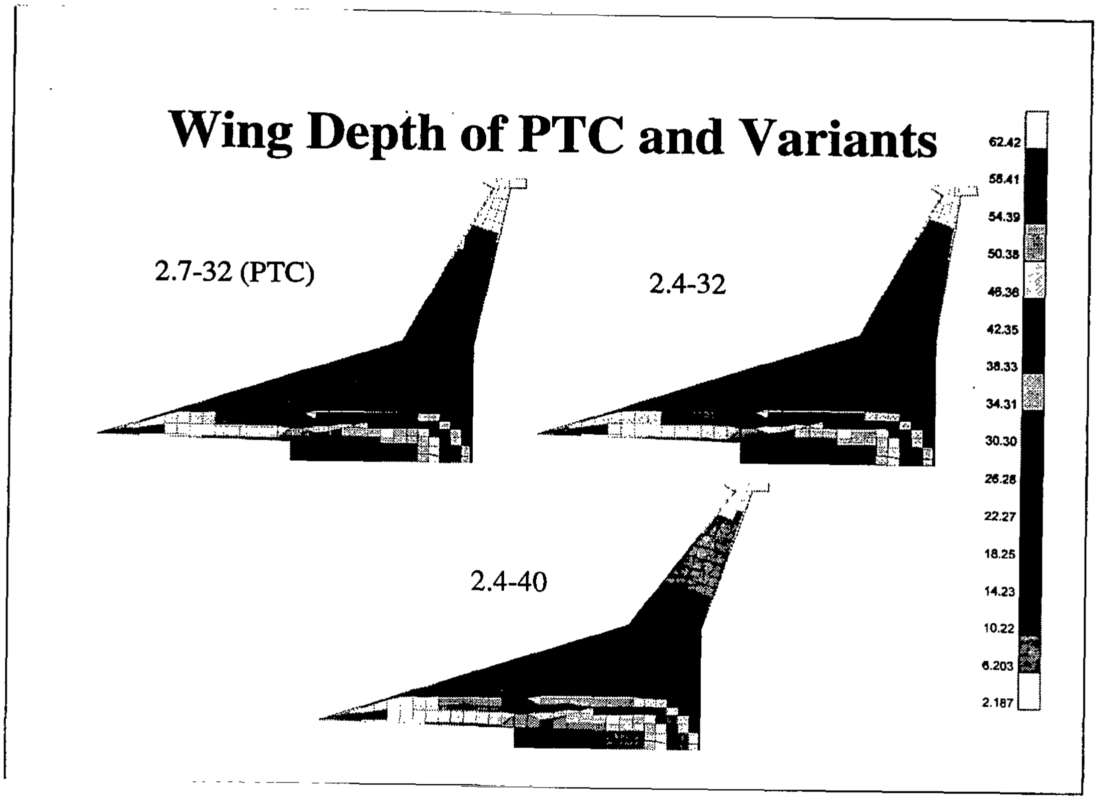
Wing Depth of PTC and Variants
2.7-32 (PTC)
2.4-32
2.4-40
62.42
58.41
54.39
50.38
46.36
42.35
38.33
34.31
30.30
26.28
22.27
18.25
14.23
10.22
6.203
2.187

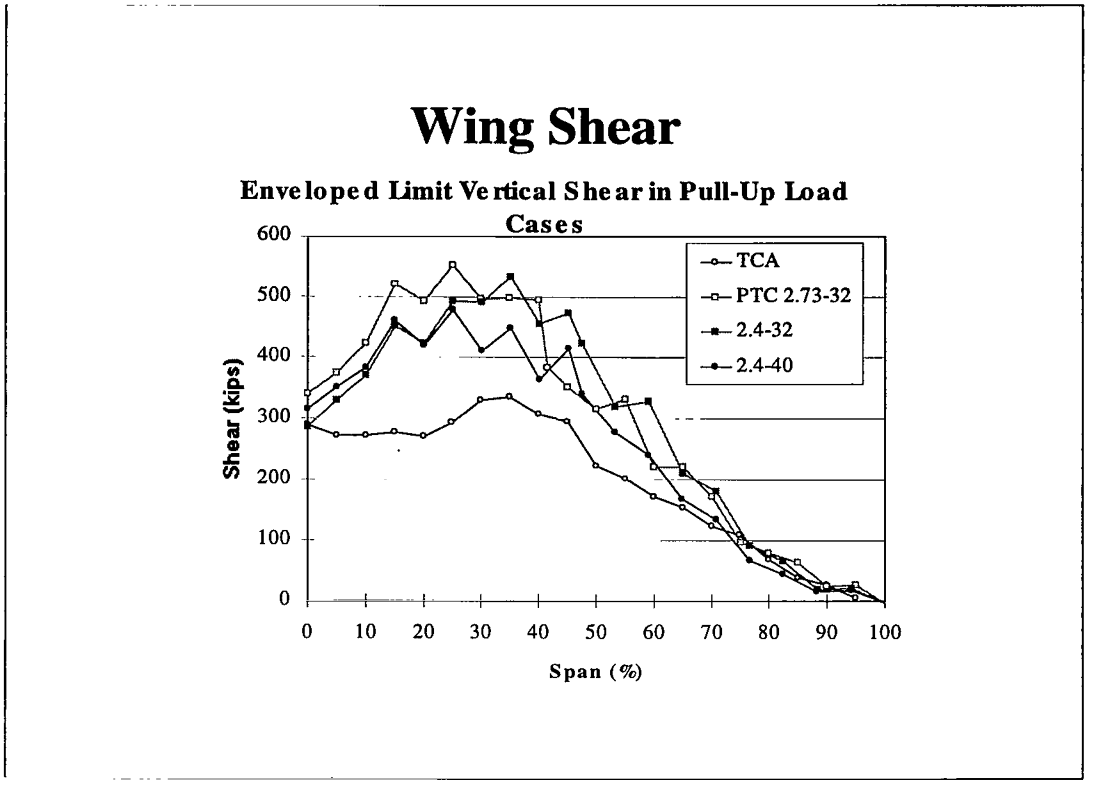

This figure illustrates the shear envelope for pull-up maneuvers for the TCA, PTC, and 2.4-32 and 2.4-40 variants to the PTC.

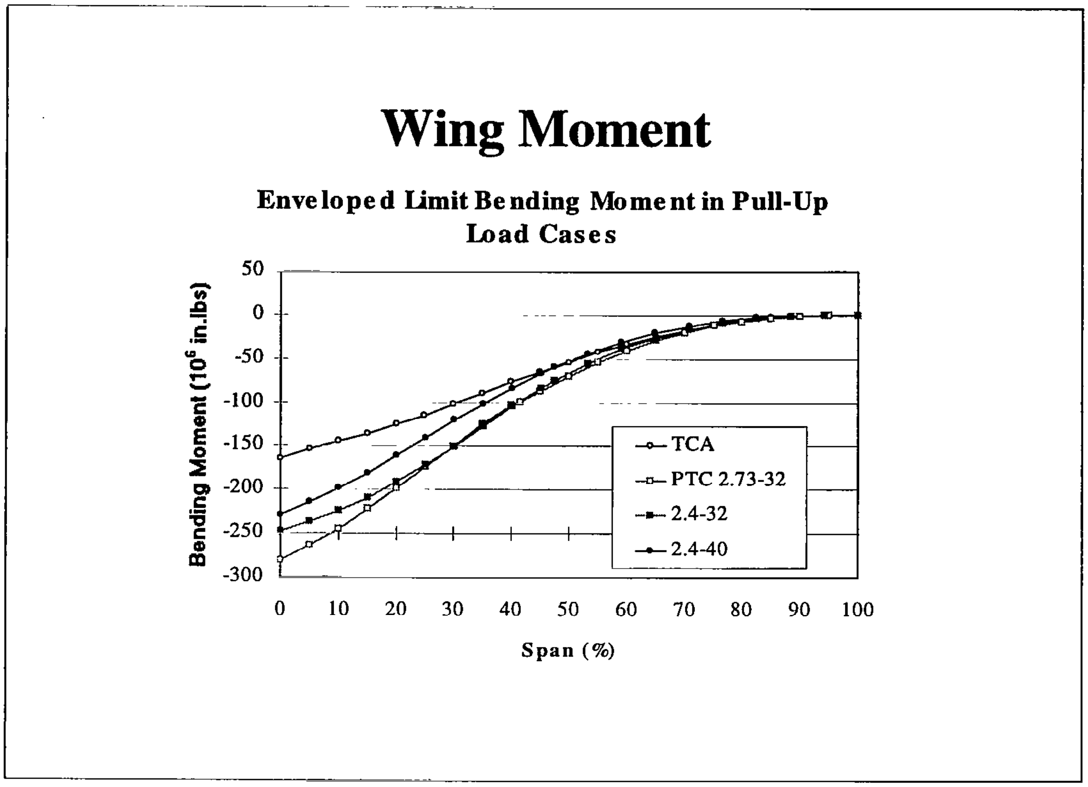

This figure illustrates the shear envelope for pull-up maneuvers for the TCA, PTC, and 2.4-32 and 2.4-40 variants to the PTC. Moments of the PTC are higher due to its larger span.

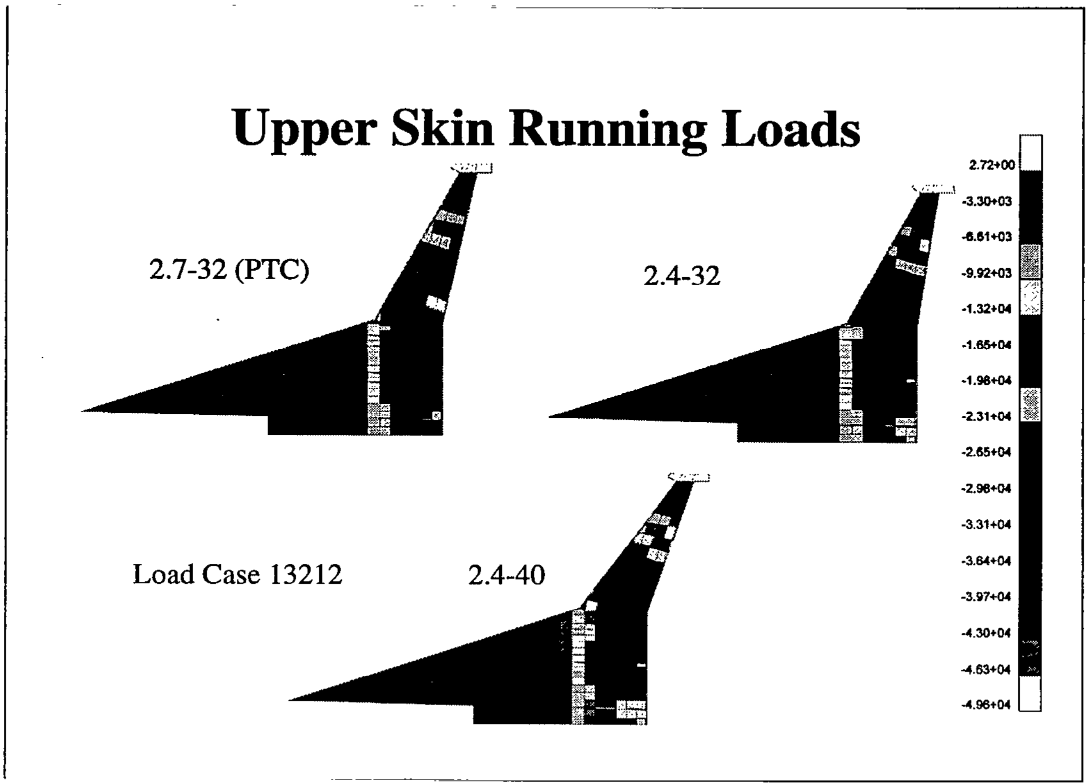

This figure illustrates internal loads in the upper skin in the spanwise direction for the critical pull-up load case.

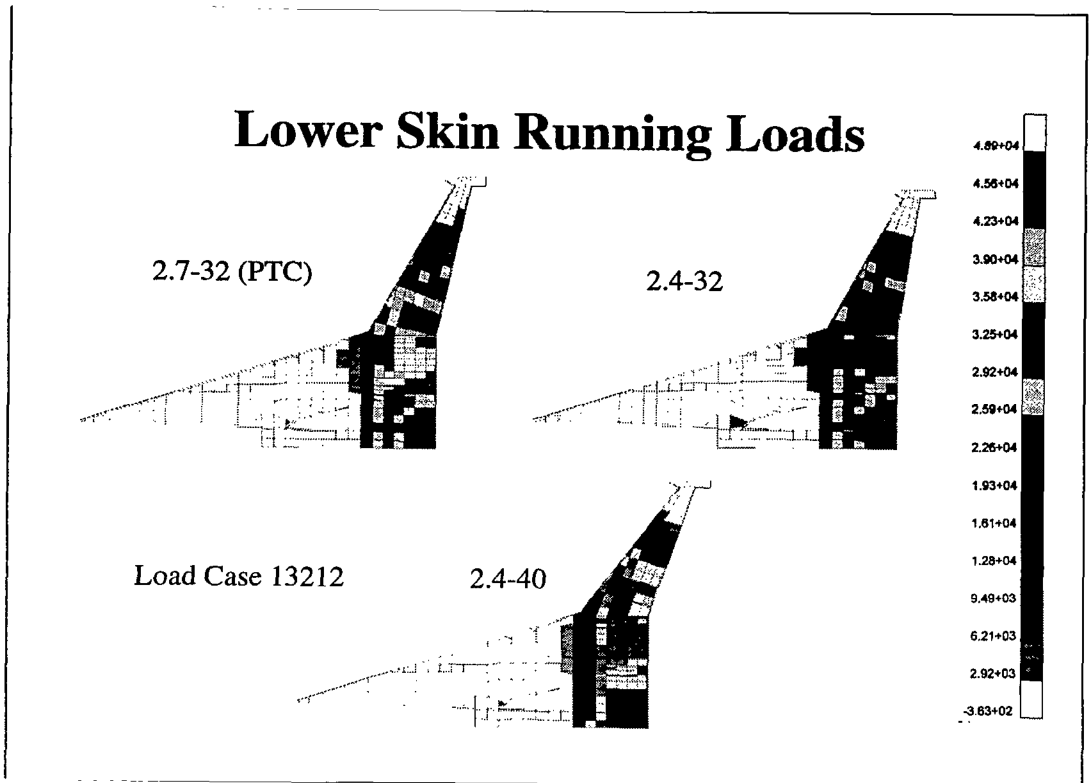

This figure illustrates internal loads in the lower skin in the spanwise direction for the critical pull-up load case.

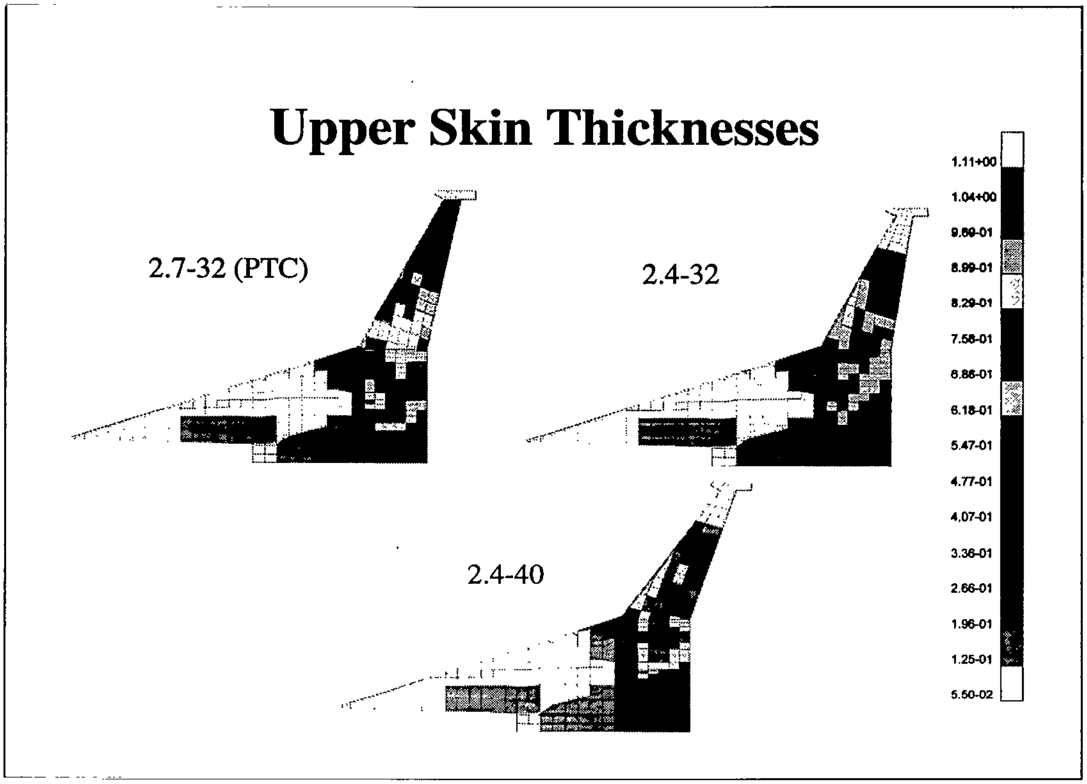

This figure illustrates the thicknesses of the sized upper skin.

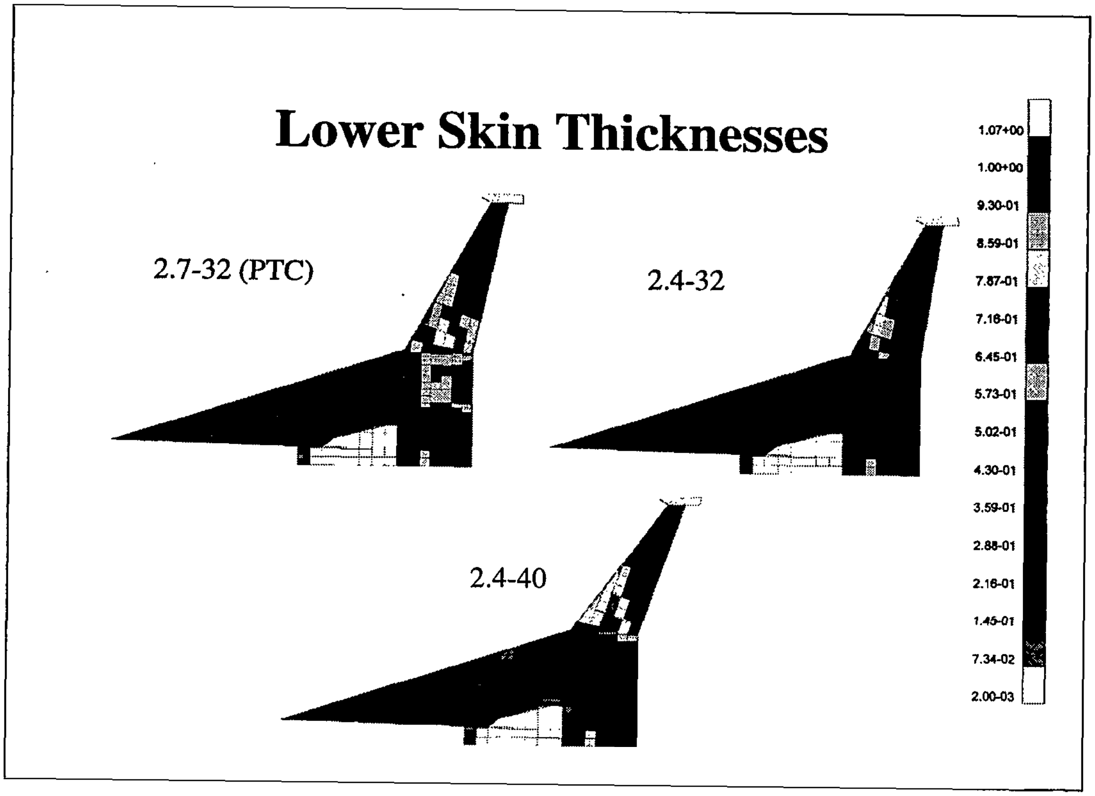

This figure illustrates the thicknesses of the sized lower skin.

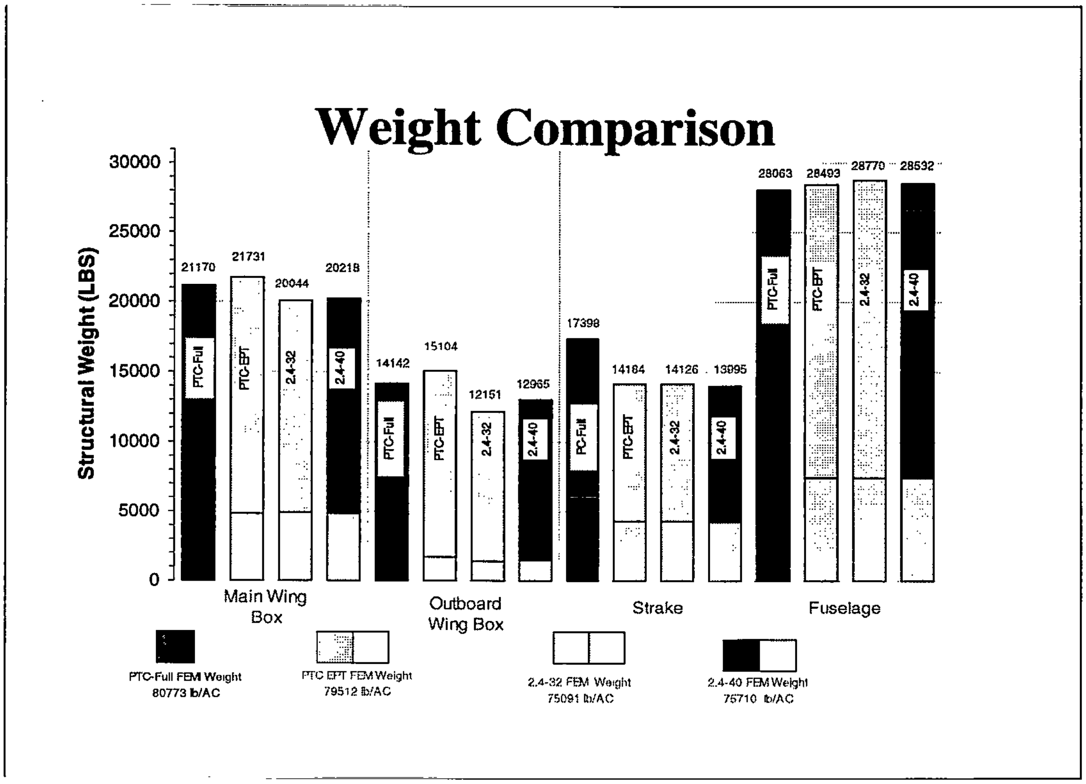

This figure compares the weights of the full PTC model, the EPT PTC model, and the two variants. The 2.4-32 is 94.4% of the weight of the baseline PTC, and the 2.4-40 is 95.2% of the baseline.

Span Time

- The three vehicles (PTC and two variants) were created by modifying and existing model, but with a new design model.
- Total time for the PTC model analysis was four months, including extensive benchmarking of the simplified leading and trailing edges, and validation of the engine, horizontal stabilizer, and canard attachments.
- Generation and sizing of the two variants was accomplished in approximately one month.
- Additional span time reductions could be accomplished with further simplification.

Representative Accuracy as a Function of Span Time

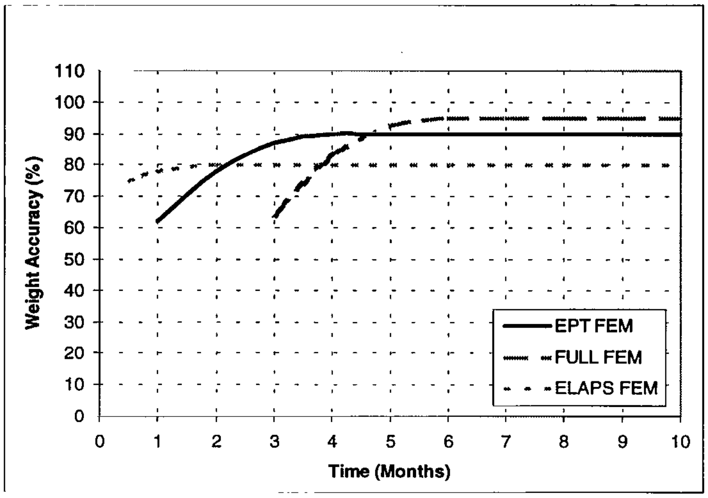

This chart is representative of the trade-off of time versus accuracy when performing structural sizing for three different finite element modeling schemes. The numbers are estimates only for illustrative purposes. All three schemes can estimate vehicle weight using simplifying assumptions, but only at the expense of time. Greater accuracy requires more elaborate estimates of as-built weights, a greater level of detail in aerodynamic, structural and design models, an extensive loads survey, etc.

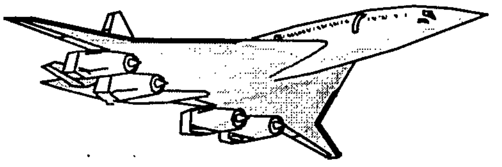

ACE Final Report

D.5 - ELAPS Process and Results

Peter Coen - NASA Langley
Greg Wrenn - NYMA
Gary Giles - NASA Langley (retired)
Matt Sexstone - NASA Langley (formerly)

December 31, 1998

Contents

This report presents a summary of the work performed in the development, validation and application of the Equivalent Laminate Plate Solution (ELAPS) based weight estimation system in the HSR Technology Integration Optimized Aeroelastic Concept (OAC) subtask The report is divided in the sections shown in the chart above. This report is an update to the earlier documentation of the Preliminary Aeroelastic Concept (PAC) subtask. Details and background information contained in the earlier report may not be repeat here. The PAC report can be found on the HSR ADAPT Document Server, in the Technology Integration Notebook, section 8.2.3.7.

ELAPS Structural Weight Estimation System Approach

Purpose

- Develop a structural analysis and sizing system that uses the improved ELAPS method as its core

Desired Capabilities

- Extremely rapid execution time
  - Complete converged structural design in one-two weeks
- Flexible modeling
  - Rapid generation of all required analysis model
  - Ability to change models quickly
    - Focus on perturbations from existing TCA
- Capture the appropriate structural phenomena
  - Aeroelastic loads
  - Flutter
  - Local sizing
- Validated results based on comparison to existing HSR TCA FEM data

Section D.4.1

The ACE weights and structures subteam was tasked with developing a structural sizing tool that could offer substantial reduction in the time required to determine the weight of a sized structure. This time savings is vital to the ACE global sensitivity analysis. It was recognized by the team that the Equivalent Laminated Plate Solution (ELAPS) code had the potential to greatly reduce the modeling and structural analysis time requirements. What was lacking was an infrastructure to integrate ELAPS into a complete structural sizing process. The original desire was to have the industry team incorporate ELAPS into their existing analysis systems. Because of budget and workforce constraints, it was not possible to do this. Therefore, the approach adopted was to have the NASA team work on both enhancing the ELAPS program and developing a structural sizing framework based on tools available at Langley and knowledge gained during the HiSAIR Pathfinder Study and the HSR LCAP. The desired capabilities of the system are indicated on this chart.

ELAPS Program Enhancements

- Fuselage Floor Plate
- Enhanced Spring Elements
- Miscellaneous Improvements

Since the publication of the PAC report, there have been a number of improvements made to the ELAPS computer program.

The first of these improvements is the implementation of a special plate element for modeling fuselage floors. This new segment provides a simplified alternative for modeling floors, by eliminating the degrees of freedom and connector springs associated with the general plates segments. The displacements of the floor are assumed to be constant in the direction perpendicular to the centerline of the fuselage. The floor is assumed to have longitudinal stretching and transverse bending connections to the fuselage shell elements only. The floor is not connected to the fuselage in the V direction.

A new option for defining the springs that are used to connect plates was implemented. This option allows the definition of springs that are parallel or perpendicular to the edges of a plate. This provides for better modeling of control surface attachments.

These options are implemented in the ELAPS version 98.10.1. They were not available at the time that the ACE sizing studies were conducted.

ACE / ELAPS Weights Estimation System Description

System Requirements:

- Fast execution
- Simplified model description
- Include static aeroelastic loads and flutter analysis
- Strength and flutter design constraints
- Unix based and portable

System Solution:

- Geometry based on WAVEDRAG geometry format
- Equivalent plate structural analysis
- Linear steady potential flow aerodynamics
- Linear unsteady doublet-lattice aerodynamics
- British-K flutter analysis
- Unix scripts to couple all codes
- Simple, portable database to control data flow

ACE / ELAPS Weights Estimation Process System Description

In response to the needs of the HSR ACE task, a system of computer programs has been developed to determine the optimum structural weight of an aerospace vehicle. The system is designed to be portable to any UNIX system, utilizing only public domain codes linked together with UNIX script files for execution control and a simple database called GRIM for data flow control. Primary requirements of the system are fast execution, simple analysis model definition and sizing for both strength and flutter constraints. The analysis models are defined in nondimensionalized form based on the WAVEDRAG geometry format. Analysis models may be perturbed for parametric studies by changing data within the WAVEDRAG data file. The ELAPS computer program is used for structural analysis for its fast execution speed and simpler model definition as compared to a finite element model. Static aeroelastic loads are computed for any number of load cases using a steady linear potential flow aerodynamics code. Unsteady linear doublet-lattice aerodynamics are coupled with a British-K flutter solution for flutter constraints. Stress and strain failure constraints and local orthotropic buckling constraints are computed from ELAPS analysis results. The optimization is performed using KSOPT, with a linearized approximate analysis. All components of the system have been written except for the interface to the optimizer. Initial testing has been performed on all completed codes to verify data flow.

ELAPS Weights Estimation Process - Optimization Cycle

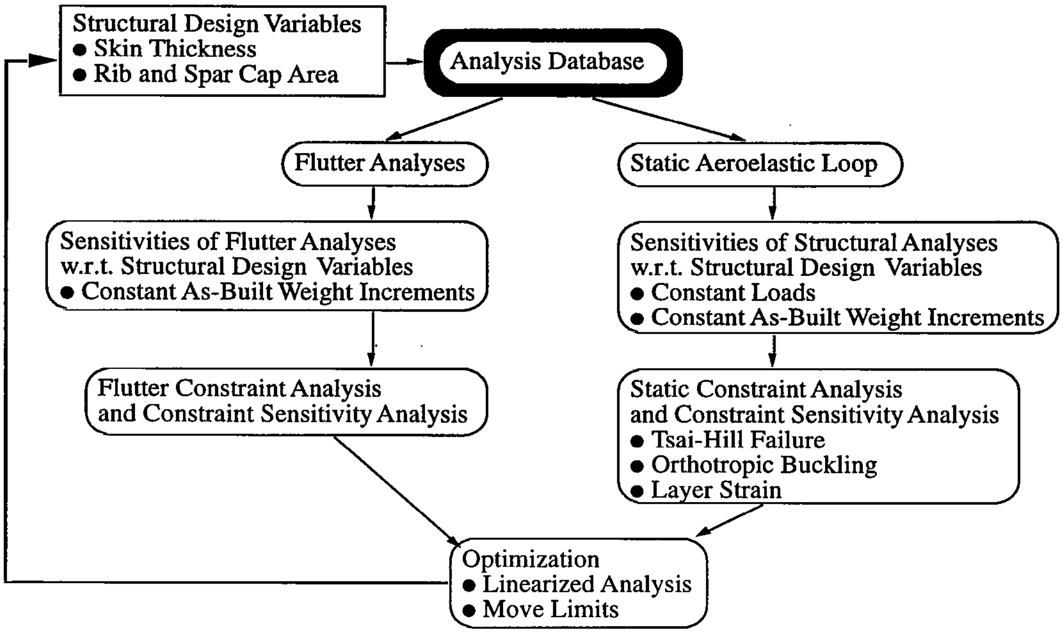

The weights estimation process combines static aeroelastic analysis and flutter analysis with a gradient based optimizer to compute the minimum weight of an aerospace vehicle. Each analysis can be performed in parallel, and each one computes constraints and their analytical sensitivity derivatives with respect to a set of structural design variables. These constraints and derivatives, and the structural weight and its derivatives are used to form an approximate linear analysis. This linearized analysis is used by the optimizer to minimize the structural weight subject to the supplied constraints. The updated design variables are then used to start the next optimization cycle. The optimization cycle terminates when convergence is achieved for the structural weight.

ELAPS Weights Estimation Process - Initialization Procedure Database Generation

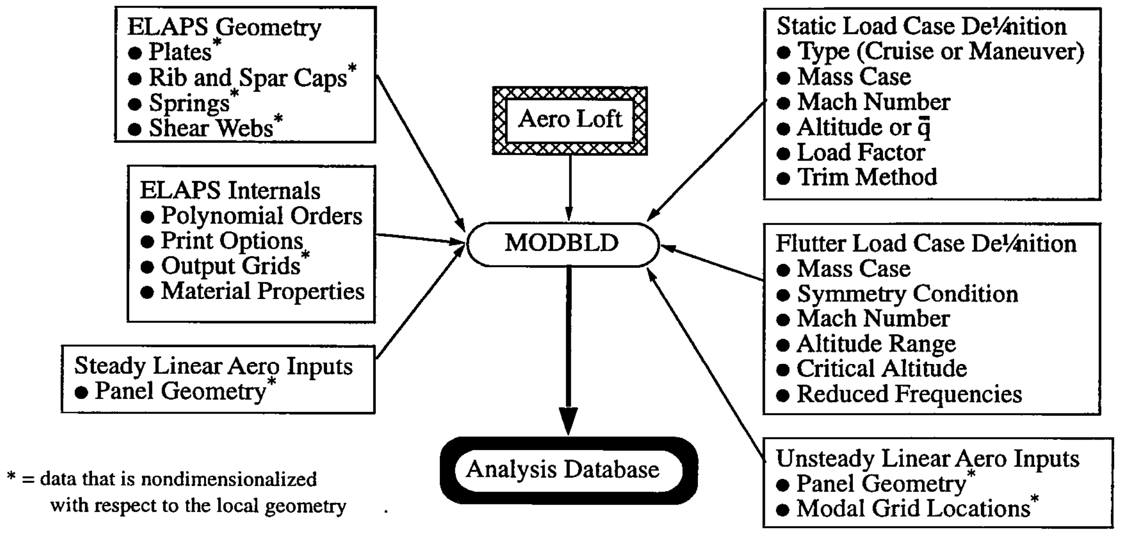

One of the key features of the ELAPS system is the use of a non-dimensionalized data description, coupled with the GRIM database. This feature allows not only rapid data access by all of the ELAPS system program elements, but provides a method of very rapidly performing parametric variation of the defined model. All model definition data is processed by program MODBLD and stored into an analysis database. The structural model and the aerodynamic models are defined in non-dimensional coordinates based on the geometry definition supplied in Harris Wavedrag format. They are converted to dimensional coordinates before being stored in the database.

The ability to perform parametric variation was utilized very effectively in the generation of the PTC model and the 5 variations run for the ACE design study.

ELAPS Based Structural Optimization Cycle Time

Set Up

- Build Models — *7 sec.**
  - Assume Wavedrag type geometry supplied
- Initiate Steady Aerodynamics — *1 min**
  - Generate AIC's, load database
- Initiate Unsteady Aerodynamics — *10 min.***

Optimization Cycle

- As built Weights — *0 min.*
  - Used using fixed data

Parallel Processes

- Static Aeroelastic Loop — *9 min.**
- Static Derivatives — *50 min.**
  and
  Static Constraints
  - 64 bit calculation
- Dynamic Derivatives — *40 min **
  - 64 bit calculation
- Flutter Analysis — *10 min per flutter case*
  - Includes flutter derivatives
  - Includes flutter constraints

Optimization — *2 min*

Problem Size

- 16 Load cases *
- 7 Steady Aero Machs *
- 5 Unsteady Aero Machs *
- 22 Flutter cases *
- 56 plates *
- 400 Design variables
- SGI Origin Computer

Sizing Cycle Time
< 3 hours !!

* Updated information based on problem definition or actual timings
** Timing per flutter Mach no. - Data generated once for specified planform geometry

High-Speed Research
Technology Integration

Langley Research Center

This chart provides a summary of the modeling and analysis times for the ELAPS based structural sizing system based on work completed to date. The modeling, static aeroelastic and flutter analysis sections have been completed and tested. Validation is in progress. Both static and dynamic analysis includes analytical sensitivity derivative calculation. Based on actual code timings obtained to date, and assuming a problem of the size described in the figure, the goal of one to two week turn around for a converged structural solution is expected to be met.

The codes required to generate the constraint data are currently being written. The only coding remaining beyond that is linking in the optimizer. It is expected that the validation phase, both for the initial model and the structural sizing will take one to two more months and will require some modifications to both the model and the system. It is anticipated that the ELAPS system will be available to support the ACE OAC process early in calendar year 1998.

TCA Model Validation

- Comparison of ELAPS model with initial thickness ELFINI and NASTRAN Results
- Validation efforts not complete
  - Insufficient personnel
  - Inefficient communication
  - Modeling difficulties
- Results to date are promising
  - Deflection under uniform load agrees well
  - Torsion agreement not as good
    - Modeling questions exist
  - Vibration results mixed
    - NASA comparison shows spurious control surface modes
    - Boeing analysis of ASE ASM model much better

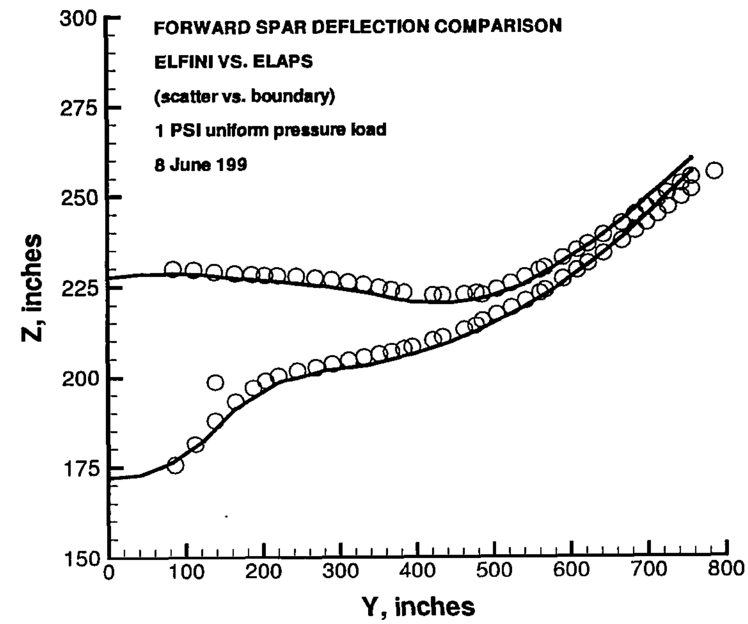
FORWARD SPAR DEFLECTION COMPARISON
ELFINI VS. ELAPS
(scatter vs. boundary)
1 PSI uniform pressure load
8 June 199
Z, inches
Y, inches
300
275
250
225
200
175
150
0
100
200
300
400
500
600
700
800

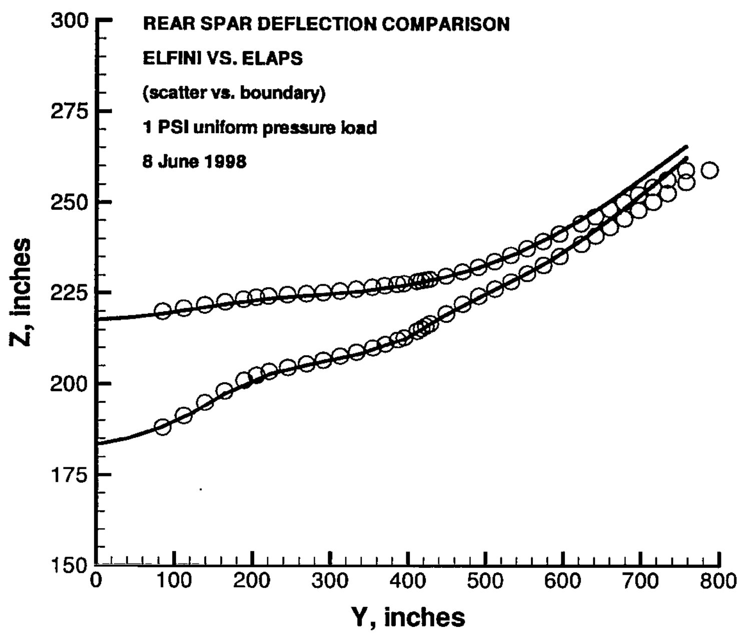
REAR SPAR DEFLECTION COMPARISON
ELFINI VS. ELAPS
(scatter vs. boundary)
1 PSI uniform pressure load
8 June 1998
Z, inches
Y, inches
300
275
250
225
200
175
150
0
100
200
300
400
500
600
700
800

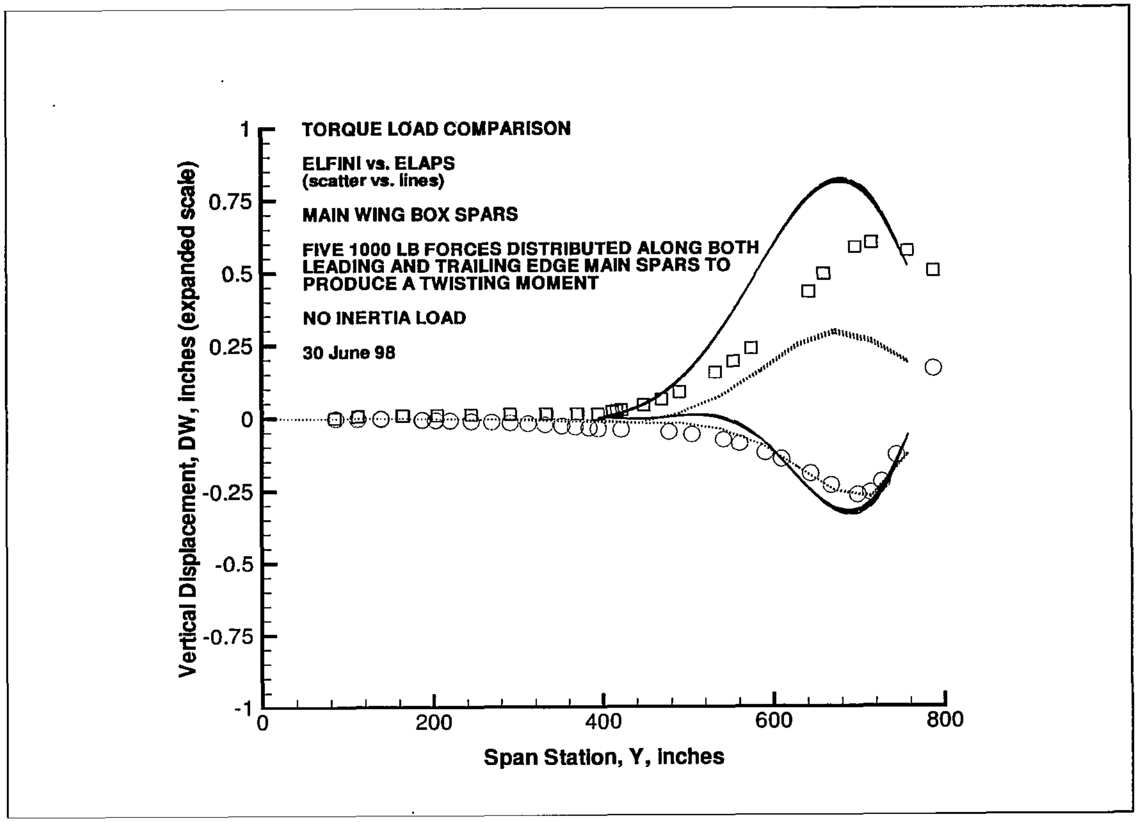
TORQUE LOAD COMPARISON
ELFINI vs. ELAPS
(scatter vs. lines)
MAIN WING BOX SPARS
FIVE 1000 LB FORCES DISTRIBUTED ALONG BOTH LEADING AND TRAILING EDGE MAIN SPARS TO PRODUCE A TWISTING MOMENT
NO INERTIA LOAD
30 June 98
Vertical Displacement, DW, Inches (expanded scale)
1
0.75
0.5
0.25
0
-0.25
-0.5
-0.75
-1
0
200
400
600
800
Span Station, Y, Inches

ASE ASM ELAPS Model Mode Shapes

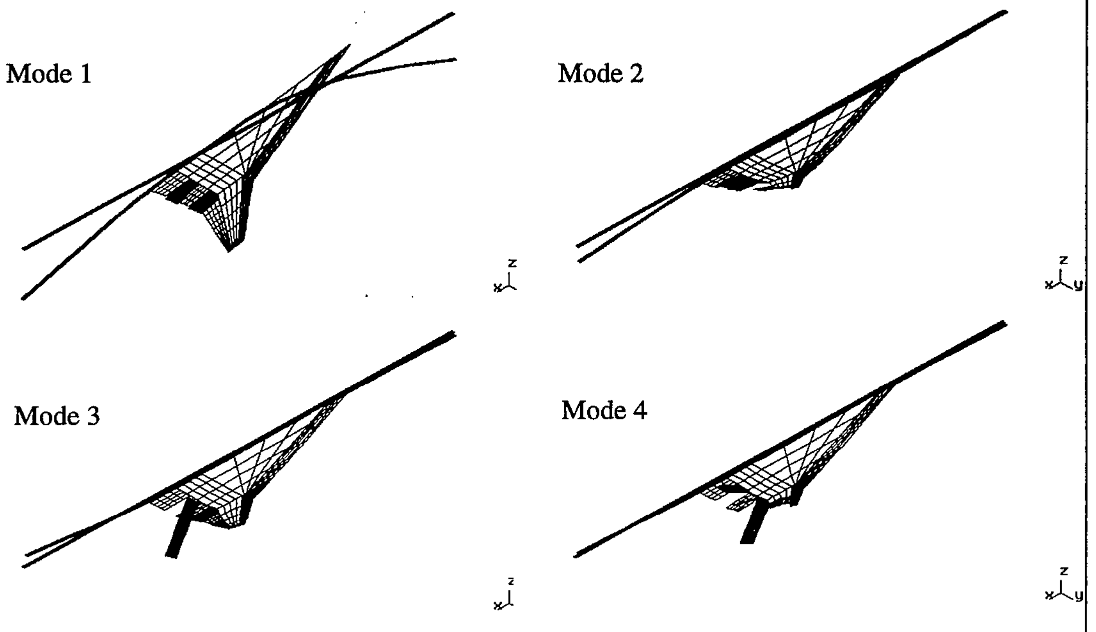

TCA Model Changes

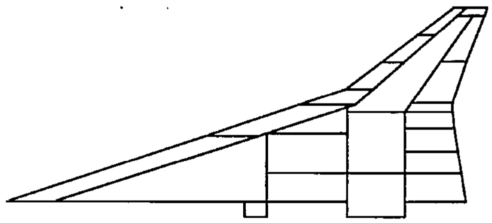

Quadratic variation of thickness on wing box plates

Original ELAPS Plate Layout

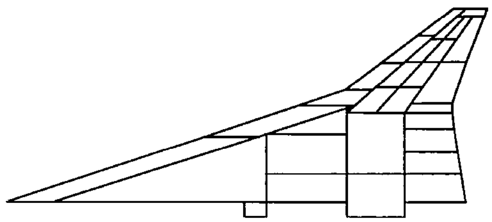

Linear variation of thickness on outboard wing box plates

Additional Segments in Outboard Wing

TCA/PTC Sizing Summary

- Strength only sizing
- Sized main box skins, spar and rib caps
- Process revealed numerous model and system weakness
  - Most fixes resulted in an improved system
- Sizing results unsatisfactory
  - Linear thickness variation unsatisfactory
  - Derivative/constraint behavior at certain locations drove design

PTC Wing Depth Variations

- Proceeded despite known difficulties with PTC sizing
- Baseline and 5 variations sized
  - Two complete sizings performed
    - main wing box skins, spar and rib caps
    - improve model, main wing box skins, smeared spar and rib caps
  - Strength only
  - 20 sizing sizing cycles
    - no convergence criteria applied, weight convergence noted
  - Average time per variation - 1.5 days
- Results Unsatisfactory
  - Wing depth changes did influence skin thickness
  - Linear design variable and derivative behavior problems invalidated results

ELAPS-ACE Structural Depth Trade Summary

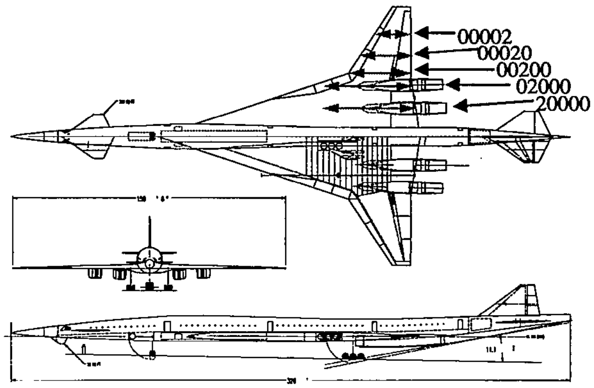

Case	Structural Wt
Base	32833
00002	32353
00020	30571
00200	30065
02000	31186
20000	32698

The Structural Weight is the ideal wt for the entire configuration, including wing, fuselage,nacelle/pylon, and tails. Only elements of the wing structure were sized during this study

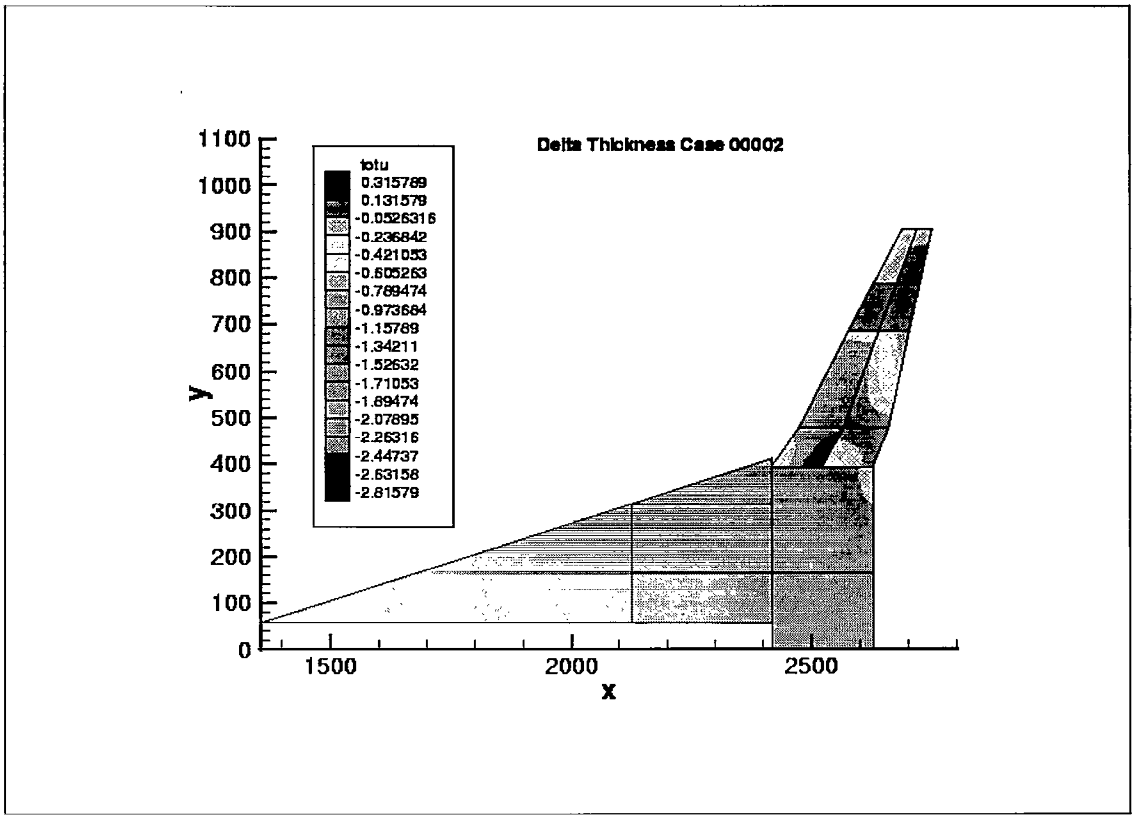
Delta Thickness Case 00002
totu
0.315789
0.131579
-0.0526316
-0.236842
-0.421053
-0.605263
-0.789474
-0.973684
-1.15789
-1.34211
-1.52632
-1.71053
-1.89474
-2.07895
-2.26316
-2.44737
-2.63158
-2.81579
y
x
0
100
200
300
400
500
600
700
800
900
1000
1100
1500
2000
2500

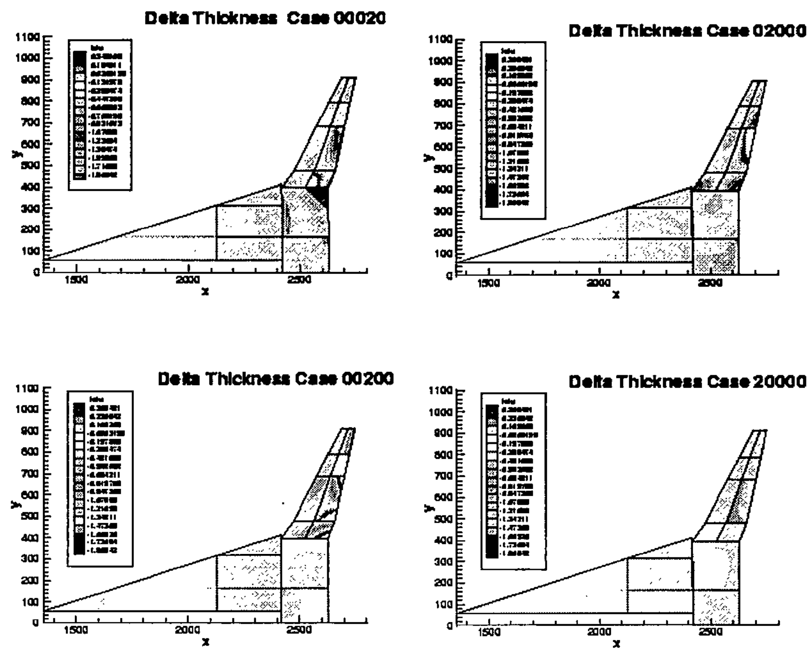
Delta Thickness Case 00020
Delta Thickness Case 02000
Delta Thickness Case 00200
Delta Thickness Case 20000
y
x

Current Activities and Plans

- ELAPS improvements implemented
  - New spring geometry flexibility
  - New plate and displacement system zone definition flexibility
- New PTC model under development
  - Better match to actual structural layout
  - Constant thickness design variable definition
  - Strength only and strength and flutter sizing to be completed
- TCA model validation with ELFINI data (NASA funded)

New PTC Model

Plate Layout

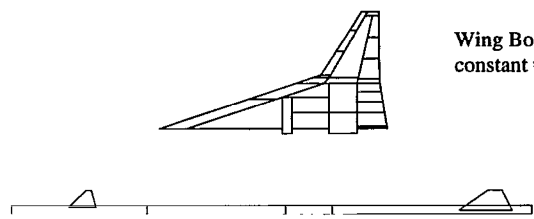

Wing Box Plates to be subdivided into constant thickness design variable zones

Aerodynamic Mesh

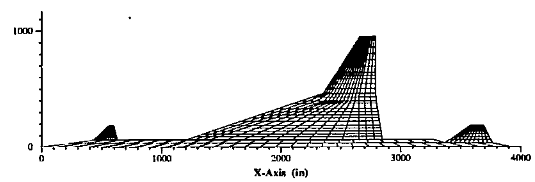

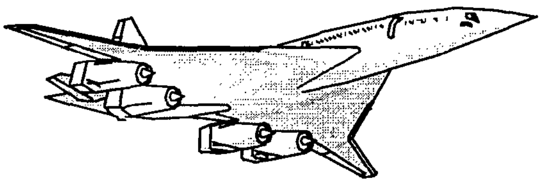

ACE Final Report

D.6 - Parametric Weights & Load Constraints

Brad Becker - Boeing Seattle
Bill Barclift - Boeing Seattle

December 31, 1998

DOSS Endload Constraint

Situation:

In the past, structural constraints due to endload limitations have not been addressed within DOSS. This has lead to configurations which are not buildable.

Target:

DOSS will have the capability to estimate endloads and will incorporate an endload limitation.

Proposal:

Develop and calibrate the algorithms to allow DOSS to estimate critical endloads for a given configuration. Provide the endload estimation routine and any additional inputs. Get buy-in from Structures.

Status:

DOSS has capability to estimate endloads. Algorithms delivered. Inputs agreed on. Structures buy-in.

Side of Body Moment Estimate

$$Moment_{ULT,SOB} = \sum Forces_{SOB} = K_{Mom} \times 3.75 \times$$
$$[(L1 \times CP) - (W1 \times CG1 + W2 \times CG2 + W3 \times CG3 + W4 \times CG4)]$$

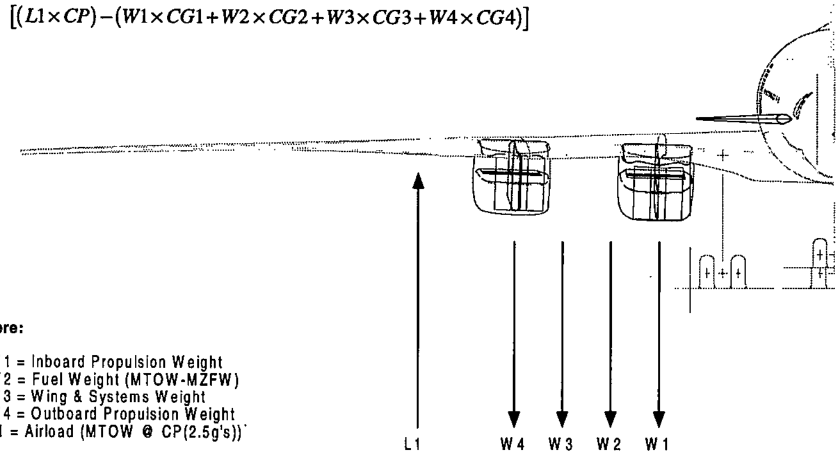

Where:

W1 = Inboard Propulsion Weight
W2 = Fuel Weight (MTOW-MZFW)
W3 = Wing & Systems Weight
W4 = Outboard Propulsion Weight
L1 = Airload (MTOW @ CP(2.5g's))

Bending Moment Distribution

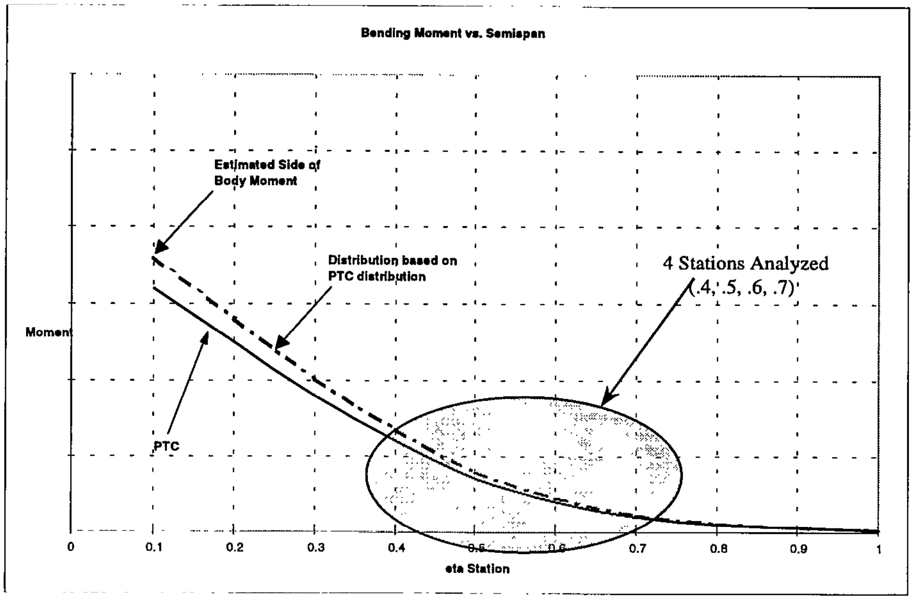

Endload Estimation

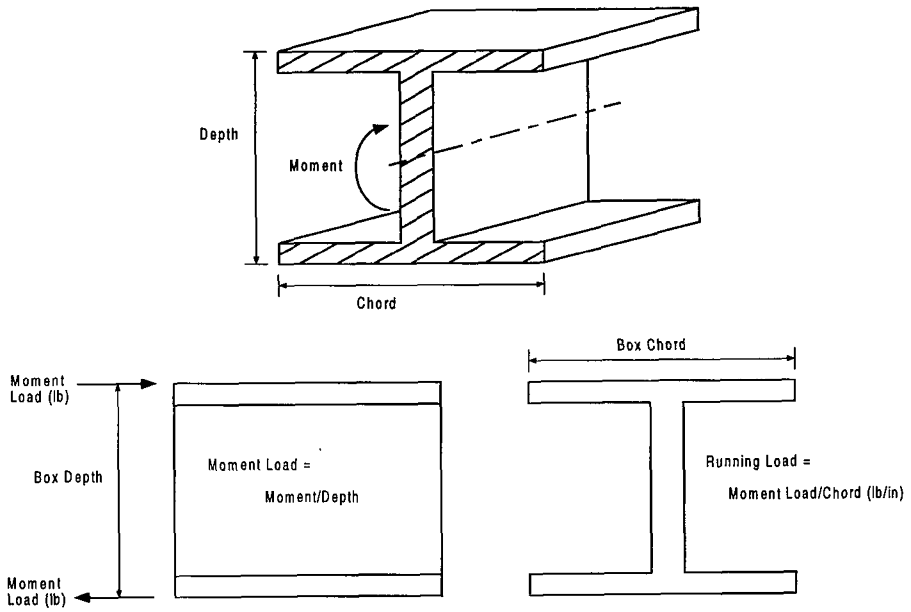

Wing Weight Parameters

Material/Structural Concept

Leading Edge Area
Leading Edge Structural Span
Tip Area

Trailing Edge Area
Trailing Edge Structural Span

Strake Area
Strake Average Thickness

Mid Box Area
Mid Box Span
Mid Box Average Thickness

Outboard Wing Box Area
Outboard Wing Box Structural Span
Outboard Wing Box Span
Outboard Wing Box Average Thickness

Inboard Wing Box Area
Inboard Wing Box Structural Span
Inboard Wing Box Span
Inboard Wing Box Average Thickness
Inboard Wing Box Chord

Effective Box Area
Front Spar Location
Leading Edge Spar Break Location

Planform Comparison

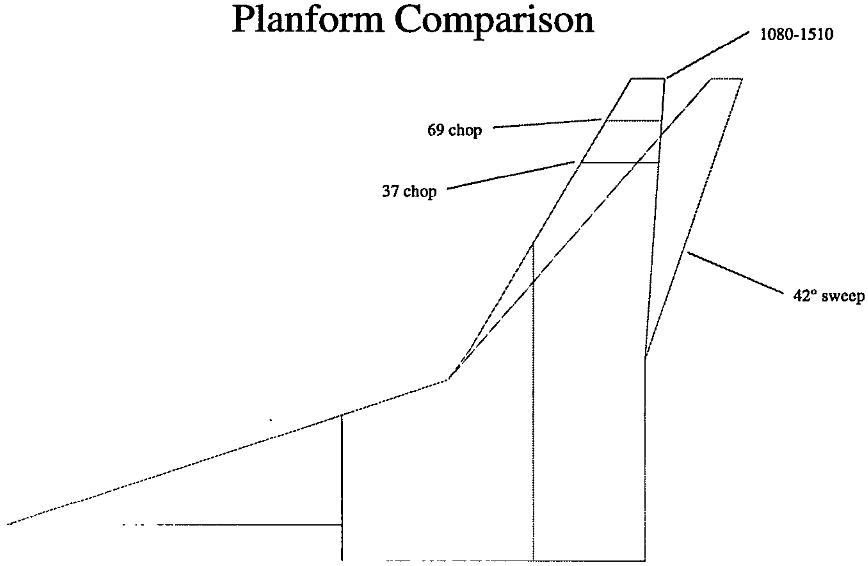

Model	Area (ft^2)	Box Area (ft^2)	Semispan (in)	Box AR	EA Semispan (in)	Box AR (EA)	Structural Tip Chord (in)
1080-1510	5415	2480	943.5	9.97	957.0	10.26	62.4
69 Chop	5316	2384	861.2	8.64	871.0	8.84	104.0
37 Chop	5169	2242	779.0	7.52	785.0	7.63	145.7
42° Sweep	5360	2524	943.5	9.80	1008.6	11.20	58.6

Wing Weight Statements

Wing Structure Weight	Strength Sized -1510 (788K) (PZSD model)		Strength Sized - 42° Sweep (SWDS model)		Strength Sized - 69 Chop (67WT model)		Strength Sized -37 Chop (37WT model)	
	Weight (lb)	Unit Weight (lb/ft^2)	Weight (lb)	Unit Weight (lb/ft^2)	Weight (lb)	Unit Weight (lb/ft^2)	Weight (lb)	Unit Weight (lb/ft^2)
TOTAL WING STRUCTURE	78,167	8.1	77,049	8.0	71,570	7.6	62,983	6.8
TOTAL WEIGHED STRUCTURE	47,942	5.0	46,824	4.8	42,548	4.5	34,643	3.8
TOTAL FIXED WEIGHT	30,225	3.1	30,225	3.1	29,022	3.1	28,340	3.1
Strake	23,219	7.74	21,987	7.74	23,906	7.97	22,926	7.68
Weighed Structure	16,421	5.48	15,189	5.35	17,097	5.70	16,130	5.38
Fixed Weight	6,798	2.27	6,798	2.39	6,798	2.27	6,798	2.27
FORWARD STRAKE	7,607	7.44	7,607	8.07	7,607	7.44	7,607	7.44
Weighed Structure	6,048	5.92	6,048	6.41	6,048	5.92	6,048	5.92
Bending Material (Skin Panels & Spar Caps)	4,718		4,719		4,717		4,717	
Shear Material (Spar Webs & Ribs)	1,258		1,258		1,258		1,258	
Lightning Protection	71		71		72		72	
Fixed Weight	1,559	1.53	1,559	1.65	1,559	1.53	1,559	1.53
Access Doors	708		708		708		708	
Wing/Fuselage Attachment	681		681		681		681	
Actuator Attachment	170		170		170		170	
MID/GEAR BOX	15,612	7.90	14,380	7.58	16,288	8.24	15,321	7.75
Weighed Structure	10,373	5.25	9,141	4.82	11,049	5.59	10,082	5.10
Bending Material (Skin Panels & Spar Caps)	7,864		6,777		8,336		7,500	
Shear Material (Spar Webs & Ribs)	2,370		2,226		2,574		2,442	
Lightning Protection	138		138		140		140	
Fixed Weight	5,239	2.65	5,239	2.76	5,239	2.65	5,239	2.65
Access Doors	852		852		852		852	
Wing/Fuselage Attachment	454		454		454		454	
Actuator Attachment	113		113		113		113	
MLG Doors & Jam/Attachment	3,820		3,820		3,820		3,820	
Main Wing Box	22,764	18.71	21,146	18.35	19,784	16.26	16,059	13.20
Weighed Structure	20,640	16.96	19,022	16.51	17,660	14.51	13,935	11.45
Bending Material (Skin Panels & Spar Caps)	16,198		14,898		13,655		10,620	
Shear Material (Spar Webs & Ribs)	4,357		4,039		3,919		3,229	
Lightning Protection	85		85		86		86	
Fixed Weight	2,124	1.75	2,124	1.84	2,124	1.75	2,124	1.75
Access Doors	819		819		819		819	
Wing/Fuselage Attachment	1,078		1,078		1,078		1,078	
Actuator Attachment	227		227		227		227	
Outboard Wing Box	12,127	9.61	13,859	10.08	8,883	8.01	5,640	5.76
Weighed Structure	10,881	8.62	12,613	9.17	7,791	7.02	4,578	4.68
Bending Material (Skin Panels & Spar Caps)	9,995		11,583		6,948		3,839	
Shear Material (Spar Webs & Ribs)	798		942		764		670	
Lightning Protection	86		88		79		69	
Fixed Weight	1,246	0.99	1,246	0.91	1,092	0.98	1,062	1.08
Access Doors	849		849		720		700	
Actuator Attachment	397		397		372		362	
Leading Edge (Fixed Weight)	7,285		7,285		6,929		6,740	
Trailing Edge (Fixed Weight)	9,679		9,679		9,278		9,022	
Fairings (Fixed Weight)	852		852		852		852	
Miscellaneous (Fixed Weight)	2,241		2,241		1,949		1,742	

Fuselage Weight Statements

Fuselage Structure Weight	Strength Sized -1510 (788K) (PZSD model)		Strength Sized - 42° Sweep (SWDS model)		Strength Sized - 69 Chop (67WT model)		Strength Sized -37 Chop (37WT model)	
	Weight (lb)	Unit Weight (lb/ft^2)	Weight (lb)	Unit Weight (lb/ft^2)	Weight (lb)	Unit Weight (lb/ft^2)	Weight (lb)	Unit Weight (lb/ft^2)
FUSELAGE STRUCTURE	**44,426**	**4.02**	**43,706**	**3.96**	**44,058**	**3.99**	**42,093**	**3.81**
Weighed Structure	**29,165**	**2.64**	**28,455**	**2.57**	**28,807**	**2.61**	**26,832**	**2.43**
Semi-Monocoque	26,548		26,144		26,207		24,484	
Skin Panels	19,386		18,987		19,050		17,328	
Frames	7,162		7,157		7,157		7,156	
Keel Beam	2,257		1,951		2,240		1,988	
Lightning Protection	360		360		360		360	
Fixed Weight Structure	**15,261**	**1.38**	**15,251**	**1.38**	**15,251**	**1.38**	**15,261**	**1.38**
Bulkheads	3,051		3,041		3,041		3,051	
Nose Gear Wheel Well	450		450		450		450	
Empennage Support	315		315		315		315	
Windows	1,120		1,120		1,120		1,120	
Passenger Windows								
Cockpit Windows								
Doors	2,911		2,911		2,911		2,911	
Pressurized								
Unpressurized								
Main Deck Floor	3,146		3,146		3,146		3,146	
Seat Tracks	713		713		713		713	
Other Items	2,049		2,049		2,049		2,049	
Tail Skid								
Seam, Seal, & Finish								
Forebody Controls								
Chines								
Fairings								
Miscellaneous	1,506		1,506		1,506		1,506	

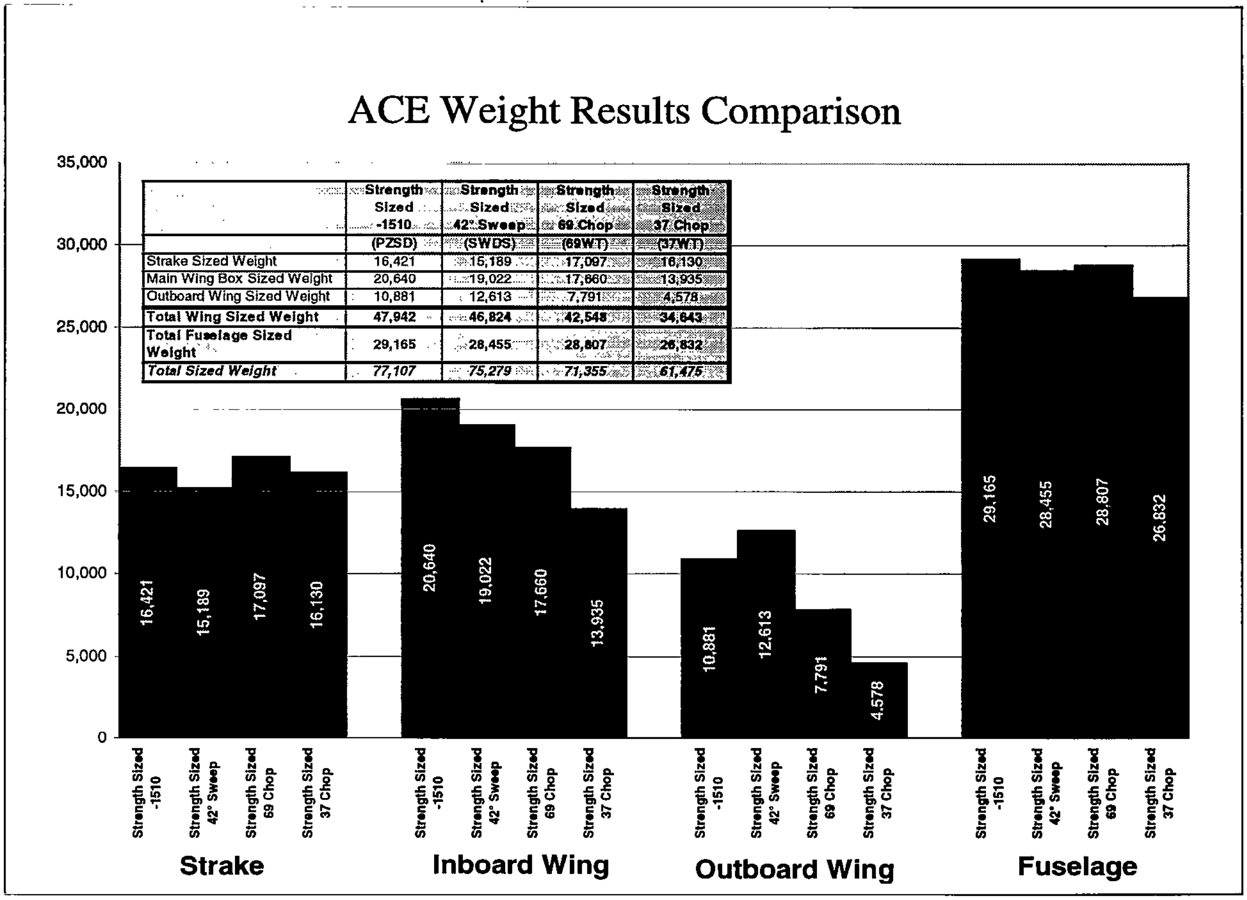

	Strength Sized -1510	Strength Sized 42° Sweep	Strength Sized 69 Chop	Strength Sized 37 Chop
	(PZSD)	(SWDS)	(69WT)	(37WT)
Strake Sized Weight	16,421	15,189	17,097	16,130
Main Wing Box Sized Weight	20,640	19,022	17,660	13,935
Outboard Wing Sized Weight	10,881	12,613	7,791	4,578
Total Wing Sized Weight	**47,942**	**46,824**	**42,548**	**34,643**
Total Fuselage Sized Weight	**29,165**	**28,455**	**28,807**	**26,832**
Total Sized Weight	***77,107***	***75,279***	***71,355***	***61,475***

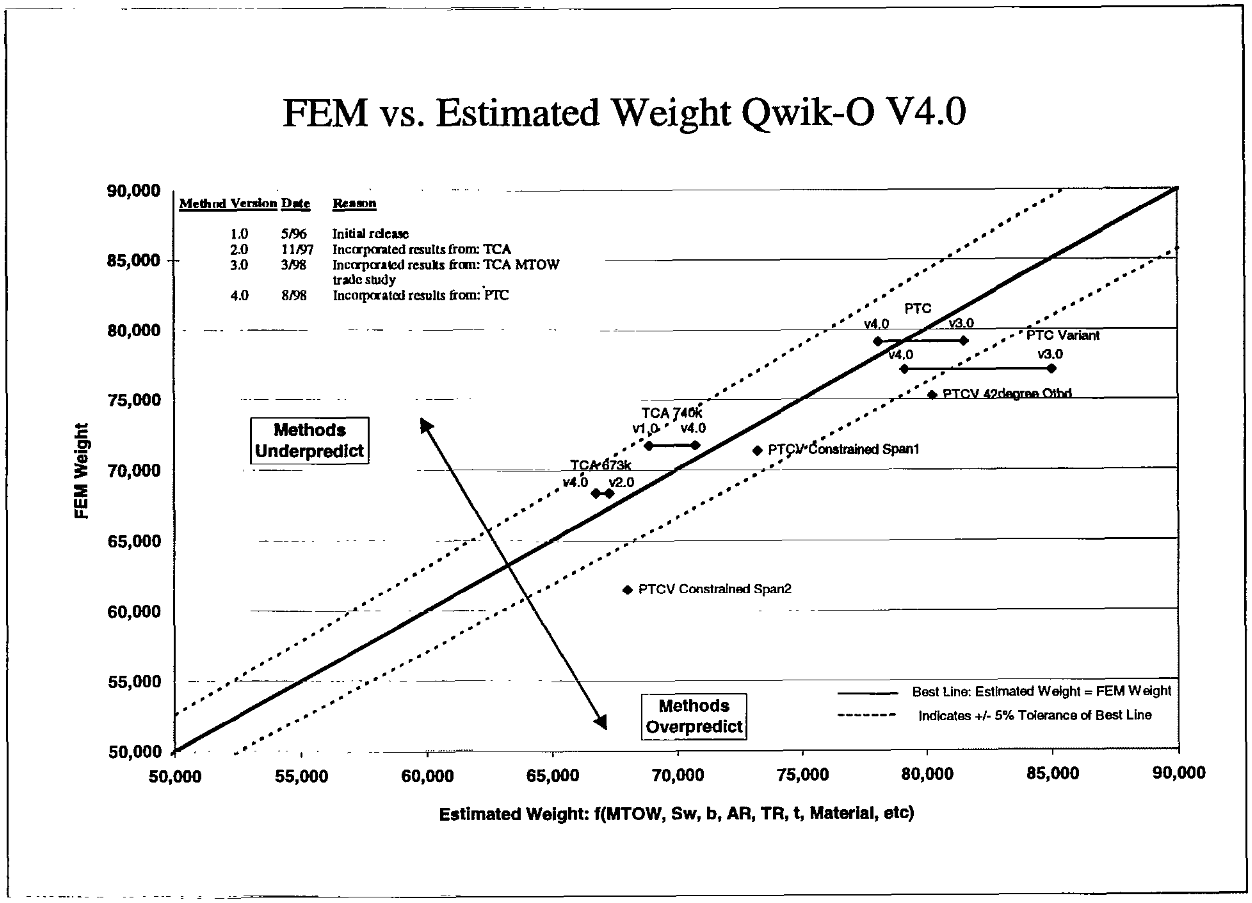
FEM vs. Estimated Weight Qwik-O V4.0
Method Version Date Reason
1.0 5/96 Initial release
2.0 11/97 Incorporated results from: TCA
3.0 3/98 Incorporated results from: TCA MTOW trade study
4.0 8/98 Incorporated results from: PTC
FEM Weight
Estimated Weight: f(MTOW, Sw, b, AR, TR, t, Material, etc)
Methods Underpredict
Methods Overpredict
PTC
v4.0
v3.0
PTC Variant
v4.0
v3.0
PTCV 42degree Otbd
TCA 740k
v1.0
v4.0
PTCV Constrained Span1
TCA 673k
v4.0
v2.0
PTCV Constrained Span2
Best Line: Estimated Weight = FEM Weight
Indicates +/- 5% Tolerance of Best Line
50,000
55,000
60,000
65,000
70,000
75,000
80,000
85,000
90,000

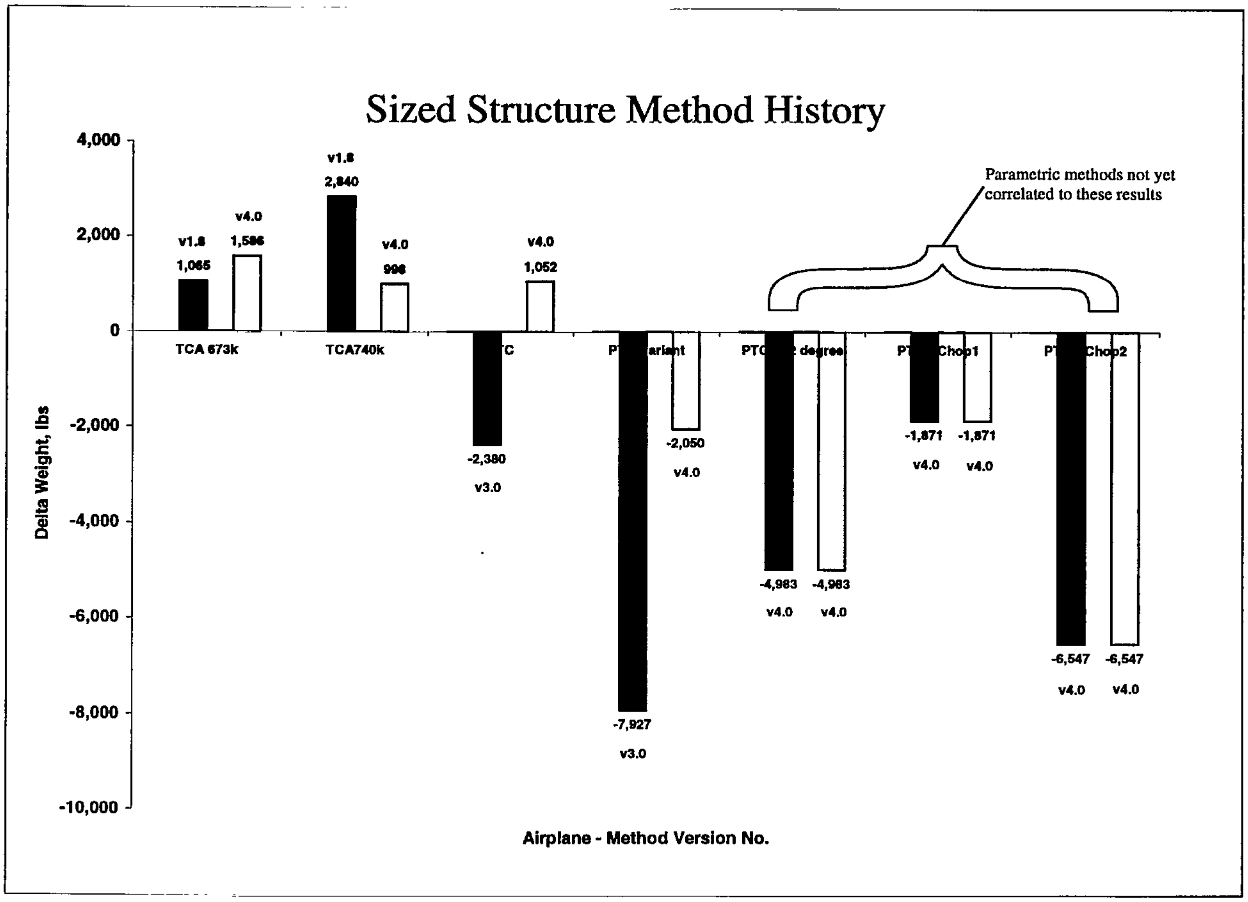
Sized Structure Method History
Delta Weight, lbs
4,000
2,000
0
-2,000
-4,000
-6,000
-8,000
-10,000
Parametric methods not yet correlated to these results
TCA 673k
TCA740k
v1.8
1,065
v4.0
1,586
v1.8
2,840
v4.0
996
v4.0
1,052
-2,380
v3.0
-7,927
v3.0
-2,050
v4.0
-4,983
v4.0
-4,983
v4.0
-1,871
v4.0
-1,871
v4.0
-6,547
v4.0
-6,547
v4.0
Airplane - Method Version No.